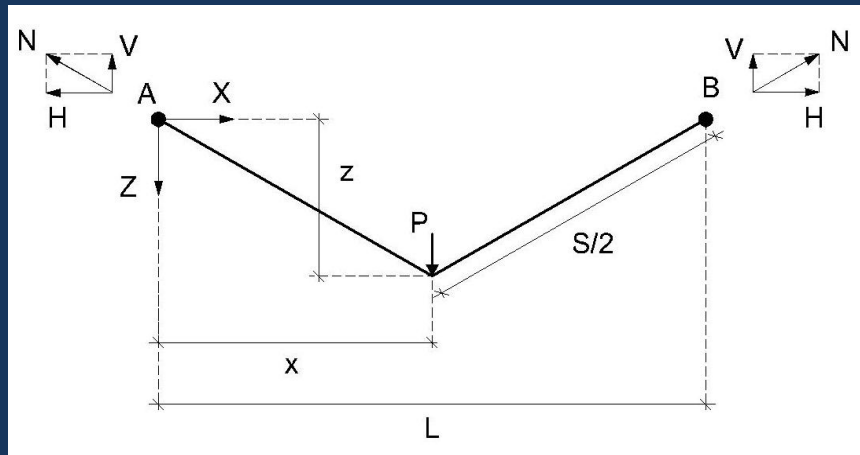


ΧΡΗΣΤΟΣ ΠΑΠΑΚΙΤΣΟΣ
CHRISTOS PAPAKITZOS

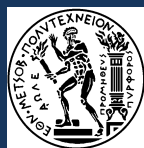
ΔΙΠΛΩΜΑΤΙΚΗ ΕΡΓΑΣΙΑ – DIPLOMA THESIS

ΜΗ ΓΡΑΜΜΙΚΗ ΣΤΑΤΙΚΗ **ΑΝΑΛΥΣΗ ΚΑΛΩΔΙΩΝ ΚΑΙ** **ΔΙΚΤΥΩΝ ΚΑΛΩΔΙΩΝ** **NONLINEAR STATIC ANALYSIS OF CABLES** **AND CABLE NETS**

ΕΠΙΒΛΕΠΩΝ: Χ. ΓΑΝΤΕΣ
SUPERVISOR: C. GANTES



ΕΘΝΙΚΟ ΜΕΤΣΟΒΙΟ ΠΟΛΥΤΕΧΝΕΙΟ
ΣΧΟΛΗ ΠΟΛΙΤΙΚΩΝ ΜΗΧΑΝΙΚΩΝ
ΕΡΓΑΣΤΗΡΙΟ ΜΕΤΑΛΛΙΚΩΝ ΚΑΤΑΣΚΕΥΩΝ



NATIONAL TECHNICAL UNIVERSITY
OF ATHENS
SCHOOL OF CIVIL ENGINEERING
INSTITUTE OF STEEL STRUCTURES

Αθήνα, Φεβρουάριος 2013
Athens, February 2013
ΕΜΚ ΔΕ 2013/46

Χ. Γ. Παπακίτσος (2013)
Μη γραμμική στατική ανάλυση καλωδίων και δικτύων καλωδίων
Διπλωματική Εργασία ΕΜΚ ΔΕ 2013/46
Εργαστήριο Μεταλλικών Κατασκευών, Εθνικό Μετσόβιο Πολυτεχνείο, Αθήνα

C. G. Papakitsos (2013)
Nonlinear static analysis of cables and cable nets
Diploma Thesis ΕΜΚ ΔΕ 2013/46
Institute of Steel Structures, National Technical University of Athens, Greece

.....
Christos G. Papakitsos
Graduate Civil Engineer N.T.U.A.

E-mail: christospapakitsos@yahoo.gr

Copyright © Christos G. Papakitsos, 2013

Με επιφύλαξη παντός δικαιώματος. All rights reserved.

Απαγορεύεται η αντιγραφή, αποθήκευση και διανομή της παρούσας εργασίας, εξ ολοκλήρου ή τμήματος αυτής, για εμπορικό σκοπό. Επιτρέπεται η ανατύπωση, αποθήκευση και διανομή για σκοπό μη κερδοσκοπικό, εκπαιδευτικής ή ερευνητικής φύσης, υπό την προϋπόθεση να αναφέρεται η πηγή προέλευσης και να διατηρείται το παρόν μήνυμα. Ερωτήματα που αφορούν τη χρήση της εργασίας για κερδοσκοπικό σκοπό πρέπει να απευθύνονται προς τον συγγραφέα.

No part of these pages, either text or image may be used for any purpose other than personal use. Therefore, reproduction, modification, storage in a retrieval system or retransmission, in any form or by any means, electronic, mechanical or otherwise, for reasons other than personal use, is strictly prohibited without prior written permission.

Contents

1	Introduction	1
1.1	Historical survey.....	1
1.2	Cables and cable structures	3
1.2.1	Cables.....	3
1.2.2	Cable structures.....	9
1.3	Cable nets	12
1.3.1	General aspects	12
1.3.2	Components of a cable net.....	13
1.3.3	Methods of structural analysis of cable nets.....	13
1.4	Source of geometric nonlinearity in cables	14
1.5	Impications of geometric nonlinearity for the static behavior.....	15
2	Analytical solutions for the static behavior of simple cables	17
2.1	Introduction.....	17
2.2	Simple cables under concentrated loads	18
2.2.1	Horizontal cable under concentrated load in the middle.....	18
2.2.2	Inclined cable under concentrated load at arbitrary position	23
2.2.3	Horizontal cable under concentrated load at arbitrary position	34
2.2.4	Inclined cable under imposed end displacement	38
2.3	Simple cables under uniformly distributed loads	46
2.3.1	Inclined cable under uniformly distributed load along its horizontal projection.....	46
2.3.2	Horizontal cable under uniformly distributed load along its horizontal projection	52
2.3.3	Inclined cable under uniformly distributed load along its arc length	57
2.3.4	Horizontal cable under uniformly distributed load along its arc length.....	63
2.4	Equivalent beam method	66
2.5	Parametric figures of a simple suspended cable	67
2.5.1	General matters	67
2.5.2	Diagrams of a horizontal cable under concentrated load in the middle.....	69
2.5.3	Diagrams of an inclined cable under concentrated load at arbitrary position.....	72
2.5.4	Diagrams of a horizontal cable under concentrated load at arbitrary position	80
2.5.5	Diagrams of an inclined cable under imposed end displacement.....	86
2.5.6	Diagrams of an inclined cable under uniformly distributed load along its horizontal projection	90
2.5.7	Diagrams of a horizontal cable under uniformly distributed load along its horizontal projection	93
2.5.8	Diagrams of an inclined cable under uniformly distributed load along its arc length	96
2.5.9	Diagrams of a horizontal cable under uniformly distributed load along its arc length.....	99
2.5.10	Annotation of parametric figures.....	102
3	Numerical solutions for the static behavior of simple cables.....	107
3.1	Numerical modeling of cables	107
3.2	Simple cables under concentrated loads	108
3.2.1	Results of comparison between analytical and numerical solutions	108
3.2.2	Comparison diagrams of a horizontal cable under concentrated load in the middle	108
3.2.3	Comparison diagrams of an inclined cable under concentrated load at arbitrary position.....	112
3.2.4	Comparison diagrams of a horizontal cable under concentrated load at arbitrary position.....	117
3.2.5	Comparison diagrams of an inclined cable under imposed end displacement	122
3.3	Simple cables under uniformly distributed loads.....	126
3.3.1	Results of comparison between analytical and numerical solutions.....	126
3.3.2	Comparison diagrams of an inclined cable under uniformly distributed load along its horizontal projection	126

3.3.3	Comparison diagrams of a horizontal cable under uniformly distributed load along its horizontal projection.....	129
3.3.4	Comparison diagrams of an inclined cable under uniformly distributed load along its arc length	130
3.3.5	Comparison diagrams of a horizontal cable under uniformly distributed load along its arc length	133
4	Static behavior of simple 1-DOF cable net under concentrated load	135
4.1	Simple 1-DOF cable net model	135
4.2	Form finding	136
4.3	Nonlinear analysis	138
4.4	Modeling with MATLAB	141
4.5	Parametric analysis.....	145
4.6	Numerical solution.....	153
5	Radio mast with pre-tensioned cables	161
5.1	Analytical solution	161
5.2	Equivalent simple 1-DOF cable net model	164
5.3	Effects of pre-tensioning.....	167
5.4	Numerical solution.....	169
6	Static behavior of cable nets.....	171
6.1	The force density method	171
6.2	Parametric analysis – The Peace and Friendship Stadium.....	173
6.2.1	The CANED program	173
6.2.2	Simulation of the Stadium of Peace and Friendship with CANED program	173
6.2.3	Parametric figures	178
7	References.....	185
	Appendix A: Hyperbolic functions.....	187
	Table of symbols	191



ΕΘΝΙΚΟ ΜΕΤΣΟΒΙΟ ΠΟΛΥΤΕΧΝΕΙΟ
ΣΧΟΛΗ ΠΟΛΙΤΙΚΩΝ ΜΗΧΑΝΙΚΩΝ
ΕΡΓΑΣΤΗΡΙΟ ΜΕΤΑΛΛΙΚΩΝ ΚΑΤΑΣΚΕΥΩΝ

ΔΙΠΛΩΜΑΤΙΚΗ ΕΡΓΑΣΙΑ
ΕΜΚ ΔΕ 2013/46

Μη γραμμική στατική ανάλυση καλωδίων και δικτύων καλωδίων

Χ. Γ. Παπακίτσος (Επιβλέπων: Χ. Γαντές)

Περίληψη

Οι καλωδιωτές κατασκευές χαίρουν της εκτίμησης των μηχανικών και των αρχιτεκτόνων, καθώς προσφέρουν υψηλή αισθητική και πλεονεκτήματα σε προβλήματα μεγάλων ανοιγμάτων, όπως οροφές σταδίων. Οι σχεδιαστές πρέπει να προσεγγίσουν αυτού του είδους τις κατασκευές με ένα μη συμβατικό τρόπο, λόγω της γεωμετρικής μη γραμμικότητας των καλωδίων. Ο σκοπός αυτής της διπλωματικής εργασίας είναι να εξετάσει αυτού του είδους τη μη γραμμικότητα έχοντας ως αφετηρία το βασικό στοιχείο των καλωδιωτών κατασκευών, που είναι ένα ανηρημένο μεμονωμένο καλώδιο, και επεκτείνοντας την ανάλυση σε 1-DOF και πιο σύνθετα δίκτυα καλωδίων.

Το πρώτο βήμα της μελέτης είναι ο προσδιορισμός της πηγής της γεωμετρικής μη γραμμικότητας συγκρίνοντας την απόκριση ενός καλωδίου και μίας δοκού σε εξωτερικά φορτία. Έπειτα, εξετάζεται ένα μεμονωμένο καλώδιο, ανηρημένο από τα δύο του άκρα. Προσδιορίζονται οι αναλυτικές εξισώσεις για διάφορα φορτία (συγκεντρωμένο φορτίο, καταναμημένο φορτίο κατά μήκος της οριζόντιας προβολής και κατά μήκος τόξου καλωδίου, μετατόπιση άκρου), για διάφορες θέσεις εφαρμογής του συγκεντρωμένου φορτίου (στο μέσο, σε τυχαία θέση) και για διάφορες κλίσεις καλωδίου (οριζόντιο, κεκλιμένο). Στην περίπτωση μετατόπισης άκρου καλωδίου, η απόκριση προσομοιάστηκε με αυτή ενός ελατηρίου και προέκυψε μία ισοδύναμη σταθερά ελατηρίου.

Οι αναλυτικές εξισώσεις για το ανηρημένο μεμονωμένο καλώδιο επεκτείνονται σε ένα δίκτυο καλωδίων ενός βαθμού ελευθερίας (1-DOF). Προσδιορίζονται οι εξισώσεις για την εύρεση σχήματος και τη στατική ανάλυση, ενώ αναπτύσσεται λογισμικό μη γραμμικής στατικής ανάλυσης 1-DOF δικτύου καλωδίου, με τη χρήση του λογισμικού MATLAB. Μια παρατήρηση στη μορφή ενός 1-DOF δικτύου καλωδίων οδηγεί στη μη γραμμική ανάλυση ενός τηλεπικοινωνιακού ιστού με προεντεταμένα υποστηρικτικά καλώδια, μία ευρέως διαδεδομένη κατασκευή. Τα αποτελέσματα της ανάλυσης αυτής παρουσιάζονται στην παρούσα διπλωματική εργασία. Εν αντιθέσει, τα σύνθετα δίκτυα καλωδίων δεν μπορούν να προσεγγιστούν με την αναλυτική μέθοδο που αναπτύχθηκε στις προηγούμενες εφαρμογές και, έτσι, αντικαθίσταται από τη μέθοδο πυκνότητας δύναμης. Βάσει αυτής της μεθόδου, προσομοιάστηκε το δίκτυο καλωδίων της οροφής του Σταδίου Ειρήνης και Φιλίας, το οποίο βρίσκεται στην Αθήνα.

Στο πλαίσιο αυτής της διπλωματικής εργασίας, οι αναλυτικές λύσεις επιβεβαιώθηκαν από αριθμητικά μοντέλα. Για αυτόν τον λόγο, χρησιμοποιήθηκαν τα λογισμικά πεπερασμένων στοιχείων SAP και ADINA. Η σύγκριση έδειξε ταύτιση μεταξύ των αναλυτικών εξισώσεων και των αριθμητικών μοντέλων, εκτός από την περίπτωση κεκλιμένου μεμονωμένου καλωδίου υπό καταναμημένο φορτίο. Η αιτία εντοπίζεται στην αγνόηση της οριζόντιας μετατόπισης, στην αναλυτική λύση, λόγω της πολυπλοκότητας των μη γραμμικών εξισώσεων. Απαιτείται περαιτέρω έρευνα, η οποία ξεπερνά τα όρια αυτής της διπλωματικής εργασίας.

Παράλληλα με τις αναλυτικές εξισώσεις και τα αριθμητικά μοντέλα, παρουσιάζονται και σχολιάζονται παραμετρικά διαγράμματα. Αυτού του είδους τα διαγράμματα εξηγούν, με ένα σφαιρικό τρόπο, την απόκριση των καλωδιωτών κατασκευών σε εξωτερικά φορτία. Θεωρήθηκαν διάφορες τιμές προέντασης, αρχικής κρέμασης καλωδίου, απαραμόρφωτου μήκους, κλίσης, θέσης εφαρμογής του συγκεντρωμένου φορτίου, μέτρου ελαστικότητας και διαμέτρου.

Λέξεις κλειδιά

ανηρημένο μεμονωμένο καλώδιο, 1-DOF δίκτυο καλωδίων, τηλεπικοινωνιακός ιστός, δίκτυο καλωδίων, γεωμετρική μη γραμμικότητα, στατική ανάλυση, αναλυτικές λύσεις, αριθμητικές λύσεις, συγκεντρωμένα φορτία, καταναμημένα φορτία, μετατοπίσεις άκρου, ισοδύναμη σταθερά ελατηρίου, προεντεταμένο καλώδιο, παραμετρικά διαγράμματα



NATIONAL TECHNICAL UNIVERSITY OF ATHENS
SCHOOL OF CIVIL ENGINEERING
INSTITUTE OF STEEL STRUCTURES

DIPLOMA THESIS
EMK ΔΕ 2013/46

Nonlinear static analysis for cables and cable nets

C. G. Papakitsos (supervised by C. Gantes)

Abstract

Cable structures have gained the regard of engineers and architects, as they offer high aesthetic and benefits in large openings, such as stadium roofs. Designers have to approach this kind of constructions in an unconventional way, due to the geometric nonlinearity of cables. The aim of this diploma thesis is to examine this kind of nonlinearity starting from the basic element of cable structures, which is a simple suspended cable, and expanding the analysis to 1-DOF and more complex cable nets.

The first step of the study is the detection of the source of the geometric nonlinearity by comparing cable and beam response to external loads. Then, a simple suspended cable is considered. Analytical equations are determined for different kind of loads (concentrated load, distributed load along horizontal projection and arc length of the cable, imposed end displacement), for different application points of concentrated load (in the middle, arbitrary) and for different inclinations (horizontal, inclined). In case of imposed end displacement, cable response is simulated with this of a spring and an equivalent spring constant is found.

The analytical equations for a simple suspended cable are extended for a cable net with one degree of freedom (1-DOF). Form finding and static analysis equations are determined, while software for nonlinear static analysis of 1-DOF cable net is developed, based on MATLAB software. An observation in the form of a 1-DOF cable net leads to the nonlinear analysis of a radio mast with pre-tensioned cables, a widely spread construction. The results of the analysis are presented in this diploma thesis. On the other hand, complex cable nets cannot be approached by the analytical method developed in previous applications and, so, it is replaced by the force density method. Based on this method, the cable net of the roof from the Stadium of Peace and Friendship, in Athens, is simulated.

In the context of this diploma thesis, the analytical solutions are verified by numerical models. For this purpose, the finite element software SAP and ADINA are used. The comparison showed identification between analytical equations and numerical models, apart from the case of an inclined simple suspended cable under distributed load. The reason is located at the omission of the horizontal deflection, in the analytical solution, due to the complexity of nonlinear equations. Further investigation, which exceeds the limits of this diploma thesis, is required.

Parallel to analytical equations and numerical models, parametric figures are presented and annotated. This kind of figures illustrates, in a spherical way, the response of cable structures to external loads. Different values of pre-tension, initial cable sag, unstressed length, inclination, application point of concentrated load, modulus of elasticity and diameter are considered.

Key words

simple suspended cable, 1-DOF cable net, radio mast, cable net, geometric nonlinearity, static analysis, analytical solutions, numerical solutions, concentrated loads, distributed loads, imposed end displacements, equivalent spring constant, pre-tensioned cable, parametric figures

Acknowledgments

First of all I would like to thank my professor, Charis Gantes, who gave me the chance to write my diploma thesis under his supervision and for his continuous support. During the period of my diploma thesis, he provided me not only high-level technical knowledge but also significant advices, gained through his long-term experience, regarding the behavior of a civil engineer, which will be my guidance for my future professional life. I would like to thank all the colleges in the Institute of Steel Structures of the School of Civil Engineering NTUA for their constructive help. I am especially grateful to all the friends for their support. But most of all, I would like to give my special thanks to my parents and my brother, Spyros, for their unconditional support.

1 INTRODUCTION

1.1 HISTORICAL SURVEY

Nature has always granted to the humanity examples to solve problems of covering spans. The vaulted caves were used as shelters, the trunks of the fallen trees formed bridges to cross streamlets or even rivers at the narrow passages and the interlaced vines constituted a sort of suspended roof, while the trees, standing upright, represented the necessary masts to support these roofs. These images, among many others, stimulated the human imagination and triggered structural engineering. The need for progress and evolution, along with the development of technology, which brought new, more efficient materials, generated the opportunity to elaborate new concepts, find new solutions, overcome the existing limits and always set new ones.

The examples are numerous, still standing over the centuries, testifying the course of the human inventiveness. Since the ancient Roman years, curves dominated in the field of engineering and architecture, substituting straight lines, made of stones or wood, which were proved to be inadequate in some cases. Arcades, arches, and domes were the best solution to cover large spans, such as aqueducts, bridges, churches, etc. Later, thin shells, made of concrete, gained the interest of architects, giving a different aspect to their creations with their lightness and captivating elegance. The function of these structures was to carry loads in pure compression, thus avoiding bending of the members. The reverse solution was realized by structures with members that operate in pure tension, which belong to the family of tensile structures. The sails of ships were among the first membrane structures ever used, providing resistance to wind, developing only tension and moving the ship over the seas. The first suspended bridges, made of ropes, were used to cross canyons, while the first suspended roof was the "velarium" of the Coliseum, built in 70 B.C. in Rome (Figure 1-1), used to protect the spectators from rain and sun. During the last six centuries, many suspended bridges were constructed, but only in the second half of the twentieth century, tensile structures became a pioneer in the field of structural engineering, opening new frontiers [1].

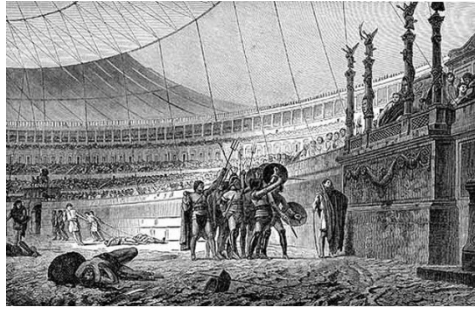


Figure 1-1: The "velarium" of the Coliseum in Rome, Italy

Cable problems have been the vehicle by which some well-known techniques, equations and mathematical functions were introduced. For example, Stevin in 1586 established the triangle of forces by experimenting with loaded strings, although Leonardo da Vinci's fifteenth-century sketches anticipated this result and several others, including the catenary and the concept of the collapse mechanism in a voussoir arch. It seems likely, according to Truesdell, that Beeckman had by 1615 solved the suspension bridge problem, namely, that in responding to load uniformly distributed in plan, a cable hangs in a parabolic arc. But nearly two centuries were to pass before this solution became well known. It was rediscovered in 1794 by the Russian engineer Fuss, who was charged with the responsibility of attempting to span the Neva River, at St. Petersburg. Galileo, in *Discourses on Two New Sciences*, published in 1638, muses on the shape of a hanging chain and concluded that it is parabolic – primarily by an analogy to the flight of a projectile. The years 1690 and 1691, Bernoulli, Leibnitz and Huygens more or less jointly discovered the catenary. In the discovery of the catenary different approaches were employed, with Huygens relying on geometrical principles, and Leibnitz and the Bernoullis using the calculus, then a comparatively recent invention.

The vibration of taut strings was studied extensively in the early part of the eighteenth century. In 1738 Daniel Bernoulli published a solution for the natural frequencies of a chain that hangs from one end. Lagrange used, a discrete, string of beads model of the taut string as an illustration of the application of his equations of motion. One could go on, but the list is sufficient to illustrate the point.

In Europe cable theory had at least a firm grounding by the nineteenth century. Outside Europe the practical aspects had received considerable attention at a much earlier date. The early civilizations of the Far East and Central and South America mastered suspension bridge construction. Needham records the existence of sophisticated suspension bridges in China before the start of the Christian era. The Native Americans did, and still do, make intricate rope pathways. Iron chain suspension bridges date from A.D. 65, when a bridge built in Yunnan, China. Thang-stong rGyal-po, a Tibetan monk in the fifteenth century, was renowned as a builder of iron chain suspension bridges. One of his iron chain suspension bridges, Chakzam Bridge, about 65 km from Lhasa, at Tsangpo, still existed in 1948 (Figure 1-2). The evolution of the suspension bridge has been given an admirable treatment by Hauri and Peters [2].



Figure 1-2: Old Chain-Bridge at Chakzam

1.2 CABLES AND CABLE STRUCTURES

1.2.1 Cables

1.2.1.1 Cable types

The basic element for cables is the steel wire with a tensile strength larger than that of ordinary structural steel. The steel wire has a cylindrical shape with a diameter of between 3 and 7 mm. A single straight wire, surrounded by a single layer of six wires with the same pitch and direction of helix, makes up the seven-wire strand, as shown in Figure 1-3.

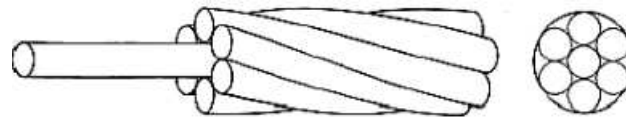


Figure 1-3: Seven-wire strand

A straight wire core surrounded by successive spinning of layers, generally with opposite direction of helix, creates the multi wire helical strands, called spiral strands. Due to the twisting of the layers, the helical strand becomes self-compacting and thus there is no need to wrap or apply bands around the strand to hold the wires together. Typical values of the elastic modulus E for a spiral strand are $E = 145 - 170$ GPa, depending on the size, almost 15 – 25 % lower than the one for the single wire. In addition, the strength of the helical strand is approximately 10 % lower than the sum of the breaking strengths of the individual wires. The way of winding defines the type of the strand. The main types of strands are those with one layer of wires (single layer strand), with two layers consisting of the same number of wires for each layer (seale strand), with two layers of wires having the same diameter for each layer (filler wire strand), with two layers of wires having different diameters in the outer layer (Warrington strand) and the multi-layer strands (combined patterns strand), as illustrated in Figure 1-4. Alternatively, the wire rope is composed by a number of steel wires spun together to form six strands, which in turn are spun together around a fiber core to form a rope (Figure 1-5).

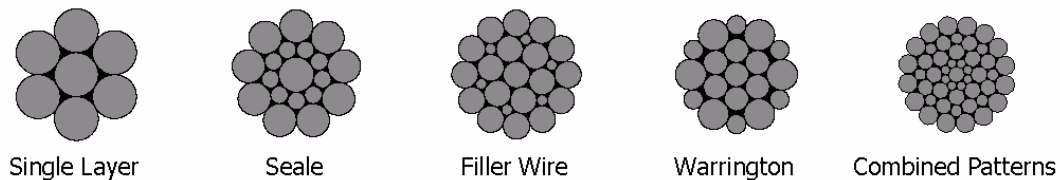


Figure 1-4: Basic strand construction

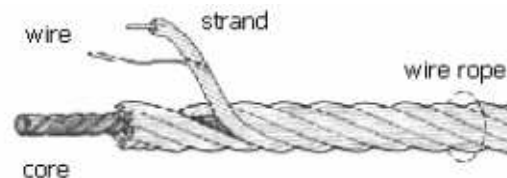


Figure 1-5: Wire rope

Locked coil strands are composed of two types of twisted wire: in the core normal round wires arranged as in a normal helical strand, and in the outer layers wires of a special Z-shape. This Z-shape is chosen so that the wires interlock which, in combination with the self-compacting effect from the spiral arrangement, ensures a tight surface (Figure 1-6). The locked-coil strands are more compact than any other type of strand. The elastic modulus E is approximately $E = 160 - 180$ MPa.

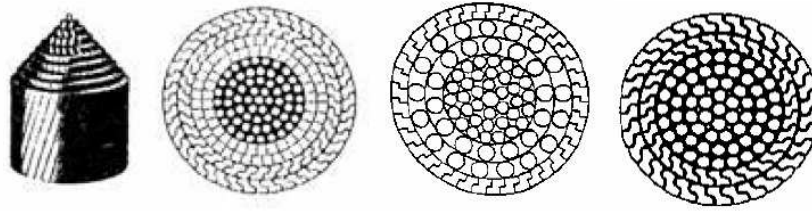


Figure 1-6: Typical cross-sections of locked coil strands

The term lay refers to the direction of the twist of the wires in a strand and to the direction that the strands are laid in the rope. In some cases, both wires in the strand and strands in the rope are laid in the same direction; otherwise, the wires are laid in one direction and the strands are laid in the opposite direction, depending on the intended use of the rope. The six types of lays used in wire ropes are as follows: 1) Right Regular Lay (RRL): The strands are laid in clockwise direction around the core and the wires in the strand are laid in a counter clockwise direction. 2) Left Regular Lay (LRL): The strands are laid in a counter clockwise direction around the core and the wires in the strand are laid in a clockwise direction. In this lay, each step of fabrication is exactly opposite from the right regular lay. In these two ways, the wires are parallel to the longitudinal axis of the strand. 3) Right Lang Lay (RLL): The strands are laid in a clockwise direction around the core and the wires in the strands are laid in clockwise direction. 4) Left Lang Lay (LLL): The strands are laid in a counter clockwise direction around the core and the wires in the strand are laid in a counter clockwise direction. These two lays are more resistant to the bending fatigue and to the abrasion than the previous two. 5) Right Alternate Lay (RAL): The strands are laid in clockwise direction. The wire in the strands are laid in a clockwise and counter clockwise direction in alternating strands and 6) Left Alternate Lay (LAL): The strands are laid in a counter clockwise direction, while the wire in the strands are laid in a counter clockwise direction in alternating strands. These six different lays of wire rope are shown in Figure 1-7.

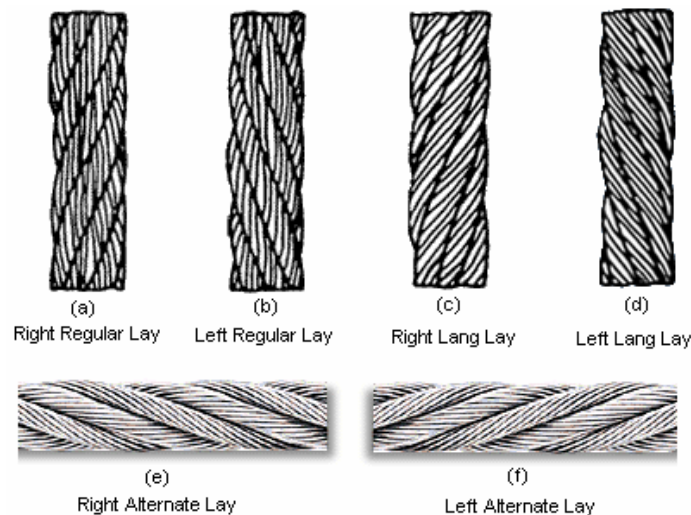


Figure 1-7: Lays of wire rope

The length of a rope lay is the distance measured parallel to the centre line of a wire rope in which a strand makes one complete spiral or turn around the rope (Figure 1-8). The length of a strand lay is the distance measured parallel to the centre line of the strand in which one wire makes one complete spiral or turnaround the strand. The lay length of a rope is the basic factor controlling the breaking load and extension characteristics of the finished cable. The breaking load is relatively low for short lay lengths and greater for longer lay lengths. Spiral strand constructions normally have lay lengths in the range 9 - 12 times the cable diameter, depending on the size of the finished strand and the number of the layers of wires. A small size strand may have long lay length, and thus large values of modulus and breaking

loads. As the spiral becomes larger and more complex, the lay has to be shortened in order to produce a good, tight strand, which leads to low values of modulus and breaking load. On the other hand, the locked coil construction may have longer lays, not depending on the size of the cable, due to the interlocking of the outer wires.

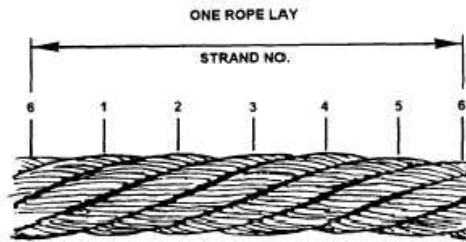


Figure 1-8: Lay length measurement

Eurocode 3, Part 1.11 [3] gives design rules for structures with tension components made of steel, which are adjustable and replaceable. These products are prefabricated, and installed into the structure on-site. For cable nets, two types of cables are recommended: the spiral strand ropes (having the characteristics of Table 1-1) and the full-locked coil ropes (with characteristics listed in Table 1-2).

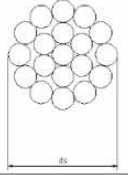

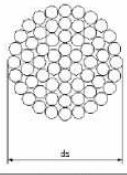
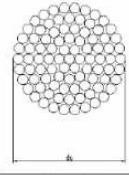
				
Construction	1 × 19	1 × 37	1 × 61	1 × 91
Diameter d_s [mm]	3 to 14	6 to 36	20 to 40	30 to 52
Wires per strand	19	37	61	91
Outer wire per strand	12	18	24	30
Breaking force factor K	0.525	0.52	0.51	0.51

Table 1-1: Spiral strand ropes (reported from [3])

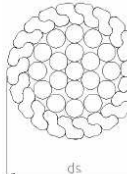
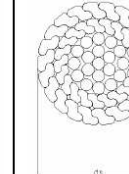
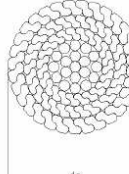
			
Construction	1 layer Z-wires	2 layer Z-wires	≥ 3 layer Z-wires
Diameter d_s [mm]	20 to 40	25 to 50	40 to 180
Tolerance d	+5%	+5%	+5%
Breaking force factor K	0.585	0.607	0.643

Table 1-2: Full-locked coil ropes (reported from [3])

The value of the rope self weight is related to the metallic cross-section and the unit length, taking account of the weight densities of steel and the corrosion protection system. For spiral strands or locked coil strands the following approximate expression for the nominal self weight may be used:

$$g_k = w_k A \quad (1-1)$$

where w_k is the unit weight in $\text{kN}/(\text{m} \cdot \text{mm}^2)$, given in Table 1-3, and A is the metallic cross-sectional area in m^2 , calculated as:

$$A = n \frac{d^2}{4} f \quad (1-2)$$

where d_A is the external diameter of the rope or strand, including sheathing for corrosion protection if used. The fill-factor f is defined as the ratio of the sum of the nominal metallic cross-sectional areas of all the wires in a rope (A) and the circumscribed area (A_u) of the rope based on its nominal diameter (d_A), also given in Table 1-3.

Ropes	Fill factor f							Unit weight $w \times 10^{-4}$ kN/(m \cdot mm 2)
	Core wires + 1 layer z-wires	Core wires + 2 layer z-wires	Core wires + >2 layer z-wires	number of wire layers around core wire				
				1	2	3-6	>6	
1	Spiral strand			0.77	0.76	0.75	0.73	830
2	Full-locked coil	0.81	0.84	0.88				830

Table 1-3: Unit weight w_k and fill-factors f (reported from [3])

Regarding the modulus of elasticity E , the exact values should be derived from tests. Notional values of elastic modulus E , for first estimations, when test results are not available, are given in Table 1-4 for locked coil strands and bundles of strands.

	High strength tension component	E_0 [kN/mm 2]	
		Steel wires	Stainless steel wires
1	Spiral strand ropes	150 \pm 10	130 \pm 10
2	Full locked coil ropes	160 \pm 10	–

Table 1-4: Notional values for the modulus of elasticity E in the range of variable loads (reported from [3])

The characteristic values of the yield stress f_y and the ultimate tensile strength f_u shall be taken from the relevant technical specifications. The following values f_u are recommended:

		f_u [N/mm 2]
steel wires	round wires	1770
	Z-wires	1570
stainless steel wires	round wires	1450

Table 1-5: Recommended nominal tensile strength values f_u for steel and stainless steel wires (reported from [3])

The minimum breaking load of the cable, in kN, is obtained as follows:

$$F^{\min} = \frac{d_A^2 R_r K_r}{1000} \quad (1-3)$$

where,

d_A is the diameter of the rope in mm

K_r is the breaking force factor

R_r is the rope grade in N/mm 2 , which is designated by a number (e.g. 1770 N/mm 2)

[1]

1.2.1.2 Materials of construction

Regarding the materials of construction, cables have been made of:

- Steel
- Kevlar (registered DuPont trademark; a synthetic aramid fiber)
- Fiberglass
- Polyester

A high-tensile breaking strength is a primary property of the wire rope. There are other important properties:

- Small cross-section
- Low weight
- Long fatigue life
- Resistance to corrosion and abrasion
- High flexibility
- Good stretch and rotational behavior

These properties depend on the rope manufacture and wire control. Cables act principally as axial elements; however, because of the helical wires, a torque may be induced as the helical wires try to "unwind" during axial loading. The effects of induced or externally applied torque may be significant; induced torque decreases the ultimate strength. A torque-balanced cable is one designed to yield zero or very small amounts of rotation under load. In addition to the stresses in the wires due to the axial force, the wound wires are subjected to bending stresses which are difficult to evaluate because of relative movements of the individual strands. Cable materials typically have linear stress-strain relationships over only a portion of their usable strength. Beyond the elastic limit, the proportional relationships do not hold. Breaking-strength efficiency is the ratio of cable strength to the sum of the individual wire strengths and is greater for ropes and strand lay. The breaking-strength efficiency is reduced as the number of wires in the strand is increased. A rope made up of brittle wires will be less able to bear pre-stressing due to unequal distribution of strains and consequently will develop lower breaking- strength efficiency than could be obtained with more ductile wire [4].

1.2.1.3 Elastic cable model

In this diploma thesis, a number of cables, with different properties, is examined. Regarding the cable response to external loads, it is considered that nonlinearity exists only in geometry and not in material. So, it is assumed that cable response is elastic until the value of the yield stress $f_y = 1.58$ GPa. If tension exceeds this limit, the cable breaks (Figure 1-9).

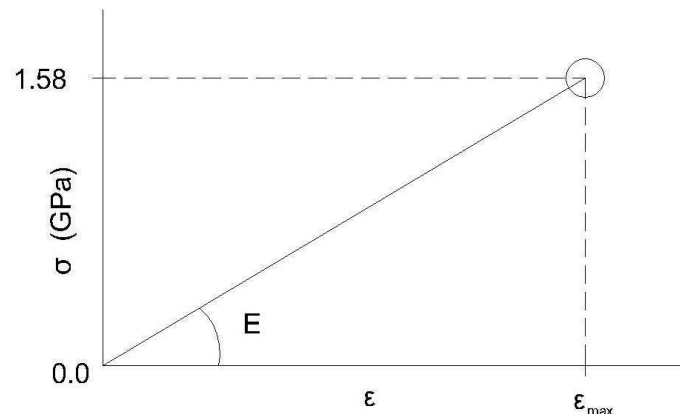


Figure 1-9: Elastic cable response

Hooke's law gives:

$$f_y = E\epsilon^{\max} \Rightarrow \epsilon^{\max} = \frac{f_y}{E} \quad (1-4)$$

Cable's axial force capacity N^{cap} comes out from the following formula:

$$f_y = \frac{N^{\text{cap}}}{A} \Rightarrow N^{\text{cap}} = f_y A \quad (1-5)$$

where A is the cross-section which is calculated as bellow:

$$A = n \frac{d_A^2}{4} \quad (1-6)$$

where d_A is the diameter of the cable.

Table 1-6 presents values of the modulus of elasticity E , diameter d_A and initial unstressed length S_0 that, mainly, have been chosen in the context of this diploma thesis.

E (GPa)	d_A (mm)	S_0 (m)
150	10	10.0
165	20	20.0
180	30	30.0

Table 1-6: Characteristic values of cable parameters

In practice, cables made of elastic materials do not exist. Paragraph 1.2.1.4 describes the post-elastic response of a cable, in order to acquire a complete knowledge of their behavior.

1.2.1.4 Post-elastic cable response

After the elastic limit of the cable is reached, the problem of the response becomes more difficult since it is nonlinear both with respect to geometry and material properties. The loading that causes a cable segment to reach the elastic limit may be found with the theory presented in this diploma thesis, but, to determine the largest load consideration must be given to the post-elastic response.

The load causing failure is always greater, sometimes substantially so, than the load pertaining to the elastic limit. A suspended cable resists applied load by changes in tension and geometry. Beyond the elastic limit changes in tension and geometry can still occur to accommodate the increased load. Tension changes occur because of the pronounced strain-hardening characteristic of the high strength steels frequently used in cables, for which there is no clearly defined yield plateau. Failure occurs when the ultimate strain is reached in some portion of the cable. For the steel typically used in cables, the ratio of strain at ultimate to strain at elastic limit is small, being of the order of 10. This may be contrasted with mild steels (which have a clearly defined yield plateau) where typically this ratio may be of the order of 100 or more. A characteristic of relatively flat suspended cables is that small changes in cable length give rise to substantial changes in cable geometry. Therefore, even though the strain ratio at ultimate may be small (and the non-recoverable strain itself be small), this behavior together with the strain-hardening effect makes it possible for the load that causes failure to be often substantially in excess of that which just exceeds the elastic limit.

Because the elastic limit is not clearly defined (see Figure 1-10), the modulus of elasticity is usually calculated from the slope of the straight line that connects the 10 % breaking load with the 90 % pre-stretching load of the cable specimen. A pre-stretching load of about 55 % of the breaking load is usually applied to remove constructional looseness in the cables—a very important prerequisite. Typically the elastic limit $\sigma_{e,r}$ is reached at about 50 % of the ultimate tensile strength σ_u . Ultimate tensile strengths of 1.500 MPa are regularly achieved, with ultimate strains around 3 % for rope and 6 % for strand; tests show that strand is stronger than the more flexible rope of the same size. Strength and stiffness, based as they are on the nominal cross-sectional areas, are affected by the class of zinc coating [2].

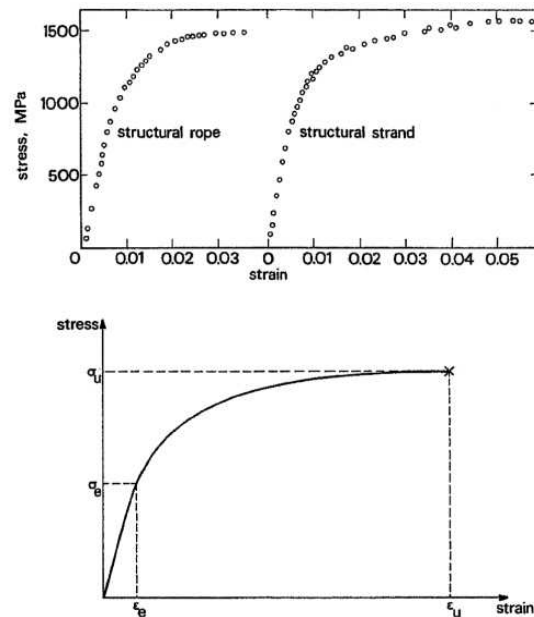


Figure 1-10: Typical stress-strain properties of structural rope and strand [2]

1.2.2 Cable structures

1.2.2.1 Types of cable structures

Tension structures are ones in which the main load-carrying members transmit applied loads to the foundations or other supporting structures by direct tensile stress without flexure or compression. Their cross-sectional dimensions and method of fabrication are such that their shear and flexural rigidities, as well as their buckling resistance, are negligible. There are two broad classes of tension structures: cable structures comprised of uniaxially stressed members, and membrane structures comprised of biaxially stressed members. The general class of cable structures can be further divided into four subclasses:

- 1) Single cables in which single cable segments, or several simply connected segments, are subjected to loads predominantly in a single plane of action, e.g., suspension cables, tether or mooring lines, guy lines for towers or tents.
- 2) Cable trusses in which pre-stressed segments are multiply connected in a single plane and loaded in that same plane, e.g., cable-stayed bridges, double-layer cable-supported roofs.
- 3) Cable nets in which pre-stressed segments are multiply connected in a curved surface (synclastic or anticlastic) and loaded predominantly normal to that surface, e.g., hanging roofs, suspended nets.
- 4) Cable networks in which cable segments are multiply connected to form a three-dimensional framework, e.g., suspension networks, trawl nets, multiple-leg.

There are four subclasses of membrane structures:

- 1) Air-supported structures in which an enclosing membrane is supported by a small differential air (or fluid) pressure, eg., stadia roofs, inflated temporary shelters or storehouses.

- 2) Inflated structures in which highly pressurized tubes or dual-walled mats are used as structural members in a space structure, e.g., inflated beams, columns, or arches; dual-walled shells; air cushion roofs.
- 3) Pre-stressed membranes in which fabric or rubberlike sheets are stretched over rigid frameworks and columns to form enclosures or diaphragms, e.g., tents, masted roofs.
- 4) Hybrid systems in which membrane panels span between primary load-carrying members such as pre-stressed cables and rigid members, e.g., reinforced fabric roofs, fluid storage tanks.

[4]

1.2.2.2 Applications of cable structures

Tension structures are well suited to support broadly distributed dead loads and live loads such as wind, ocean currents, and drift forces due to waves. It should not be surprising that lightweight tension structures resemble biological forms, since such forms also support loads by tension in pneumatically pre-stressed skins and fibers. Some of the advantages of tension members for use as structural components are:

- 1) They are lightweight and collapsible and therefore easy to transport and erect.
- 2) They can be prefabricated in a factory, have low installation costs, and are potentially relocatable.
- 3) For air-supported structures, the primary load-carrying mechanism is the habitable environment itself, i.e., a pressurized mixture of gases.
- 4) The environmental loads are efficiently carried by direct stress without bending.
- 5) They are load-adaptive in that the members change geometry to better if accommodates changes in load patterns and magnitudes.

[4]

1.2.2.3 Examples of cable structures

In this chapter, images of cables structures all over the world are presented.

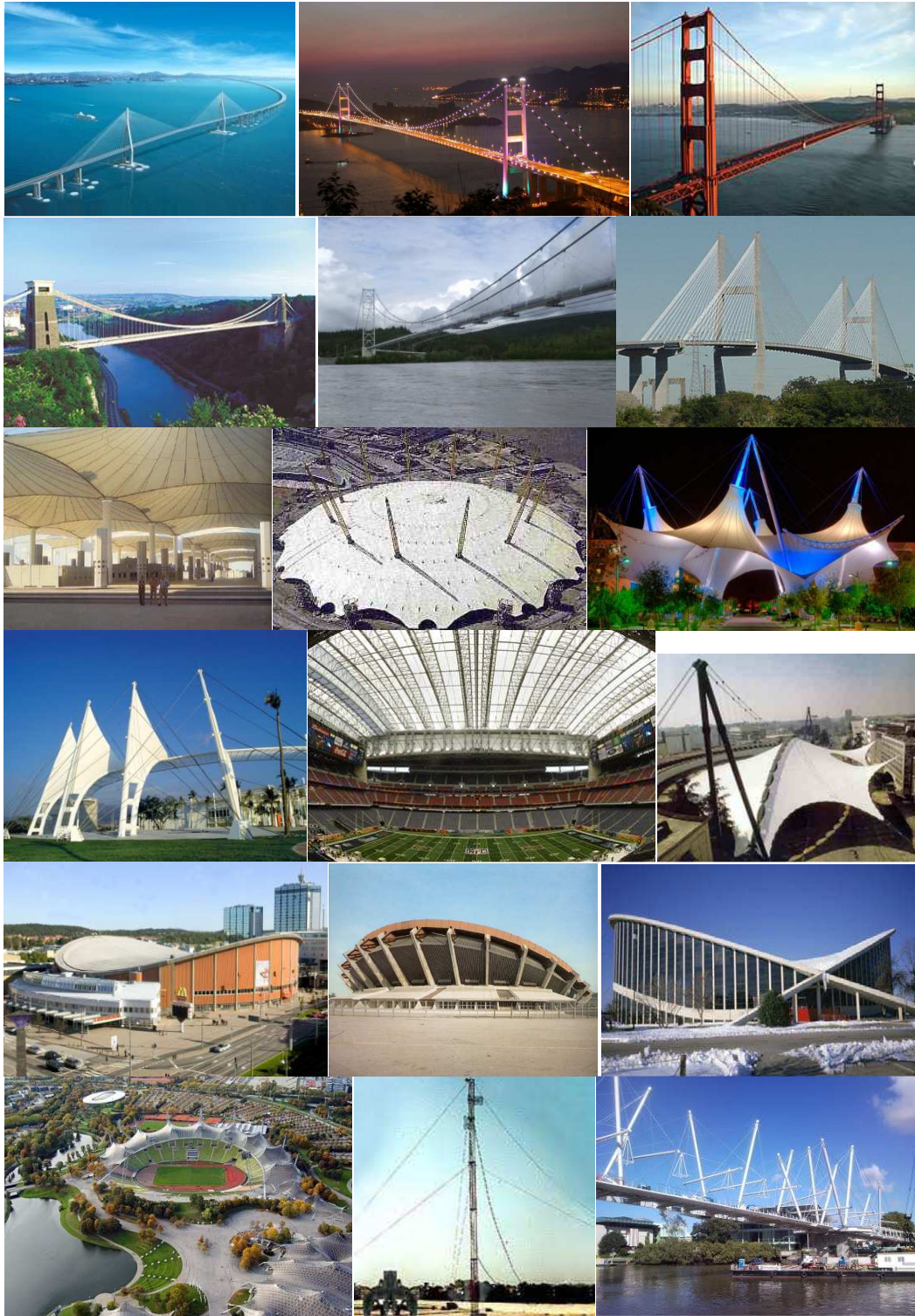


Figure 1-11: Cable structures around the world



Figure 1-12: Cable structures around Greece

1.3 CABLE NETS

1.3.1 General aspects

Cable nets belong to the family of tensile structures. They are characterized by their capacity to cover long spans without intermediate supports and to carry loads much heavier than their own weight. They are structures that always stimulate the interest and the imagination of both structural engineers and architects, demanding their collaboration, as their structural behavior and geometry are closely related. The shape of the final surface depends on the geometry of their boundaries, the curvatures, the levels of cable pre-tension and the eventual internal supports. The most common shape of cable nets is the hyperbolic paraboloid with a surface that is convex about one axis and concave about the other, with a rectangular, rhomboid, circular or elliptical plan. The net consists of two families of pre-stressed cables, the main or carrying cables, which are suspended from the highest points of the boundary and the secondary or stabilizing ones, which are anchored at the lowest points of the boundary. The difference of height between the highest or lowest points and the central node is called sag of the roof in the direction of the main or stabilizing cables, respectively. The boundary is usually a pre-stressed reinforced concrete ring with a box cross-section. These structures are very efficient, because the loads are transmitted through tension of the cables, usually made of high-strength steel, having thus the best exploitation of the material. In addition, with their unusual forms they differ from all other, conventional structures, something that makes them extremely elegant.

These characteristics render them one of the most attractive alternatives for covering hangars, stadiums, swimming pools, ice rinks, exhibition halls, theatres, concert halls, churches and other long-span structures. On the other hand, these structures experience large deformations, mainly because, due to their lack of shear rigidity, the cables change their shape in order to equilibrate the loads without shear. The large deflections can be alleviated by appropriate level of pre-tension. The design of such structures aims at

maintaining all cables in tension under any load combination; in case of cable slackening, the net may exhibit large deformations. Opposite curvatures enable pre-tension in both directions, providing bearing capacity for loads directed downwards, such as snow and wind pressure and upwards, such as wind suction. Flat or nearly flat regions of the cable net surface should be avoided, because their stiffness is insufficient and they may easily flutter. In general, however, the suspended roofs cannot be calculated on the basis of linear theory, due to the large difference between their un-deformed and their deformed shape. Thus, their analysis should be geometrical nonlinear. The principle of superposition does not apply and separate nonlinear analyses must be performed for each loading combination [1].

1.3.2 Components of a cable net

A saddle-form cable network consists of two families of pre-stressed cables, which projected in plan create an orthogonal grid. The cables that are suspended from the highest points of the boundary are called carrying or main cables, while the stabilizing or secondary cables are anchored at the lowest points of the boundary (Figure 1-13).

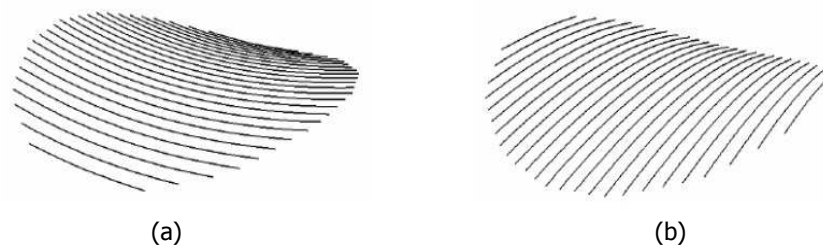


Figure 1-13: Components of a cable net: (a) main cables, (b) secondary cables

The cables are anchored to a boundary ring usually made of pre-stressed concrete with a closed box cross-section. It is supported by columns arranged radially and it is either rigidly connected with the columns or it seats on bearings placed on the top of the columns [1].

1.3.3 Methods of structural analysis of cable nets

Cable nets are multiply connected systems. In a multiply connected system more than two segments may meet at a node and closed loops may be formed. Such systems are highly redundant, and the deformations of the individual segments play an important role in determining the stresses in the segments. If the segments all lie in a single curved surface and are loaded principally transverse to that surface, then analytical and numerical methods based on a membrane analogy can be used. That is, the net is replaced by an equivalent pre-stressed membrane and solution methods available for that type of problem can be adopted.

More generally, multiply connected segments will form a three-dimensional network. Methods of redundant structural analysis are needed to predict both the pre-stressed configuration and the in-service response. The pre-stressed configuration and stress state can be determined either by an inverse method or by nonlinear analysis. Sometimes a combination of both is needed. Often, if in the in-service phase the added loads are small, the response can be modeled by linearized equations. But the essential nonlinearity of the system remains, and care must be exercised in superposing responses and extreme in-service loads must also be handled with nonlinear techniques.

Of the two principal methods redundant structural analysis, flexibility and stiffness methods, stiffness methods have proved to be more useful in the analysis of highly redundant cable systems. In stiffness methods the fundamental unknowns of the equations formulated are the displacements of the nodal points connecting segments. In that class of methods, the lumped

parameter method (analogous to the finite difference method) was the first to be applied to cable systems. In the lumped parameter method all loads (concentrated and distributed) are "lumped" at the nodal points, and attention is focused on the static equilibrium of the nodes. The effects of the segments are replaced by forces in equivalent straight and weightless springs, which may be nonlinear, and a system of simultaneous algebraic equations is generated from the nodal equilibrium conditions.

The finite element method of stiffness analysis has gradually supplanted the lumped parameter method in the analysis of cable systems. The advantages of the finite element method are (1) the numerical modeling has a clearer physical interpretation; (2) the approximations for a particular problem are more flexible (refined approximating functions can be used for higher-order effects such as segment curvature); (3) the refinement of the elements in regions of particular interest is more readily implemented; (4) comparable accuracy can be obtained with less computational effort and mesh refinement; (5) efficient matrix manipulation and solution routines can be used; and (6) variable grid sizes and layouts can be easily generated and changed. Also, the finite element method is less problem-dependent, i.e., with a set of standard cable elements as subroutines in a computer program it is possible to handle with a single program various configurations and loadings of networks and to include other structural elements, such as beams, in the model [4].

1.4 SOURCE OF GEOMETRIC NONLINEARITY IN CABLES

Because of their reduced stiffness, tension structures are susceptible to large motions due to concentrated loads and dynamic effects. Figure 1-14 illustrates the difference in the response to an external vertical uniformly distributed load between a beam and a cable. Beam develops shear and moment tensions in order to lift loads to its supports. In contrast, cable, due to its cross-section, cannot develop shear and moment. The only way to lift external loads is to change its geometry so the multiplication of the sag and the horizontal component of the axial tension at any arbitrary position equals to the moment of external loads [5].

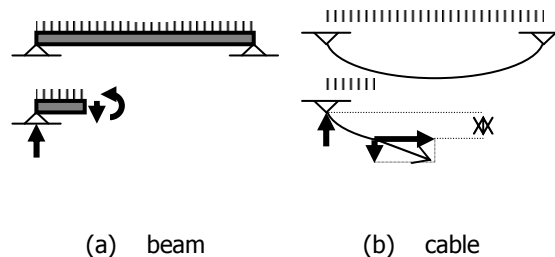


Figure 1-14: Response of beam and cable to external vertical load [5]

Cables respond in a nonlinear fashion to both pre-stressing forces and in-service forces, regardless of linearity of material or loads. Pre-stressing forces are those forces (edge loads, self weight, or pressure) which act on a predominant configuration of static equilibrium for the structure. They stabilize the structure and provide stiffness against further deflection. The response of a tension structure to pre-stressing forces is always nonlinear in that the equilibrium configurations, as well as the state of stress, are depended on those forces.

In-service forces are those variable live loads, static or dynamics, which the structure may be expected to encounter during its service life. They are superposed upon the pre-stressing forces. The response to in-service forces may be nonlinear or quasi-linear, depending on the directions and magnitudes of the in-service forces relative to the state of stress in, and configuration of, the pre-stressed structure.

It is usually sufficient to consider only linear (possibly piecewise linear) material behavior for tension structures. There are instances, however, where nonlinear material characteristics should be considered: hyperelastic and viscoelastic behavior of polymer cables and membranes; nonisotropic woven fabrics; and thermal-elastic and elastoplastic behavior under extreme loads. Another potential source of nonlinearities of response is the interaction of tension structures with hydrostatic and hydrodynamic loads. Not only are the magnitudes of drag force nonlinear, but they are also nonconservative in that directions of pressure loads are dependent on orientations of the cable axes and membrane surfaces, which may undergo considerable rotation during loading [4].

1.5 IMPLICATIONS OF GEOMETRIC NONLINEARITY FOR THE STATIC BEHAVIOR

The unstressed and stressed geometry of cable structures differ, significantly, due to large displacements, when external loads are applied. Cable's equilibrium under external load is implemented at stressed geometry and, as a consequence, equations of cable structures must refer to the stressed and not to the unstressed geometry. However, the stressed geometry cannot be defined in advance. So, static analysis of such structures involves loops in order to find the final state. The equilibrium path is a curve, in contrast to the linear figure of structures having small displacements, such as beams, as illustrated in Figure 1-15.

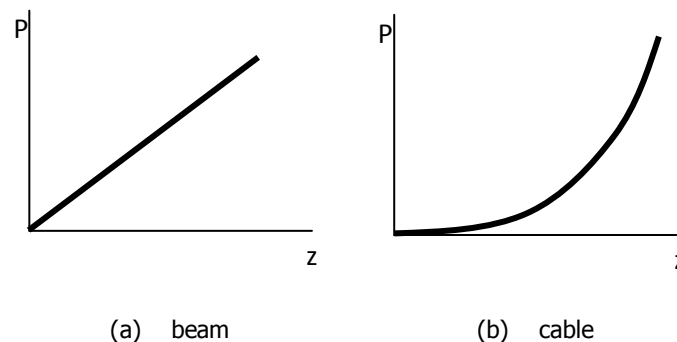


Figure 1-15: Equilibrium path of a beam and a cable

The response is not linear and, therefore, superposition of results for different in-service loading conditions is not strictly valid and, if it is done, must be done carefully. Conventional methods of static analysis have no implementation in cable structures. This particularity is known as geometric nonlinearity and is the main feature of the static response of tension structures.

Figure 1-16 indicates the error that appears in case that the geometric nonlinearity is neglected and the calculation of cable's response is based on the unstressed geometry and the initial stiffness matrix. Given an external load P , the response z_2 , based on the linear theory, can be significantly larger than the real one, which is z_1 . It is considered that cable's length is larger than the distance spanned and, so, the equilibrium path starts from a positive value of displacement [5].

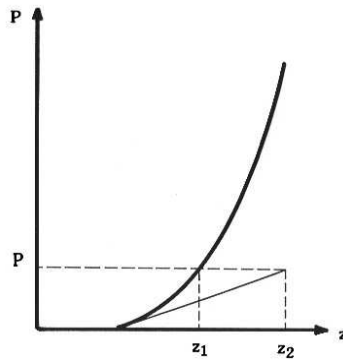


Figure 1-16: Implication of geometric nonlinearity into cable response

2 ANALYTICAL SOLUTIONS FOR THE STATIC BEHAVIOR OF SIMPLE CABLES

2.1 INTRODUCTION

In this chapter, simple suspended cables are studied. Their geometry and loading retain that the unstressed geometry, the loads and the stressed geometry belong to one single plane. Analytical solutions of the problem provide qualitative features of the response of cable structures, through diagrams, comparisons etc. Such solutions are used leading to figures that show the relationship between important parameters, dimensional or not.

The self weight of the cable is neglected, comparing it to the external pre-tension and live loads. The reader can include cable self weight into his analysis using the analytical solutions of Paragraphs 2.3.3 and 2.3.4, as it is a uniformly distributed load along its arc length. Figures of Chapter 2 present the position of the examined point using the horizontal u and the vertical v deflection, which are defined as:

$$u = x - x^* \quad (2-1)$$

$$v = z - z^* \quad (2-2)$$

where,

x, z are the coordinates of the examined point after the application of the load P, p or q , in m

x^*, z^* are the coordinates of the point from which cable tension, due to the load P, p or q , occurs, in m.

regardless if it is defined with x - and z - coordinates in analytical equations. This happens as the comparison between cables, varying in properties, becomes more comprehensive because curves have as common starting point the start of the axes. For instance, cables differing in inclination, but with the same loading condition, conclude to z -coordinates of the examined point within a wide range of values.

2.2 SIMPLE CABLES UNDER CONCENTRATED LOADS

2.2.1 Horizontal cable under concentrated load in the middle

A concentrated load P is applied at middle span of a horizontal cable, which stretches, until an equilibrium position is obtained with z -coordinate at the midpoint, as shown in Figure 2-1. At point i , the reaction N_i , the horizontal reaction H_i and the vertical reaction V_i are developed, where $i = A, B$. The static response of the cable is described by using three different equations: (a) the equation of static equilibrium, (b) the geometric compatibility equation, (c) the material constitutive equation. The cable spans the distance $S_{AB} = L$, where S_{AB} is the distance between points A and B.

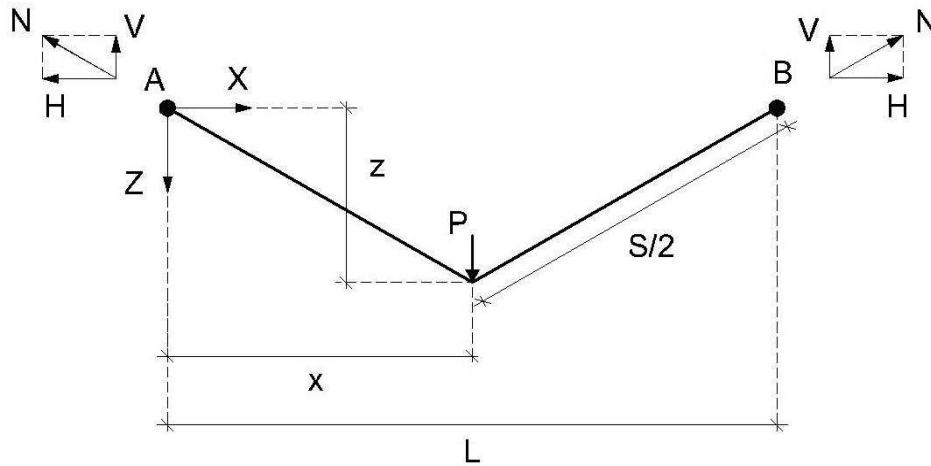


Figure 2-1: Equilibrium position of a cable under concentrated load at middle span

Due to the symmetric geometry and loading, there is no horizontal deflection u . The vertical deflection v of the cable, due to the concentrated load P , is significant and cannot be neglected. This is the reason why the equations of static equilibrium must refer to the stressed geometry and not to the unstressed geometry. This characteristic of cable structures is called geometric nonlinearity and leads to different static analysis methods comparing to the conventional structures.

The vertical component V of axial force N is:

$$V = \frac{P}{2} \quad (2-3)$$

$$\text{where } V_A = V_B = V. \quad (2-4)$$

The sum of moments about the equilibrium point gives:

$$Hz = V \frac{L}{2} \Rightarrow H = \frac{P}{4} \left(\frac{L}{z} \right) \quad (2-5)$$

$$\text{where } H_A = H_B = H, \text{ from the equilibrium of horizontal forces.} \quad (2-6)$$

The axial force N of the cable is:

$$N = \sqrt{V^2 + H^2} = \frac{P}{2} \sqrt{1 + \frac{L^2}{4z^2}} \quad (2-7)$$

$$\text{where } N_A = N_B = N. \quad (2-8)$$

Eq. (2-7) contains an unknown parameter, the z -coordinate at the midpoint. Additional equations are needed in order to define the solution, in contrast with conventional structures which are solved using only the equations of equilibrium. So, assuming the material as linearly elastic and using the material constitutive equation, Hooke's law gives:

$$\sigma = E\varepsilon \Rightarrow \frac{N}{A} = E \frac{\Delta S}{S_0} \Rightarrow N = EA \frac{S - S_0}{S_0} \quad (2-9)$$

where,

A is the cross-section of the cable, in m^2
 E is the modulus of elasticity of the cable, in GPa
 S is the stressed length of the cable, in m.

The geometric compatibility equation gives:

$$\frac{S}{2} = \sqrt{\left(\frac{L}{2}\right)^2 + z^2} \Rightarrow S = 2z \sqrt{1 + \frac{L^2}{4z^2}} \quad (2-10)$$

Combining Eqs. (2-7), (2-9) and (2-10) and eliminating N and S , the following equation occurs:

$$\frac{P}{2} \sqrt{1 + \frac{L^2}{4z^2}} = EA \left(\frac{2z}{S_0} \sqrt{1 + \frac{L^2}{4z^2}} - 1 \right) \Rightarrow P = 2EA \left(\frac{2}{S_0} - \frac{1}{\sqrt{z^2 + \frac{L^2}{4}}} \right) z \quad (2-11)$$

Eq. (2-11) relates the external concentrated load P with the z -coordinate the midpoint. This is a nonlinear relationship. Contrary to cable structures, conventional structures provide a linear relationship between P and z , the response is proportional to the load, and the superposition principle is valid. Obviously, in cable structures this principle cannot be used. Defining:

$$z' = \frac{z}{L}, \quad S'_0 = \frac{S_0}{L}, \quad P' = \frac{P}{EA} \quad (2-12)$$

Eq. (2-11) turns into non-dimensional:

$$(2-11) \Rightarrow P' = 2z' \left[\frac{2}{S'_0} - \frac{1}{\sqrt{(z')^2 + \frac{1}{4}}} \right] \quad (2-13)$$

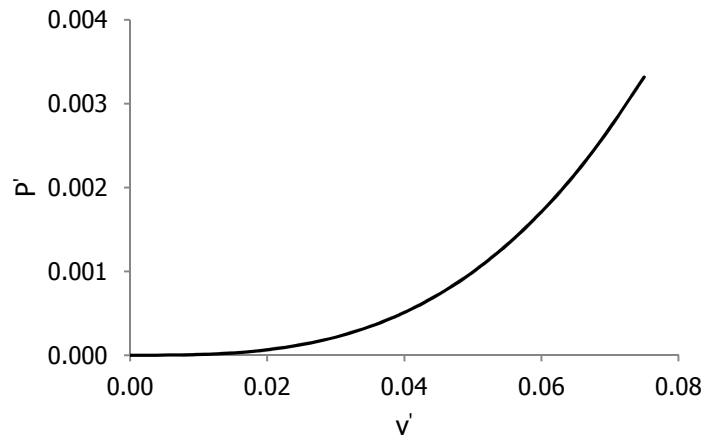


Figure 2-2: Applied load P' as function of vertical deflection v' , in case that $S_0 = S_{AB}$

Figure 2-2 shows the equilibrium path of the cable. Here, $z^* = 0$ as $S_0 = S_{AB}$ and, so, $v = z$ or $v' = z'$, where $v' = \frac{v}{L}$ is the vertical deflection in non-dimensional form. Easy to notice that diagram are not line but a curve. The slope, which indicates cable's stiffness, increases as load P' increases. So, the cable becomes stiffer as the load and the corresponding deflection increase. Giving a qualitative explanation, larger deflection means the increment of the slope of cable's segments left and right from the applied load, leading to the increment of the vertical component of cable's axial force, the component that balances the external load.

Replacing Eq. (2-11) into Eq. (2-7), the axial force N of the cable is calculated:

$$N = EA \left(\frac{2z}{S_0} \sqrt{1 + \frac{L^2}{4z^2}} - 1 \right) \quad (2-14)$$

So, not only the concentrated load P but also the axial force N of the cable, which means the total response, is described by nonlinear equations. Defining:

$$N' = \frac{N}{EA} \quad (2-15)$$

the previous equation turns into non-dimensional, as below:

$$(2-14) \Rightarrow N' = \frac{2z'}{S_0'} \sqrt{1 + \frac{1}{4(z')^2}} - 1 \quad (2-16)$$

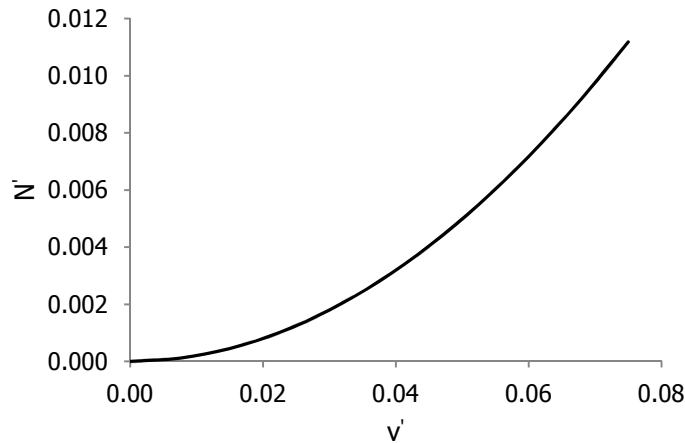


Figure 2-3: Cable's axial force N' as function of vertical deflection v' , in case that $S_0 = S_{AB}$

Figure 2-3 describes the cable's axial force N' as function of vertical deflection v' . Here, $z^* = 0$ as $S_0 = S_{AB}$ and, so, $v = z$ or $v' = z'$. The slope of the curve increases as the vertical deflection v' , in other words the concentrated load P , increases due to the geometric nonlinearity.

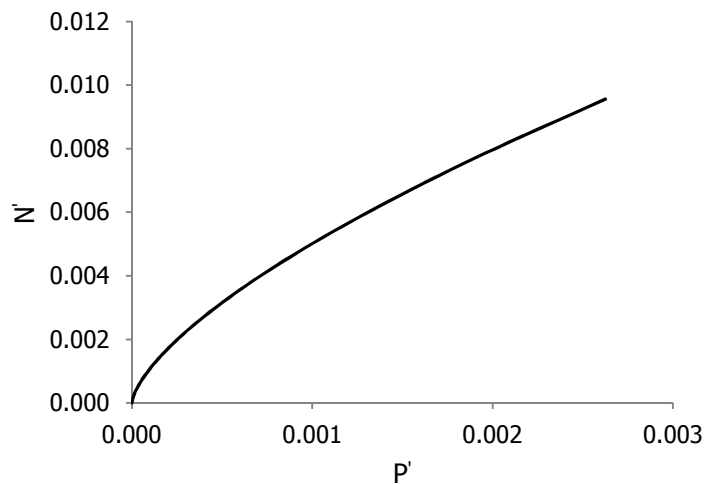


Figure 2-4: Cable's axial force N' as function of applied load P' , in case that $S_0 = S_{AB}$

The slope of Figure 2-4 decreases as applied load P increases, indicating that the rate of axial force's increment decreases as the load increases. This observation verifies that cable structures respond to the increment of external loads by mainly adapting their geometry and less by changing their developed tensions.

The stiffness K of the cable is tangential to the diagram P - z . So:

$$K = \frac{\partial P}{\partial z} = 2EA \left[\frac{2}{S_0} - \left(1 + \frac{L^2}{4z^2} \right)^{-3/2} \left(-\frac{1}{2} \right) \frac{L^2}{4} \left(-\frac{2}{z^3} \right) \right] \Rightarrow$$

$$\Rightarrow K = \frac{4EA}{L} \left\{ \frac{L}{S_0} - \frac{\left(\frac{L}{2z} \right)^3}{\left[1 + \left(\frac{L}{2z} \right)^2 \right]^{3/2}} \right\} \quad (2-17)$$

Defining:

$$K' = \frac{K}{\frac{EA}{L}} \quad (2-18)$$

Eq. (2-17) turns into non-dimensional, as:

$$(2-17) \Rightarrow K' = 4 \left\{ \frac{1}{S_0'} - \frac{\left(\frac{1}{2z'} \right)^3}{\left[1 + \left(\frac{1}{2z'} \right)^2 \right]^{3/2}} \right\} \quad (2-19)$$

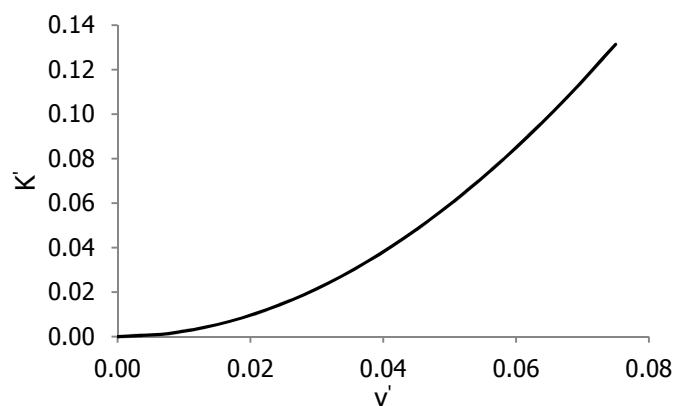


Figure 2-5: Cable's stiffness K' as function of vertical deflection v' , in case that $S_0 = S_{AB}$

Figure 2-5 describes the cable's stiffness K' as function of vertical deflection v' . Here, $z^* = 0$ as $S_0 = S_{AB}$ and, so, $v = z$ or $v' = z'$. The stiffness K' increases as the vertical deflection v' , in other words the concentrated load P , increases due to the geometric nonlinearity. The increase of stiffness K' is presented, in Figures 2-2 and 2-3, with the increase of the slope of the curves. The abrupt decrease of the slope in Figure 2-4, or correspondingly the abrupt increase of the slope in Figures 2-2 and 2-3, near the start of the axes is consistent with the abrupt increase of the slope in Figure 2-5. This observation indicates that geometric nonlinearity is evident, mainly, for small values of concentrated load P and for larger values of P the response tends to be linear. Pre-tensioned cables make advantage of this incident responding, almost, linear with large values of stiffness K .

$$(2-5) \Rightarrow H' = \frac{P'}{4z'} \quad (2-20)$$

$$\text{where } H' = \frac{H}{EA} \quad (2-21)$$

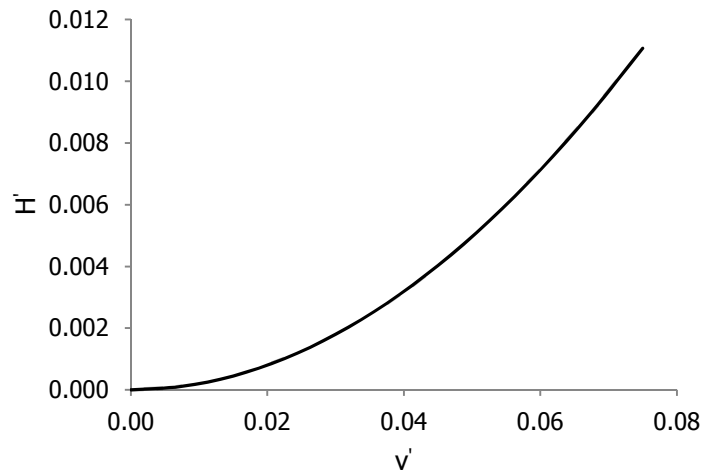


Figure 2-6: Horizontal component H' of the axial force as function of vertical deflection v' , in case that $S_0 = S_{AB}$

Figure 2-6 describes the horizontal component H' of the axial force as function of vertical deflection v' . Here, $z^* = 0$ as $S_0 = S_{AB}$ and, so, $v = z$ or $v' = z'$. The slope of the curve increases as the vertical deflection v' , in other words the concentrated load P , increases due to the geometric nonlinearity.

Next paragraph generalizes the cable geometry and loading conditions. The implementation of the cable model, as presented in Paragraph 2.2.1, into the general equations leads to the same results.

2.2.2 Inclined cable under concentrated load at arbitrary position

A simple inclined cable is subjected to a concentrated load P at arbitrary position, as illustrated in Figure 2-7. The cable spans the distance S_{AB} , which is the distance between points A and B. There is not only vertical deflection v but also horizontal u from the application point, determined by the physical path of response. After load application, the redefined application point can lie over or below the horizontal level of support B. Here, both cases are examined. If the application point stands at the level of support B, the mentioned alternative procedures give same results. Notice that diagrams are designed through ADINA models, for case A, and SAP model, for case B, (contained in the accompanied CD, commented in the list of numerical models with 'analytical'), due to the complexity of the 2-degree polynomial solution. ADINA cable models contain all the appropriate information, regarding loading conditions and cable properties. Paragraph 3.2.3 verifies the identification between analytical solution and numerical models.

A) Application point lies over the horizontal level of support B

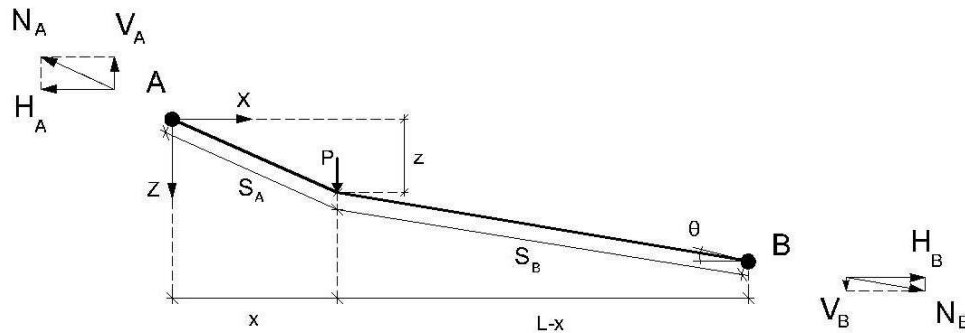


Figure 2-7: Simple inclined cable under concentrated load at arbitrary position, for case A

The equilibrium of horizontal forces leads to:

$$H = H_A = H_B \quad (2-22)$$

Vertical reactions are defined from the equations of static equilibrium:

$$\Sigma M_A = 0 \Rightarrow V_B = H \tan \theta - \frac{Px}{L} \quad (2-23)$$

$$\Sigma M_B = 0 \Rightarrow V_A = H \tan \theta + \frac{P(L-x)}{L} \quad (2-24)$$

The proportionality of the sides of the two pairs of similar triangles, as shown below:

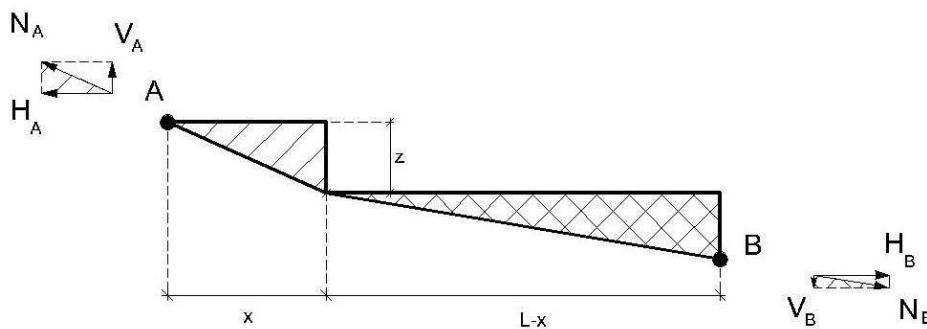


Figure 2-8: Similar triangles in stressed situation, for case A

gives for left pair:

$$\frac{H}{V_A} = \frac{x}{z} \Rightarrow H = V_A \frac{x}{z} \quad (2-25)$$

and for right pair:

$$\frac{H}{V_B} = \frac{L-x}{\tan \theta L - z} \Rightarrow H = V_B \frac{L-x}{\tan \theta L - z} \quad (2-26)$$

The axial force and its vertical component of the cable segment, supported at point i , are equal to the corresponding reactions at point i , where $i = A, B$. So:

$$N_A = \sqrt{V_A^2 + H^2} = V_A \sqrt{1 + \left(\frac{x}{z}\right)^2} = \left[H \tan \theta + \frac{P(L-x)}{L} \right] \sqrt{1 + \left(\frac{x}{z}\right)^2} \quad (2-27)$$

$$N_B = \sqrt{V_B^2 + H^2} = V_B \sqrt{1 + \left(\frac{L-x}{\tan \theta L - z}\right)^2} = \left(H \tan \theta - \frac{Px}{L} \right) \sqrt{1 + \left(\frac{L-x}{\tan \theta L - z}\right)^2} \quad (2-28)$$

Assuming the material as linearly elastic and using the material constitutive equation, Hooke's law gives:

$$\begin{aligned} \sigma_i &= E \epsilon_i \Rightarrow \frac{N_i}{A} = E \frac{\Delta S_i}{S_{0i}} \Rightarrow \\ \Rightarrow N_i &= EA \frac{S_i - S_{0i}}{S_{0i}} \Rightarrow S_i = S_{0i} \left(1 + \frac{N_i}{EA} \right), \text{ where } i = A, B \end{aligned} \quad (2-29)$$

Using the geometric compatibility equation:

$$S_A = \sqrt{x^2 + z^2} = S_{0A} \left(1 + \frac{N_A}{EA} \right) \Rightarrow S_{0A} = \frac{\sqrt{x^2 + z^2}}{1 + \frac{N_A}{EA}} \quad (2-30)$$

$$S_B = \sqrt{(L-x)^2 + (\tan \theta L - z)^2} = S_{0B} \left(1 + \frac{N_B}{EA} \right) \Rightarrow S_{0B} = \frac{\sqrt{(L-x)^2 + (\tan \theta L - z)^2}}{1 + \frac{N_B}{EA}} \quad (2-31)$$

Adding Eqs. (2-30) and (2-31):

$$S_0 = S_{0A} + S_{0B} \quad (2-32)$$

Replacing N_A and N_B from Eqs. (2-27) and (2-28), correspondingly, the following equation occurs:

$$(2-32) \Rightarrow S_0 = \frac{z}{\frac{1}{\sqrt{\left(\frac{x}{z}\right)^2 + 1}} + \frac{1}{EA} \left[H \tan \theta + \frac{P(L-x)}{L} \right]} + \frac{\tan \theta L - z}{\frac{1}{\sqrt{\left(\frac{L-x}{\tan \theta L - z}\right)^2 + 1}} + \frac{1}{EA} \left(H \tan \theta - \frac{Px}{L} \right)} \quad (2-33)$$

This nonlinear equation describes the equilibrium path of the cable. For simplification reasons, the following non-dimensional parameters are considered:

$$x' = \frac{x}{L}, z' = \frac{z}{L}, \beta = \frac{L-x}{L} = 1-x', \gamma = \frac{\tan\theta L - z}{L} = \tan\theta - z',$$

$$P' = \frac{P}{EA}, H' = \frac{H}{EA}, S'_0 = \frac{S_0}{L}, \quad (2-34)$$

$$c_1 = \frac{1}{\sqrt{\left(\frac{x'}{z'}\right)^2 + 1}}, c_2 = \frac{1}{\sqrt{\left(\frac{\beta}{\gamma}\right)^2 + 1}}$$

So, Eq. (2-33) turns into the following simplified equation:

$$(2-33) \Rightarrow S'_0 = \frac{z'}{c_1 + H' \tan\theta + P' \beta} + \frac{\gamma}{c_2 + H' \tan\theta - P' x'} \quad (2-35)$$

Replacing V_A from Eq. (2-24) into (2-25), H can be defined as function of P , as shown below:

$$zH = xH \tan\theta + \frac{P(L-x)x}{L} \Rightarrow H = \left(\frac{1}{z-x \tan\theta} \right) \frac{P(L-x)x}{L} \quad (2-36)$$

Replacing Eq. (2-34) into (2-36):

$$(2-36) \Rightarrow z'H' = x'H' \tan\theta + x'\beta P' \Rightarrow H' = \frac{x'\beta P'}{z'-x' \tan\theta} \quad (2-37)$$

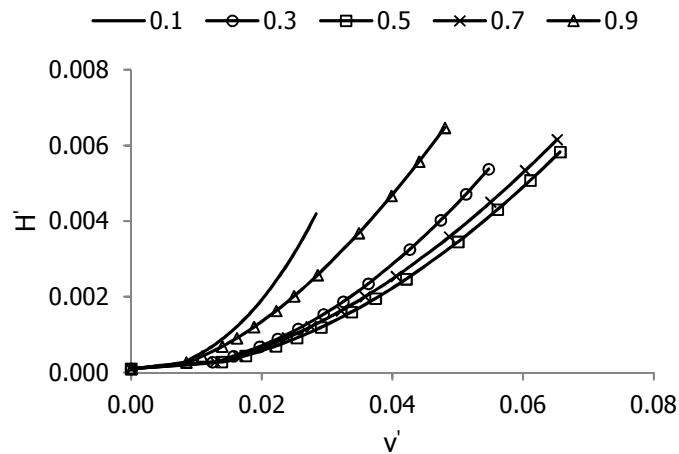


Figure 2-9: Horizontal component H' of the axial force as function of vertical deflection v' for different values of α , in case that $\theta = 45$ deg and $S_0 = S_{AB}$

Figure 2-9 describes the horizontal component H' of the axial force as function of vertical deflection v' for different values of α . The parameter α is defined as:

$$\alpha = \frac{x^*}{L} \quad (2-38)$$

The coordinates x^* , z^* are identical to the coordinates x_p , z_p , which are the coordinates of the starting application point of the concentrated load P , as defined in ADINA cable models. In a general cable model with $S_0 > S_{AB}$, $z^* \neq z_p$.

The combination of Eqs. (2-35) and (2-37) gives:

$$S_0' = \frac{z'}{c_1 + \frac{x'\beta P'}{z-x'\tan\theta} \tan\theta + P'\beta} + \frac{Y}{c_2 + \frac{x'\beta P'}{z-x'\tan\theta} \tan\theta - P'x'} \Rightarrow \quad (2-39)$$

$$\Rightarrow S_0' = \frac{z'}{c_1 + P'\Gamma} + \frac{Y}{c_2 + P'\Delta}$$

$$\text{where } \Gamma = \frac{x'\beta \tan\theta}{z-x'\tan\theta} + \beta \quad \text{and} \quad \Delta = \frac{x'\beta \tan\theta}{z-x'\tan\theta} - x' \quad (2-40)$$

P' can be expressed, transforming Eq. (2-39), into a form of a 2-degree polynomial equation. Elaboration of Eq. (2-39) leads to:

$$\Theta(P')^2 + \Lambda P' + \Xi = 0 \quad (2-41)$$

where,

$$\Theta = S_0' \Gamma \Delta \quad (2-42)$$

$$\Lambda = S_0' c_1 \Delta + S_0' c_2 \Gamma - z' \Delta - Y \Gamma \quad (2-43)$$

$$\Xi = S_0' c_1 c_2 - z' c_2 - Y c_1 \quad (2-44)$$

Now, the 2-degree polynomial equation indicates a relationship between P' , x' and z' , bearing in mind the geometry of the cable that defines the rest parameters.

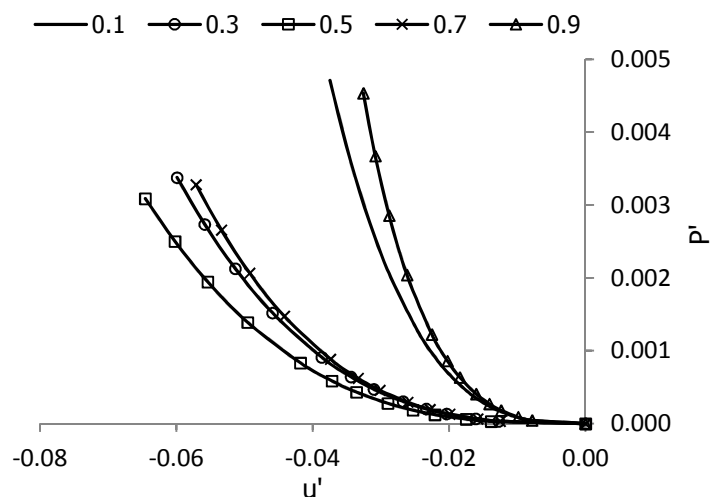


Figure 2-10: Applied load P' as function of horizontal deflection u' for different values of α , in case that $\theta = 45$ deg and $S_0 = S_{AB}$

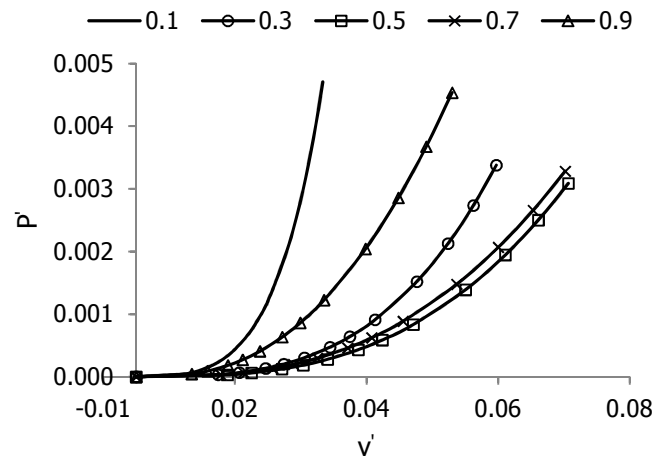


Figure 2-11: Applied load P' as function of vertical deflection v' for different values of α , in case that $\theta = 45$ deg and $S_0 = S_{AB}$

Figures 2-10 and 2-11 present the applied load P' as function of horizontal u' and vertical v' deflection for different values of α , where $u' = \frac{u}{L}$ is the horizontal deflection in non-dimensional form.

Cable's axial force can be easily determined, as function of P' , by replacing Eqs. (2-34) and (2-40) into Eqs. (2-27) and (2-28):

$$(2-27) \Rightarrow N'_A = \frac{P'\Gamma}{C_1} \quad (2-45)$$

$$\text{where } N'_A = \frac{N_A}{EA} \quad (2-46)$$

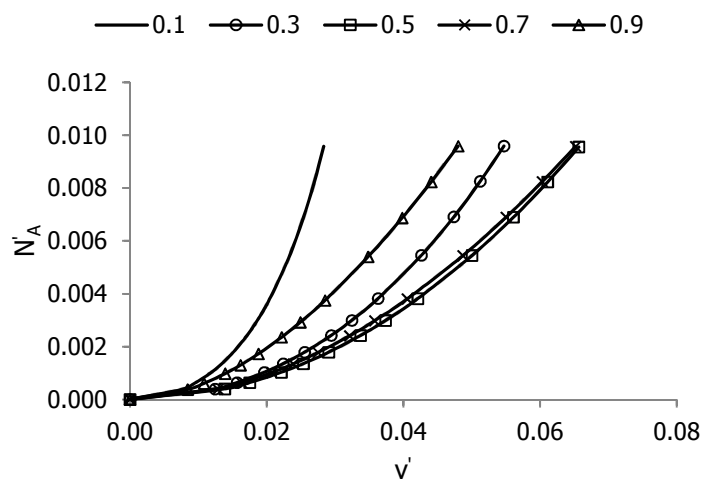


Figure 2-12: Cable's axial force N'_A as function of vertical deflection v' for different values of α , in case that $\theta = 45$ deg and $S_0 = S_{AB}$

Figures 2-12 presents the cable's axial force N'_A as function of vertical deflection v' for different values of α .

$$(2-28) \Rightarrow N'_B = \frac{P'\Delta}{c_2} \quad (2-47)$$

$$\text{where } N'_B = \frac{N_B}{EA} \quad (2-48)$$

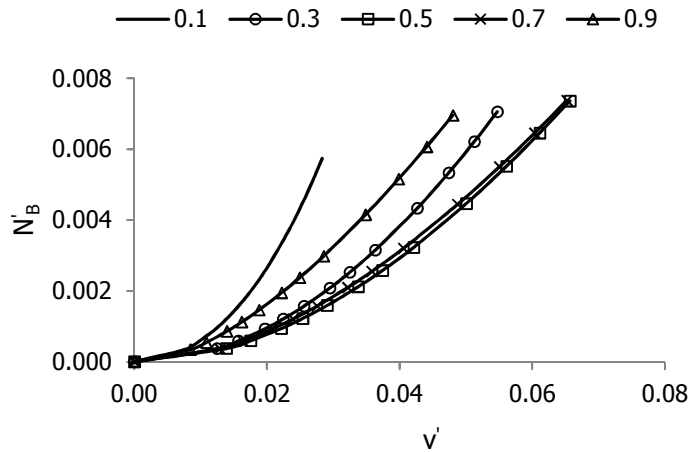


Figure 2-13: Cable's axial force N'_B as function of vertical deflection v' for different values of α , in case that $\theta = 45$ deg and $S_0 = S_{AB}$

Figures 2-13 presents the cable's axial force N'_B as function of vertical deflection v' for different values of α .

A common observation in Figures 2-9 to 2-13 is that, the nearer to the points of support the application point of the concentrated load P is the larger cable stiffness K is developed. In general, the shorter a cable is the smaller deflections can develop, increasing its stiffness K . As the concentrated load P reaches point A, the length of the left cable segment shortens provoking smaller positive vertical deflections v , increasing the stiffness in this kind of deflection. In case that the concentrated load P reaches point B, the length of the right cable segment shortens provoking smaller negative horizontal deflections u , increasing the stiffness in this kind of deflection. Comparing Figures 2-10 and 2-11, the stiffness in horizontal deflection u , as shown in Figure 2-10, is larger in case of $\alpha = 0.9$, as the concentrated load P reaches point B, and the stiffness in vertical deflection v , as shown in Figure 2-11, is larger in case of $\alpha = 0.1$, as the concentrated load P reaches point A. The response of the cable to a deflection is the development of the corresponding tension. So, a vertical (horizontal) deflection v (u) provokes increase of the vertical (horizontal) component V_i (H_i) of the axial force N_i , where $i = A, B$, increasing the stiffness in vertical (horizontal) deflections v (u). For a vertical concentrated load, large values of angle θ give large values of the vertical component V_i and small values of the horizontal H_i one, concluding to large stiffness in vertical deflections v . The total deflection is the vector sum of horizontal u and the vertical v one and, so, the increase of stiffness in one deflection leads to the increase of stiffness in the other due to stretch limitations. This is the reason why, in Figure 2-10, cable with $\alpha = 0.1$ seems to be stiffer in horizontal deflections u that the cable with $\alpha = 0.5$.

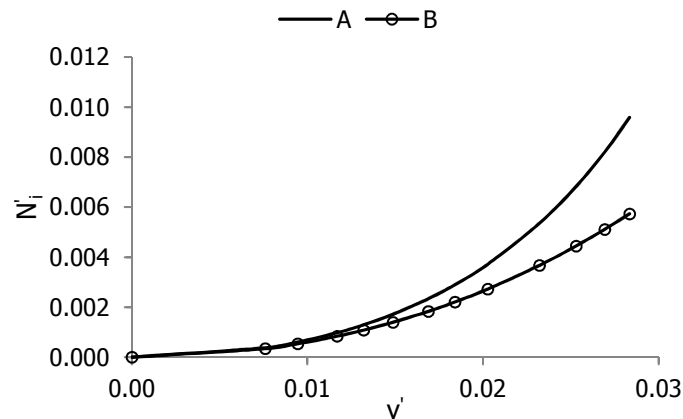


Figure 2-14: Cable's axial forces N_i as function of vertical deflection v' , in case that $\theta = 45$ deg, $S_0 = S_{AB}$ and $\alpha = 0.1$

Figure 2-14 describes cable's axial forces N_i as function of vertical deflection v' , in case that $\theta = 45$ deg, $S_0 = S_{AB}$ and $\alpha = 0.1$, where $i = A, B$. The left cable segment, with axial force N_A , is stiffer in vertical deflections v , as the concentrated load P is near point A.

Parametric diagrams of cables with different angle θ can be found in Paragraph 2.5.3- case 2.

B) Application point lies below the horizontal level of support B

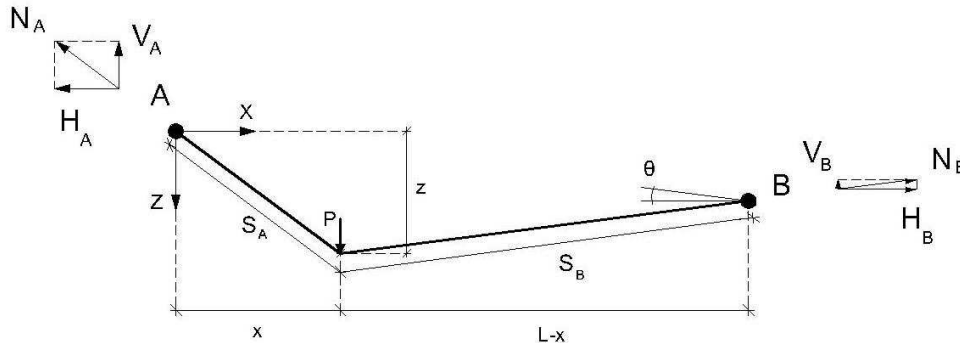


Figure 2-15: Simple inclined cable under concentrated load at arbitrary position, for case B

The procedure for case B differs from this of case A in the following equation of static equilibrium:

$$\Sigma M_A = 0 \Rightarrow V_B = \frac{Px}{L} - H \tan \theta \quad (2-49)$$

and in pairs of similar triangles, as:

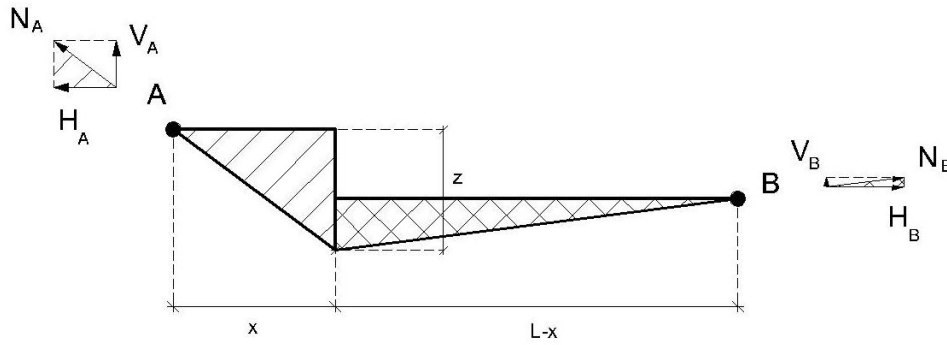


Figure 2-16: Similar triangles in stressed situation, for case B

So,

$$\frac{H}{V_B} = \frac{L-x}{z - \tan\theta L} \Rightarrow H = V_B \frac{L-x}{z - \tan\theta L} \quad (2-50)$$

Final equations, in case B, are presented below:

$$(2-41) \Rightarrow \Theta^\# (P')^2 + \Lambda^\# P' + \Xi^\# = 0 \quad (2-51)$$

where,

$$(2-42) \Rightarrow \Theta^\# = S_0' \Gamma^\# \Delta^\# \quad (2-52)$$

$$(2-43) \Rightarrow \Lambda^\# = S_0' c_1^\# \Delta^\# + S_0' c_2^\# \Gamma^\# - z' \Delta^\# - \gamma^\# \Gamma^\# \quad (2-53)$$

$$(2-44) \Rightarrow \Xi^\# = S_0' c_1^\# c_2^\# - z' c_2^\# - \gamma^\# c_1^\# \quad (2-54)$$

and

$$(2-34) \Rightarrow \beta^\# = 1 - x', \gamma^\# = z' - \tan\theta,$$

$$c_1^\# = \frac{1}{\sqrt{\left(\frac{x'}{z'}\right)^2 + 1}}, c_2^\# = \frac{1}{\sqrt{\left(\frac{\beta^\#}{\gamma^\#}\right)^2 + 1}} \quad (2-55)$$

$$(2-40) \Rightarrow \Gamma^\# = \frac{x' \beta^\# \tan\theta}{z' - x' \tan\theta} + \beta^\#, \Delta^\# = x' - \frac{x' \beta^\# \tan\theta}{z' - x' \tan\theta} \quad (2-56)$$

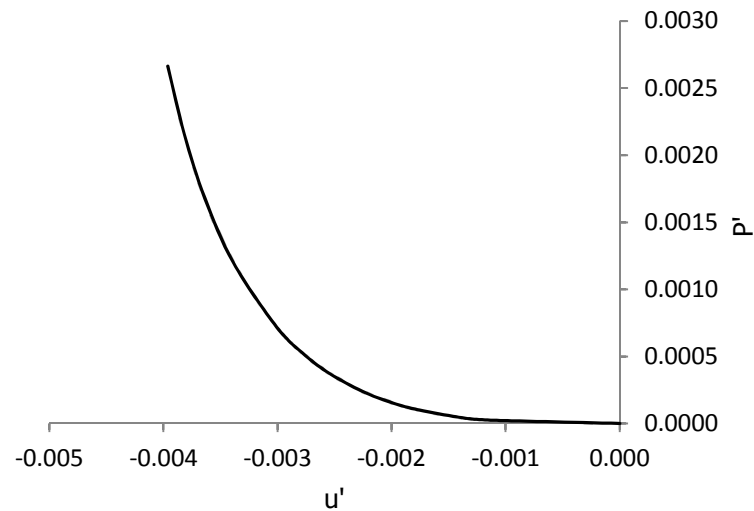


Figure 2-17: Applied load P' as function of horizontal deflection u' , in case that $\theta = 5$ deg, $S_0 = S_{AB}$ and $\alpha = 0.6$

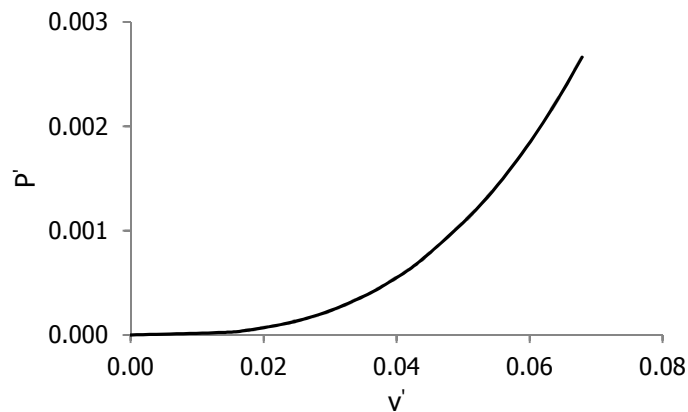


Figure 2-18: Applied load P' as function of vertical deflection v' , in case that $\theta = 5$ deg, $S_0 = S_{AB}$ and $\alpha = 0.6$

Figures 2-17 and 2-18 show the equilibrium path of the cable, in case that $\theta = 5$ deg, $S_0 = S_{AB}$ and $\alpha = 0.6$. The slope, which indicates cable's stiffness K , increases as load P increases, due to the geometric nonlinearity.

Axial forces N'_i , where $i = A, B$, are calculated from the following equations:

$$(2-45) \Rightarrow N'_A = \frac{P' \Gamma^\#}{c_1^\#} \quad (2-57)$$

$$(2-47) \Rightarrow N'_B = \frac{P' \Delta^\#}{c_2^\#} \quad (2-58)$$

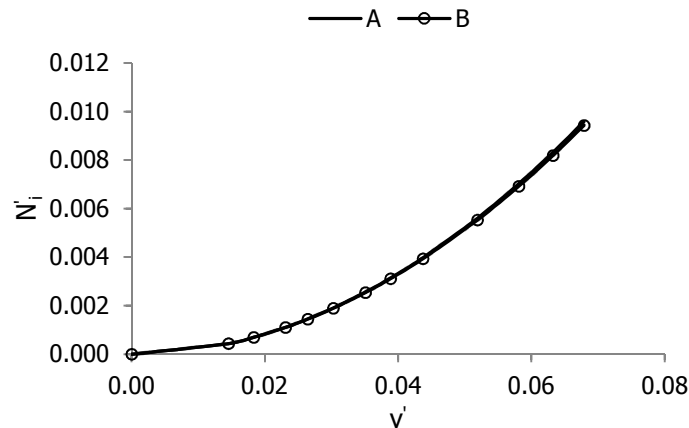


Figure 2-19: Cable's axial forces N_i as function of vertical deflection v_i , in case that $\theta = 5$ deg, $S_0 = S_{AB}$ and $\alpha = 0.6$

Figure 2-19 describes cable's axial forces N_i as function of vertical deflection v_i , in case that $\theta = 5$ deg, $S_0 = S_{AB}$ and $\alpha = 0.6$, where $i = A, B$. The slope of the curves increases as the vertical deflection v_i , in other words the concentrated load P , increases due to the geometric nonlinearity. The difference between two cable segments is slight, as the cable is almost horizontal ($\theta = 5$ deg) and the concentrated load P is applied near the midpoint ($\alpha = 0.6$), eliminating the differences in stiffness in horizontal u and vertical v deflections.

The horizontal component H' of the axial force is defined as:

$$(2-37) \Rightarrow H' = \frac{x' \beta^{\#} P'}{z - x \tan \theta} \quad (2-59)$$

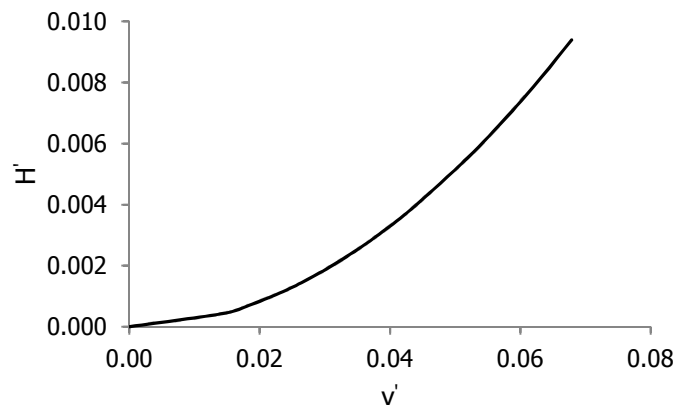


Figure 2-20: Horizontal component H' of the axial force as function of vertical deflection v_i , in case that $\theta = 5$ deg, $S_0 = S_{AB}$ and $\alpha = 0.6$

Figure 2-20 describes the horizontal component H' of the axial force as function of vertical deflection v_i , in case that $\theta = 5$ deg, $S_0 = S_{AB}$ and $\alpha = 0.6$. The slope of the curve increases as the vertical deflection v_i , in other words the concentrated load P , increases due to the geometric nonlinearity. The smooth angle in the curve is due to load steps in SAP model.

Unspecified parameters remain the same as in case A.

2.2.3 Horizontal cable under concentrated load at arbitrary position

A simple horizontal cable is subjected to a concentrated load at arbitrary position, as shown in Figure 2-21. The cable spans the distance S_{AB} , which is the distance between points A and B. The analytical equations derive from Paragraph 2.2.2 - case B, taking into account the new geometry. Notice that diagrams are designed through ADINA models (contained in the accompanied CD, commented in the list of numerical models with 'analytical'), due to the complexity of the 2-degree polynomial solution. ADINA cable models contain all the appropriate information, regarding loading conditions and cable properties. Paragraph 3.2.4 verifies the identification between analytical solution and numerical models.

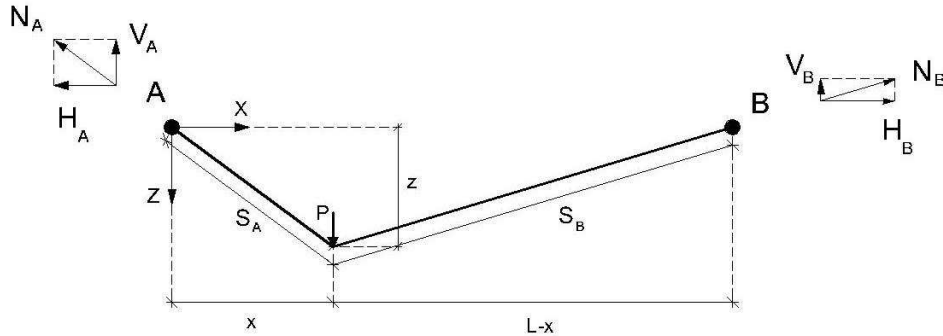


Figure 2-21: Simple horizontal cable under concentrated load at arbitrary position

Replacing $\theta = 0$ deg into the equations of Paragraph 2.2.2 – case B, the analytical solution for a horizontal cable under concentrated load at arbitrary position occurs.

$$(2-51) \Rightarrow \Theta^h (P')^2 + \Lambda^h P' + \Xi^h = 0 \quad (2-60)$$

where,

$$(2-52) \Rightarrow \Theta^h = S'_0 \Gamma^h \Delta^h \quad (2-61)$$

$$(2-53) \Rightarrow \Lambda^h = S'_0 c_1^h \Delta^h + S'_0 c_2^h \Gamma^h - z' \Delta^h - \gamma^h \Gamma^h \quad (2-62)$$

$$(2-54) \Rightarrow \Xi^h = S'_0 c_1^h c_2^h - z' c_2^h - \gamma^h c_1^h \quad (2-63)$$

and

$$(2-55) \Rightarrow \beta^h = 1 - x', \gamma^h = z',$$

$$c_1^h = \frac{1}{\sqrt{\left(\frac{x'}{z'}\right)^2 + 1}}, c_2^h = \frac{1}{\sqrt{\left(\frac{\beta^h}{\gamma^h}\right)^2 + 1}} \quad (2-64)$$

$$(2-56) \Rightarrow \Gamma^h = \beta^h, \Delta^h = x' \quad (2-65)$$

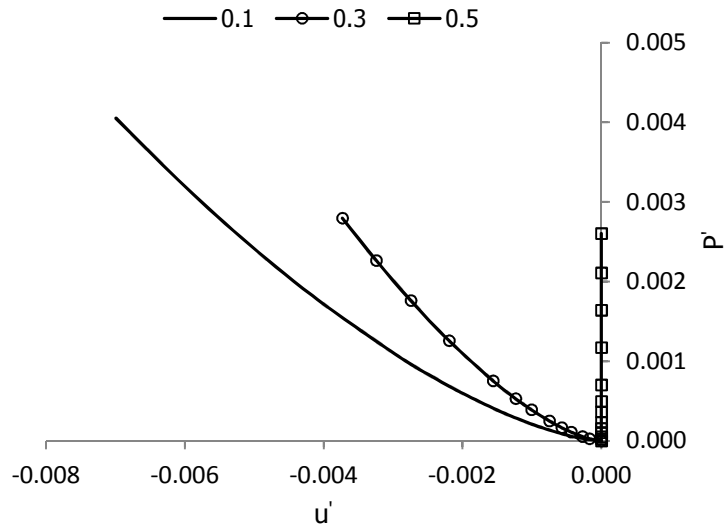


Figure 2-22: Applied load P' as function of horizontal deflection u' for different values of α , in case that $S_0 = S_{AB}$

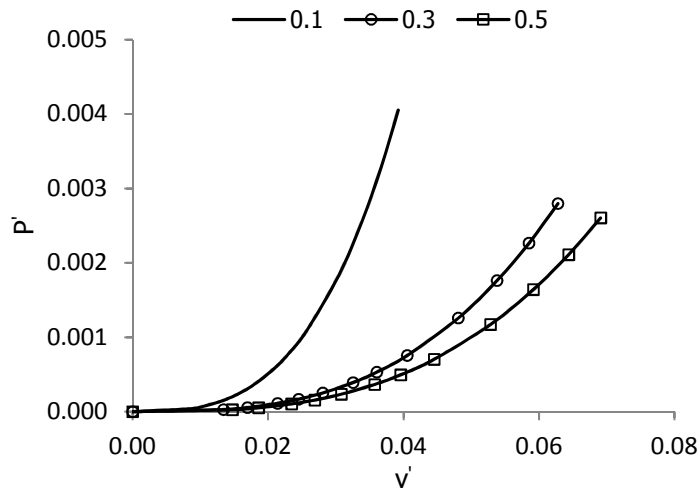


Figure 2-23: Applied load P' as function of vertical deflection v' for different values of α , in case that $S_0 = S_{AB}$

Figures 2-22 and 2-23 present the applied load P' as function of horizontal u' and vertical v' deflection, correspondingly, for different values of α . Here, $z^* = 0$ as $S_0 = S_{AB}$ and, so, $v = z$ or $v' = z'$.

Axial forces N'_i , where $i = A, B$, are calculated from the following equations:

$$(2-57) \Rightarrow N'_A = \frac{P' \Gamma^h}{c_1^h} \tag{2-66}$$

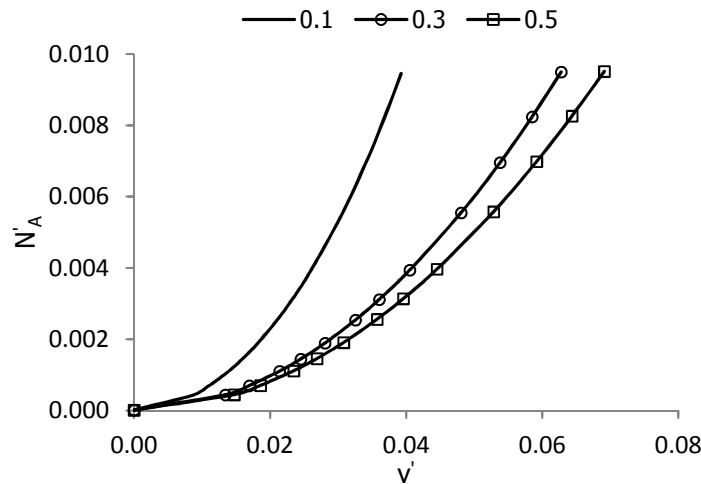


Figure 2-24: Cable's axial force N'_A as function of vertical deflection v' for different values of α , in case that $S_0 = S_{AB}$

Figure 2-24 presents the cable's axial force N'_A as function of vertical deflection v' for different values of α . Here, $z^* = 0$ as $S_0 = S_{AB}$ and, so, $v = z$ or $v' = z'$. The smooth angle, in case that $\alpha = 0.1$, is due to load steps in ADINA models.

$$(2-58) \Rightarrow N'_B = \frac{P' \Delta^h}{c_2^h} \quad (2-67)$$

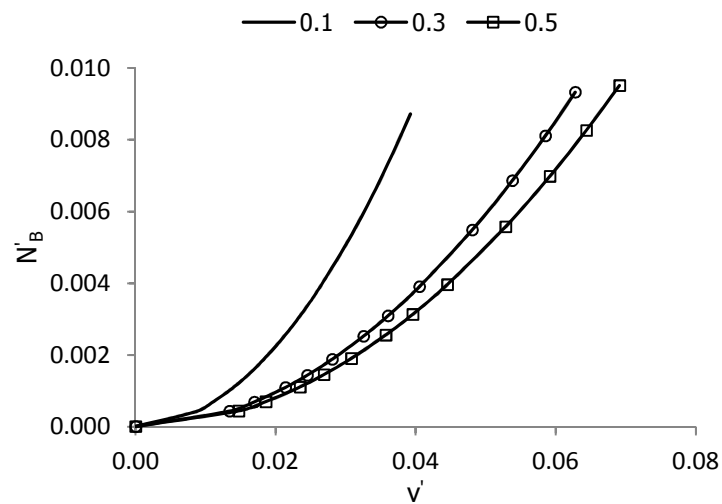


Figure 2-25: Cable's axial force N'_B as function of vertical deflection v' for different values of α , in case that $S_0 = S_{AB}$

Figure 2-25 presents the cable's axial force N'_B as function of vertical deflection v' for different values of α . Here, $z^* = 0$ as $S_0 = S_{AB}$ and, so, $v = z$ or $v' = z'$. The smooth angle, in case that $\alpha = 0.1$, is due to load steps in ADINA models.

A common observation in Figures 2-23 to 2-25 is that, the nearer to the point of support the application point of the concentrated load P is the larger cable stiffness K in vertical deflection v is developed. In the other hand, according to Figure 2-22, the farther from the point of support the application point of the concentrated load P is the larger cable stiffness K in horizontal deflection u is developed. In general, the shorter a cable is the smaller deflections can develop, increasing its stiffness K . As the concentrated load P reaches point A, the length of the left cable segment shortens provoking smaller positive vertical deflections v , increasing the stiffness in this kind of deflection. In case that the concentrated load P reaches the midpoint, the length of the right cable segment shortens provoking smaller negative horizontal deflections u , increasing the stiffness in this kind of deflection. Comparing Figures 2-22 and 2-23, the stiffness in horizontal deflection u , as shown in Figure 2-22, is larger in case of $\alpha = 0.3$, as the concentrated load P reaches the midpoint, and the stiffness in vertical deflection v , as shown in Figure 2-23, is larger in case of $\alpha = 0.1$, as the concentrated load P reaches point A. For $\alpha = 0.5$ there is no horizontal deflection u due to the geometry cable symmetry. Here, $\theta = 0$ deg and the development of stiffness in one kind of deflection is independent from the stiffness in the other deflection.

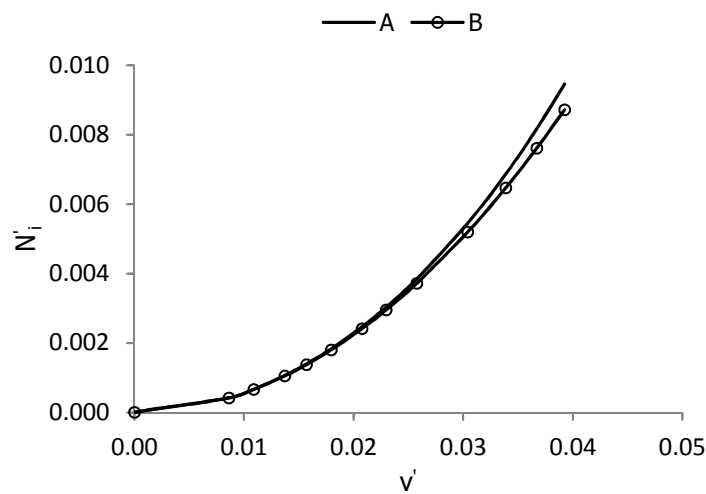


Figure 2-26: Cable's axial forces N'_i as function of vertical deflection v' , in case that $S_0 = S_{AB}$ and $\alpha = 0.1$

Figure 2-26 describes cable's axial forces N'_i as function of vertical deflection v' , in case that $S_0 = S_{AB}$ and $\alpha = 0.1$, where $i = A, B$. Here, $z^* = 0$ as $S_0 = S_{AB}$ and, so, $v = z$ or $v' = z'$. The slope of the curves increases as the vertical deflection v' , in other words the concentrated load P , increases due to the geometric nonlinearity. There is difference between two cable segments, as the concentrated load P is applied near to the point A ($\alpha = 0.1$), increasing the stiffness in vertical v deflections of the left cable segment. The smooth angle is due to load steps in ADINA models.

The horizontal component H' of the axial force is defined as:

$$(2-59) \Rightarrow H' = \frac{x' \beta^h P'}{z'} \quad (2-68)$$

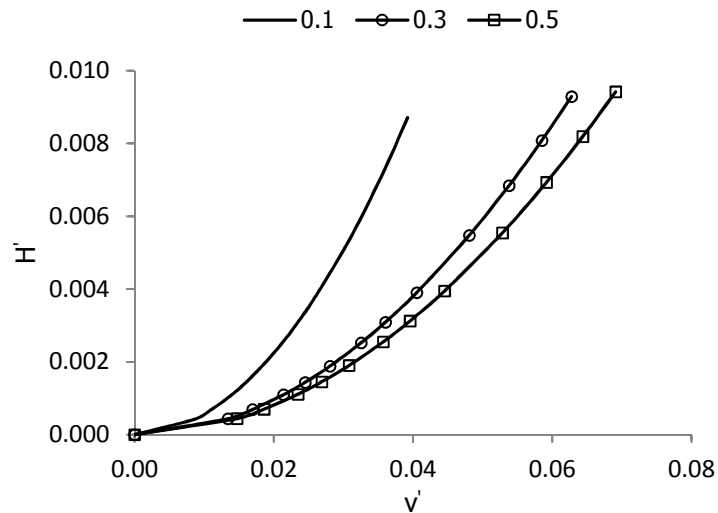


Figure 2-27: Horizontal component H' of the axial force as function of vertical deflection v' for different values of α , in case that $S_0 = S_{AB}$

Figure 2-27 describes the horizontal component H' of the axial force as function of vertical deflection v' for different values of α , following the reasoning of Figures 2-23 to 2-25. Here, $z^* = 0$ as $S_0 = S_{AB}$ and, so, $v = z$ or $v' = z'$.

The smooth angle in the figures of Paragraph 2.2.3 is caused by the load steps in ADINA models.

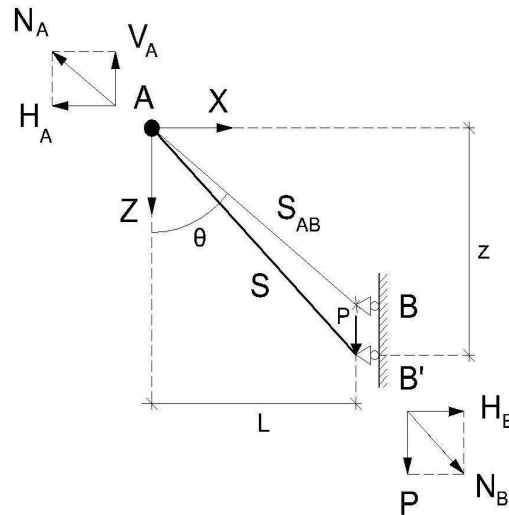
2.2.4 Inclined cable under imposed end displacement

2.2.4.1 Response of an inclined cable under imposed end displacement

In this paragraph, two kinds of imposed end displacement are presented, the vertical v and horizontal u . Vertical imposed end displacements v can be detected at the deck of a cable-braced bridge while a horizontal imposed end displacement u can occur at a radio mast, for instance due to a seismic load. The analytical solution can be derived considering the half of a horizontal cable under concentrated load in the middle - Paragraph 2.2.1.

A) Vertical imposed end displacement v

A simple inclined cable, with initial unstressed length S_0 , is subjected to a vertical imposed end displacement v by the application of a concentrated load P , as shown in Figure 2-28.


 Figure 2-28: Simple inclined cable under vertical imposed end displacement v

Replacing the following parameters for the half cable:

$$\frac{P}{2} \rightarrow P, \quad \frac{L}{2} \rightarrow L, \quad \frac{S_0}{2} \rightarrow S_0$$

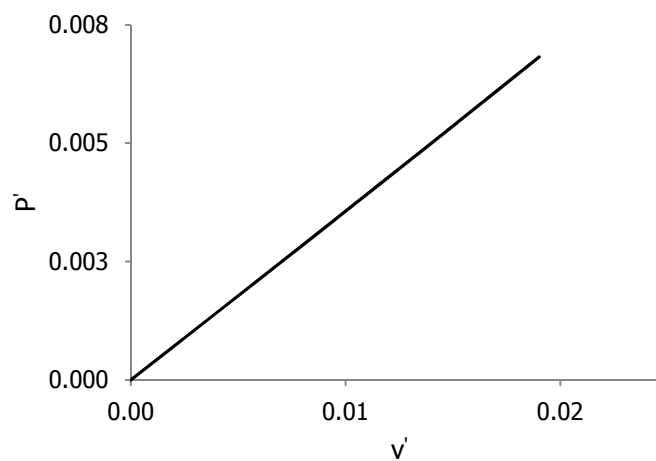
equations for a vertical imposed end displacement v are acquired.

The concentrated load P as function of the z -coordinate of the equilibrium point is defined as:

$$(2-11) \Rightarrow P = EA \left(\frac{1}{S_0} - \frac{1}{\sqrt{z^2 + L^2}} \right) z \quad (2-69)$$

Using the replacements of Eq. (2-12), the non-dimensional form of Eq. (2-69) occurs:

$$(2-69) \Rightarrow P' = \frac{z'}{S_0} - \frac{1}{\sqrt{1 + \left(\frac{1}{z'}\right)^2}} \quad (2-70)$$


 Figure 2-29: Applied load P' as function of vertical deflection v' , in case that $S_0 = S_{AB}$ and $\theta = 30$ deg

Figures 2-29 presents the applied load P' as function of vertical v' deflection, in case that $S_0 = S_{AB}$ and $\theta = 30$ deg. The response is almost linear, as the geometric nonlinearity is mild.

The axial force N is expressed as function of the z -coordinate of the equilibrium point as:

$$(2-14) \Rightarrow N = EA \left[\frac{z}{S_0} \sqrt{1 + \left(\frac{L}{z}\right)^2} - 1 \right] \quad (2-71)$$

Using the replacements of Eqs. (2-12) and (2-15), the non-dimensional form of Eq. (2-71) occurs:

$$(2-71) \Rightarrow N' = \frac{z'}{S_0'} \sqrt{1 + \left(\frac{1}{z'}\right)^2} - 1 \quad (2-72)$$

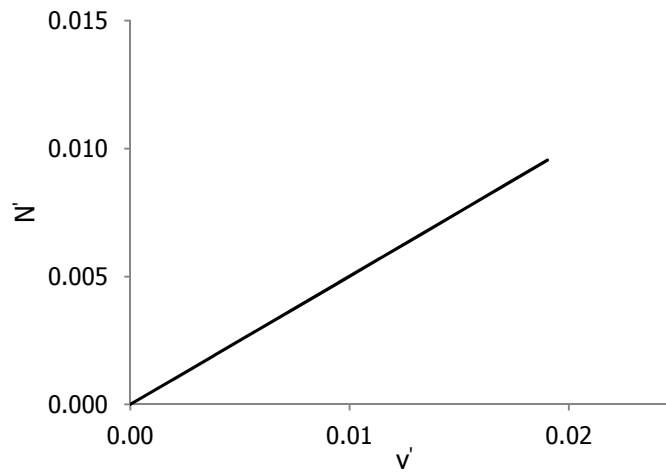


Figure 2-30: Cable's axial force N' as function of vertical deflection v' , in case that $S_0 = S_{AB}$ and $\theta = 30$ deg

Figures 2-30 presents the axial force N' as function of vertical v' deflection, in case that $S_0 = S_{AB}$ and $\theta = 30$ deg. The response is almost linear, as the geometric nonlinearity is mild.

The horizontal component H of the axial force as function of the z -coordinate of the equilibrium point is shown below:

$$(2-5) \Rightarrow H = \frac{PL}{z} \quad (2-73)$$

Using the replacements of Eqs. (2-12) and (2-21), the non-dimensional form of Eq. (2-73) occurs:

$$(2-73) \Rightarrow H' = \frac{P'}{z'} \quad (2-74)$$

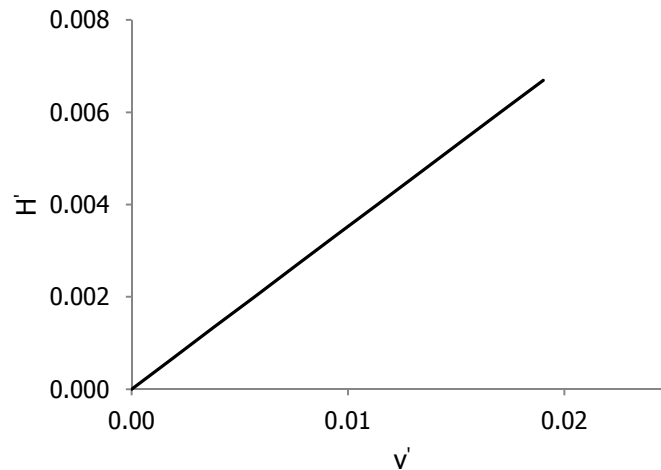


Figure 2-31: Horizontal component H' of the axial force as function of vertical deflection v' , in case that $S_0 = S_{AB}$ and $\theta = 30$ deg

Figure 2-31 presents the horizontal component H' of the axial force as function of vertical v' deflection, in case that $S_0 = S_{AB}$ and $\theta = 30$ deg. The response is almost linear, as the geometric nonlinearity is mild.

Figures 2-29 to 2-31 indicate an almost linear cable response. The vertical imposed end displacement v is the vector sum of a displacement perpendicular to the cable, which rotates it, and a displacement parallel to the cable, which elongates it in a linear way. This is the reason why the geometric nonlinearity is not intense.

Eqs. (2-69) to (2-74) are valid for $z \geq z^* = \sqrt{S_0^2 - L^2}$. In case that $S_0 \neq S_{AB}$, $z^* \neq \cos\theta S_{AB}$.

B) Horizontal imposed end displacement u

In this case, a simple inclined cable, with initial unstressed length S_0 , is subjected to a horizontal imposed end displacement u . The cause of this displacement is the concentrated load P , as shown in Figure 2-32.

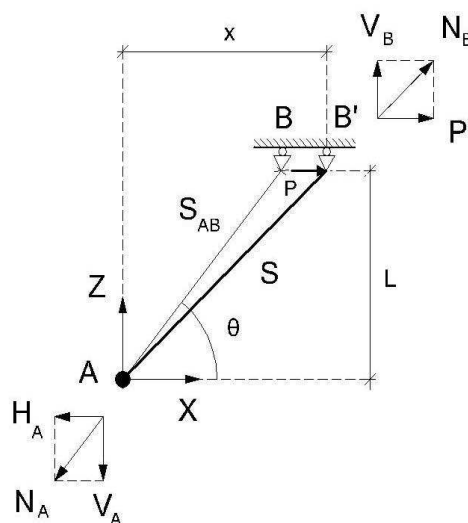


Figure 2-32: Simple inclined cable under horizontal imposed end displacement u

The corresponding cable equations, based on case A, are presented below.

For the concentrated load P:

$$(2-69) \Rightarrow P = EA \left(\frac{1}{S_0} - \frac{1}{\sqrt{x^2 + L^2}} \right) x \quad (2-75)$$

$$(2-70) \Rightarrow P' = \frac{x'}{S_0} - \frac{1}{\sqrt{1 + \left(\frac{1}{x'}\right)^2}} \quad (2-76)$$

For the axial force N:

$$(2-71) \Rightarrow N = EA \left[\frac{x}{S_0} \sqrt{1 + \left(\frac{L}{x}\right)^2} - 1 \right] \quad (2-77)$$

$$(2-72) \Rightarrow N' = \frac{x'}{S_0} \sqrt{1 + \left(\frac{1}{x'}\right)^2} - 1 \quad (2-78)$$

For the horizontal component H of the axial force:

$$(2-73) \Rightarrow H = \frac{PL}{x} \quad (2-79)$$

$$(2-74) \Rightarrow H' = \frac{P'}{x} \quad (2-80)$$

Eqs. (2-75) to (2-80) are valid for $x \geq x^* = \sqrt{S_0^2 - L^2}$. In case that $S_0 \neq S_{AB}$, $x^* \neq \cos\theta S_{AB}$.

Diagrams, and their qualitative explanation, are the same with case A.

2.2.4.2 Examination of a simple inclined cable as spring

An inclined cable under imposed end displacement can be simulated with an equivalent spring, simplifying the analysis procedure in case of a construction with many cables, for instance a cable-braced bridge. Generally, spring's reaction is subjected to Hooke's law, which states that:

$$F = K_S u \quad (2-81)$$

where,

u is the displacement of the spring's end from its equilibrium position, in m
F is the restoring force exerted by the spring on that end, in kN, and
K_S is a constant called the rate or spring constant, in kN/m.

The spring simulation concerns the calculation of the equivalent spring constant K_S of the cable. It is assumed that cable's material is linearly elastic. In case of an end displacement parallel to the cable ($\theta = 0$ deg), the material constitutive equation gives:

$$N = EA \frac{\Delta S}{S_0} = K_S \Delta S \quad (2-82)$$

where,

$$K_S = \frac{EA}{S_0} \quad \text{and} \quad \Delta S = u \text{ or } v. \quad (2-83)$$

K_S is the equivalent spring constant of the cable, in kN/m. The response is linear.

In case of an inclined cable imposed to a vertical/horizontal end displacement the analysis is more complicated. Eqs. (2-69) and (2-75) are equivalent to Eq. (2-81), as the restoring force F corresponds to the external load P and the displacement of spring's end u to the horizontal u or vertical v end displacement. Considering a vertical imposed end displacement v , the expansion of Eq. (2-69) in Taylor series around the point $z = z^*$ gives:

$$(2-69) \Rightarrow P = P(z) = EA \left\{ \frac{1}{S_0} + \frac{(z^*)^2}{[(z^*)^2 + L^2]^{3/2}} - \frac{1}{\sqrt{(z^*)^2 + L^2}} \right\} (z - z^*) +$$

$$+ \frac{EA}{2} \left\{ \frac{3z^*}{[(z^*)^2 + L^2]^{3/2}} - \frac{3(z^*)^3}{[(z^*)^2 + L^2]^{5/2}} \right\} (z - z^*)^2 + \dots \quad (2-84)$$

The first term of Eq. (2-84) represents the approximate equivalent linear spring, as:

$$(2-84) \Rightarrow P = K_S v \quad (2-85)$$

with equivalent spring constant K_S , in kN/m:

$$K_S = EA \left\{ \frac{1}{S_0} + \frac{(z^*)^2}{[(z^*)^2 + L^2]^{3/2}} - \frac{1}{\sqrt{(z^*)^2 + L^2}} \right\} = EA \left[\frac{S_0^2 - (\sin\theta S_{AB})^2}{S_0^3} \right] \quad (2-86)$$

where $L = \sin\theta S_{AB}$, from Figure 2-28.

For $\theta = 0$ deg, Eq. (2-86) turns into Eq. (2-83).

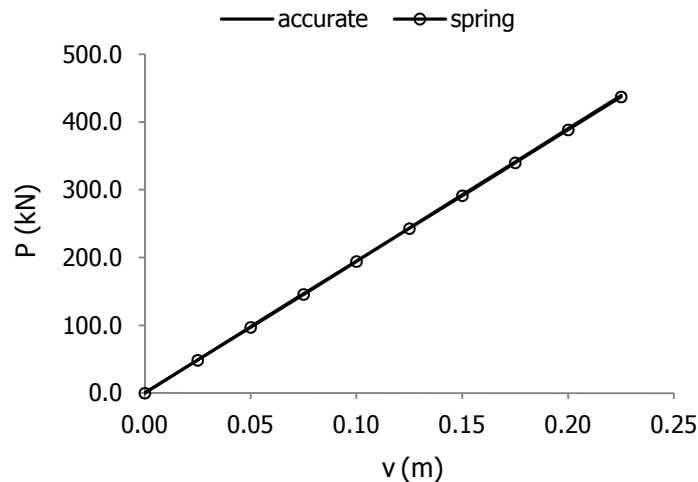


Figure 2-33: P – v curves considering the accurate solution and the equivalent linear spring equation, in case that $\theta = 30$ deg, $S_0 = S_{AB} = 20$ m, $E = 165$ GPa and $d = 20$ mm

Figure 2-33 compares the accurate solution, from Eq. (2-69), with the equivalent linear spring, from Eq. (2-85), in case that $\theta = 30$ deg, $S_0 = S_{AB} = 20$ m, $E = 165$ GPa and $d = 20$ mm. Curves are almost identical, proving the lack of geometric nonlinearity in diagrams of Paragraph 2.2.4.1 – case A.

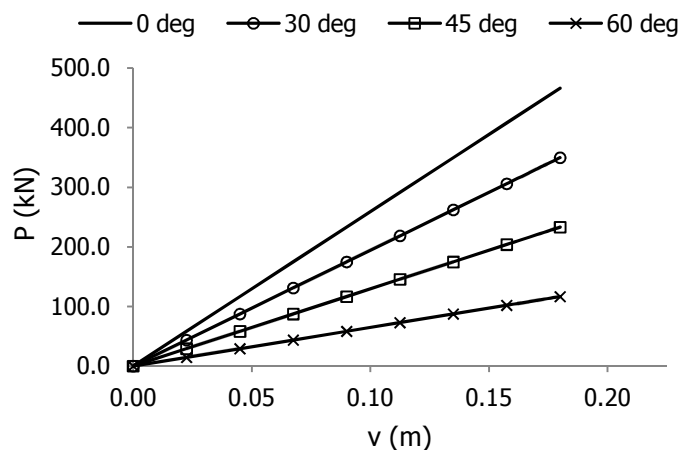


Figure 2-34: P – v curves of the equivalent spring for different values of angle θ , in case that $S_0 = S_{AB} = 20$ m, $E = 165$ GPa and $d = 20$ mm

Figure 2-34 presents the response of the equivalent spring for different values of angle θ , in case that $S_0 = S_{AB} = 20$ m, $E = 165$ GPa and $d = 20$ mm. The slope of curves is invariable and equals to the equivalent spring constant K_S . The smaller the angle θ is the stiffer the equivalent spring becomes. The response of the cable to a vertical imposed end displacement v is the development of the corresponding tension, which is the vertical component V of the axial force N , increasing the stiffness in this kind of deflections. A small value of angle θ means large value of the vertical component V and small value of the horizontal H one, concluding to large stiffness in vertical deflections v . This is the reason why cables with small inclination are stiffer in vertical imposed end displacements v .

In non-dimensional form:

$$(2-85) \Rightarrow P' = K_S' v' \quad (2-87)$$

where,

$$K'_S = \frac{(S'_0)^2 - 1}{(S'_0)^3} \quad (2-88)$$

Eqs. (2-84) to (2-88) are valid for $z \geq z^* = \sqrt{S_0^2 - L^2}$. Starting from Eq. (2-75), the equivalent spring constant K_S for horizontal displacement u occurs.

2.2.4.3 Implementations in cable structures

The analytical solutions of Paragraphs 2.2.4.1 and 2.2.4.2 can be implemented in cable structures. The static analysis of a cable-braced bridge, subjected to vertical end displacements v , is an example. In such structures, which contain long cables, self weight provokes curvature and cannot be omitted during the design procedure.

Figure 2-35 illustrates a model of a cable-braced bridge. The weight of a moving vehicle can be regarded as a concentrated load P_i applied on bridge's deck. This load provokes vertical displacement of the deck and, as a consequence, vertical end displacement v_i of cable i . Replacing cable i with a spring having equivalent spring constant K_{Si} , as shown in Figure 2-36, the vertical imposed end displacement v_i can be calculated. Rest cables are replaced with the corresponding springs.

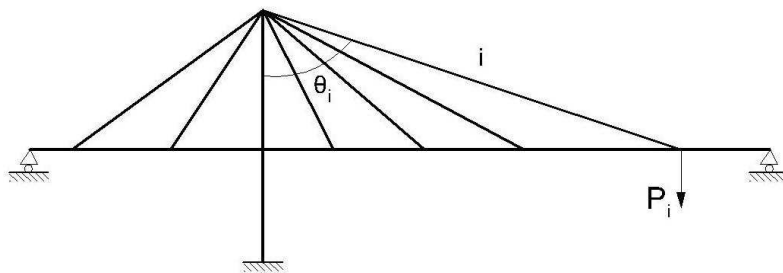


Figure 2-35: Cable-braced bridge subjected to moving concentrated load P_i

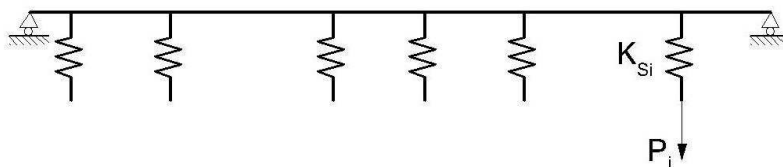


Figure 2-36: Equivalent model of a cable-braced bridge with linear springs

In a real model case, cables are pre-tensioned due to the weight of the deck. Initially unstressed cables are placed in order to deliver dead loads of the deck. These loads provoke permanent vertical imposed end displacements v , and corresponding pre-tensions, at cables. During the service phase, live loads add vertical imposed end displacements v and tensions to the pre-tensioned cables.

Regarding the horizontal imposed end displacements u , a radio mast is a cable structure subjected in such displacements. A detailed analysis, taking into account the pre-tension, is presented in Chapter 5.

2.3 SIMPLE CABLES UNDER UNIFORMLY DISTRIBUTED LOADS

2.3.1 Inclined cable under uniformly distributed load along its horizontal projection

A simple inclined cable, with initial unstressed length S_0 , spans the distance S_{AB} , where S_{AB} is the distance between points A and B. A uniformly distributed load p along cable's horizontal projection is applied, as shown in Figure 2-37. The horizontal deflection u of the cable is not taken into account in this analysis, for simplification reasons.

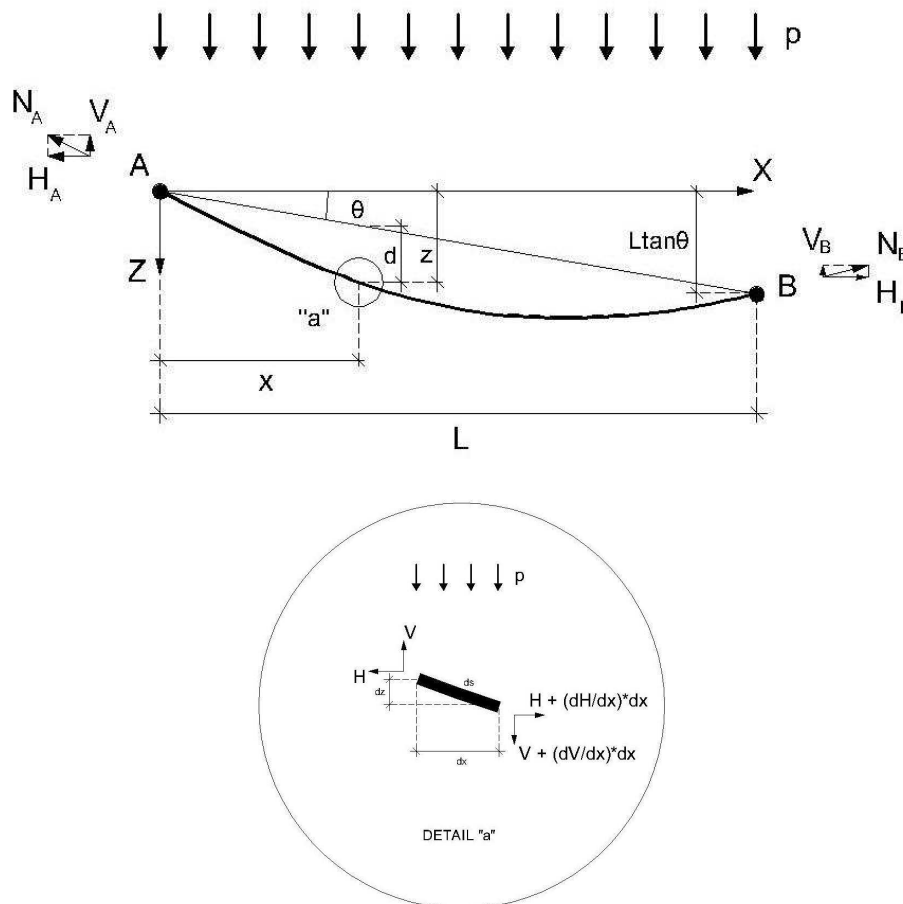


Figure 2 -37: Inclined cable under uniformly distributed load p along its horizontal projection

The x -coordinate is assumed as independent variable. The horizontal component H and vertical component V of the axial force, the z -coordinate and the stressed cable length S are considered as dependent variables.

The equilibrium of forces on the differential length ds is expressed as:

$$\frac{dH}{dx} = 0 \Rightarrow H = H_A = H_B \quad (2-89)$$

$$\frac{dV}{dx} dx = -p dx \Rightarrow V = V_A - px \quad (2-90)$$

where H_A and V_A are the horizontal and vertical reactions at point A. So:

$$N_A = \sqrt{H_A^2 + V_A^2} \quad (2-91)$$

The axial force N at distance x from endpoint A, is given as:

$$N = \sqrt{H^2 + V^2} = \sqrt{H^2 + (V_A - px)^2} \quad (2-92)$$

Using the equations of geometry and taking into account that the force N is axial, in other words tangent to the stressed cable, the following equations occur:

$$\frac{dz}{dx} = \frac{V}{H} = \frac{V_A - px}{H} \Rightarrow z = \frac{x}{H} \left(V_A - \frac{px}{2} \right) \quad (2-93)$$

$$\frac{ds}{dx} = \frac{N}{H} \Rightarrow s = \frac{H}{2p} \left[\frac{V_A N_A - V_B N_B}{H} + \log \left(\frac{N - V}{N_A - V_A} \right) \right] \quad (2-94)$$

where s is the stressed length of the cable from the start of the axes to the point (x, z) .

The analytical form of Eqs. (2-93) and (2-94) derives from their integration from $x = 0$ to x , where for $x = 0$:

$$z = s = 0 \quad (2-95)$$

$$N = N_A \quad (2-96)$$

$$H = H_A \quad (2-97)$$

$$V = V_A \quad (2-98)$$

Applying the boundary conditions of right support B:

$$z = L \tan \theta \quad \text{and} \quad x = L \quad (2-99)$$

Eq. (2-93) turns into:

$$(2-93) \Rightarrow V_A = H \tan \theta + \frac{pL}{2} \quad (2-100)$$

Combing Eqs. (2-92) and (2-100), cable's axial force N at distance x from endpoint A is defined as:

$$N = H \sqrt{1 + \left[\tan \theta + \frac{pL}{2H} \left(1 - \frac{2x}{L} \right) \right]^2} \quad (2-101)$$

Replacing Eq. (2-100) into (2-93), the z -coordinate of the point (x, z) is:

$$z = x \tan \theta + d \quad (2-102)$$

where,

$$d = \frac{xp(L-x)}{2H} \quad (2-103)$$

Notice from Figure 2-37 that, d is the vertical distance of the stressed cable from the chord AB . In case that, $S_0 \leq S_{AB}$, $d = v$.

Eqs. (2-101) and (2-102) describe the axial force N and the z -coordinate as function of the horizontal component H of the axial force, which is generally not known. In some occasions, H can be defined from the reader directly or indirectly, for instance if d is known at some point.

If the vertical distance d of the cable at midpoint is defined as:

$$d_m = d'_m L \quad (2-104)$$

the horizontal component H of the axial force comes out from the following equation:

$$(2-103) \Rightarrow d_m = \frac{pL}{4H} \left(L - \frac{L}{2} \right) \Rightarrow H = \frac{pL}{8d'_m} \quad (2-105)$$

and previous equations turn into:

$$(2-101) \Rightarrow N = \frac{pL}{8d'_m} \sqrt{1 + \left[\tan\theta + 4d'_m \left(1 - \frac{2x}{L} \right) \right]^2} \quad (2-106)$$

$$(2-102) \Rightarrow z = x \left[\tan\theta + 4d'_m \left(1 - \frac{x}{L} \right) \right] \quad (2-107)$$

In case that, the horizontal component H of the axial force and/or the vertical distance d for each point are unknown, the material constitutive equation is used in calculations. Assuming the material as linearly elastic, Hooke's law gives for the differential length ds of DETAIL "a" - Figure 2-37:

$$\sigma = E\varepsilon \Rightarrow N = EA \left(\frac{ds - ds_0}{ds_0} \right) \Rightarrow \frac{ds}{dx} = \frac{ds_0}{dx} \left(1 + \frac{N}{EA} \right) \quad (2-108)$$

The combination of Eqs. (2-94) and (2-108) leads to:

$$\frac{N}{H} = \frac{ds_0}{dx} \left(1 + \frac{N}{EA} \right) \Rightarrow \frac{ds_0}{dx} = \frac{\frac{N}{H}}{\left(1 + \frac{N}{EA} \right)} \quad (2-109)$$

Replacing Eq. (2-101) into (2-109) and integrating from $x = 0$ to L , in the left part derives the known cable's unstressed length S_0 and in the right part a function of the horizontal component H of the axial force. Eq. (2-109) is too complex to determine an analytical solution from its integral. The right part should be simplified. Expanding to series according to:

$$\frac{1}{1+x} = 1 - x + x^2 - x^3 + \dots \quad (2-110)$$

[6]

and assuming that $\frac{N}{EA} \ll 1$, the terms $\frac{N}{EA}$ of higher order are neglected. Then, Eq. (2-109) becomes:

$$(2-109) \Rightarrow \frac{ds_0}{dx} = \frac{N}{H} \left(1 - \frac{N}{EA} \right) \quad (2-111)$$

Replacing the horizontal component H of the axial force from Eq. (2-105) and the axial force N from Eq. (2-106) into (2-111):

$$(2-111) \Rightarrow \frac{ds_0}{dx} = \sqrt{1 + \left[\tan\theta + 4d'_m \left(1 - \frac{2x}{L} \right) \right]^2} \left\{ 1 - \frac{pL}{8d'_m EA} \sqrt{1 + \left[\tan\theta + 4d'_m \left(1 - \frac{2x}{L} \right) \right]^2} \right\} \quad (2-112)$$

For simplification reasons, the following non-dimensional parameters are used:

$$\rho' = \frac{pL}{2EA} \quad (2-113)$$

$$\rho = \tan\theta + 4d'_m \left(1 - \frac{2x}{L} \right)$$

Then, the horizontal component H' of the axial force in non-dimensional form is defined as:

$$(2-105) \Rightarrow H' = \frac{\rho'}{4d'_m} \quad (2-114)$$

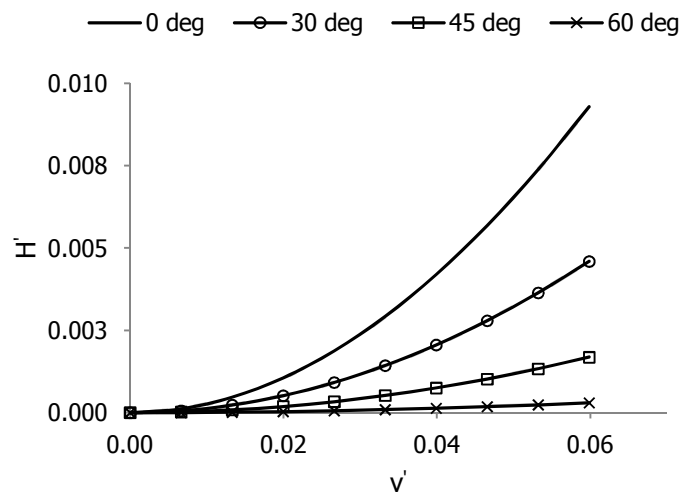


Figure 2-38: Horizontal component H' of the axial force as function of vertical deflection v' ($= d'_m$) for different values of angle θ , in case that $S_0 = S_{AB}$

Figure 2-38 describes the horizontal component H' of the axial force as function of vertical deflection v' ($= d'_m$) for different values of angle θ , in case that $S_0 = S_{AB}$.

Eq. (2-112) turns into:

$$(2-112) \Rightarrow \frac{ds_0}{dx} = \sqrt{1 + \rho^2} \left(1 - \frac{p'}{4d_m'} \sqrt{1 + \rho^2} \right) \quad (2-115)$$

The integration of Eq. (2-115) from $x = 0$ to L gives:

$$(2-115) \Rightarrow S_0' = \frac{1}{16d_m'} \left\{ \left[\left(\rho_A \sqrt{1 + \rho_A^2} - \rho_B \sqrt{1 + \rho_B^2} \right) + \ln \left(\frac{\rho_A + \sqrt{1 + \rho_A^2}}{\rho_B + \sqrt{1 + \rho_B^2}} \right) \right] + \right. \\ \left. + \frac{p'}{2d_m'} \left[(\rho_B - \rho_A) + \frac{\rho_B^3 - \rho_A^3}{3} \right] \right\} \quad (2-116)$$

where,

$$\rho_A = \rho(x=0) = \tan\theta + 4d_m' \\ \rho_B = \rho(x=L) = \tan\theta - 4d_m' \quad (2-117)$$

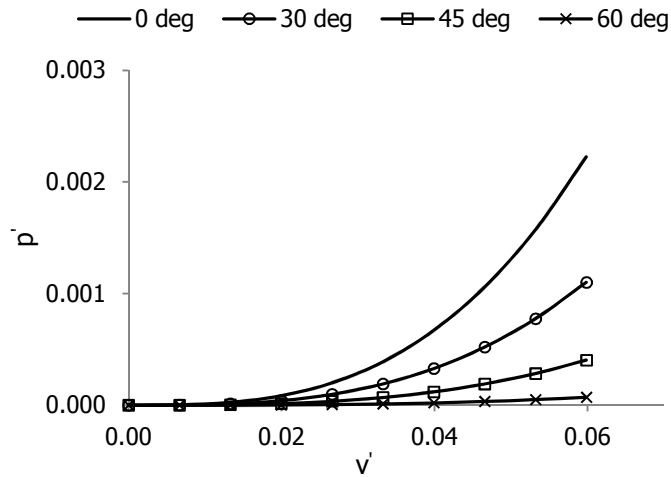


Figure 2-39: Applied load p' as function of vertical deflection v' ($= d_m'$) for different values of angle θ , in case that $S_0 = S_{AB}$

Figure 2-39 describes the equilibrium path of the cable for different values of angle θ , in case that $S_0 = S_{AB}$.

Cable's axial force gets the maximum value at endpoint A, according to Eq. (2-106):

$$(2-106) \Rightarrow N^{\max} = \frac{pL}{8d_m'} \sqrt{1 + (\tan\theta + 4d_m')^2} \quad (2-118)$$

or in non-dimensional form:

$$(2-118) \Rightarrow N^{\max'} = \frac{p'}{4d_m'} \sqrt{1 + \rho_A^2} \quad (2-119)$$

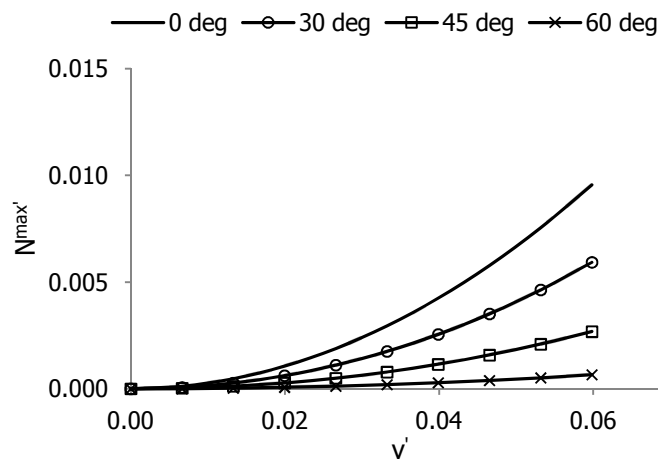


Figure 2-40: Maximum axial force $N^{\max'}$ as function of vertical deflection $v' (= d_m')$ for different values of angle θ , in case that $S_0 = S_{AB}$

Figure 2-40 describes the maximum axial force $N^{\max'}$ as function of vertical deflection $v' (= d_m')$ for different values of angle θ , in case that $S_0 = S_{AB}$.

Figures 2-38 to 2-40 have the same qualitative behavior. The slope of the curves increase as the vertical deflection v' , in other words the applied load p , increases due to the geometric nonlinearity. For larger values of the vertical deflection v' , the curves tend to become linear, as the geometric nonlinearity is eliminated. Moreover, the smaller the angle θ is the stiffer the cable becomes. According to Figure 2-41, applied load p is analyzed into a component p_{\perp} perpendicular to the differential length ds and a parallel one p_{\parallel} , where:

$$p_{\perp} = \cos\theta p \quad (2-120)$$

$$p_{\parallel} = \sin\theta p \quad (2-121)$$

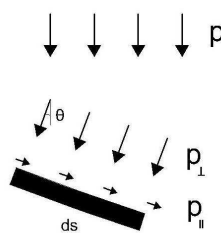


Figure 2-41: Analysis of the applied load p into p_{\perp} and p_{\parallel} components

The component p_{\perp} displaces the differential length ds along its direction, while the component p_{\parallel} elongates it according to Hooke's law, Eq. (2-108). Larger values of angle θ lead to larger values of the component p_{\parallel} and, given a constant value of the modulus of elasticity E , larger elongations ϵ . As elongations ϵ increase, cable's stiffness K decreases. This is the reason why the smaller the angle θ is the stiffer the cable becomes. Notice that, in case of a concentrated load P the opposite qualitative behavior occurs, according to Paragraph 2.5.3 – case 2, as the response mechanism of the cable differs.

2.3.2 Horizontal cable under uniformly distributed load along its horizontal projection

In this section, a horizontal cable under uniformly distributed load p along its horizontal projection is examined. The model of the cable is illustrated on Figure 2-37, for $\theta = 0$ deg. Due to the geometric symmetry, there are no horizontal deflection u . Eq. (2-116) is simplified as follows:

$$(2-116) \Rightarrow S'_0 = \frac{1}{16d'_m} \left\{ 8d'_m \sqrt{1+(4d'_m)^2} + \ln \left[\frac{\sqrt{1+(4d'_m)^2} + 4d'_m}{\sqrt{1+(4d'_m)^2} - 4d'_m} \right] - 4p' \left[1 + \frac{(4d'_m)^2}{3} \right] \right\} \quad (2-122)$$

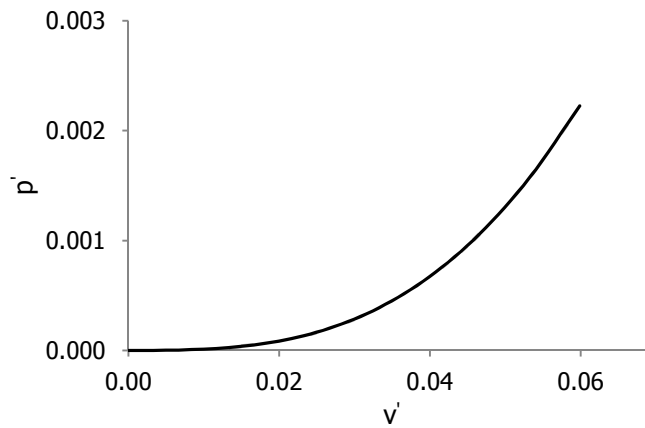


Figure 2-42: Applied load p' as function of vertical deflection v' ($= d'_m$), in case that $S_0 = S_{AB}$

Figure 2-42 shows the equilibrium path of the cable, in case that $S_0 = S_{AB}$. The slope, which indicates cable's stiffness K , increases as the applied load p' increases, due to the geometric nonlinearity. Here, $z^* = 0$ as $S_0 = S_{AB}$ and, so, $v = z$ or $v' = z'$.

Using Eq. (2-106), the expression of the cable's axial force N is:

$$(2-106) \Rightarrow N = \frac{pL}{2} \sqrt{\frac{1}{(4d'_m)^2} + \left(1 - \frac{2x}{L}\right)^2} \quad (2-123)$$

and is maximum at endpoint A:

$$(2-123) \Rightarrow N^{\max} = \frac{pL}{2} \sqrt{\frac{1}{(4d'_m)^2} + 1} \quad (2-124)$$

or in non-dimensional form:

$$(2-124) \Rightarrow N^{\max'} = p' \sqrt{\frac{1}{(4d'_m)^2} + 1} \quad (2-125)$$

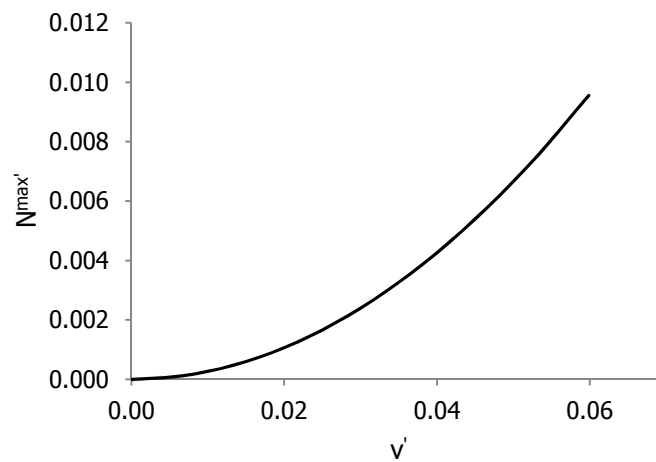


Figure 2-43: Maximum axial force $N^{\max'}$ as function of vertical deflection v' ($= d_m'$), in case that $S_0 = S_{AB}$

Figure 2-43 describes cable's maximum axial forces $N^{\max'}$ as function of vertical deflection v' ($= d_m'$), in case that $S_0 = S_{AB}$. The slope of the curve increases as the vertical deflection v' , in other words the applied load p' , increases due to the geometric nonlinearity. Here, $z^* = 0$ as $S_0 = S_{AB}$ and, so, $v = z$ or $v' = z'$.

The horizontal component H of the axial force comes out from:

$$(2-105) \Rightarrow H = \frac{pL}{8d_m'} \quad (2-126)$$

or in non-dimensional form:

$$(2-126) \Rightarrow H' = \frac{p'}{4d_m'} \quad (2-127)$$

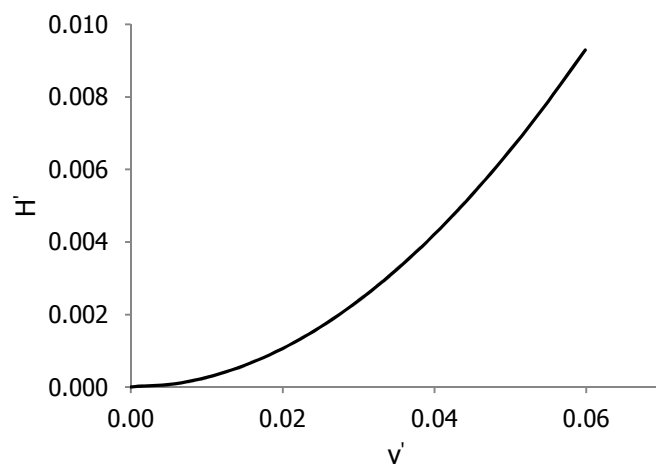


Figure 2-44: Horizontal component H' of the axial force as function of vertical deflection v' ($= d_m'$), in case that $S_0 = S_{AB}$

Figure 2-44 describes the horizontal component H' of the axial forces as function of vertical deflection v' ($=d'_m$), in case that $S_0 = S_{AB}$. The slope of the curve increases as the vertical deflection v' , in other words the applied load p' , increases due to the geometric nonlinearity. Here, $z^* = 0$ as $S_0 = S_{AB}$ and, so, $v = z$ or $v' = z$.

In case that the vertical deflection d'_m at midpoint is small, in other words $d'_m \ll 1$, Eq. (2-122) can be developed in Taylor series, after multiplication with $16d'_m$. The result is:

$$(2-122) \Rightarrow 16d'_m S'_0 = -4p' + 16d'_m - \frac{64}{3} p' (d'_m)^2 + \frac{128}{3} (d'_m)^3 - \frac{512}{5} (d'_m)^5 + \frac{4096}{7} (d'_m)^7 + \dots \quad (2-128)$$

Neglecting the terms of fifth and higher order, Eq. (2-128) is a 3rd degree equation and can be written as follows:

$$(2-128) \Rightarrow (4d'_m)^3 - 2p' (4d'_m)^2 - 6(S'_0 - 1)(4d'_m) - 6p' = 0 \quad (2-129)$$

The solution of Eq. (2-129) defines the vertical deflection d'_m in case that the initial unstressed length S_0 and the load p' are known.

For horizontal inextensible cables, which are cables with quite large stiffness with $EA \rightarrow \infty$ and, so, $p' = 0$, Eq. (2-122) turns into:

$$(2-122) \Rightarrow S'_0 = \frac{1}{16d'_m} \left\{ 8d'_m \sqrt{1+(4d'_m)^2} + \ln \left[\frac{\sqrt{1+(4d'_m)^2} + 4d'_m}{\sqrt{1+(4d'_m)^2} - 4d'_m} \right] \right\} \quad (2-130)$$

The corresponding approximate Eq. (2-129) turns into:

$$(2-129) \Rightarrow d'_m = \sqrt{\frac{3}{8}(S'_0 - 1)} \quad (2-131)$$

or, alternatively:

$$(2-131) \Rightarrow S'_0 = 1 + \frac{8}{3}(d'_m)^2 \quad (2-132)$$

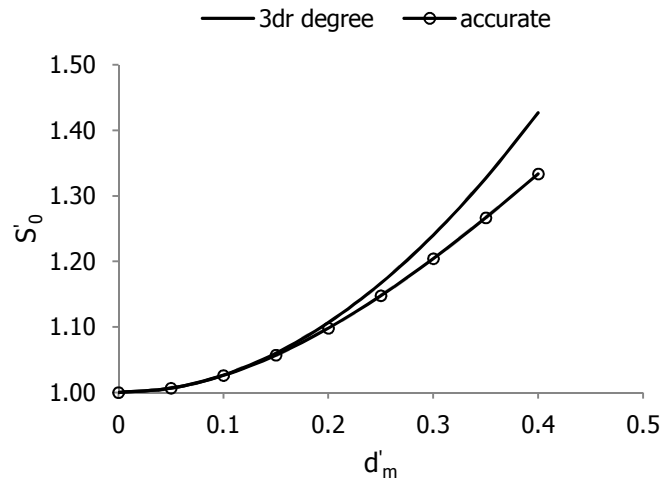


Figure 2-45: Comparison between accurate and approximate solution, in case of a horizontal inextensible cable

Figure 2-45 indicates the difference between the accurate solution, Eq. (2-130), and the approximation using Taylor series, Eq. (2-132), in case of a horizontal inextensible cable. Notice that, 3rd degree approximation is sufficient for $f \leq 0.2$.

In case of an inclined inextensible cable:

$$d'_m = \sqrt{\frac{3}{8} \left[S'_0 - 1 - \frac{1}{2} (\tan\theta)^2 \right]} \quad (2-133)$$

or

$$(2-133) \Rightarrow S'_0 = 1 + \frac{8}{3} (d'_m)^2 + \frac{1}{2} (\tan\theta)^2 \quad (2-134)$$

which are equivalent to Eqs. (2-131) and (2-132), [4].

It is useful to present the comparison of the response of a horizontal inextensible cable subjected to a uniformly distributed load p along its horizontal projection and to an equivalent concentrated load $P = pL$ at midpoint, in case that $S_0 = S_{AB}$. Here, $z^* = 0$ and, so, $v = z = d'_m$ or $v' = z' = d'_m$. Eq. (2-13) for $P' = 0$, as $EA \rightarrow \infty$, gives the vertical deflection d'_{mP} for the equivalent concentrated load P' at midpoint as:

$$(2-13) \Rightarrow d'_{mP} = \frac{1}{2} \sqrt{(S'_0)^2 - 1} \quad (2-135)$$

The corresponding axial force N_p comes out from the combination of Eqs. (2-7) and (2-104) as:

$$N_p = \frac{pL}{2} \sqrt{1 + \frac{1}{4(d'_{mP})^2}} = \frac{pL}{2} \sqrt{\frac{(S'_0)^2}{(S'_0)^2 - 1}} \quad (2-136)$$

The combination of Eqs. (2-124) and (2-131) gives the maximum axial force N^{\max} , in case of a uniformly distributed load p along cable's horizontal projection as:

$$N^{\max} = \frac{pL}{2} \sqrt{\frac{1}{6(S'_0 - 1)} + 1} \quad (2-137)$$

The ratios of the vertical deflection and the axial force are:

$$\frac{d'_{mP}}{d'_m} = \frac{\frac{1}{2} \sqrt{(S'_0)^2 - 1}}{\sqrt{\frac{3}{8}(S'_0 - 1)}} = \sqrt{\frac{2}{3}(S'_0 + 1)} \quad (2-138)$$

$$\frac{N_p}{N^{\max}} = \frac{\frac{pL}{2} \sqrt{\frac{(S'_0)^2}{(S'_0)^2 - 1}}}{\frac{pL}{2} \sqrt{\frac{1}{6(S'_0 - 1)} + 1}} = S'_0 \sqrt{\frac{6(S'_0 - 1)}{[(S'_0)^2 - 1][1 + 6(S'_0 - 1)]}} \quad (2-139)$$

Eqs. (2-138) and (2-139) are presented graphically below.

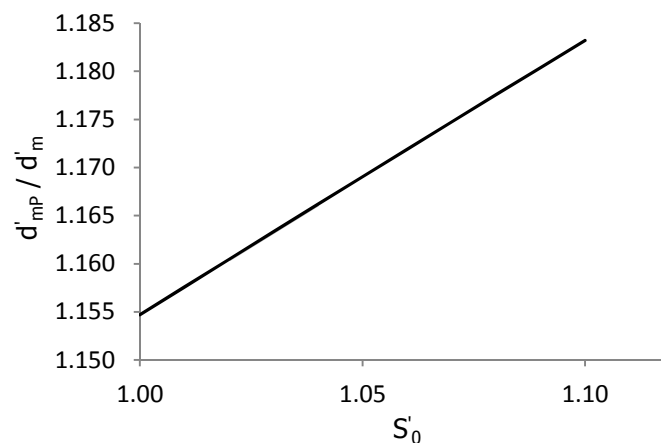


Figure 2-46: Ratio of the vertical deflection of a horizontal inextensible cable subjected to distributed p and to equivalent concentrated P load

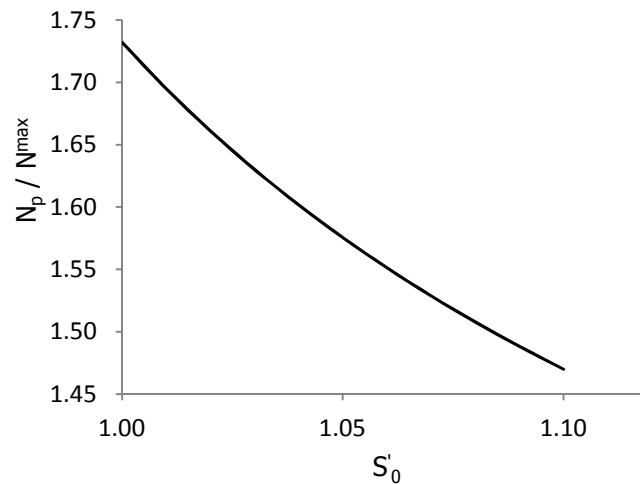


Figure 2-47: Ratio of the axial force of a horizontal inextensible cable subjected to distributed p and to equivalent concentrated P load

Figures 2-46 and 2-47 indicate that the vertical deflection and the axial force due to a uniformly distributed load p along cable's horizontal projection are smaller than these due to an equivalent concentrated load P at midpoint. So, distributed loads are delivered from a simple cable in a smoother way, in comparison to concentrated loads.

2.3.3 Inclined cable under uniformly distributed load along its arc length

A simple inclined cable, with initial unstressed length S_0 , spans the distance S_{AB} , where S_{AB} is the distance between points A and B. A uniformly distributed load q along cable's arc length is applied, as shown in Figure 2-48. The horizontal deflection u of the cable is not taken into account in this analysis, for simplification reasons.

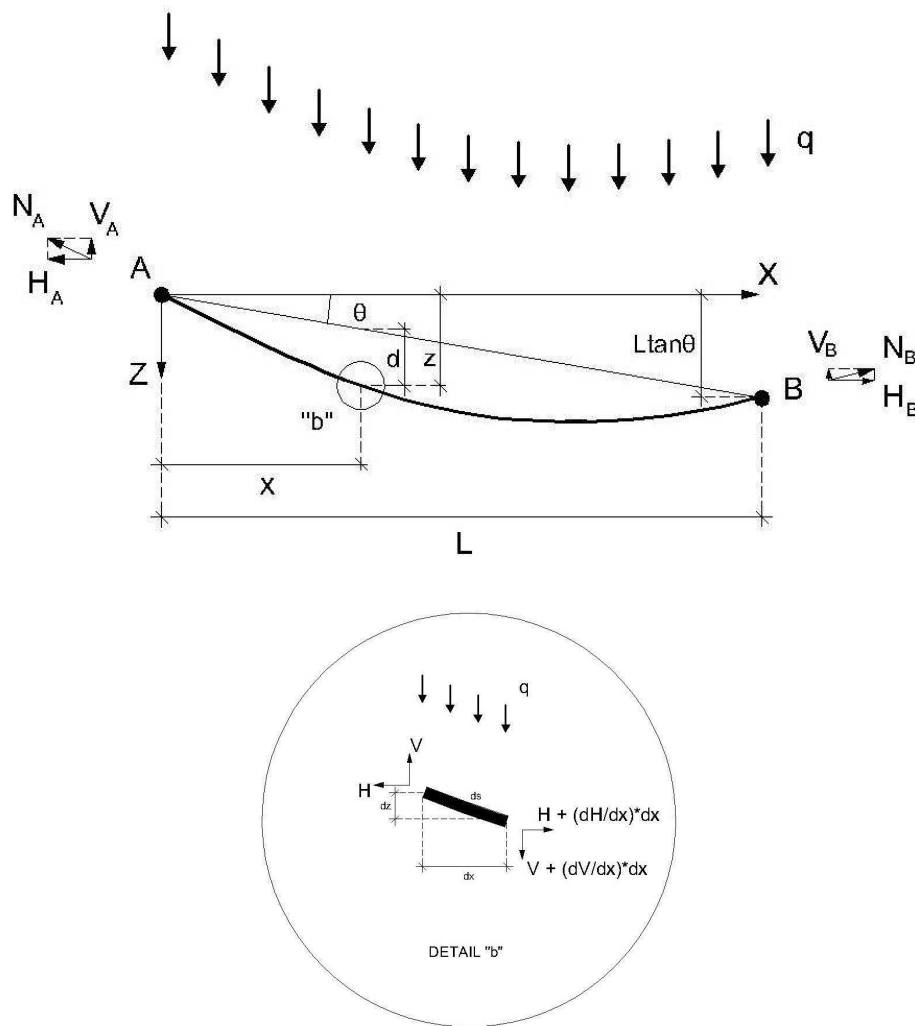


Figure 2-48: Inclined cable under uniformly distributed load q along its arc length

The stressed length s of the cable from the start of the axes to the point (x,z) is assumed as independent variable.

The equilibrium of forces on the differential length ds is expressed as:

$$\frac{dH}{dx} = 0 \Rightarrow H = H_A = H_B \quad (2-140)$$

$$\frac{dV}{dx} = -q \frac{ds}{dx} \quad (2-141)$$

Using the equations of geometry and taking into account that the force N is axial, in other words tangent to the stressed cable, the following equations occur:

$$\frac{dz}{dx} = \frac{V}{H} \Rightarrow V = H \frac{dz}{dx} \quad (2-142)$$

$$\frac{ds}{dx} = \frac{N}{H} \quad (2-143)$$

The derivative of x of Eq. (2-142) is:

$$(2-142) \Rightarrow \frac{dV}{dx} = H \frac{d^2z}{dx^2} \quad (2-144)$$

The combination of Eqs. (2-141) and (2-144) leads to:

$$H \frac{d^2z}{dx^2} = -q \frac{ds}{dx} \quad (2-145)$$

According to Figure 2-48 – DETAIL “b”, the differential length ds equals to:

$$ds = \sqrt{dx^2 + dz^2} \quad (2-146)$$

So, Eq. (2-145) turns into:

$$(2-145) \Rightarrow \frac{d^2z}{dx^2} + \frac{q}{H} \sqrt{1 + \left(\frac{dz}{dx}\right)^2} = 0 \quad (2-147)$$

Eq. (2-147) is the equilibrium differential equation of a cable subjected to its self weight or to a uniformly distributed load q along its arc length. The solution of this equation is called catenary, as describes the curve of a hanging chain subjected to its own weight.

Assuming that the horizontal component H of the axial force is given, the integration of Eq. (2-147) twice and the application of the boundary conditions:

$$z = 0 \text{ at } x = 0 \quad (2-148)$$

$$z = L \tan \theta \text{ at } x = L \quad (2-149)$$

define the solution of the equilibrium differential equation as:

$$(2-147) \Rightarrow z = d + x \tan \theta = \frac{L}{2\delta} \left\{ \cosh(\zeta + \delta) - \cosh \left[\zeta + \delta \left(1 - \frac{2x}{L} \right) \right] \right\} \quad (2-150)$$

where,

$$\delta = \frac{qL}{2H} \quad (2-151)$$

$$\zeta = \sinh^{-1} \left(\tan \theta \frac{\delta}{\sinh \delta} \right)$$

[4]

Appendix A presents the main properties of hyperbolic functions. Notice from Figure 2-48 that, d is the vertical distance of the stressed cable from the chord AB. In case that, $S_0 \leq S_{AB}$, $d = v$.

The axial force N is defined as:

$$N = \sqrt{V^2 + H^2} = \sqrt{H^2 \left(\frac{dz}{dx} \right)^2 + H^2} \Rightarrow N = H \sqrt{1 + \left(\frac{dz}{dx} \right)^2} \quad (2-152)$$

The derivative of x of Eq. (2-150) is:

$$(2-150) \Rightarrow \frac{dz}{dx} = \sinh \left[\zeta + \delta \left(1 - \frac{2x}{L} \right) \right] \quad (2-153)$$

So:

$$(2-152) \Rightarrow N = \frac{qL}{2\delta} \cosh \left[\zeta + \delta \left(1 - \frac{2x}{L} \right) \right] \quad (2-154)$$

$$(2-142) \Rightarrow V = \frac{qL}{2\delta} \sinh \left[\zeta + \delta \left(1 - \frac{2x}{L} \right) \right] \quad (2-155)$$

where,

$$(2-151) \Rightarrow H = \frac{qL}{2\delta} \quad (2-156)$$

In case that, the horizontal component H of the axial force is unknown, the material constitutive equation is used in calculations. Assuming the material as linearly elastic, Hooke's law gives for the differential length ds of DETAIL "b" - Figure 2-48:

$$\sigma = E\varepsilon \Rightarrow N = EA \left(\frac{ds - ds_0}{ds_0} \right) \Rightarrow \frac{ds}{dx} = \frac{ds_0}{dx} \left(1 + \frac{N}{EA} \right) \quad (2-157)$$

Replacing Eqs. (2-143), (2-154) and (2-156) into (2-157) and integrating from x = 0 to L, the analytical solution for the response of the cable is determined. The integration is too complex and, so, the right part should be simplified. Expanding to series according to Eq. (2-110) and

assuming that $\frac{N}{EA} \ll 1$, Eq. (2-157) becomes:

$$(2-157) \Rightarrow \frac{ds_0}{dx} = \frac{N}{H} \left(1 - \frac{N}{EA} \right) \quad (2-158)$$

Substituting the axial force N from Eq. (2-154) and using Eq. (2-156), the solution of the differential equation Eq. (2-158) is:

$$(2-158) \Rightarrow S_0(x) = \frac{1}{8EA\delta} \left[-4\delta Hx + 4EAL \sinh(\zeta + \delta) - HL \sinh(2\zeta + 2\delta) - 4EAL \sinh \left(\zeta + \delta - \frac{2\delta x}{L} \right) + HL \sinh \left(2\zeta + 2\delta - \frac{4\delta x}{L} \right) \right] \quad (2-159)$$

The condition $S_0(L) = S_0$ gives:

$$(2-159) \Rightarrow S_0 = \frac{1}{8EA\delta} \left[-4\delta HL + 4EAL \sinh(\zeta + \delta) - HL \sinh(2\zeta + 2\delta) - 4EAL \sinh(\zeta - \delta) + HL \sinh(2\zeta - 2\delta) \right] \Rightarrow \quad (2-160)$$

$$\Rightarrow \frac{S_0}{L} = -\frac{H}{2EA} + \frac{\sinh(\zeta + \delta) - \sinh(\zeta - \delta)}{2\delta} + \frac{H}{2EA} \left[\frac{\sinh(2\zeta - 2\delta) - \sinh(2\zeta + 2\delta)}{4\delta} \right]$$

Defining $q' = \frac{qL}{2EA}$, Eq. (2-160) is changed as follows:

$$(2-160) \Rightarrow 2\delta S_0' - \sinh(\zeta + \delta) + \sinh(\zeta - \delta) = q' \left[\frac{\sinh(2\zeta - 2\delta) - \sinh(2\delta + 2\zeta)}{4\delta} - 1 \right] \quad (2-161)$$

In case that S_0 is defined, q is calculated from Eq. (2-161) using numerical methods. The vertical distance $d_m' = \frac{d_m}{L}$ at midpoint is defined from Eq. (2-150) for $x = \frac{L}{2}$:

$$(2-150) \Rightarrow d_m' = \frac{1}{2\delta} \left[\cosh(\zeta + \delta) - \cosh(\zeta) \right] - \frac{1}{2} \tan\theta \quad (2-162)$$

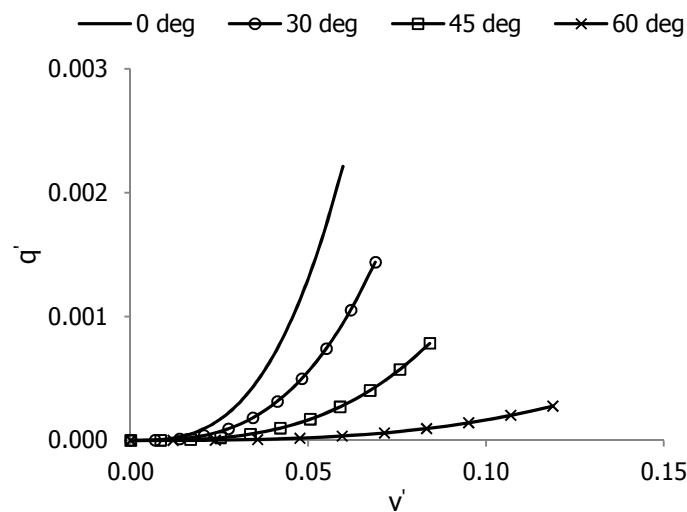


Figure 2-49: Applied load q' as function of vertical deflection v' ($= d_m'$) for different values of angle θ , in case that $S_0 = S_{AB}$

Figure 2-49 describes the equilibrium path of the cable for different values of angle θ , in case that $S_0 = S_{AB}$.

Cable's axial force gets the maximum value at endpoint A, according to Eq. (2-154):

$$(2-154) \Rightarrow N^{\max} = \frac{qL}{2\delta} \cosh(\zeta + \delta) \quad (2-163)$$

or in non-dimensional form:

$$(2-163) \Rightarrow N^{\max'} = \frac{q'}{\delta} \cosh(\zeta + \delta) \quad (2-164)$$

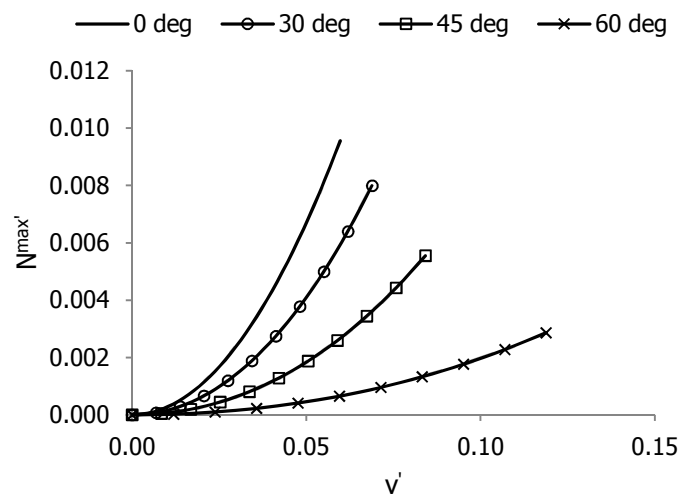


Figure 2-50: Maximum axial force $N^{\max'}$ as function of vertical deflection $v' (= d_m')$ for different values of angle θ , in case that $S_0 = S_{AB}$

Figure 2-50 describes the maximum axial force $N^{\max'}$ as function of vertical deflection $v' (= d_m')$ for different values of angle θ , in case that $S_0 = S_{AB}$.

The horizontal component H of the axial force, in non-dimensional form, comes out from Eq. (2-156) as:

$$(2-156) \Rightarrow H' = \frac{q'}{\delta} \quad (2-165)$$

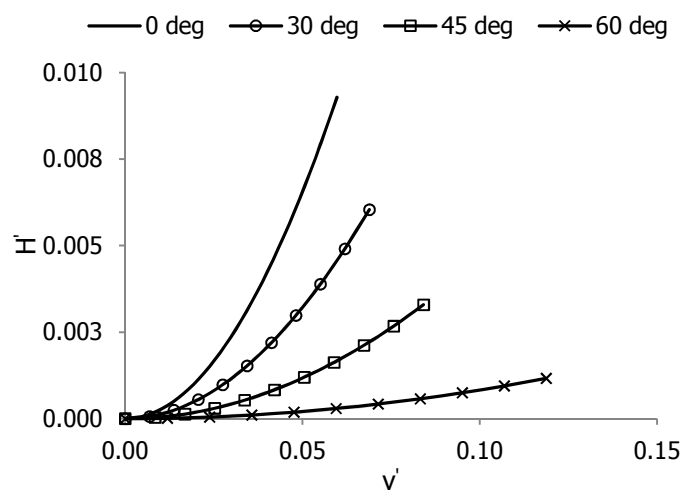


Figure 2-51: Horizontal component H' of the axial force as function of vertical deflection $v' (= d_m')$ for different values of angle θ , in case that $S_0 = S_{AB}$

Figure 2-51 describes the horizontal component H' of the axial force as function of vertical deflection v' ($= d'_m$) for different values of angle θ , in case that $S_0 = S_{AB}$.

Figures 2-49 to 2-51 have the same qualitative behavior. The slope of the curves increase as the vertical deflection v' , in other words the applied load q , increases due to the geometric nonlinearity. For larger values of the vertical deflection v' , the curves tend to become linear, as the geometric nonlinearity is eliminated. Moreover, the smaller the angle θ is the stiffer the cable becomes. According to Figure 2-52, applied load q is analyzed into a component q_{\perp} perpendicular to the differential length ds and a parallel one q_{\parallel} , where:

$$q_{\perp} = \cos\theta q \quad (2-166)$$

$$q_{\parallel} = \sin\theta q \quad (2-167)$$

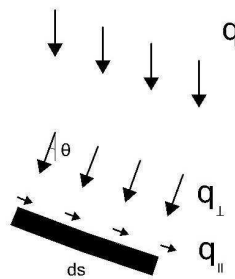


Figure 2-52: Analysis of the applied load q into q_{\perp} and q_{\parallel} components

The component q_{\perp} displaces the differential length ds along its direction, while the component q_{\parallel} elongates it according to Hooke's law, Eq. (2-157). Larger values of angle θ lead to larger values of the component q_{\parallel} and, given a constant value of the modulus of elasticity E , larger elongations ϵ . As elongations ϵ increase, cable's stiffness K decreases. This is the reason why the smaller the angle θ is the stiffer the cable becomes. Notice that, in case of a concentrated load P the opposite qualitative behavior occurs, according to Paragraph 2.5.3 – case 2, as the response mechanism of the cable differs.

2.3.4 Horizontal cable under uniformly distributed load along its arc length

A horizontal cable under uniformly distributed load q along its arc length is examined. The model of the cable is illustrated on Figure 2-48, for $\theta = 0$ deg. Due to the geometric symmetry, there are no horizontal deflection u . Equations of Paragraph 2.3.3 are simplified, replacing $\theta = 0$ deg, as follows:

$$(2-151) \Rightarrow \zeta = 0 \quad (2-168)$$

$$(2-150) \Rightarrow z = d = \frac{L}{2\delta} \left\{ \cosh\delta - \cosh \left[\delta \left(1 - \frac{2x}{L} \right) \right] \right\} \quad (2-169)$$

$$(2-154) \Rightarrow N = \frac{qL}{2\delta} \cosh \left[\delta \left(1 - \frac{2x}{L} \right) \right] \quad (2-170)$$

$$(2-155) \Rightarrow v = \frac{qL}{2\delta} \sinh \left[\delta \left(1 - \frac{2x}{L} \right) \right] \quad (2-171)$$

$$(2-161) \Rightarrow 2(\sinh\delta - S_0'\delta) = q' \left[\frac{\sinh(2\delta)}{2\delta} + 1 \right] \quad (2-172)$$

$$(2-162) \Rightarrow d_m' = \frac{\cosh\delta - 1}{2\delta} \quad (2-173)$$

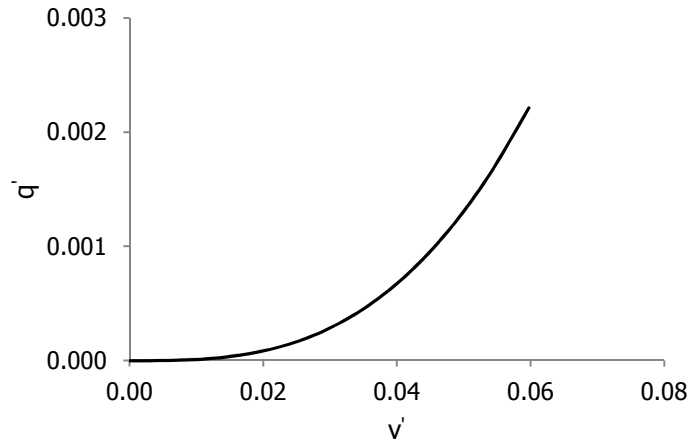


Figure 2-53: Applied load q' as function of vertical deflection v' ($= d_m'$), in case that $S_0 = S_{AB}$

Figure 2-53 shows the equilibrium path of the cable, in case that $S_0 = S_{AB}$. The slope, which indicates cable's stiffness K , increases as the applied load q' increases, due to the geometric nonlinearity. Here, $z^* = 0$ as $S_0 = S_{AB}$ and, so, $v = z$ or $v' = z$.

Cable's axial force is maximum at endpoint A, where:

$$(2-170) \Rightarrow N^{\max} = \frac{qL}{2\delta} \cosh\delta \quad (2-174)$$

or in non-dimensional form:

$$(2-174) \Rightarrow N^{\max'} = \frac{q'}{\delta} \cosh\delta \quad (2-175)$$

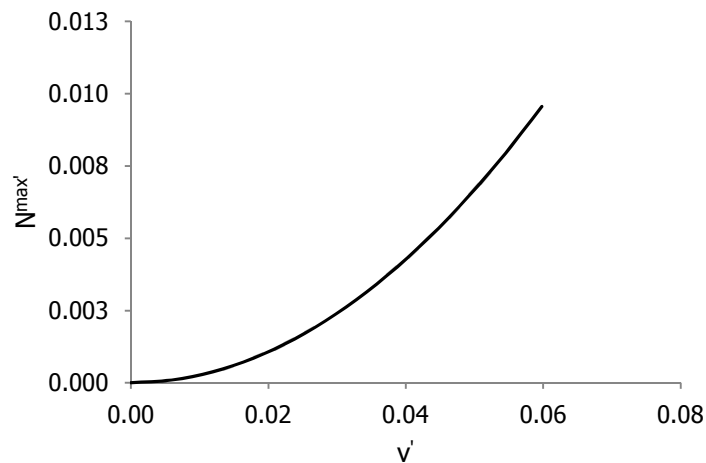


Figure 2-54: Maximum axial force $N^{\max'}$ as function of vertical deflection $v' (= d'_m)$, in case that $S_0 = S_{AB}$

Figure 2-54 describes cable's maximum axial forces $N^{\max'}$ as function of vertical deflection $v' (= d'_m)$, in case that $S_0 = S_{AB}$. The slope of the curve increases as the vertical deflection v' , in other words the applied load q' , increases due to the geometric nonlinearity. Here, $z^* = 0$ as $S_0 = S_{AB}$ and, so, $v = z$ or $v' = z'$.

The horizontal component H of the axial force is defined from Eq. (2-156) or from Eq. (2-165) in non-dimensional form.

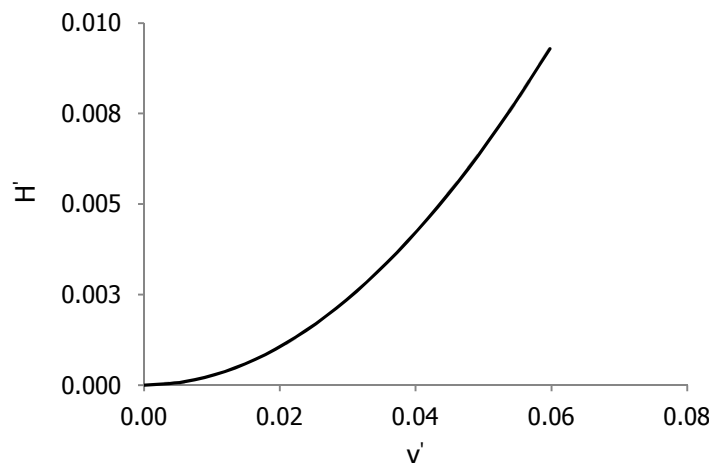


Figure 2-55: Horizontal component H' of the axial force as function of vertical deflection $v' (= d'_m)$, in case that $S_0 = S_{AB}$

Figure 2-55 describes the horizontal component H' of the axial forces as function of vertical deflection $v' (= d'_m)$, in case that $S_0 = S_{AB}$. The slope of the curve increases as the vertical deflection v' , in other words the applied load q' , increases due to the geometric nonlinearity. Here, $z^* = 0$ as $S_0 = S_{AB}$ and, so, $v = z$ or $v' = z'$. Appendix A presents the main properties of hyperbolic functions.

2.4 EQUIVALENT BEAM METHOD

Cable response in concentrated or distributed loads shows similarities with this of a simply supported beam. Regarding a concentrated load P at arbitrary position, as presented in Paragraph 2.2.3:

- the stressed geometry of the cable is similar to the bending moment diagram of an equivalent simple supported beam with the same span and loads
- the horizontal component H of the axial force remains unchanged along cable's length, as external horizontal loads do not exist

The previous observations are expressed as:

$$Hz = M \quad (2-176)$$

where M is the bending moment of the equivalent beam, in kNm.

According to Eq. (2-177), in case that z -coordinate, for each cable point, is unknown, the stressed geometry is defined from the known value of H .

$$Hz = M = \begin{cases} \frac{Px_p(L-x_p)}{L} \frac{x}{x_p} & 0 \leq x \leq x_p \\ \frac{Px_p(L-x_p)}{L} \frac{L-x}{L-x_p} & x_p \leq x \leq L \end{cases} \quad (2-177)$$

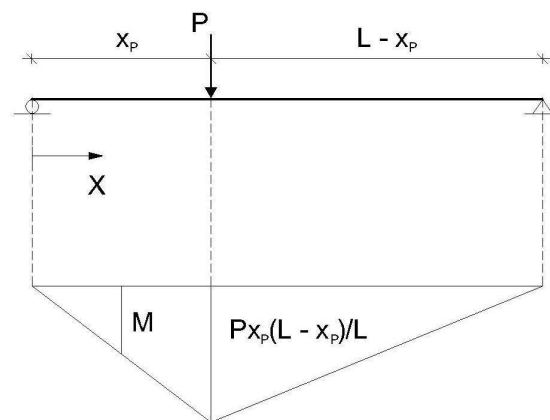


Figure 2-56: Bending moment diagram of a simple supported beam

In case of an inclined cable subjected to uniformly distributed load p along its horizontal projection, as defined in Paragraph 2.3.1, the vertical distance d of the stressed cable from the chord AB is given as:

$$d = \frac{M}{H} \quad (2-178)$$

where M is the moment of an equivalent simply supported beam, in kNm.

In other words, the bending moment M , due to external distributed load p applied at an equivalent simply supported beam, is equal to the bending moment M of the horizontal component H of the axial force applied at vertical distance d from the chord AB [5].

2.5 PARAMETRIC FIGURES OF A SIMPLE SUSPENDED CABLE

2.5.1 General matters

Paragraph 2.5 examines the impact of important cable parameters, such as the initial unstressed length S_0 , the modulus of elasticity E , the diameter d_A and the angle θ , into its response to external loads. The results are presented in parametric figures, in which one single parameter changes each time. Paragraphs 2.2 and 2.3 present general equations of cable response to different types of loads and the corresponding figures for $S_0 = S_{AB}$. In these equations, the initial unstressed cable length S_0 is assumed as accidental. The general case of a cable with initial unstressed length S_0 , spanning the distance S_{AB} , which is the distance between points A and B, is shown in Figure 2-57. The geometry gives:

$$L = S_{AB} \cos\theta \quad (2-179)$$

In case of a horizontal cable, in other words $\theta = 0$ deg, $S_{AB} = L$.

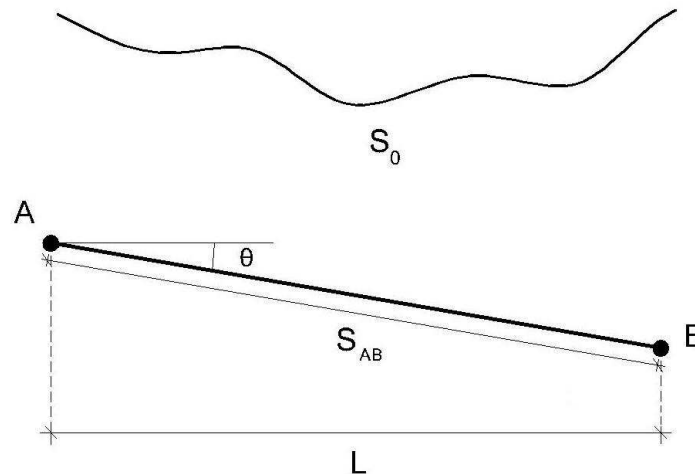


Figure 2-57: Initial unstressed state of a cable

The correlation between lengths S_0 and S_{AB} determines the response of the cable to external loads. Three cases can be detected:

1) $S_0 \leq S_{AB}$

In this case, the cable acquires pre-tension. Pre-tensioned cables respond more efficient to external loads, as their stiffness is increased and, so, develop smaller deflections. Pre-tension can be implemented either by the elongation of an initially unstressed cable or by the application of an initial external load. This paragraph examines the first one. According to Eq. (2-17), the stiffness K of a cable equals to the slope of its equilibrium path. So:

$$\Delta z = \frac{\Delta P}{K} \quad (2-180)$$

Figures 2-11 and 2-18 of Paragraph 2.2.2, which refer to the general case of an inclined cable under concentrated load P at arbitrary position, show that as the applied load P increases, cable's stiffness K increases and, for constant additional load ΔP , additional deflection Δz decreases, according to Eq. (2-180). Pre-tension gives initial stiffness to the cable, which develops smaller deflections. For large values of pre-tension and/or external loads, cable response tends to be linear. The same behavior occurs for distributed loads p and q .

Assuming the cable material as linearly elastic, Hooke's law gives:

$$\sigma^{\text{pre}} = E\varepsilon \Rightarrow \frac{N^{\text{pre}}}{A} = E \frac{\Delta S}{S_0} \Rightarrow N^{\text{pre}} = EA \left(\frac{S_{AB}-1}{S_0} \right) \quad (2-181)$$

where A is the cross-section and E the modulus of elasticity of the cable.

It is useful to express the axial force N^{pre} of the cable due to pre-tension as a percentage w^{pre} of the axial force capacity N^{cap} , which is defined below:

$$N^{\text{cap}} = Af_y \quad (2-182)$$

where f_y is the yield stress of the cable.

So:

$$w^{\text{pre}} = 100 \frac{N^{\text{pre}}}{N^{\text{cap}}} = 100 \frac{EA \left(\frac{S_{AB}-1}{S_0} \right)}{Af_y} \Rightarrow w^{\text{pre}} = 100 \frac{E \left(\frac{S_{AB}-1}{S_0} \right)}{f_y} \quad (2-183)$$

$$2) \quad S_0 = S_{AB}$$

Cable's initial unstressed length S_0 equals to the distance S_{AB} spanned. In this case, the cable remains unstressed until the application of the external loads. There is no pre-tension, as:

$$(2-183) \Rightarrow w^{\text{pre}} = 100 \frac{E \left(\frac{S_0-1}{S_0} \right)}{f_y} = 0 \% \quad (2-184)$$

$$3) \quad S_0 \geq S_{AB}$$

Cable's initial unstressed length S_0 is larger than the distance S_{AB} spanned. Cable remains unstressed until its total deployment, caused by the application of external loads. Then, it responds with the development of tension. Cable's equations are valid for $z \geq z^*$ and $x \geq x^*$, where z^*, x^* define the coordinates of the point from which cable tension, due to the load P, p or q, occurs. In other case, cable's tension and joint reactions are zero.

The coordinates z^*, x^* are calculated from the geometric compatibility equations, in case of a concentrated load P, as below:

- Horizontal cable under concentrated load P in the middle – Figure 2-1

$$z^* = \frac{\sqrt{S_0^2 - L^2}}{2} \quad (2-185)$$

- Inclined cable under concentrated load P at arbitrary position - Figures 2-7 and 2-15

$$S_0 = \sqrt{(x^*)^2 + (z^*)^2} + \sqrt{(L-x^*)^2 + (\tan\theta L - z^*)^2} \quad (2-186)$$

- Horizontal cable under concentrated load P at arbitrary position – Figure 2-21

$$S_0 = \sqrt{(x^*)^2 + (z^*)^2} + \sqrt{(L-x^*)^2 + (z^*)^2} \quad (2-187)$$

- Inclined cable under imposed end displacement v or u - Figures 2-28 and 2-32

$$z^* = \sqrt{S_0^2 - L^2} \quad \text{or} \quad x^* = \sqrt{S_0^2 - L^2} \quad (2-188)$$

where $x^* = x_p$, except for Eq. (2-188). The coordinates z_p , x_p refer to the starting application point of the concentrated load P. In case that $S_0 > S_{AB}$, $z^* \neq z_p$.

The impact of cable's initial unstressed length S_0 and of other parameters into its response to external loads is illustrated in the following diagrams, for a number of cable types and loads. Dimensional and non-dimensional diagrams are presented. Curves' limits are defined by the axial force capacity N^{cap} of each cable. Default values of cable parameters, mentioned in Table 2-1, are valid for the following diagrams in case that they are not specified in the text.

E	165	GPa
f_y	1.58	GPa
d_A	20	mm
S_{AB}	20.0	m
w^{pre}	10.0	%
α	0.10	-
θ	45	deg
S₀/S_{AB}	1.10	-

Table 2-1: Default values of cable parameters

The annotation of the parametric figures is placed at Paragraph 2.5.10, in order to highlight the common qualitative behavior of a cable in different kinds of load.

2.5.2 Diagrams of a horizontal cable under concentrated load in the middle

In this section, parametric diagrams for the case of Paragraph 2.2.1 are presented. The cable is horizontal, in other words $S_{AB} = L$.

$$1) \quad S_0 \leq S_{AB}$$

Here, $z^* = 0$ as $S_0 \leq S_{AB}$ and, so, $v' = z'$.

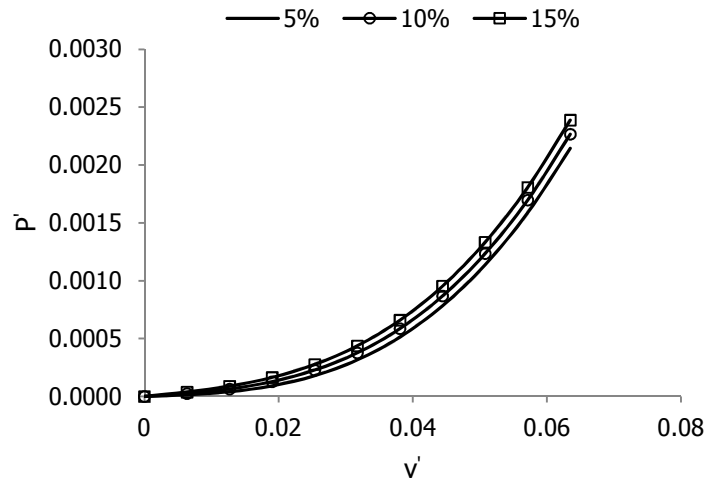


Figure 2-58: Applied load P' as function of vertical deflection v' for different values of pre-tension w^{pre}

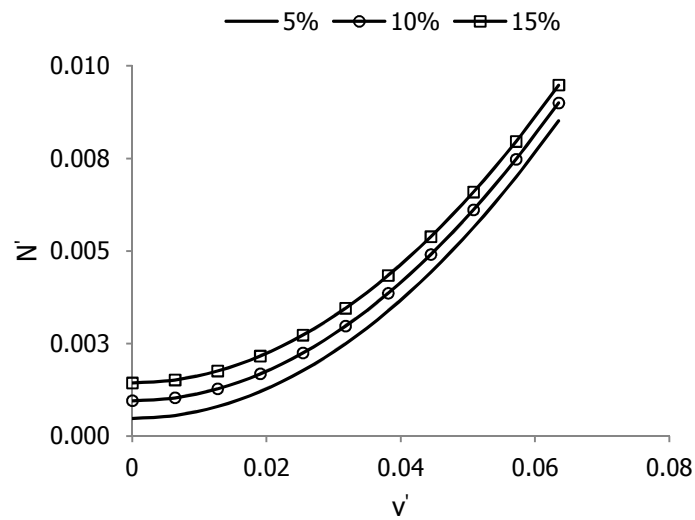


Figure 2-59: Cable's axial force N' as function of vertical deflection v' for different values of pre-tension w^{pre}

$$2) \quad S_0 = S_{AB}$$

Here, $z^* = 0$ as $S_0 = S_{AB}$ and, so, $v = z$.

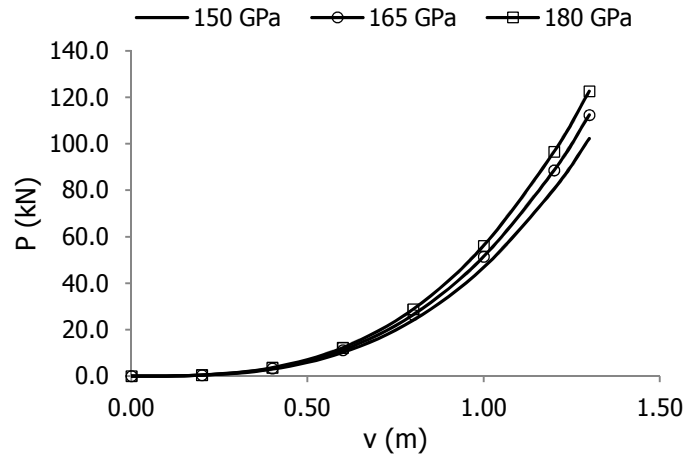


Figure 2-60: Applied load P as function of vertical deflection v for different values of the modulus of elasticity E

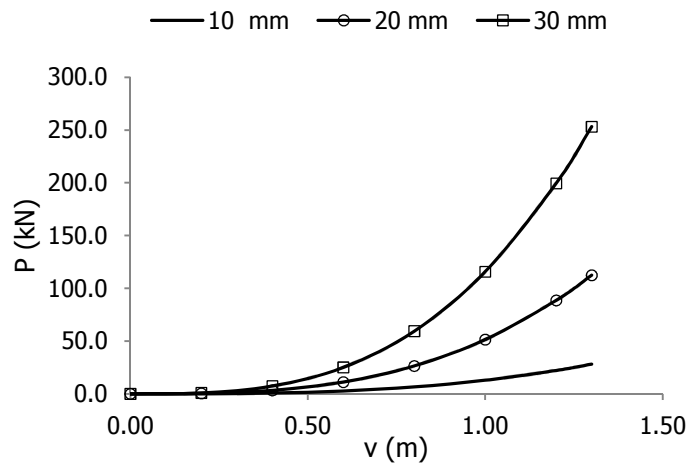


Figure 2-61: Applied load P as function of vertical deflection v for different values of diameter d_A

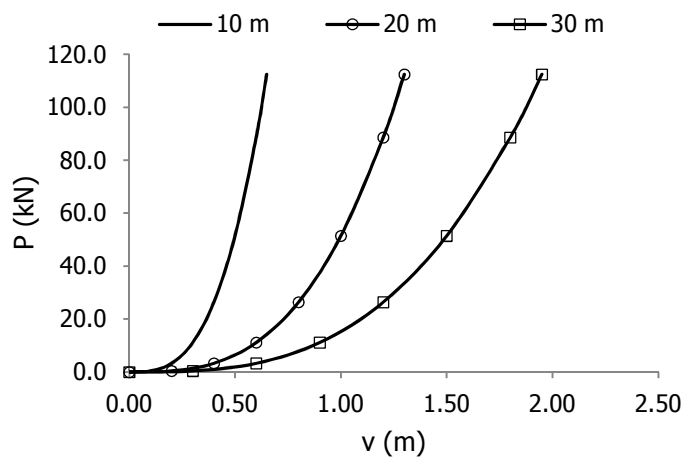


Figure 2-62: Applied load P as function of vertical deflection v for different values of initial unstressed length S_0

3) $S_0 \geq S_{AB}$

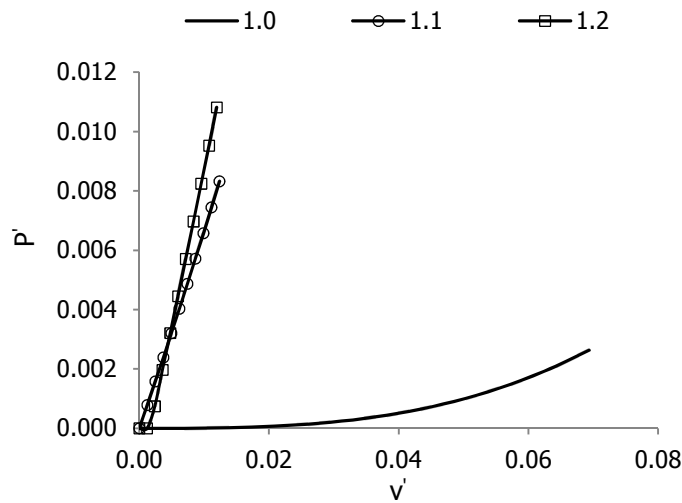


Figure 2-63: Applied load P' as function of vertical deflection v' for different values of ratio S_0/S_{AB}

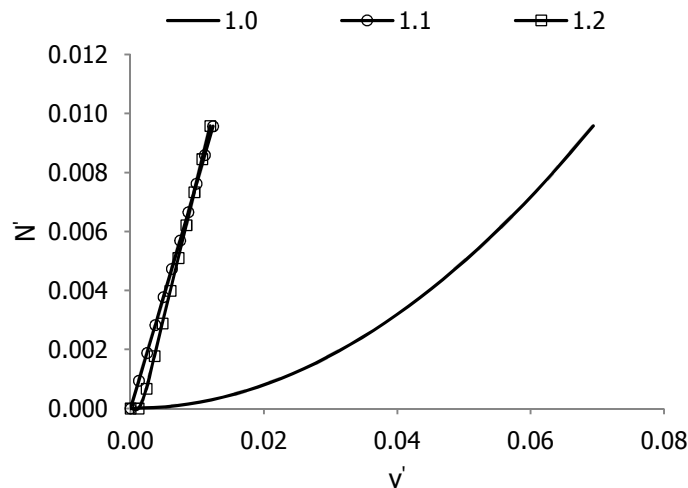


Figure 2-64: Cable's axial force N' as function of vertical deflection v' for different values of ratio S_0/S_{AB}

2.5.3 Diagrams of an inclined cable under concentrated load at arbitrary position

The following diagrams refer to the analysis of Paragraph 2.2.2 – case A. Notice that diagrams are designed through ADINA models (contained in the accompanied CD, commented in the list of numerical models with 'analytical') due to the complexity of the 2-degree polynomial solution. Paragraph 3.2.3 verifies the identification between analytical solution and numerical models.

1) $S_0 \leq S_{AB}$

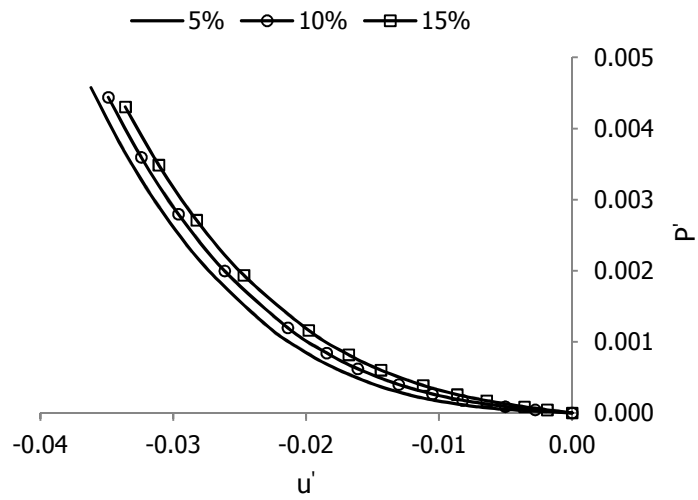


Figure 2-65: Applied load P' as function of horizontal deflection u' for different values of pre-tension w^{pre}

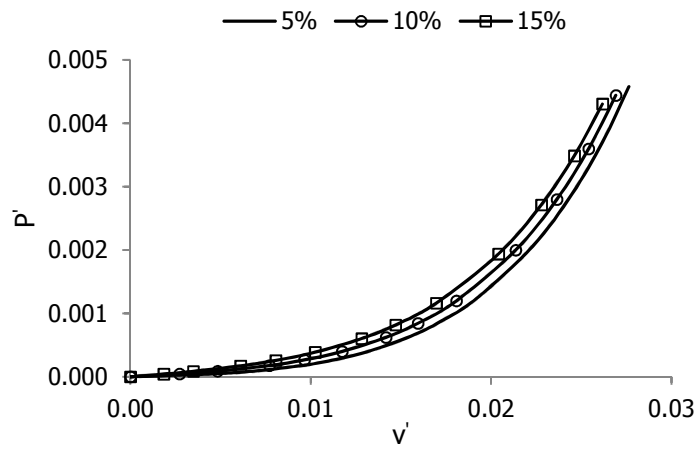


Figure 2-66: Applied load P' as function of vertical deflection v' for different values of pre-tension w^{pre}

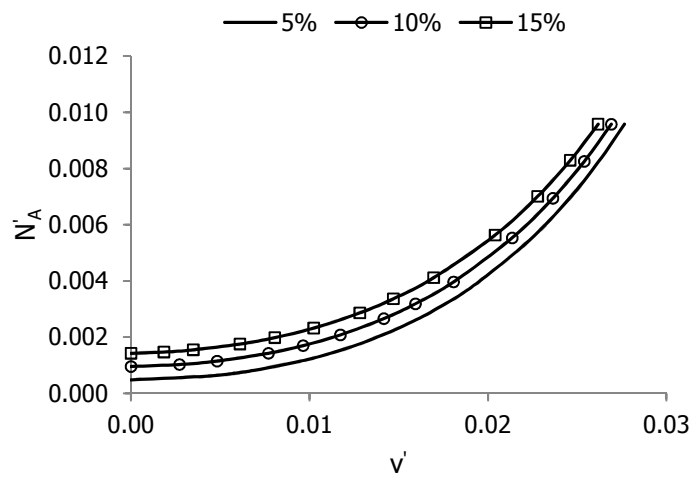


Figure 2-67: Cable's axial force N'_A as function of vertical deflection v' for different values of pre-tension w^{pre}

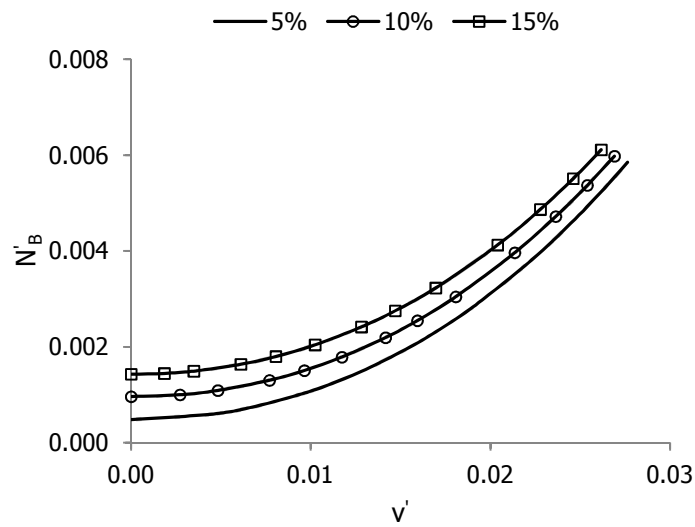


Figure 2-68: Cable's axial force N_B^i as function of vertical deflection v' for different values of pre-tension w^{pre}

The initial curve angle, in case of $w^{pre} = 5\%$, derives from the number of load steps in ADINA model.

2) $S_0 = S_{AB}$

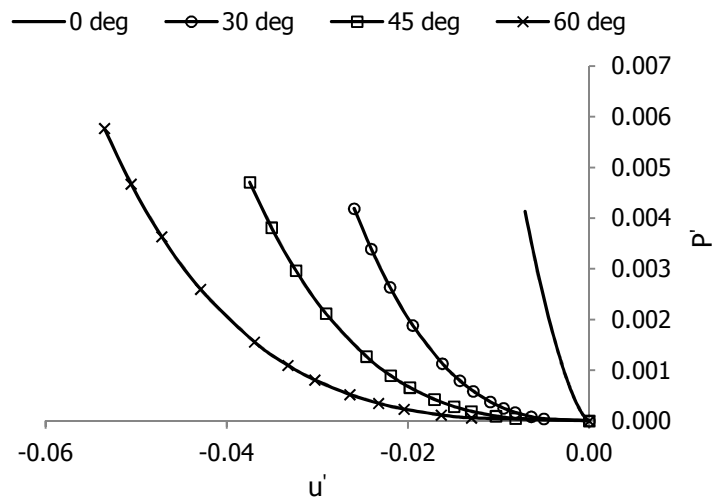


Figure 2-69: Applied load P' as function of horizontal deflection u' for different values of angle θ

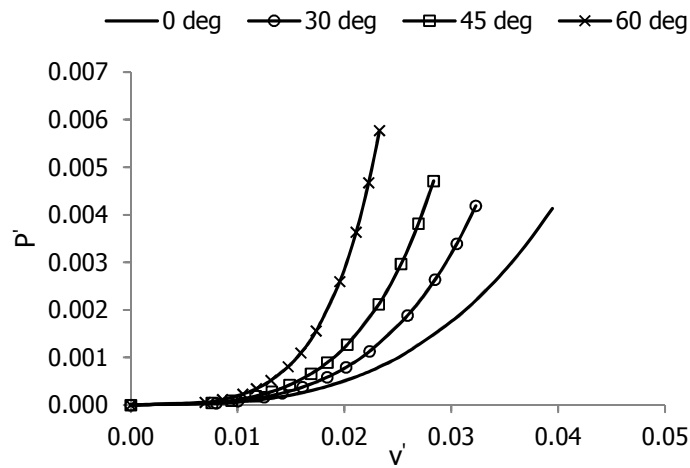


Figure 2-70: Applied load P' as function of vertical deflection v' for different values of angle θ

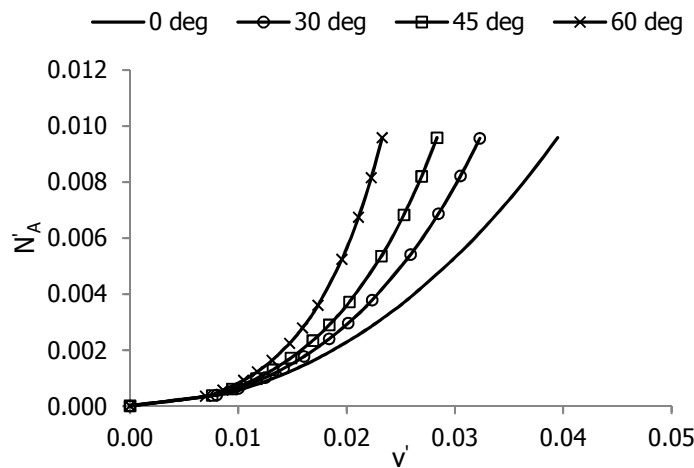


Figure 2-71: Cable's axial force N'_A as function of vertical deflection v' for different values of angle θ

The initial common curve section derives from the number of load steps in ADINA model.

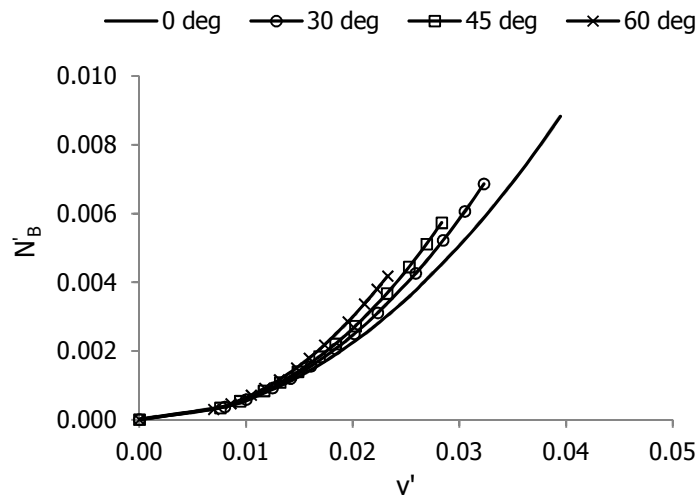


Figure 2-72: Cable's axial force N'_B as function of vertical deflection v' for different values of angle θ

The initial common curve section derives from the number of load steps in ADINA model.

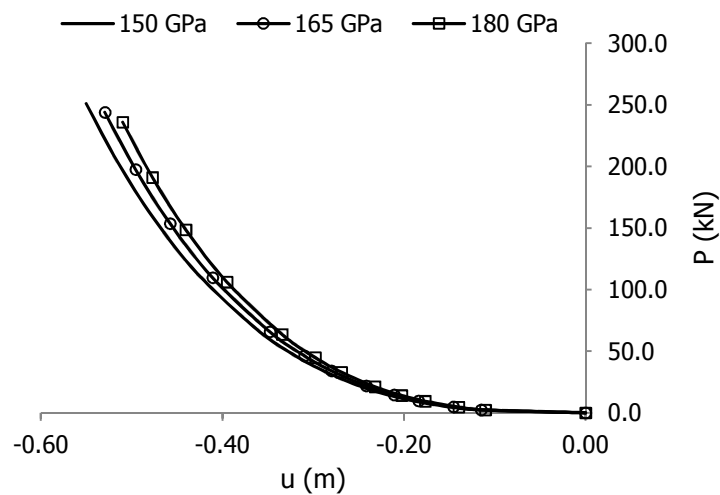


Figure 2-73: Applied load P as function of horizontal deflection u for different values of the modulus of elasticity E

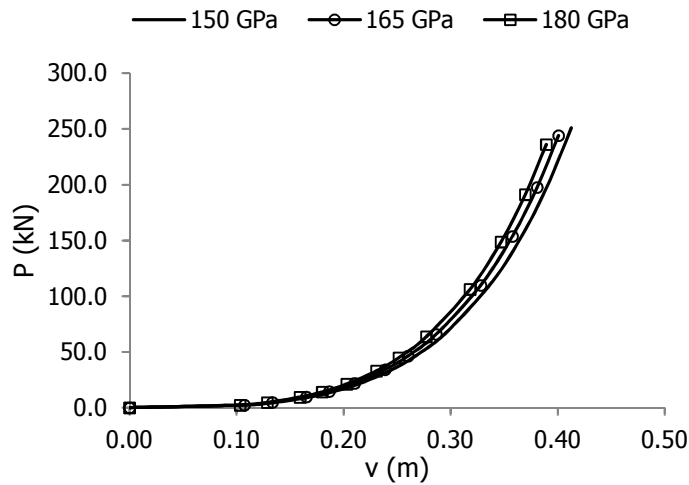


Figure 2-74 Applied load P as function of vertical deflection v for different values of the modulus of elasticity E

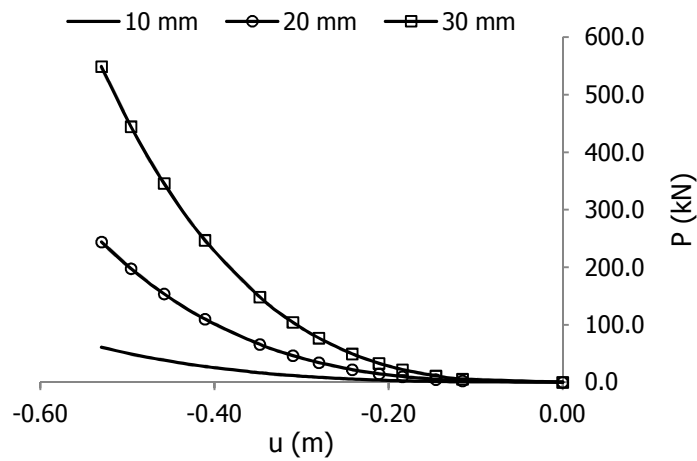


Figure 2-75: Applied load P as function of horizontal deflection u for different values of diameter d_A

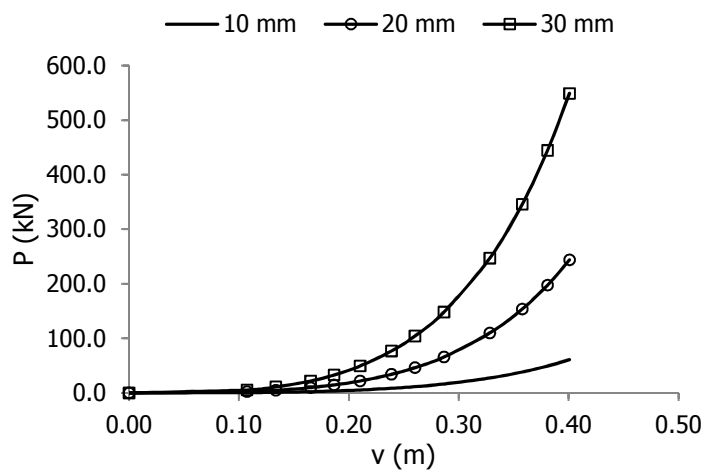


Figure 2-76: Applied load P as function of vertical deflection v for different values of diameter d_A

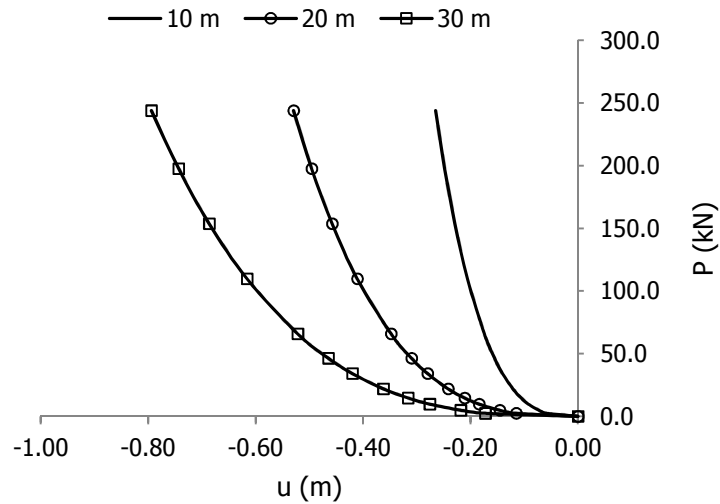


Figure 2-77: Applied load P as function of horizontal deflection u for different values of initial unstressed length S_0

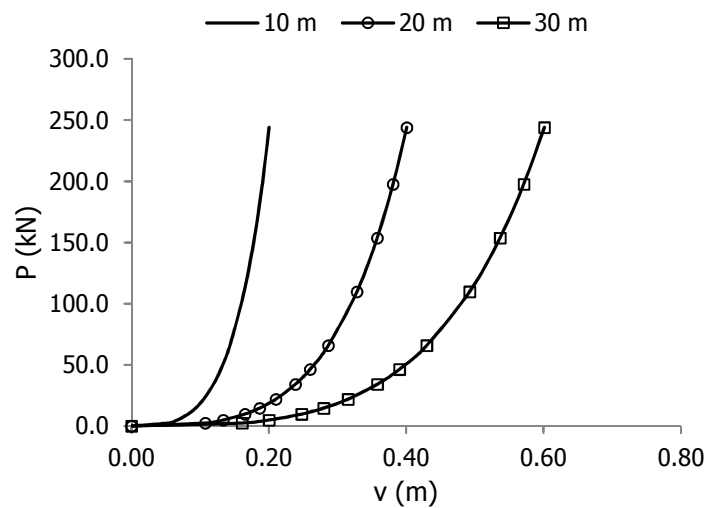


Figure 2-78: Applied load P as function of vertical deflection v for different values of initial unstressed length S_0

3) $S_0 \geq S_{AB}$

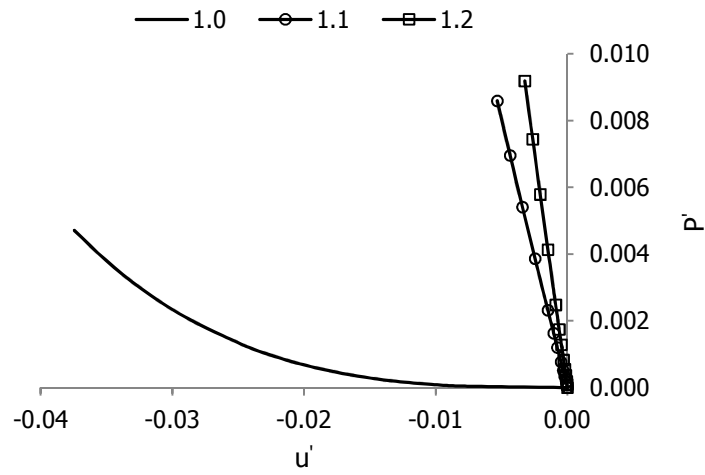


Figure 2-79: Applied load P' as function of horizontal deflection u' for different values of ratio S_0/S_{AB}

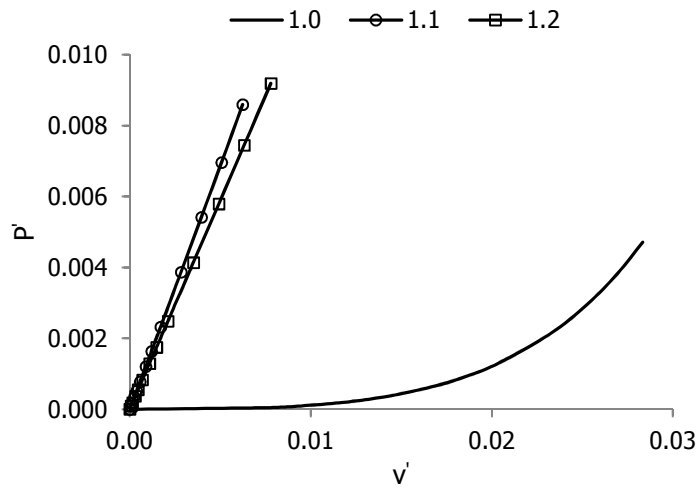


Figure 2-80: Applied load P' as function of vertical deflection v' for different values of ratio S_0/S_{AB}

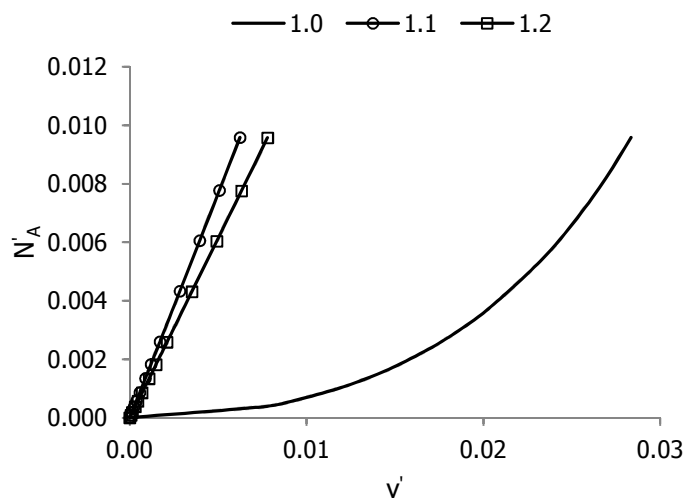


Figure 2-81: Cable's axial force N'_A as function of vertical deflection v' for different values of ratio S_0/S_{AB}

The initial curve angle, in case of $S_0/S_{AB} = 1.0$, derives from the number of load steps in ADINA model.

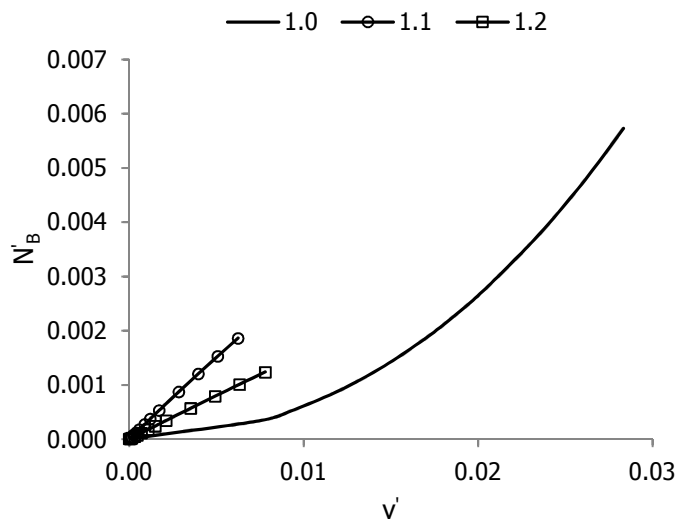


Figure 2-82: Cable's axial force N'_B as function of vertical deflection v' for different values of ratio S_0/S_{AB}

The initial curve angle, in case of $S_0/S_{AB} = 1.0$, derives from the number of load steps in ADINA model.

2.5.4 Diagrams of a horizontal cable under concentrated load at arbitrary position

Diagrams for the case of Paragraph 2.2.3 are presented. Notice that diagrams are designed through ADINA models (contained in the accompanied CD, commented in the list of numerical models with 'analytical') due to the complexity of the 2-degree polynomial solution. Paragraph 3.2.4 verifies the identification between analytical solution and numerical models.

1) $S_0 \leq S_{AB}$

Here, $z^* = 0$ as $S_0 \leq S_{AB}$ and, so, $v' = z'$.

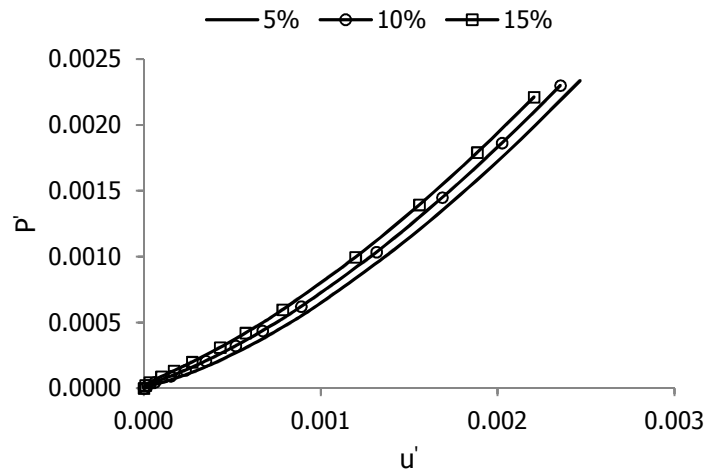


Figure 2-83: Applied load P' as function of horizontal deflection u' for different values of pre-tension w^{pre} , in case that $\alpha = 0.65$

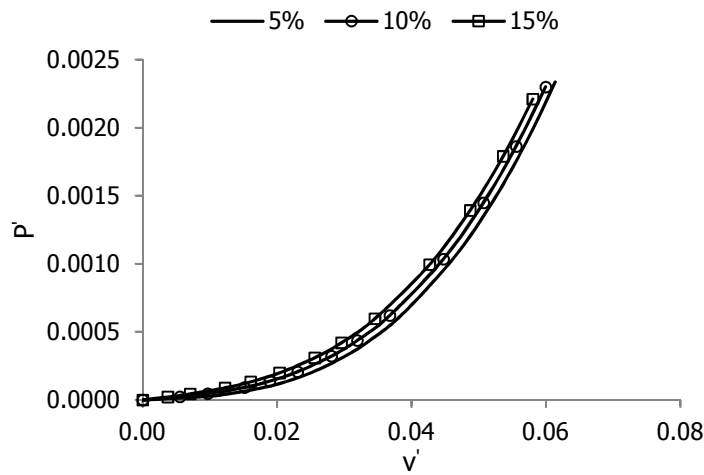


Figure 2-84: Applied load P' as function of vertical deflection v' for different values of pre-tension w^{pre} , in case that $\alpha = 0.65$

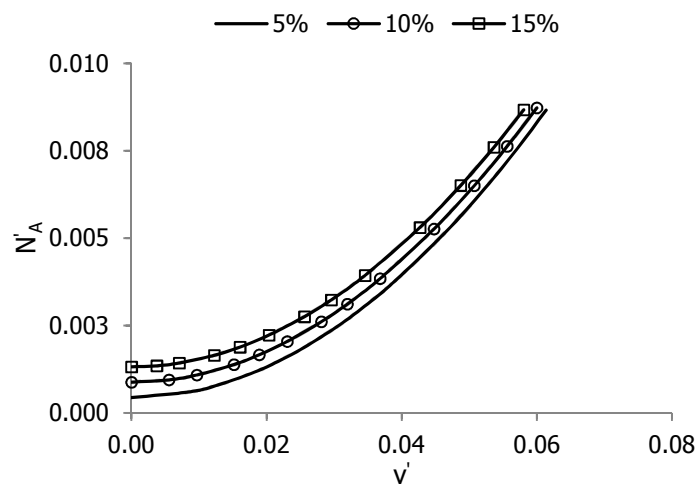


Figure 2-85: Cable's axial force N_A' as function of vertical deflection v' for different values of pre-tension w^{pre} , in case that $\alpha = 0.65$

The initial curve angle, in case of $w^{\text{pre}} = 5\%$, derives from the number of load steps in ADINA model.

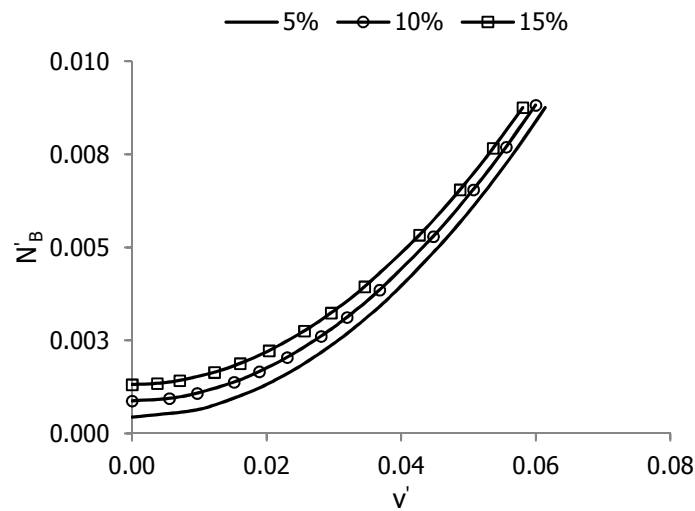


Figure 2-86: Cable's axial force N_B^i as function of vertical deflection v^i for different values of pre-tension w^{pre} , in case that $\alpha = 0.65$

The initial curve angle, in case of $w^{\text{pre}} = 5\%$, derives from the number of load steps in ADINA model.

$$2) \quad S_0 = S_{AB}$$

Here, $z^* = 0$ as $S_0 = S_{AB}$ and, so, $v = z$.

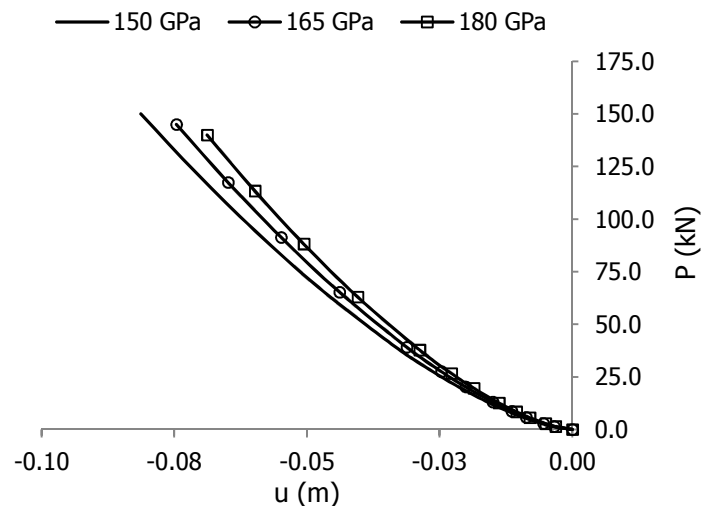


Figure 2-87: Applied load P as function of horizontal deflection u for different values of the modulus of elasticity E , in case that $\alpha = 0.30$

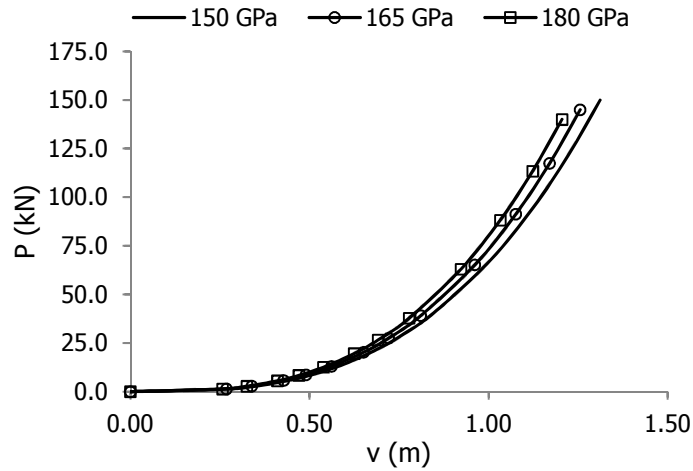


Figure 2-88 Applied load P as function of vertical deflection v for different values of the modulus of elasticity E , in case that $\alpha = 0.30$

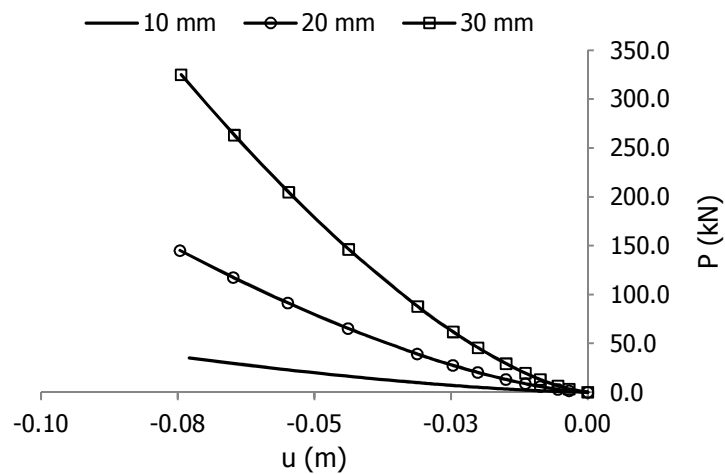


Figure 2-89: Applied load P as function of horizontal deflection u for different values of diameter d_A , in case that $\alpha = 0.30$

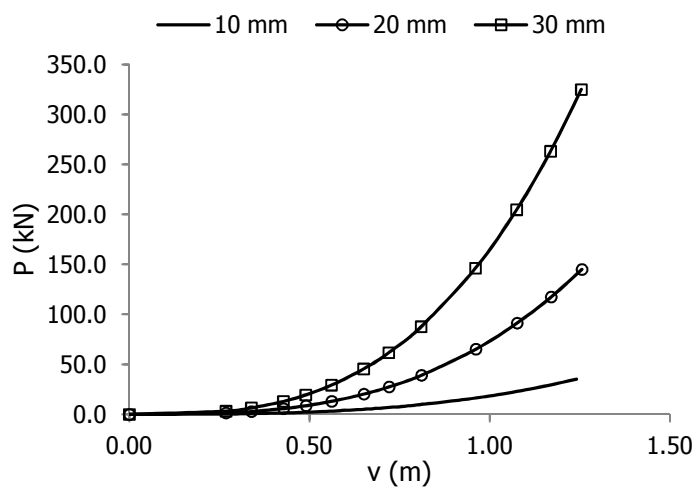


Figure 2-90: Applied load P as function of vertical deflection v for different values of diameter d_A , in case that $\alpha = 0.30$

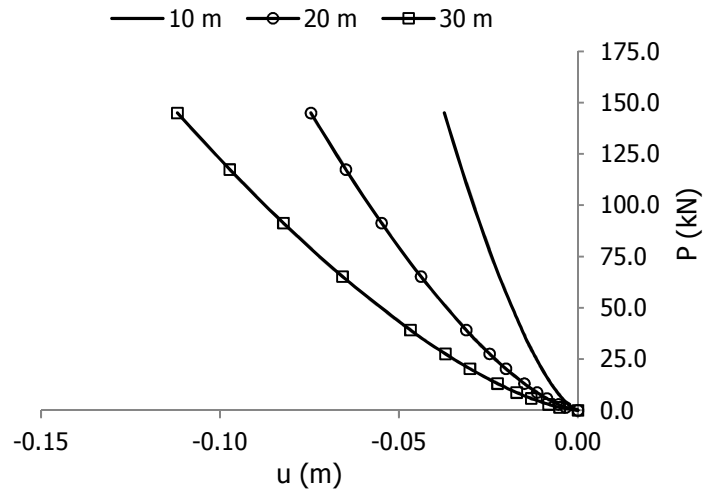


Figure 2-91: Applied load P as function of horizontal deflection u for different values of initial unstressed length S_0 , in case that $\alpha = 0.30$

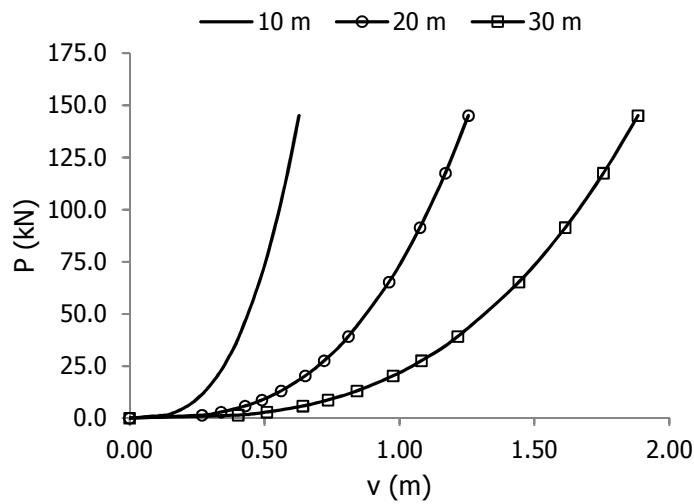


Figure 2-92: Applied load P as function of vertical deflection v for different values of initial unstressed length S_0 , in case that $\alpha = 0.30$

3) $S_0 \geq S_{AB}$

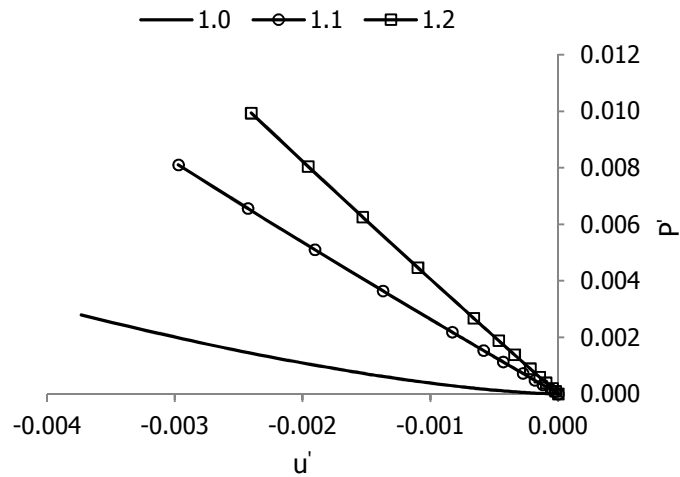


Figure 2-93: Applied load P' as function of horizontal deflection u' for different values of ratio S_0/S_{AB} , in case that $\alpha = 0.30$

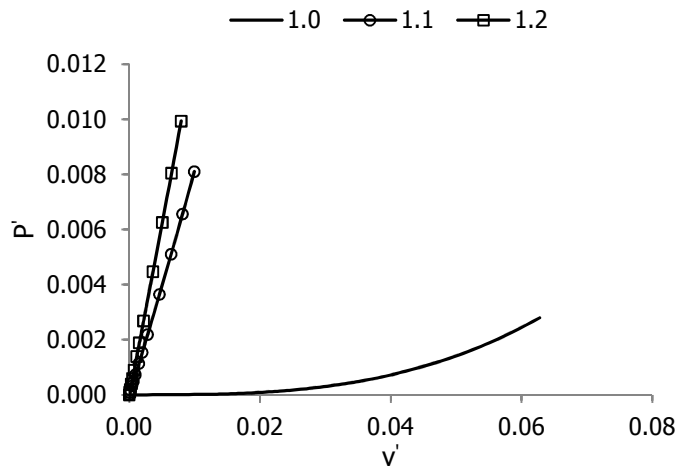


Figure 2-94: Applied load P' as function of vertical deflection v' for different values of ratio S_0/S_{AB} , in case that $\alpha = 0.30$

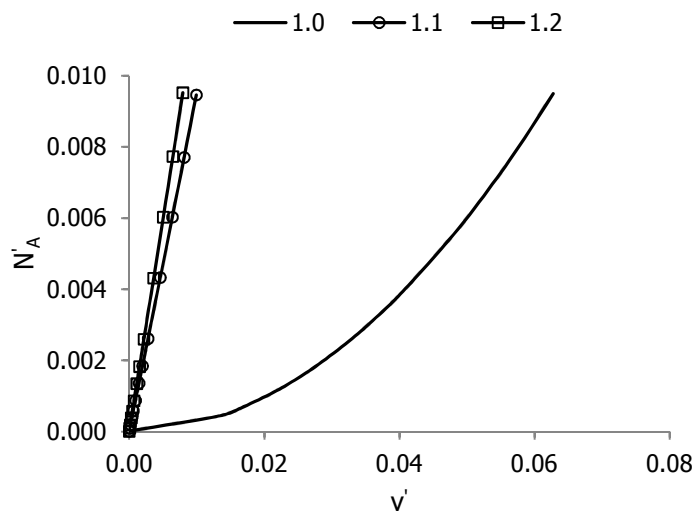


Figure 2-95: Cable's axial force N'_A as function of vertical deflection v' for different values of ratio S_0/S_{AB} , in case that $\alpha = 0.30$

The initial curve angle, in case of $S_0/S_{AB} = 1.0$, derives from the number of load steps in ADINA model.

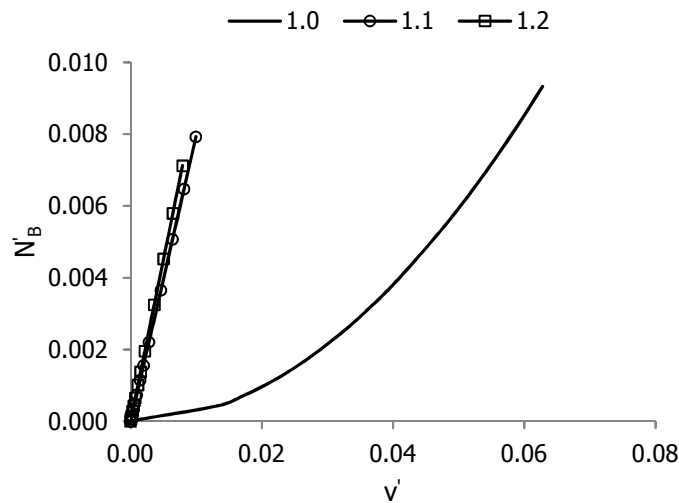


Figure 2-96: Cable's axial force N'_B as function of vertical deflection v' for different values of ratio S_0/S_{AB} , in case that $\alpha = 0.30$

The initial curve angle, in case of $S_0/S_{AB} = 1.0$, derives from the number of load steps in ADINA model.

2.5.5 Diagrams of an inclined cable under imposed end displacement

Using the analysis of Paragraph 2.2.4.1 – case A, the corresponding diagrams are designed. For case B, in other words for an inclined cable under horizontal imposed end displacement u , parametric diagrams are identical with these of case A. Moreover, based on Figure 2-33, which shows identification between the solution for case A and the equivalent linear spring, the following parametric diagrams are valid for this kind of spring.

$$1) \quad S_0 \leq S_{AB}$$

Cables, in this case, are not pre-tensioned as support B is free to move vertical and balance to an unstressed position. Inclined pre-tensioned cables under imposed end displacement are presented analytically in Chapter 5.

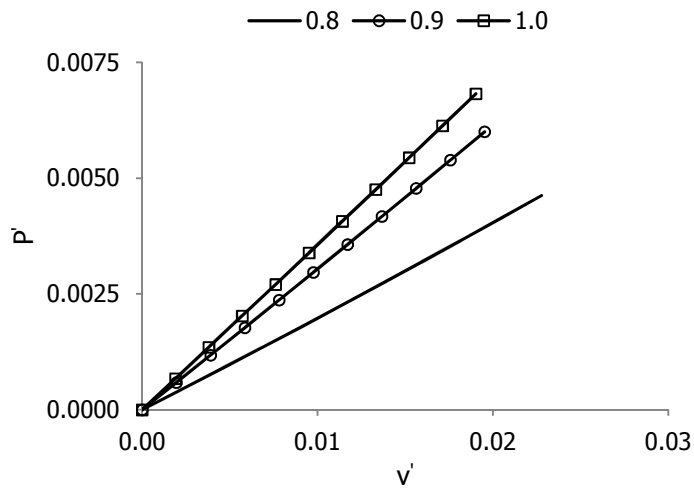


Figure 2-97: Applied load P' as function of vertical deflection v' for different values of ratio S_0/S_{AB}

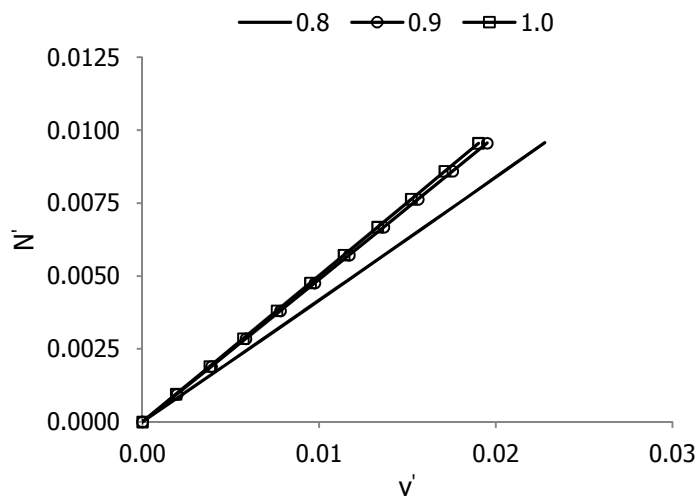


Figure 2-98: Cable's axial force N' as function of vertical deflection v' for different values of ratio S_0/S_{AB}

2) $S_0 = S_{AB}$

Figure for the case of $\theta = 0$ deg cannot be designed as $L = 0$ and, so, $v' = \frac{v}{L}$ cannot be defined.

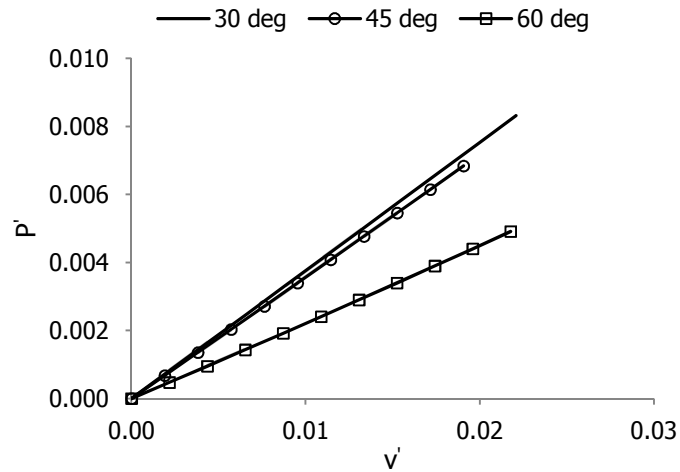


Figure 2-99: Applied load P' as function of vertical deflection v' for different values of angle θ

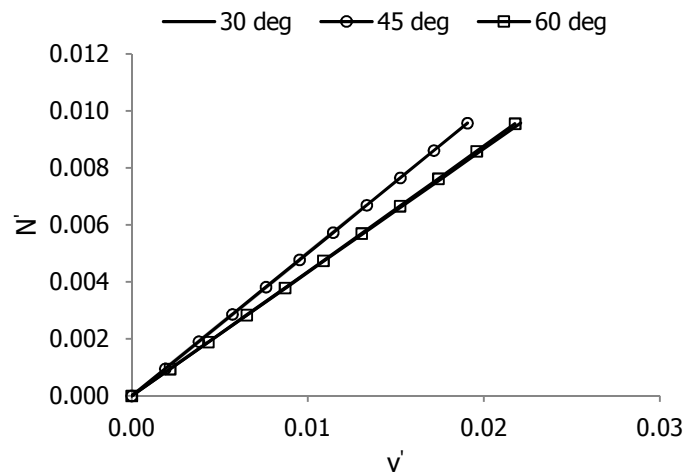


Figure 2-100: Cable's axial force N' as function of vertical deflection v' for different values of angle θ

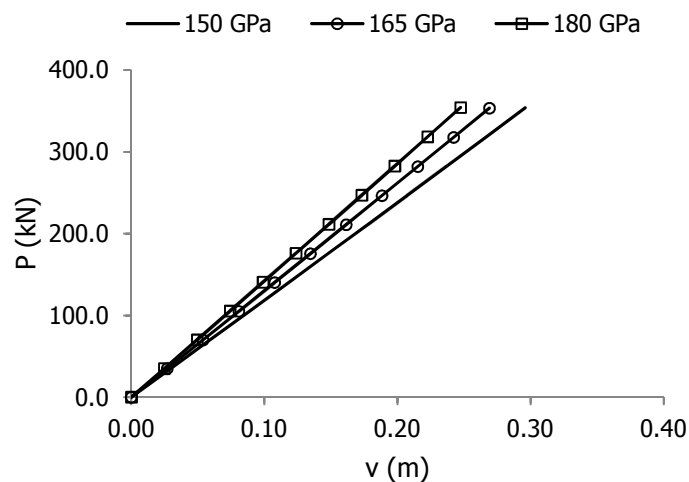


Figure 2-101: Applied load P as function of vertical deflection v for different values of the modulus of elasticity E

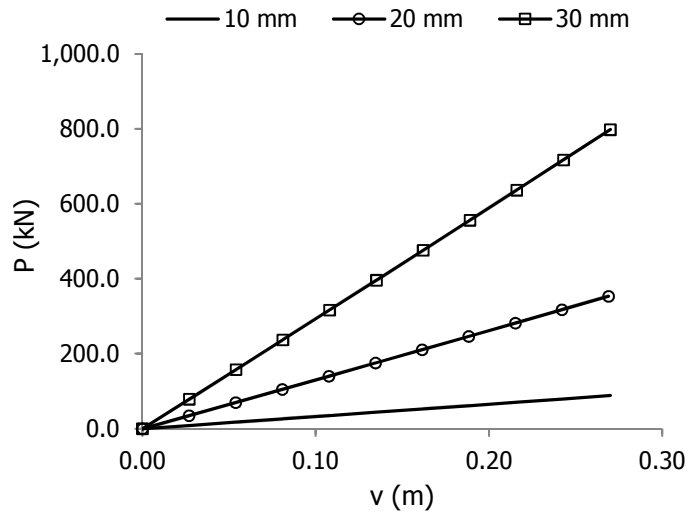


Figure 2-102: Applied load P as function of vertical deflection v for different values of diameter d_A

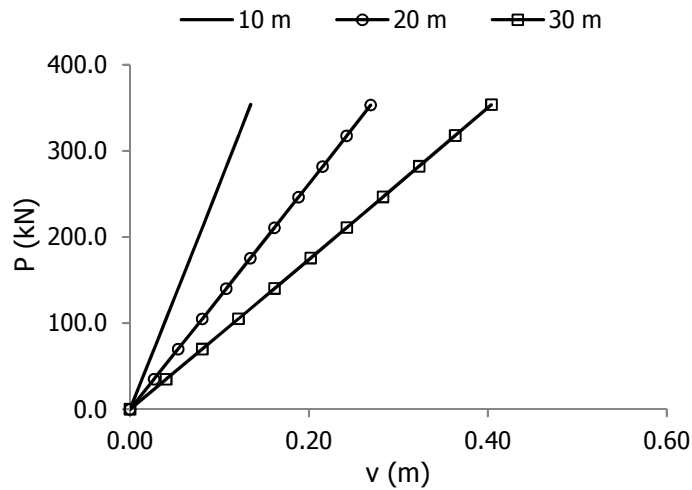


Figure 2-103: Applied load P as function of vertical deflection v for different values of initial unstressed length S_0

3) $S_0 \geq S_{AB}$

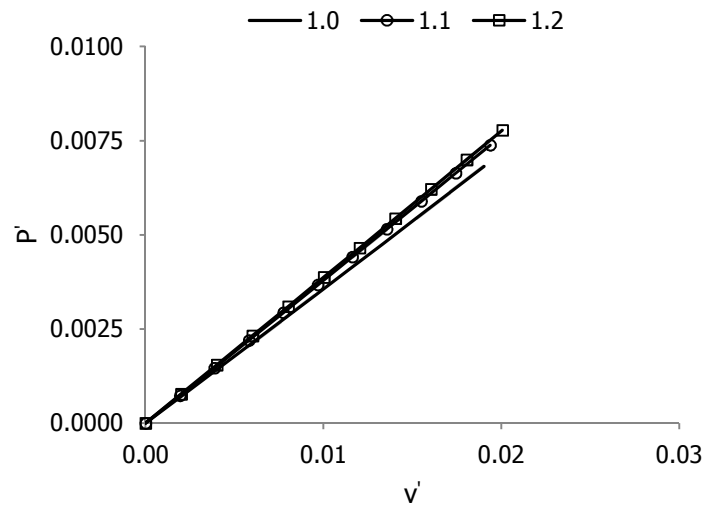


Figure 2-104: Applied load P' as function of vertical deflection v' for different values of ratio S_0/S_{AB}

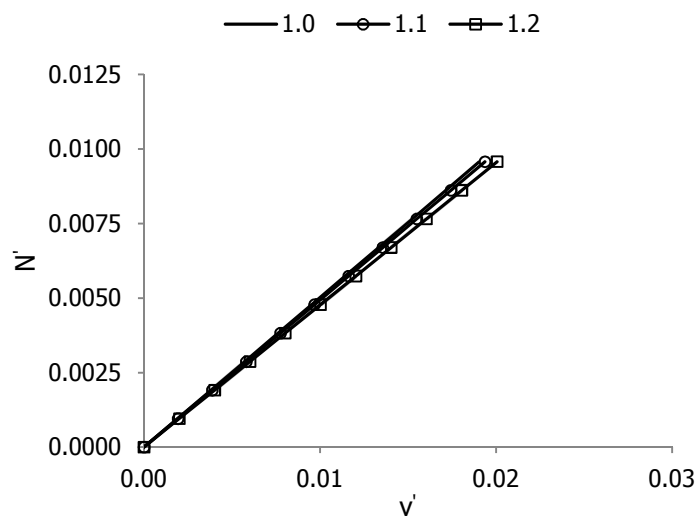


Figure 2-105: Cable's axial force N' as function of vertical deflection v' for different values of ratio S_0/S_{AB}

2.5.6 Diagrams of an inclined cable under uniformly distributed load along its horizontal projection

Diagrams for the cable of Paragraph 2.3.1 are presented.

1) $S_0 \leq S_{AB}$

Here, $v' = d'_m$ as $S_0 \leq S_{AB}$.

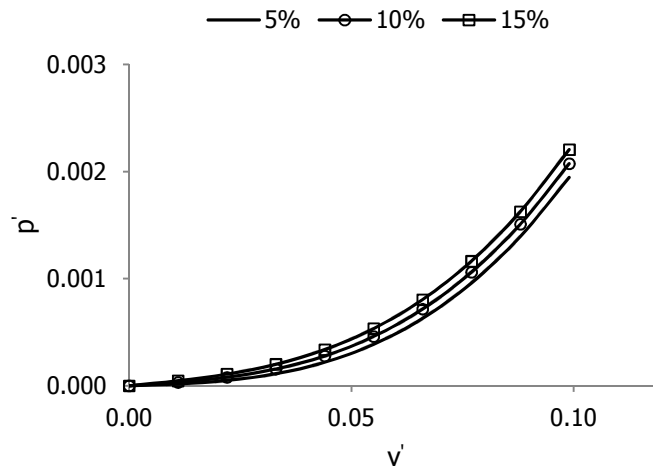


Figure 2-106: Applied load p' as function of vertical deflection v' for different values of pre-tension w^{pre}

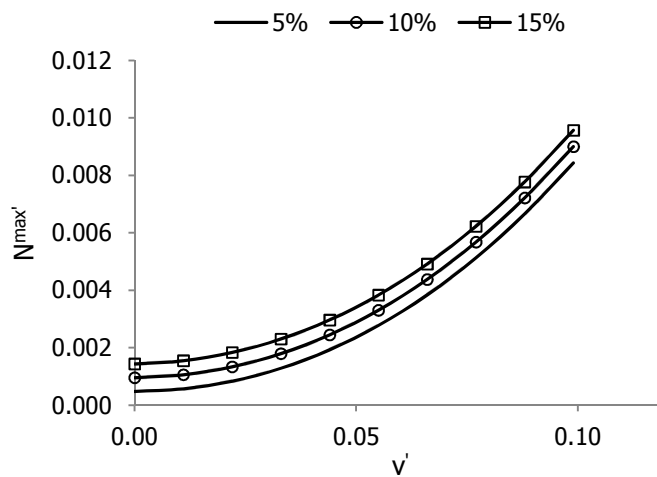


Figure 2-107: Maximum axial force $N^{max'}$ as function of vertical deflection v' for different values of pre-tension w^{pre}

2) $S_0 = S_{AB}$

Here, $v = d_m$ as $S_0 = S_{AB}$.

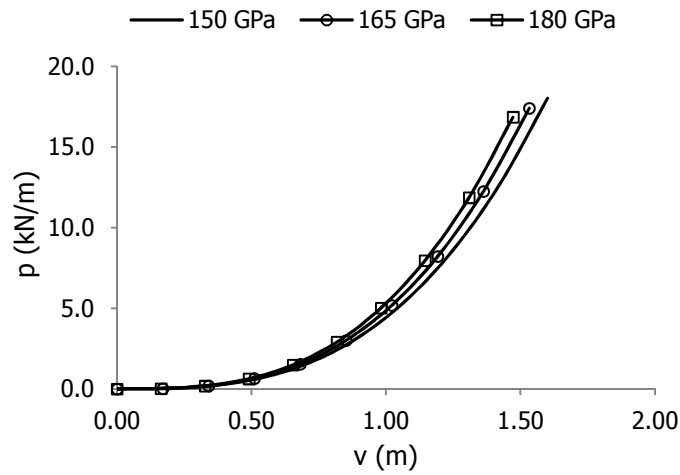


Figure 2-108: Applied load p as function of vertical deflection v for different values of the modulus of elasticity E

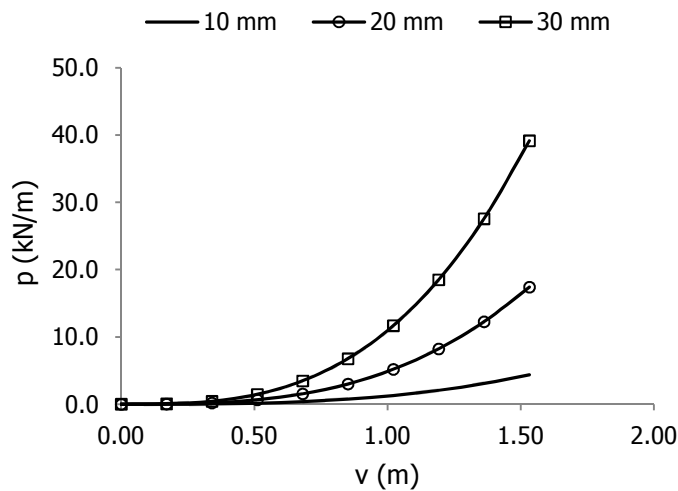


Figure 2-109: Applied load p as function of vertical deflection v for different values of diameter d_A

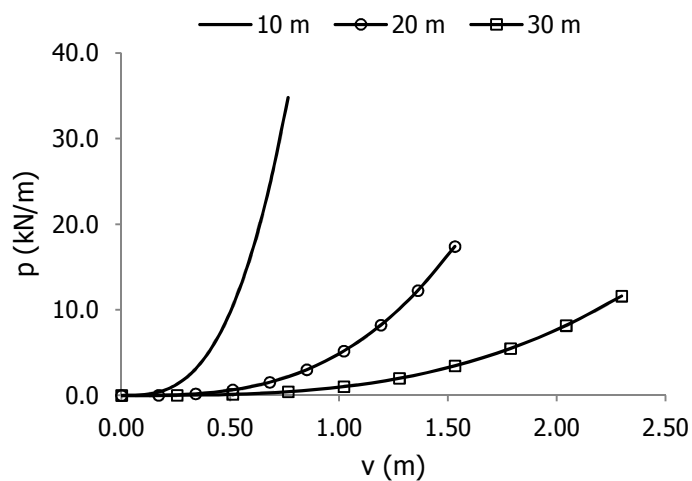


Figure 2-110: Applied load p as function of vertical deflection v for different values of initial unstressed length S_0

3) $S_0 \geq S_{AB}$

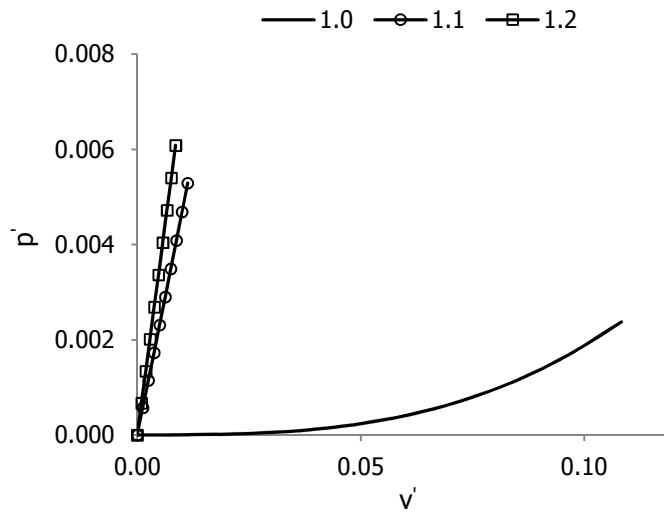


Figure 2-111: Applied load p' as function of vertical deflection v' for different values of ratio S_0/S_{AB}

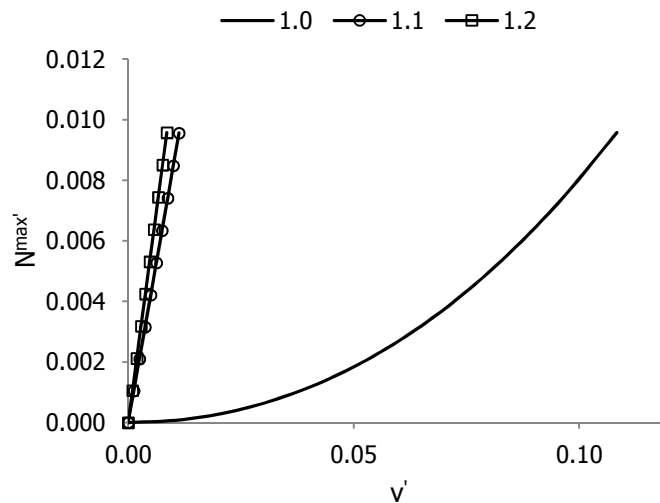


Figure 2-112: Maximum axial force $N^{\max'}$ as function of vertical deflection v' for different values of ratio S_0/S_{AB}

2.5.7 Diagrams of a horizontal cable under uniformly distributed load along its horizontal projection

Diagrams for the case of Paragraph 2.3.2 are designed using the corresponding formulas.

1) $S_0 \leq S_{AB}$

Here, $z^* = 0$ as $S_0 \leq S_{AB}$ and, so, $v' = z' = d_m'$.

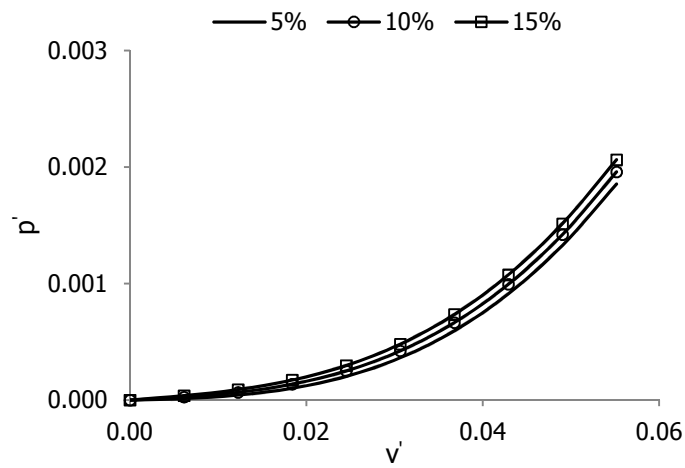


Figure 2-113: Applied load p' as function of vertical deflection v' for different values of pre-tension w^{pre}

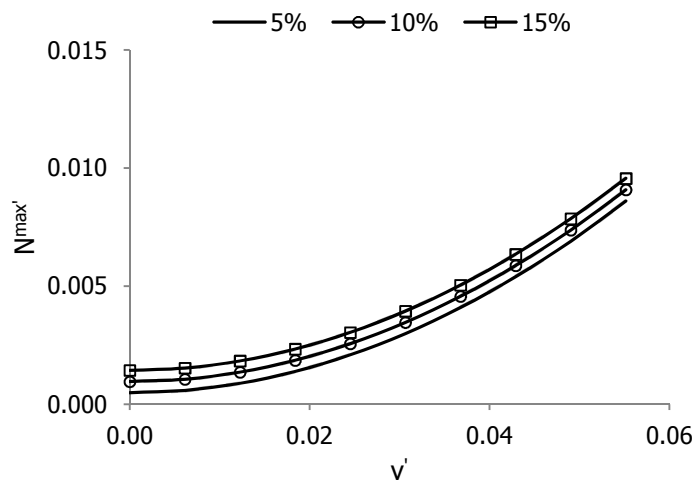


Figure 2-114: Maximum axial force $N^{max'}$ as function of vertical deflection v' for different values of pre-tension w^{pre}

$$2) \quad S_0 = S_{AB}$$

Here, $z^* = 0$ as $S_0 = S_{AB}$ and, so, $v = z = d_m$.

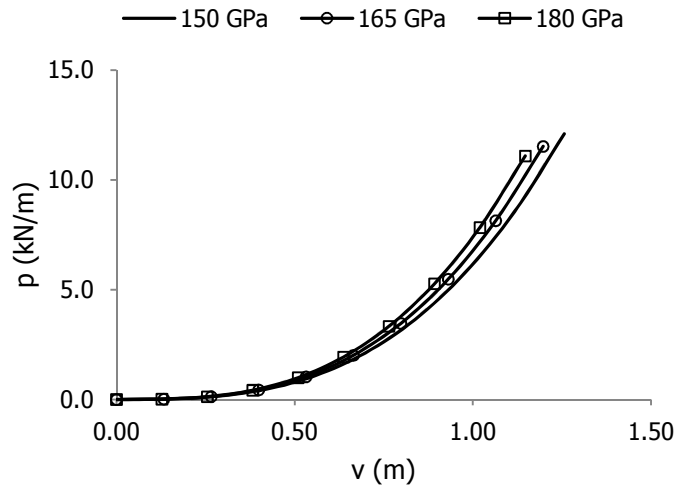


Figure 2-115: Applied load p as function of vertical deflection v for different values of the modulus of elasticity E

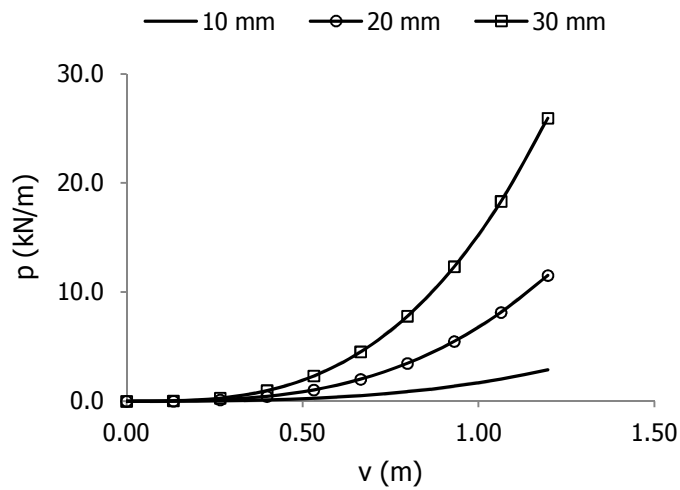


Figure 2-116: Applied load p as function of vertical deflection v for different values of diameter d_A

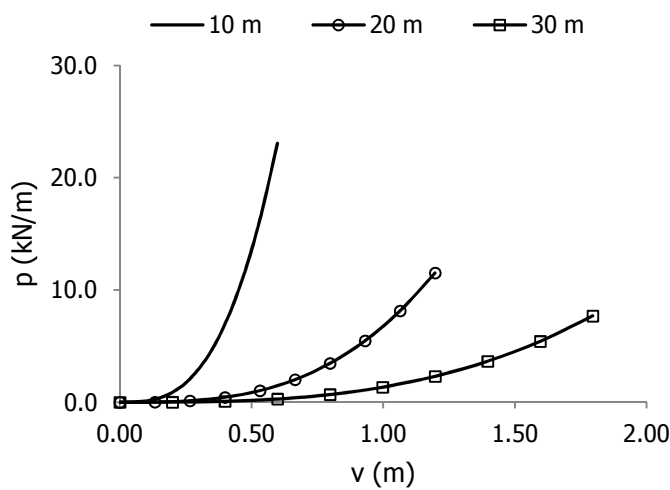


Figure 2-117: Applied load p as function of vertical deflection v for different values of initial unstressed length S_0

3) $S_0 \geq S_{AB}$

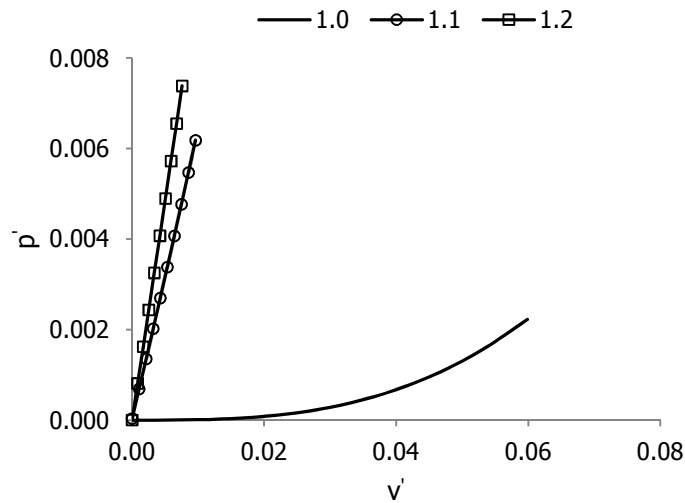


Figure 2-118: Applied load p' as function of vertical deflection v' for different values of ratio S_0/S_{AB}

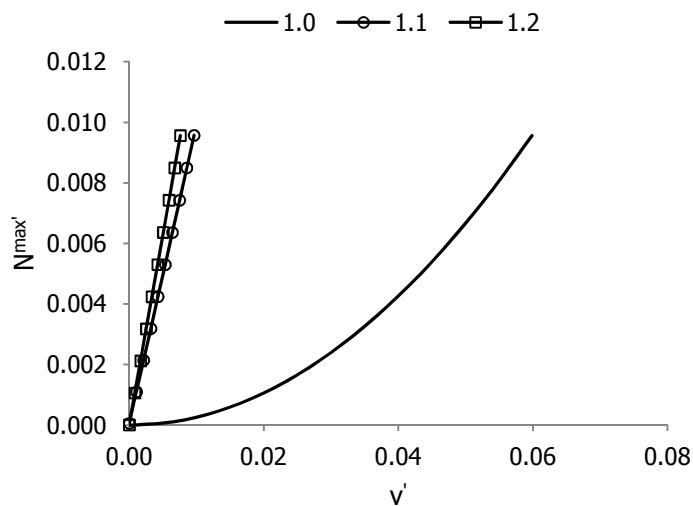


Figure 2-119: Maximum axial force $N^{\max'}$ as function of vertical deflection v' for different values of ratio S_0/S_{AB}

2.5.8 Diagrams of an inclined cable under uniformly distributed load along its arc length

Using analysis of Paragraph 2.3.3, the following comparison diagrams are designed.

1) $S_0 \leq S_{AB}$

Here, $v' = d'_m$ as $S_0 \leq S_{AB}$.

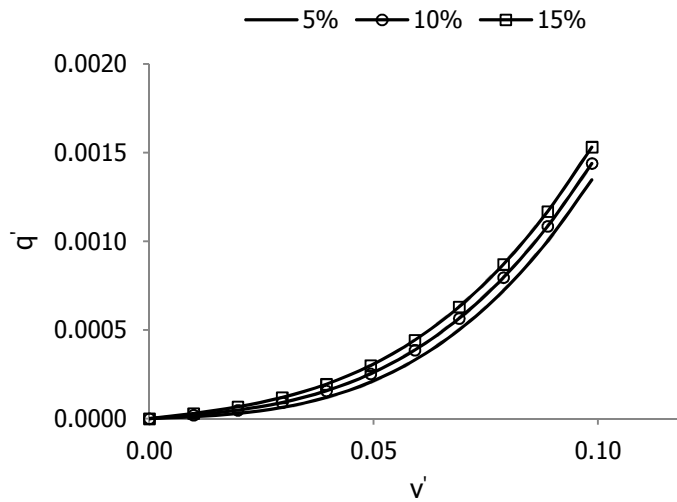


Figure 2-120: Applied load q' as function of vertical deflection v' for different values of pre-tension w^{pre}

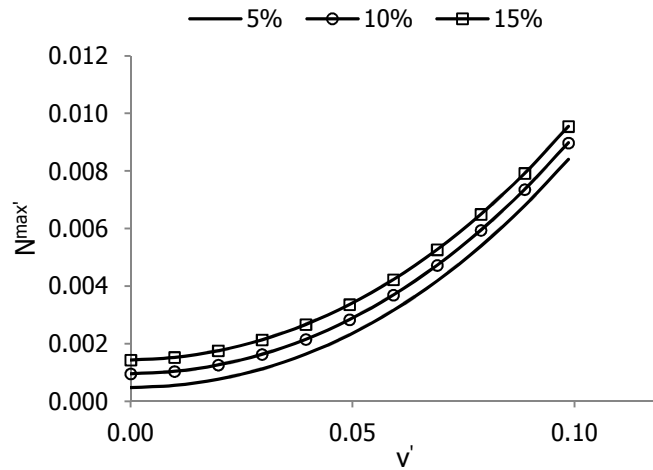


Figure 2-121: Maximum axial force $N^{\text{max}'}$ as function of vertical deflection v' for different values of pre-tension w^{pre}

2) $S_0 = S_{AB}$

Here, $v = d_m$ as $S_0 = S_{AB}$.

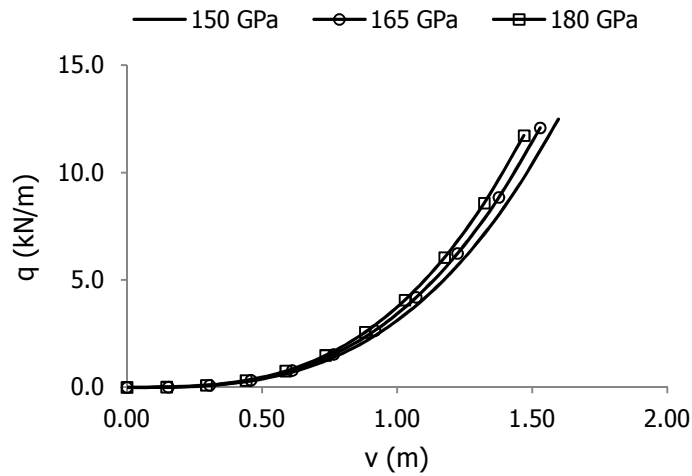


Figure 2-122: Applied load q as function of vertical deflection v for different values of the modulus of elasticity E

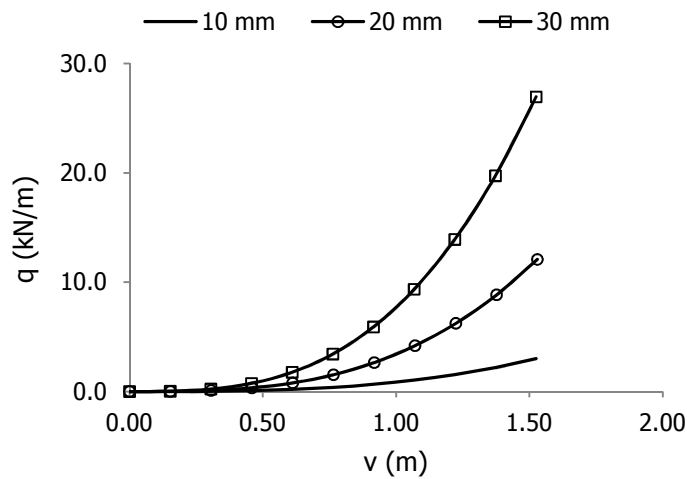


Figure 2-123: Applied load q as function of vertical deflection v for different values of diameter d_A

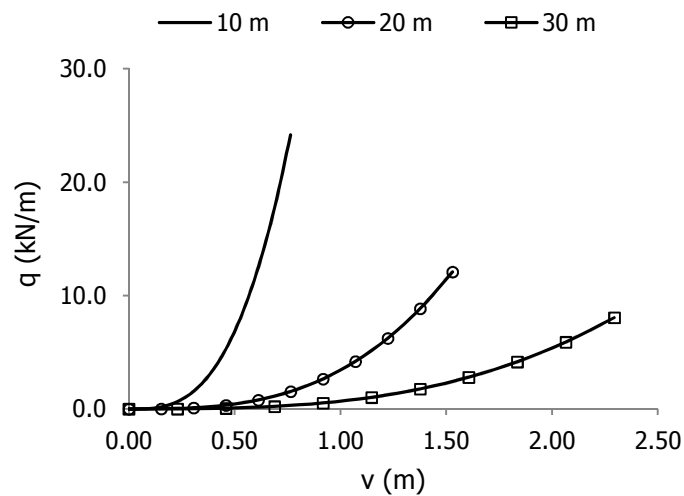


Figure 2-124: Applied load q as function of vertical deflection v for different values of initial unstressed length S_0

3) $S_0 \geq S_{AB}$

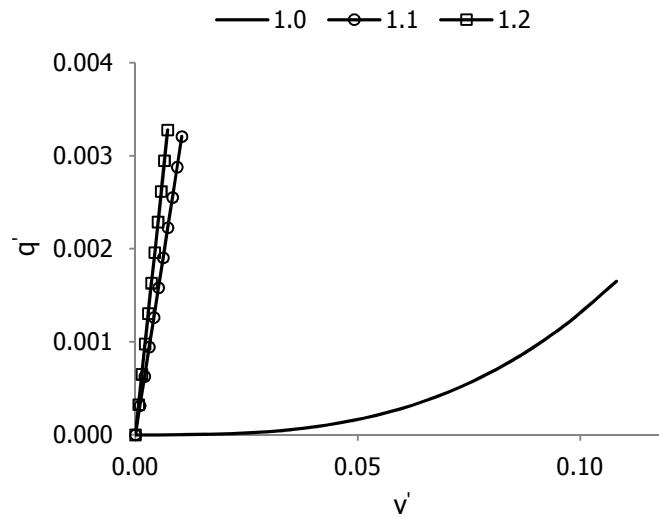


Figure 2-125: Applied load q' as function of vertical deflection v' for different values of ratio S_0/S_{AB}

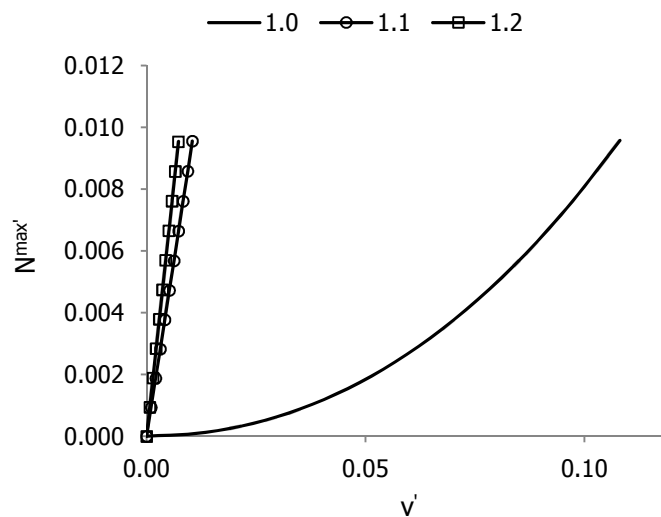


Figure 2-126: Maximum axial force $N^{\max'}$ as function of vertical deflection v' for different values of ratio S_0/S_{AB}

2.5.9 Diagrams of a horizontal cable under uniformly distributed load along its arc length

The response of a horizontal cable under uniformly distributed load along its length is illustrated by the following diagrams, based on Paragraph 2.3.4.

1) $S_0 \leq S_{AB}$

Here, $z^* = 0$ as $S_0 \leq S_{AB}$ and, so, $v' = z' = d'_m$.

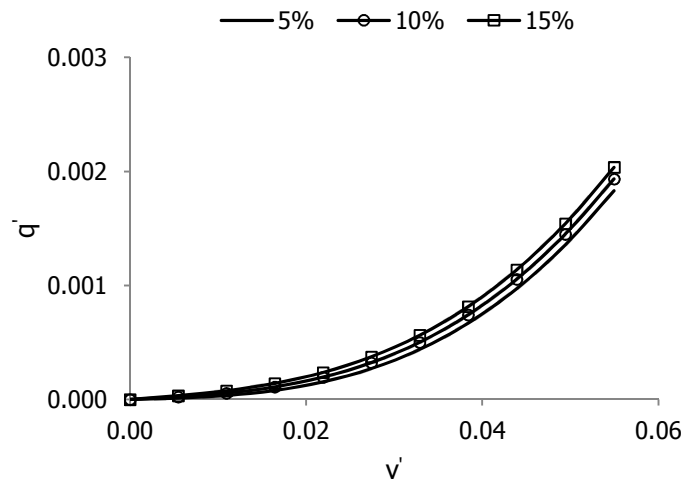


Figure 2-127: Applied load q' as function of vertical deflection v' for different values of pre-tension w^{pre}

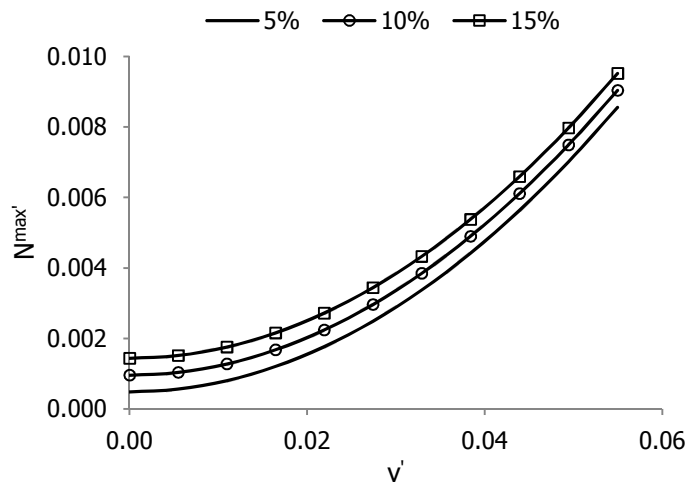


Figure 2-128: Maximum axial force $N^{\text{max}'}$ as function of vertical deflection v' for different values of pre-tension w^{pre}

2) $S_0 = S_{AB}$

Here, $z^* = 0$ as $S_0 = S_{AB}$ and, so, $v = z = d_m$.

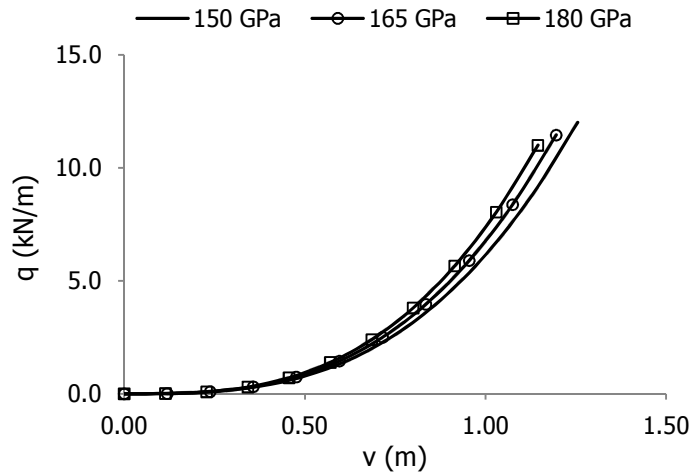


Figure 2-129: Applied load q as function of vertical deflection v for different values of the modulus of elasticity E

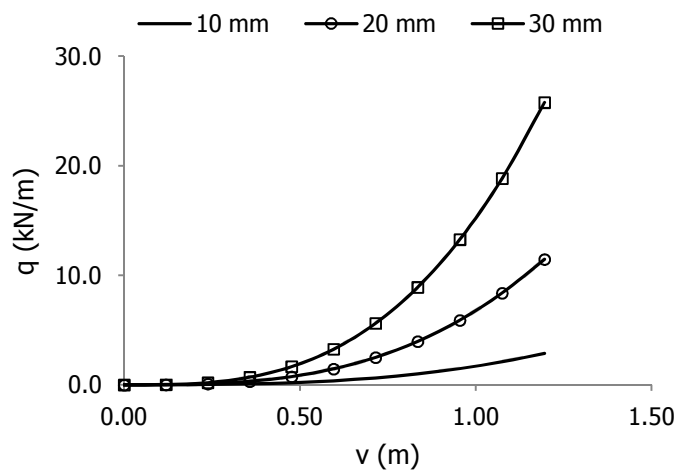


Figure 2-130: Applied load q as function of vertical deflection v for different values of diameter d_A

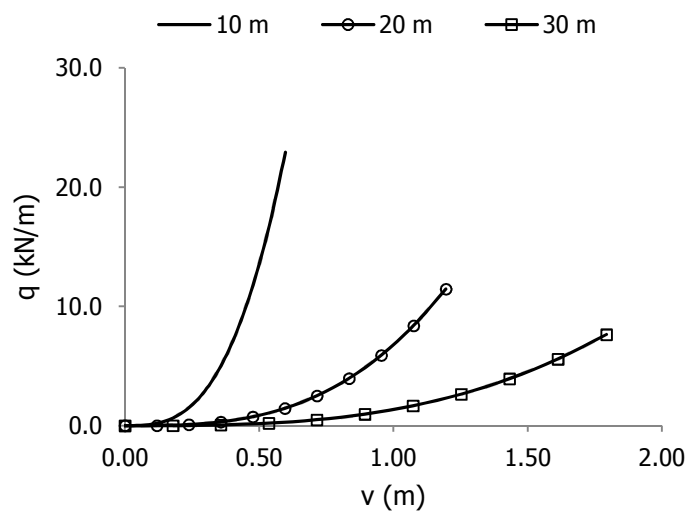


Figure 2-131: Applied load q as function of vertical deflection v for different values of initial unstressed length S_0

3) $S_0 \geq S_{AB}$

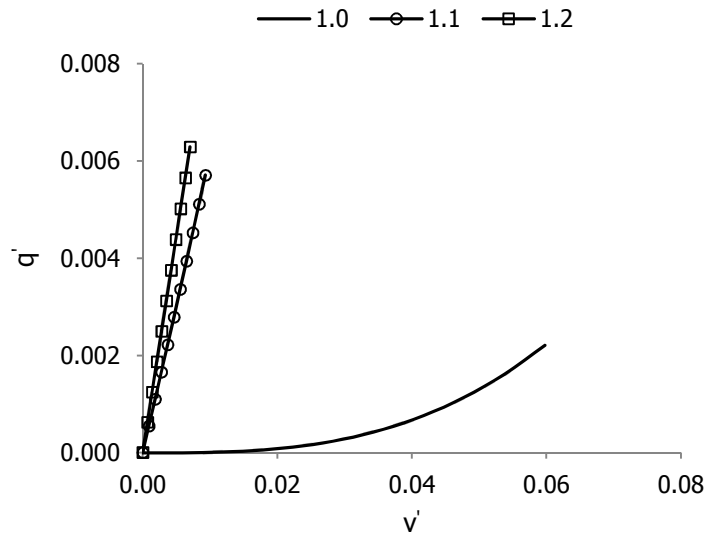


Figure 2-132: Applied load q' as function of vertical deflection v' for different values of ratio S_0/S_{AB}

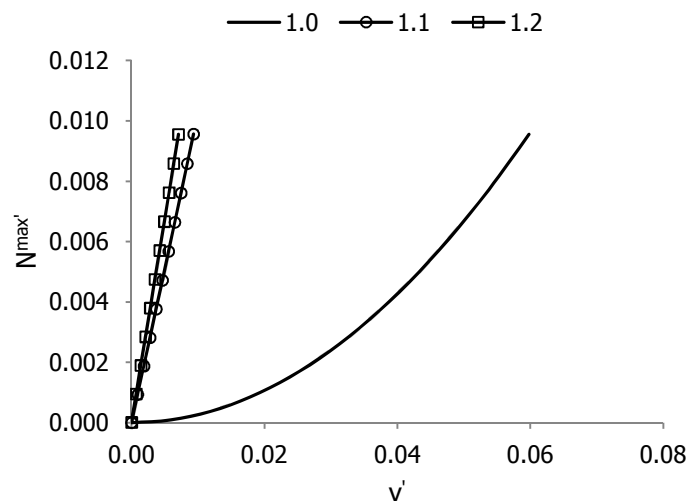


Figure 2-133: Maximum axial force $N^{\max'}$ as function of vertical deflection v' for different values of ratio S_0/S_{AB}

2.5.10 Annotation of parametric figures

Parametric figures of Paragraphs 2.5.2 to 2.5.9 have the same qualitative behavior independently the kind of load, concentrated or distributed, the load position and the inclination of the cable, except from the case of imposed end displacement. Paragraph 2.5.10 describes cable response, in different circumstances, and gives a physical explanation for each one. The aim of this paragraph is to define a catholic behavior of the simple suspended cable.

A simple suspended cable responds to an external load with a combination of geometric adaption and elongation ϵ of the linearly elastic material. The development of deflection

causes axial force N of the cable, which can be analyzed into its horizontal component H and its vertical one V . The more horizontal a cable is the larger the horizontal component H is and the smaller the vertical one V is. The adaption of the cable, which occurs by the development of deflection, introduces the geometric nonlinearity and, according to Eqs. (2-176) to (2-178) of the equivalent beam method, in combination with the horizontal component H of the axial force balance the bending moment of an equivalent beam. In the other hand, the vertical component V of the axial force is opponent to the deflection and is responsible for the development of stiffness in this kind of deflection. The axial force N causes the elongation ε of the cable.

1) $S_0 \leq S_{AB}$

- Applied load as function of deflection for different values of pre-tension w^{pre}

Paragraph 2.5.2 \ Figure 2-58

Paragraph 2.5.3 \ Figures 2-65 and 2-66

Paragraph 2.5.4 \ Figures 2-83 and 2-84

Paragraph 2.5.6 \ Figure 2-106

Paragraph 2.5.7 \ Figure 2-113

Paragraph 2.5.8 \ Figure 2-120

Paragraph 2.5.9 \ Figure 2-127

Given a constant value of applied load, the larger the pre-tension w^{pre} is the smaller deflection (in absolute values) occurs. Pre-tension w^{pre} gives initial stiffness to the cable. It is applied by the elongation of an initial unstressed cable, with length $S_0 \leq S_{AB}$. The stressed state of a pre-tensioned cable is equivalent to this of a non pre-tensioned cable imposed to a load, in other words the corresponding point at equilibrium path is placed at an intermediate position with increased stiffness. This stiffness is regarding as the initial one due to pre-tension w^{pre} . Curves seems to be parallel, as pre-tension w^{pre} does not affect the way the stiffness increases, and shifted in a constant value, as pre-tension step is constant. Pre-tension cables fulfill more efficient service demands.

Paragraph 2.5.5 \ Figure 2-97

Given a constant value of applied load, the smaller the ratio S_0/S_{AB} is the larger deflection occurs. As the ratio S_0/S_{AB} decreases, the cable is more horizontal. So, the vertical component V of the axial force decreases, in other words the stiffness in vertical deflection decreases, and the horizontal component H of the axial force increases. So, geometric nonlinearity is more intense, as for $S_0/S_{AB} = 0.8$ the curve is less linear. Bear in mind that, as the ratio S_0/S_{AB} decreases the initial unstressed length S_0 decreases and for a constant elongation ε , where:

$$\varepsilon = \frac{\Delta S}{S_0}, \quad (2-189)$$

the amount ΔS , in other words the deflection, decreases. In the same time two contradictory tendencies, regarding the relationship S_0/S_{AB} and deflection, take place. In Figure 2-97, the first one prevails.

- Axial force of the cable as function of deflection for different values of pre-tension w^{pre}

Paragraph 2.5.2 \ Figure 2-59

Paragraph 2.5.3 \ Figures 2-67 and 2-68

Paragraph 2.5.4 \ Figures 2-85 and 2-86

Paragraph 2.5.6 \ Figure 2-107

Paragraph 2.5.7 \ Figure 2-114

Paragraph 2.5.8 \ Figure 2-121

Paragraph 2.5.9 \ Figure 2-128

Given a constant value of deflection, the larger the pre-tension w^{pre} is the larger axial force of the cable occurs. Larger values of pre-tension w^{pre} means larger value of elongation ΔS and, based on Hooke's law, in case of pre-tension w^{pre} :

$$\sigma^{\text{pre}} = E\varepsilon \Rightarrow \frac{N^{\text{pre}}}{A} = E \frac{\Delta S}{S_0} \quad (2-190)$$

larger value of N^{pre} . This increase provokes corresponding increase in the axial force of the cable imposed to a load.

Paragraph 2.5.5 \ Figure 2-98

Given a constant value of axial force of the cable, the smaller the ratio S_0/S_{AB} is the larger deflection occurs and the more intense the geometric nonlinearity is. Figure 2-98 follows the qualitative behavior and the reasoning of Figure 2-97.

2) $S_0 = S_{AB}$

- Applied load as function of deflection for different values of angle θ

Paragraph 2.5.3 \ Figures 2-69

Given a constant value of applied load, the smaller the angle θ is, in other words the more horizontal the cable is, the smaller horizontal deflection occurs. The horizontal component H of the axial force increases, in other words the stiffness in horizontal deflection increases.

Paragraph 2.5.3 \ Figures 2-70

Given a constant value of applied load, the smaller the angle θ is, in other words the more horizontal the cable is, the larger vertical deflection occurs. The vertical component V of the axial force decreases, in other words the stiffness in vertical deflection decreases. Notice that, in case of distributed loads the opposite qualitative behavior occurs, according to Figures 2-39 and 2-49, as the response mechanism of the cable differs.

Paragraph 2.5.5 \ Figure 2-99

Given a constant value of applied load, the smaller the angle θ is, in other words the less horizontal the cable is, the smaller deflection occurs. Figure 2-99 follows the qualitative behavior and the reasoning of Figure 2-97.

- Axial force of the cable as function of deflection for different values of angle θ

Paragraph 2.5.3 \ Figures 2-71 and 2-72

Given a constant value of axial force of the cable, the smaller the angle θ is, in other words the more horizontal the cable is, the larger deflection occurs. The vertical component V of the axial force decreases, in other words the stiffness in vertical deflection decreases. Notice that, in case of distributed loads the opposite qualitative behavior occurs, according to Figures 2-40 and 2-50, as the response mechanism of the cable differs.

Paragraph 2.5.5 \ Figure 2-100

Figure 2-100 follows the qualitative behavior and the reasoning of Figure 2-97. There is not clear prevalence of one single tendency, regarding the relationship S_0/S_{AB} and deflection.

- Applied load as function of deflection for different values of the modulus of elasticity E

Paragraph 2.5.2 \ Figure 2-60
 Paragraph 2.5.3 \ Figures 2-73 and 2-74
 Paragraph 2.5.4 \ Figures 2-87 and 2-88
 Paragraph 2.5.5 \ Figure 2-101
 Paragraph 2.5.6 \ Figure 2-108
 Paragraph 2.5.7 \ Figure 2-115
 Paragraph 2.5.8 \ Figure 2-122
 Paragraph 2.5.9 \ Figure 2-129

Given a constant value of applied load, the larger the modulus of elasticity E the smaller deflection (in absolute values) occurs. Assuming that constant value of applied load gives constant value of axial force of the cable, the increase of the modulus of elasticity E in Hooke's law:

$$\sigma = E\varepsilon \Rightarrow \sigma = \frac{N}{A} = E \frac{\Delta S}{S_0} \quad (2-191)$$

leads to decrease of the elongation ε , in other words to the deflection. In case of an imposed end displacement, curves are almost linear as the applied load P is delivered mainly by the elongation ε of the cable, whose material is linearly elastic, and less by adapting cable geometry, which causes nonlinearity.

- Applied load as function of deflection for different values of diameter d_A

Paragraph 2.5.2 \ Figure 2-61
 Paragraph 2.5.3 \ Figures 2-75 and 2-76
 Paragraph 2.5.4 \ Figures 2-89 and 2-90
 Paragraph 2.5.5 \ Figure 2-102
 Paragraph 2.5.6 \ Figure 2-109
 Paragraph 2.5.7 \ Figure 2-116
 Paragraph 2.5.8 \ Figure 2-123
 Paragraph 2.5.9 \ Figure 2-130

Given a constant value of applied load, the larger the diameter d_A the smaller deflection (in absolute values) occurs. Assuming that constant value of applied load gives constant value of axial force of the cable, the increase of diameter d_A , in other words of the cross-section A, in Hooke's law of Eq. (2-191) leads to decrease of the elongation ε , in other words to the deflection. In case of an imposed end displacement, curves are almost linear as the applied load P is delivered mainly by the elongation ε of the cable, whose material is linearly elastic, and less by adapting cable geometry, which causes nonlinearity.

- Applied load as function of deflection for different values of initial unstressed length S_0

Paragraph 2.5.2 \ Figure 2-62
 Paragraph 2.5.3 \ Figures 2-77 and 2-78
 Paragraph 2.5.4 \ Figures 2-91 and 2-92
 Paragraph 2.5.5 \ Figure 2-103
 Paragraph 2.5.6 \ Figure 2-110
 Paragraph 2.5.7 \ Figure 2-117
 Paragraph 2.5.8 \ Figure 2-124
 Paragraph 2.5.9 \ Figure 2-131

Given a constant value of applied load, the larger the initial unstressed length S_0 the larger deflection (in absolute values) occurs. Assuming that constant value of applied load gives constant value of axial force of the cable, the elongation ϵ is constant in Hooke's law of Eq. (2-191). The increase of initial unstressed length S_0 leads to the increase of the amount ΔS , which indicates the deflection. In case of an imposed end displacement, curves are almost linear as the applied load P is delivered mainly by the elongation ϵ of the cable, whose material is linearly elastic, and less by adapting cable geometry, which causes nonlinearity.

3) $S_0 \geq S_{AB}$

- Applied load as function of deflection for different values of ratio S_0/S_{AB}

Paragraph 2.5.2 \ Figure 2-63

Paragraph 2.5.3 \ Figures 2-79 and 2-80

Paragraph 2.5.4 \ Figures 2-93 and 2-94

Paragraph 2.5.6 \ Figure 2-111

Paragraph 2.5.7 \ Figure 2-118

Paragraph 2.5.8 \ Figure 2-125

Paragraph 2.5.9 \ Figure 2-132

Given a constant value of applied load, the larger the ratio S_0/S_{AB} is the smaller deflection occurs and the less intense the geometric nonlinearity is. As the ratio S_0/S_{AB} increases, cable segments, after its deployment and before the development of axial force N , is less horizontal. So, the vertical component V of the axial force increases, in other words the stiffness in vertical deflection increases, and the horizontal component H of the axial force significantly decreases. So, geometric nonlinearity is eliminated, as in case that $S_0/S_{AB} = 1.1$ and 1.2 . In the same time, the second tendency, regarding the relationship S_0/S_{AB} and deflection, which is analyzed in Eq. (2-189), takes place reasoning the curve for $S_0/S_{AB} = 1.1$ in relevance with this for $S_0/S_{AB} = 1.2$.

Paragraph 2.5.5 \ Figure 2-104

Figure 2-104 follows the qualitative behavior and the reasoning of Figure 2-97.

- Axial force of the cable as function of deflection for different values of ratio S_0/S_{AB}

Paragraph 2.5.2 \ Figure 2-64

Paragraph 2.5.3 \ Figures 2-81 and 2-82

Paragraph 2.5.4 \ Figures 2-95 and 2-96

Paragraph 2.5.6 \ Figure 2-112

Paragraph 2.5.7 \ Figure 2-119

Paragraph 2.5.8 \ Figure 2-126

Paragraph 2.5.9 \ Figure 2-133

Figures follow the qualitative behavior and the reasoning of figures for applied load as function of deflection for different values of ratio S_0/S_{AB} .

Paragraph 2.5.5 \ Figure 2-105

Given a constant value of axial force of the cable, the smaller the ratio S_0/S_{AB} is the smaller deflection occurs. Here, taking into account Hooke's law of Eq. (2-191), the second tendency, regarding the relationship S_0/S_{AB} and deflection, which is analyzed in Eq. (2-189), prevails.

3. NUMERICAL SOLUTIONS FOR THE STATIC BEHAVIOUR OF SIMPLE CABLES

3.1 NUMERICAL MODELING OF CABLES

This chapter presents the numerical solutions for the static behavior of simple suspended cables. In Chapter 2, analytical expressions for simple cables have been derived, describing their response taking into account their geometric nonlinearity. However, material nonlinearity was neglected and simplifications were made in order to overcome the difficulty of complex mathematics.

The scope of this chapter is to compare the results from finite element software with those derived from analytical solutions, thus to confirm the rightness of cable analytical equations. The comparison is carried out for a simple suspended cable for different properties and load conditions. Cables are modeled to sustain only tension.

The finite element analysis software that are used are ADINA and SAP, which can perform linear and nonlinear analyses of structures, including effects of material nonlinearities and large deformations. They offer versatile and, generally, applicable finite elements for solids, trusses, beams, pipes, plates, shells, etc. Material models for steel, concrete etc. are available. They can include initial strains or stresses in order to consider a deformed state from a previous analysis. The results can be plotted in figures or listed in tables. Snapshots of the cable model can also be taken. More information can be found at references [7] and [8].

Regarding the numerical analyses performed in this chapter, the following assumptions are adopted:

- the cables are modeled as 10 truss elements
- the cross-sectional area of the element remains unchanged
- large displacements – small strains are assumed

Each model case is analyzed by both programs, ADINA and SAP. The name given to models identifies the paragraph of the corresponding analytical solution and their major properties. Here are the parameters which are taken into account during the cable modeling.

loading: a cable is imposed under concentrated loads varying in their application position a , end displacements and uniformly distributed loads along its horizontal projection and along its arc length

cable's properties: there is a variation in the inclination (angle θ), the initial unstressed length S_0 , the modulus of elasticity E and the diameter d_A of the cross-section

effects of cable length: cable's initial unstressed length S_0 is considered shorter (pre-tension), equal and larger than the distance spanned S_{AB}

X-axis in numerical models is identical with this defined in Chapter 2 but z-axis is opposite and, so, change in \pm signs of the numerical results should be made before the design of figures. The coordinates x^* , z^* , which define the coordinates of the point from which cable tension, due to the load P , p or q , occurs, are identical to the coordinates x_p , z_p , which are the coordinates of the starting application point of the concentrated load P , and they are defined in numerical cable models. The number of load steps is chosen depended on the wished detailed results. Then, 10 load values and the corresponding cable analysis results are used to design the figures. Exception is the SAP models of a simple cable under uniformly distributed load along its arc length, where 10 separate one step analyses are made. In this kind of load, SAP program does not divide equidistantly the maximum load value. Curves' limits are defined by the axial force capacity N^{cap} of each cable. ADINA and SAP programs extract results as deflections u and v .

In the accompanied CD, there is a list of the numerical models, which contains the attributes of each model case. The models used in this chapter are commented with the word 'comparison'. In the same CD, the .idb file for ADINA and the .sdb file for SAP can be found, for each model case. Tutorials for ADINA and SAP programs, oriented to simple cables, can be found at the link of reference [9] or requested from the author via e-mail.

Note: In some operating systems, user must save SAP models with a simple name, without symbols, at the following path:

c:\Program Files\Computers and Structures\

in order to run the analysis.

3.2 SIMPLE CABLES UNDER CONCENTRATED LOADS

3.2.1 Results of comparison between analytical and numerical solutions

The comparison between analytical and numerical curves, in case of concentrated loads or imposed end displacements, verifies the rightness of the analytical solutions developed in Paragraph 2.2. Reader can use either analytical formulas or the finite element software ADINA and SAP for the analysis of a simple cable under concentrated loads or imposed end displacements, as identical results occur.

3.2.2 Comparison diagrams of a horizontal cable under concentrated load in the middle

Analytical solution: Paragraph 2.2.1

Parametric figures: Paragraph 2.5.2

- 1) $S_0 \leq S_{AB}$

Here, $z^* = 0$ as $S_0 \leq S_{AB}$ and, so, $v = z$.

2.2.1~ $S_{AB}=30m \sim \theta=0deg \sim \alpha=0.5 \sim 15\%$		
θ	0	deg
S_0	29.957	m
S_{AB}	30.000	m
w^{pre}	15.0	%
N^{pre}	74.418	kN
E	165	GPa
d_A	20	mm
α	0.50	-
p^{max}	125	kN

Table 3-1: Properties of the numerical cable model

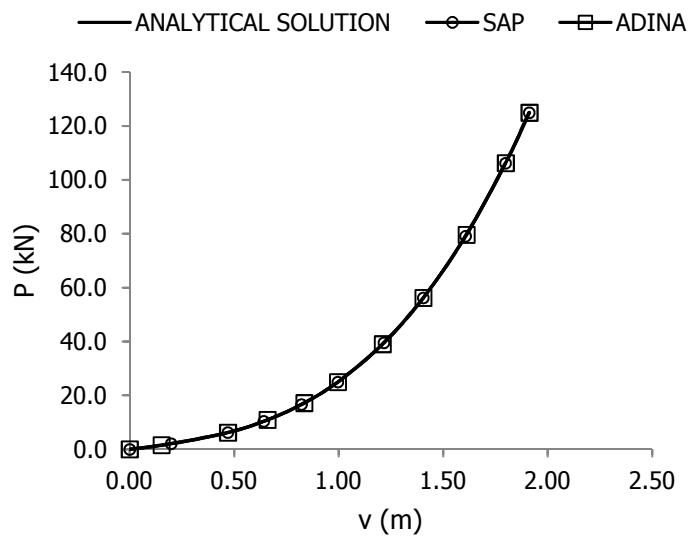


Figure 3-1: Applied load P as function of vertical deflection v

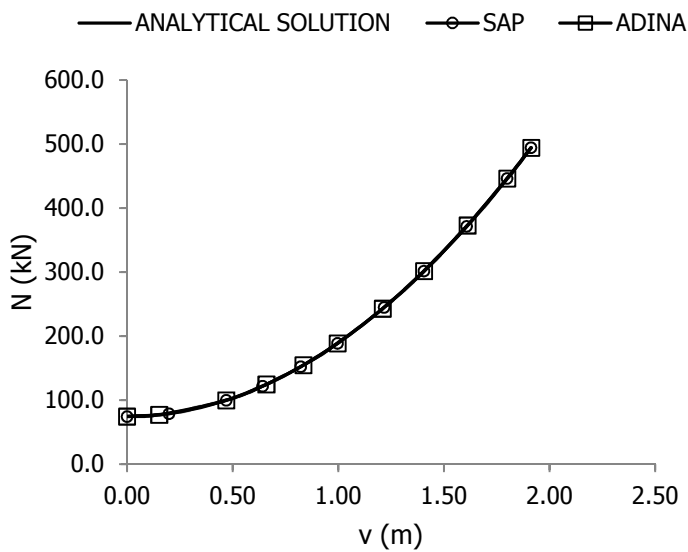


Figure 3-2: Cable's axial force N as function of vertical deflection v

2) $S_0 = S_{AB}$

Here, $z^* = 0$ as $S_0 \leq S_{AB}$ and, so, $v = z$.

2.2.1~SAB=10m~θ=0deg~α=0.5~0%		
θ	0	deg
S₀	10.000	m
E	150	GPa
d_A	10	mm
α	0.50	-
p^{max}	35.5	kN

Table 3-2: Properties of the numerical cable model

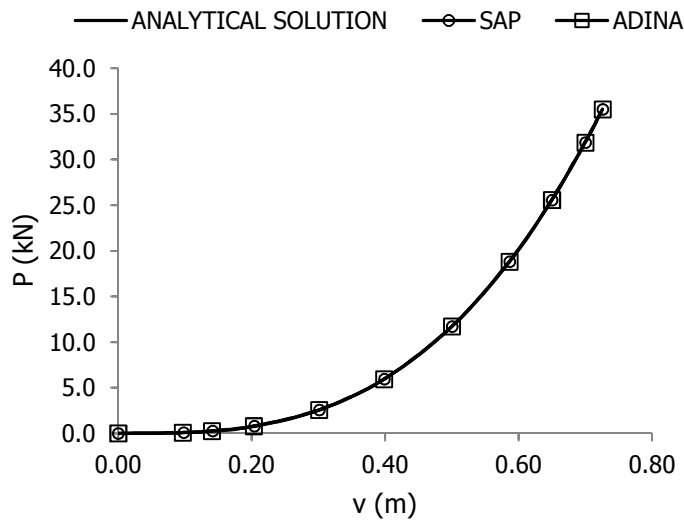


Figure 3-3: Applied load P as function of vertical deflection v

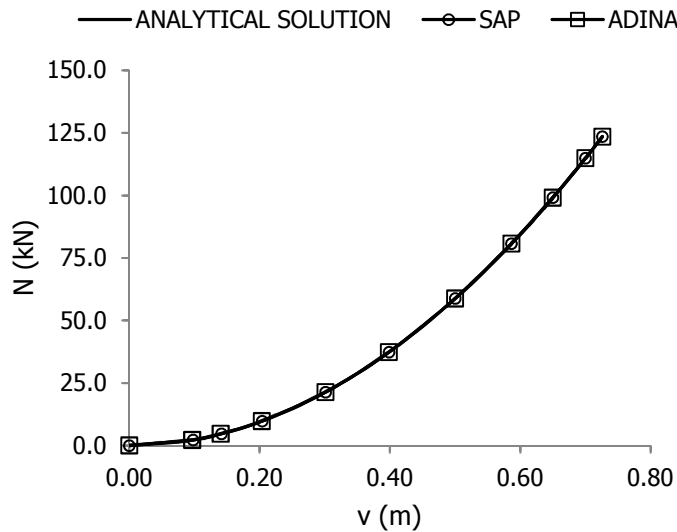


Figure 3-4: Cable's axial force N as function of vertical deflection v

3) $S_0 \geq S_{AB}$

2.2.1~SAB=20m~θ=0deg~α=0.5~1.2		
θ	0	deg
S₀	24.000	m
S_{AB}	20.000	m
S₀/S_{AB}	1.20	-
E	165	GPa
d_A	20	mm
α	0.50	-
p^{max}	560	kN

Table 3-3: Properties of the numerical cable model

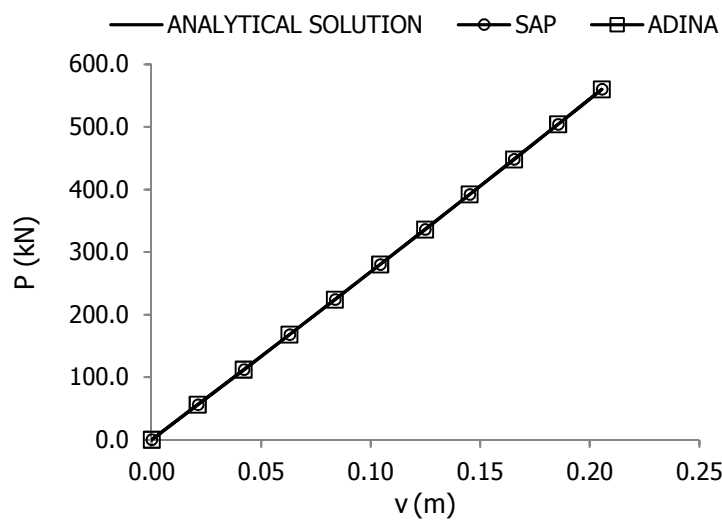


Figure 3-5: Applied load P as function of vertical deflection v

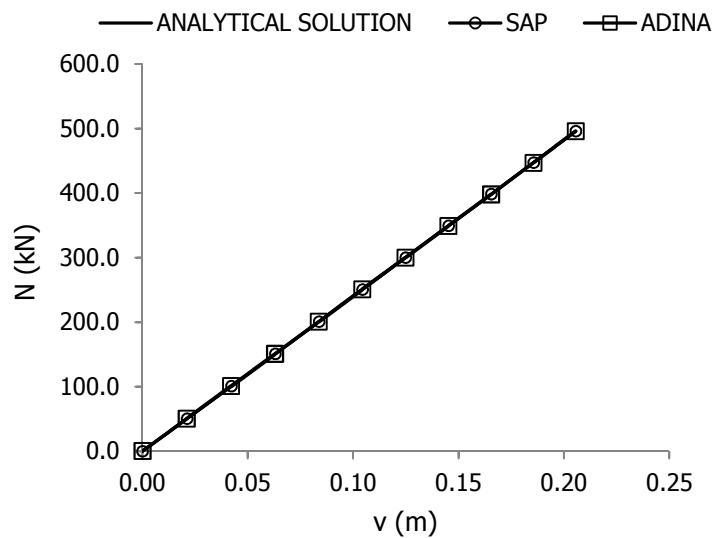


Figure 3-6: Cable's axial force N as function of vertical deflection v

3.2.3 Comparison diagrams of an inclined cable under concentrated load at arbitrary position

Analytical solution: Paragraph 2.2.2

Parametric figures: Paragraph 2.5.3

The complexity of the analytical solution prohibits the immediate design of the curves from it. Thus, the following design procedure is applied: pairs (u,v) are taken from the numerical solution, ADINA or SAP, and taking into account the point (x^*,z^*) , from the numerical model, pairs (x,z) are extracted. These pairs are input in the 2-degree polynomial equation, Eq. (2-41) in case A and Eq. (2-51) in case B, with output the value of the concentrated load P , in non-dimensional form. The values of the concentrated load P , in dimensional form, and of the cable's axial forces N_A and N_B derive from the corresponding equations of Paragraph 2.2.2.

$$1) \quad S_0 \leq S_{AB}$$

2.2.2~ $S_{AB}=30m \sim \theta=5deg \sim \alpha=0.6 \sim 10\%$ - case A and B -		
θ	5	deg
S_0	29.971	m
S_{AB}	30.000	m
w^{pre}	10.0	%
N^{pre}	49.612	kN
E	165	GPa
d_A	20	mm
α	0.60	-
p^{max}	130	kN

Table 3-4: Properties of the numerical cable model

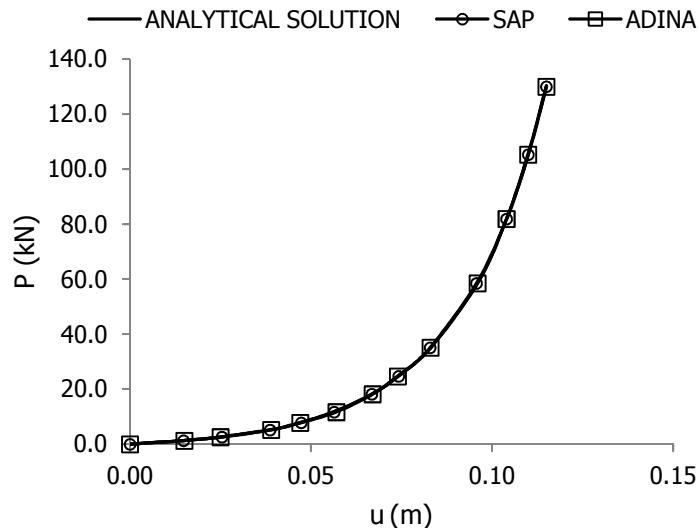


Figure 3-7: Applied load P as function of horizontal deflection u

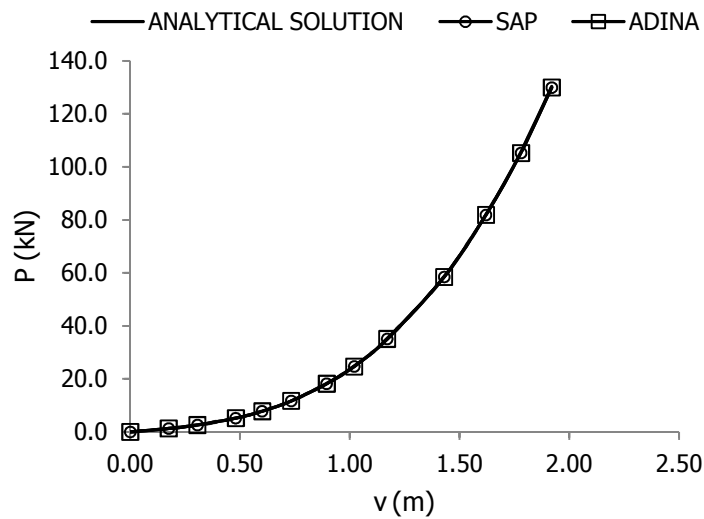


Figure 3-8: Applied load P as function of vertical deflection v

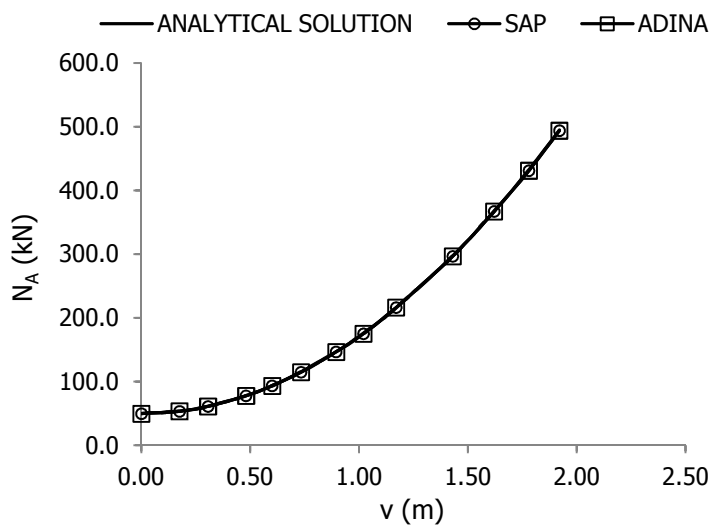


Figure 3-9: Cable's axial force N_A as function of vertical deflection v

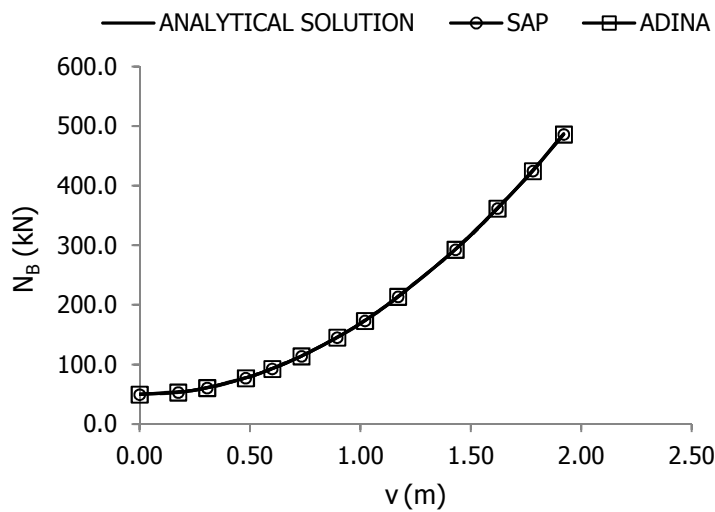


Figure 3-10: Cable's axial force N_B as function of vertical deflection v

$$2) S_0 = S_{AB}$$

2.2.2~SAB=20m~θ=10deg~α=0.3~0%		
- case A -		
θ	10	deg
S₀	20.000	m
E	165	GPa
d_A	20	mm
α	0.30	-
p^{max}	144	kN

Table 3-5: Properties of the numerical cable model

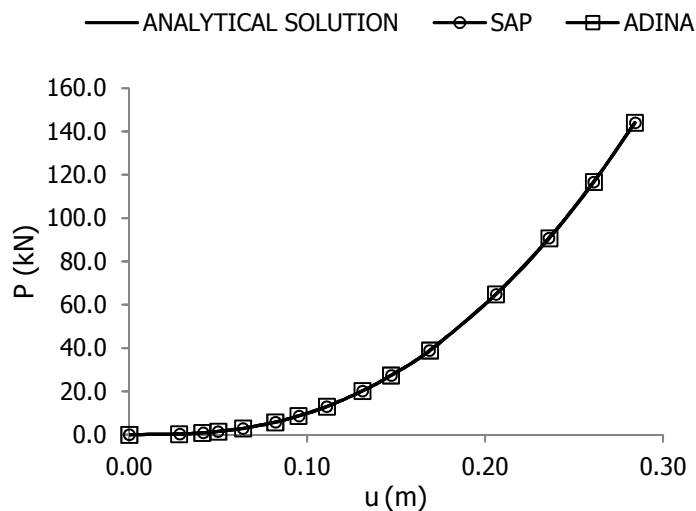


Figure 3-11: Applied load P as function of horizontal deflection u

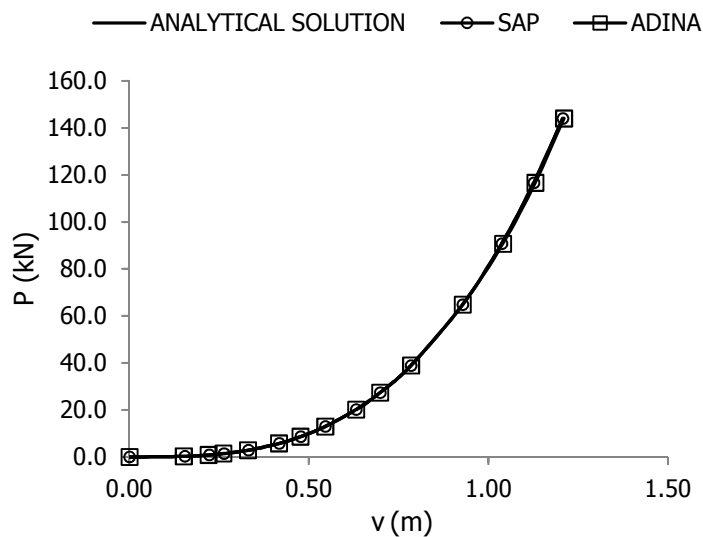


Figure 3-12: Applied load P as function of vertical deflection v

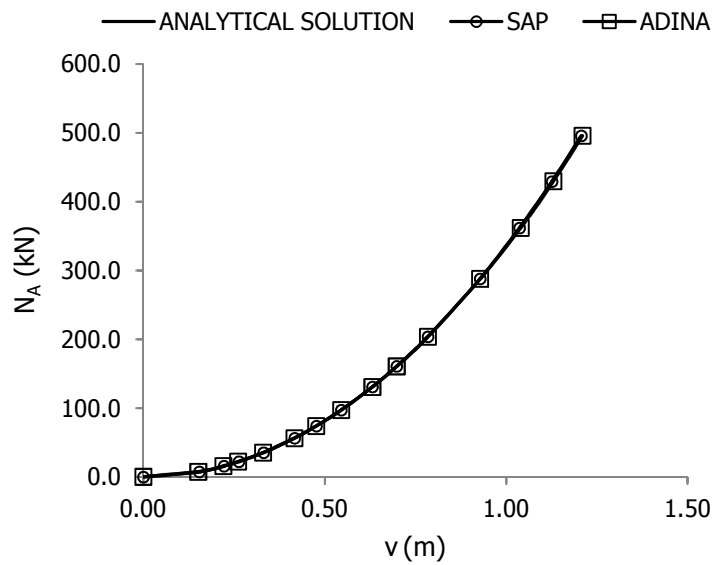


Figure 3-13: Cable's axial force N_A as function of vertical deflection v

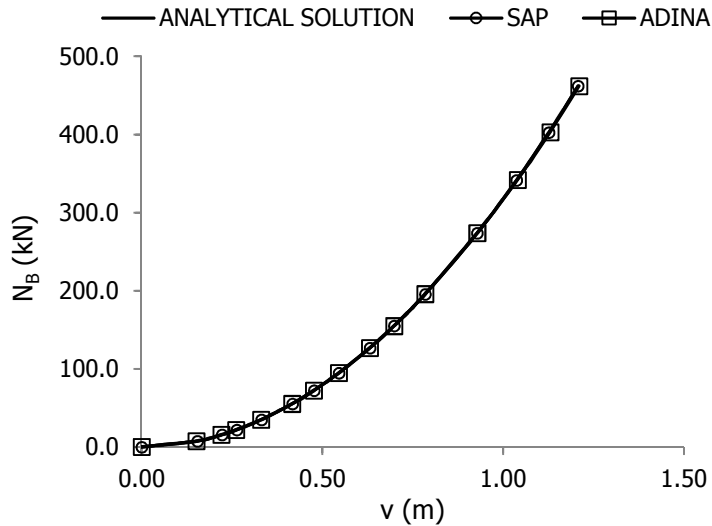


Figure 3-14: Cable's axial force N_B as function of vertical deflection v

3) $S_0 \geq S_{AB}$

2.2.2~SAB=20m~θ=20deg~α=0.4~1.1		
- case B -		
θ	20	deg
S₀	22.000	m
S_{AB}	20.000	m
S₀/S_{AB}	1.10	-
E	165	GPa
d_A	20	mm
α	0.40	-
p^{max}	388	kN

Table 3-6: Properties of the numerical cable model

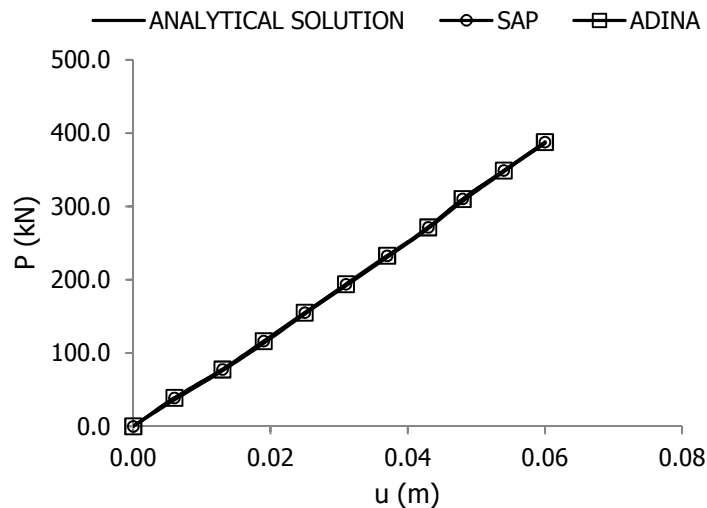


Figure 3-15: Applied load P as function of horizontal deflection u

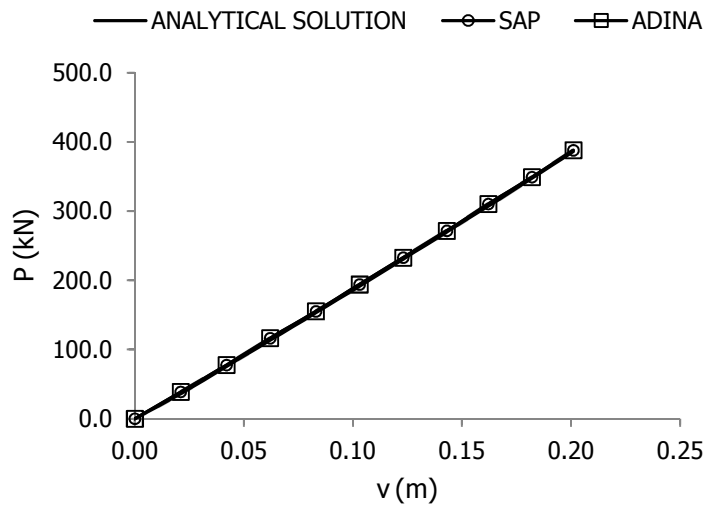
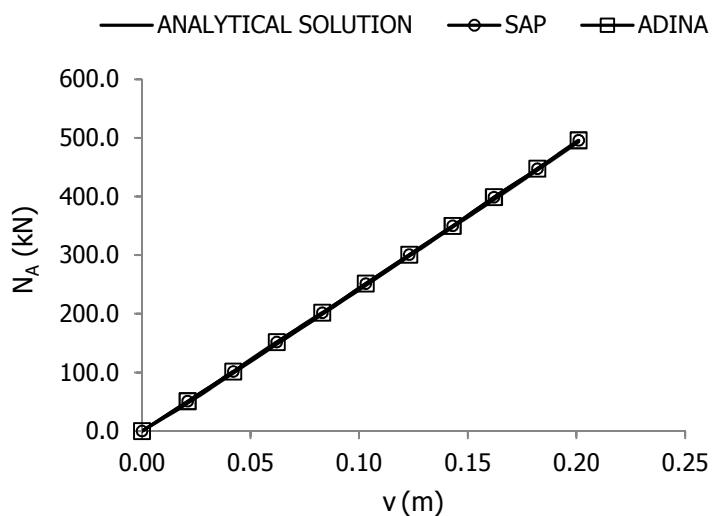


Figure 3-16: Applied load P as function of vertical deflection v

Figure 3-17: Cable's axial force N_A as function of vertical deflection v

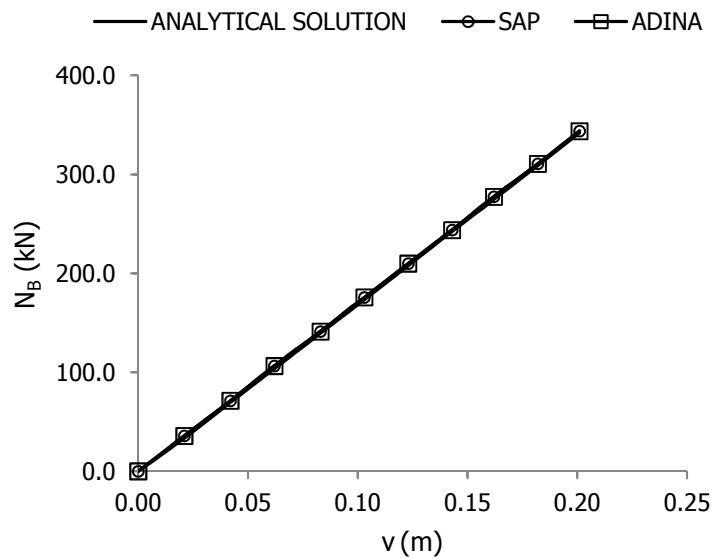


Figure 3-18: Cable's axial force N_B as function of vertical deflection v

3.2.4 Comparison diagrams of a horizontal cable under concentrated load at arbitrary position

Analytical solution: Paragraph 2.2.3

Parametric figures: Paragraph 2.5.4

The complexity of the analytical solution prohibits the immediate design of the curves from it. Thus, the following design procedure is applied: pairs (u,v) are taken from the numerical solution, ADINA or SAP, and taking into account the point (x^*,z^*) , from the numerical model, pairs (x,z) are extracted. These pairs are input in the 2-degree polynomial equation, Eq. (2-60), with output the value of the concentrated load P' , in non-dimensional form. The values of the concentrated load P in dimensional form and of the cable's axial forces N_A and N_B derive from the corresponding equations of Paragraph 2.2.3.

1) $S_0 \leq S_{AB}$

Here, $z^* = 0$ as $S_0 \leq S_{AB}$ and, so, $v = z$.

2.2.3~SAB=10m~θ=0deg~α=0.65~15%		
θ	0	deg
S₀	9.987	m
S_{AB}	10.000	m
w^{pre}	15.0	%
N^{pre}	74.418	kN
E	180	GPa
d_A	20	mm
α	0.65	-
p^{max}	125	kN

Table 3-7: Properties of the numerical cable model

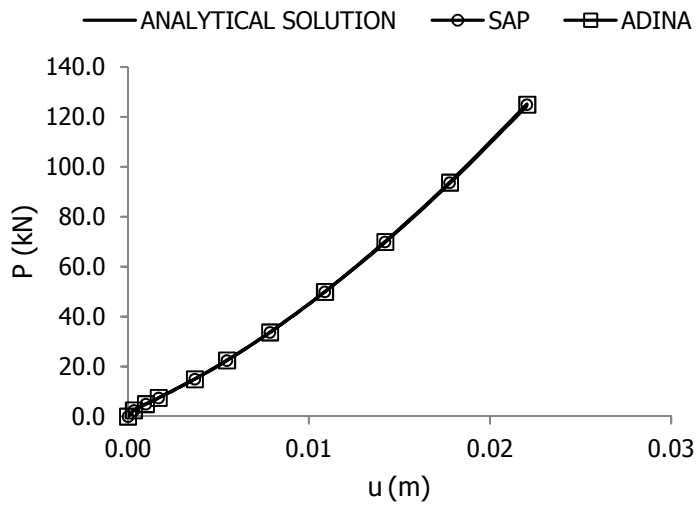


Figure 3-19: Applied load P as function of horizontal deflection u

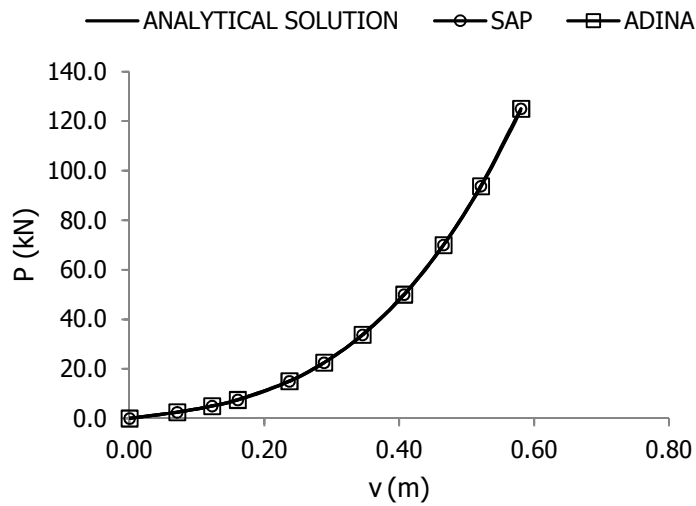


Figure 3-20: Applied load P as function of vertical deflection v

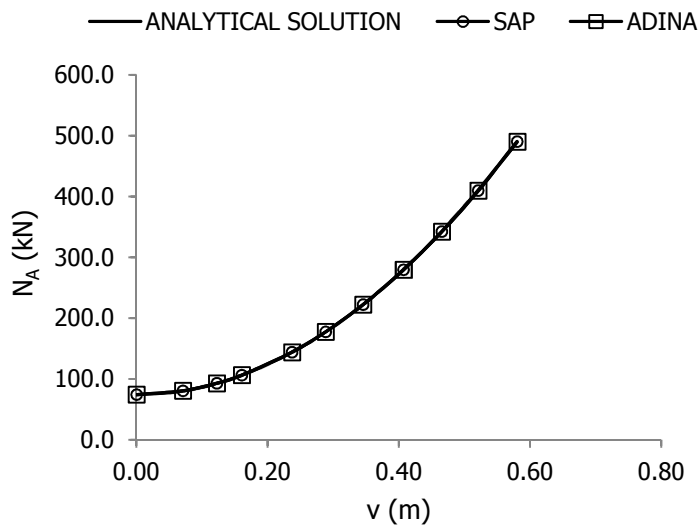


Figure 3-21: Cable's axial force N_A as function of vertical deflection v

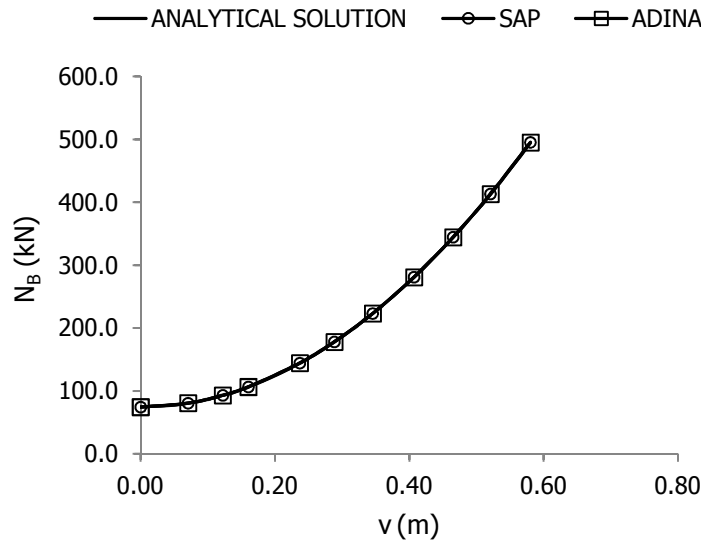


Figure 3-22: Cable's axial force N_B as function of vertical deflection v

2) $S_0 = S_{AB}$

Here, $z^* = 0$ as $S_0 \leq S_{AB}$ and, so, $v = z$.

2.2.3~SAB=20m~θ=0deg~α=0.3~0%		
θ	0	deg
S_0	20.000	m
E	165	GPa
d_A	20	mm
α	0.30	-
p^{max}	145	kN

Table 3-8: Properties of the numerical cable model

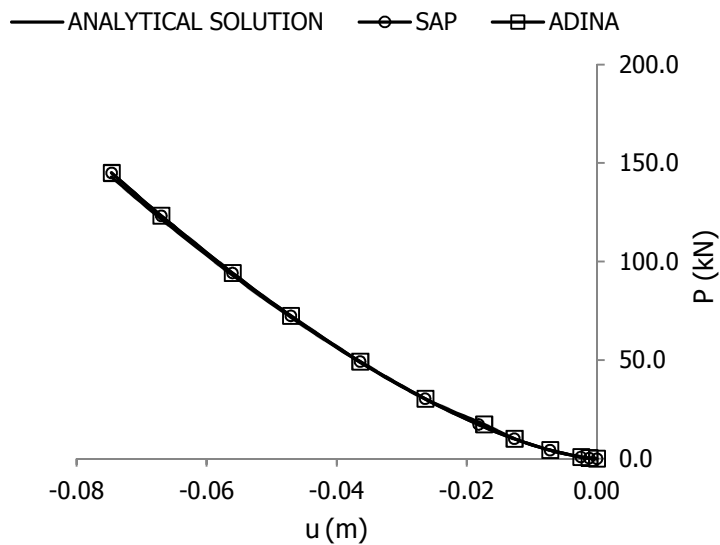
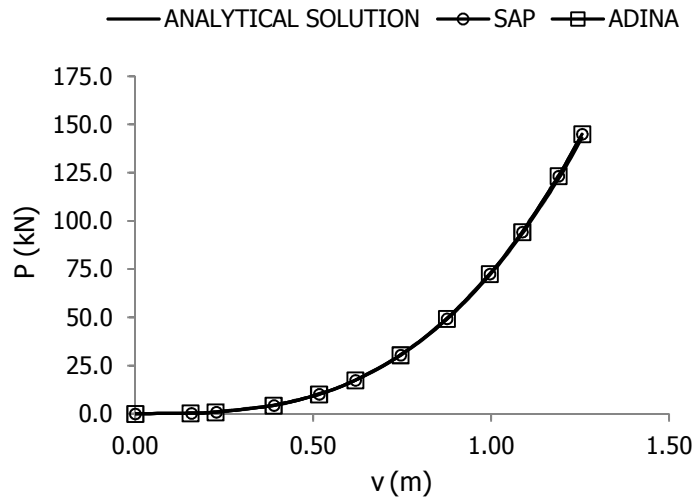
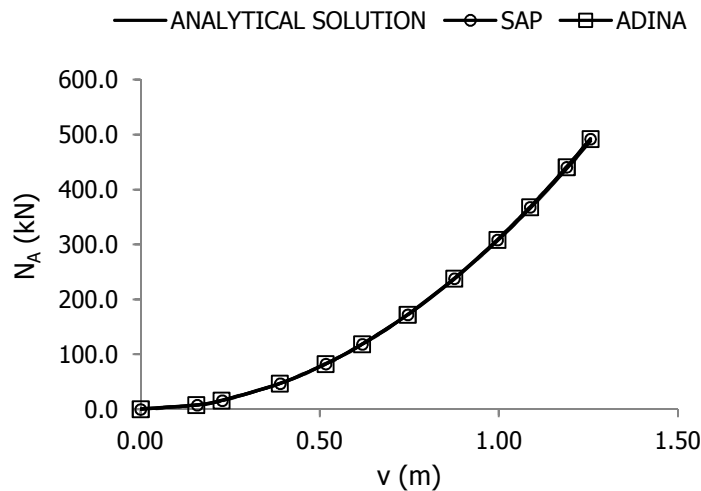
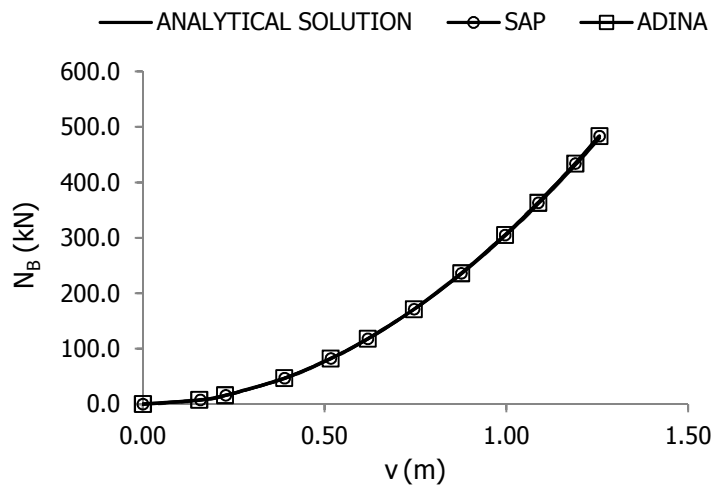


Figure 3-23: Applied load P as function of horizontal deflection u

Figure 3-24: Applied load P as function of vertical deflection v Figure 3-25: Cable's axial force N_A as function of vertical deflection v Figure 3-26: Cable's axial force N_B as function of vertical deflection v

3) $S_0 \geq S_{AB}$

2.2.3~SAB=30m~θ=0deg~α=0.4~1.1		
θ	0	deg
S₀	33.000	m
S_{AB}	30.000	m
S₀/S_{AB}	1.10	-
E	165	GPa
d_A	20	mm
α	0.40	-
p^{max}	421	kN

Table 3-9: Properties of the numerical cable model

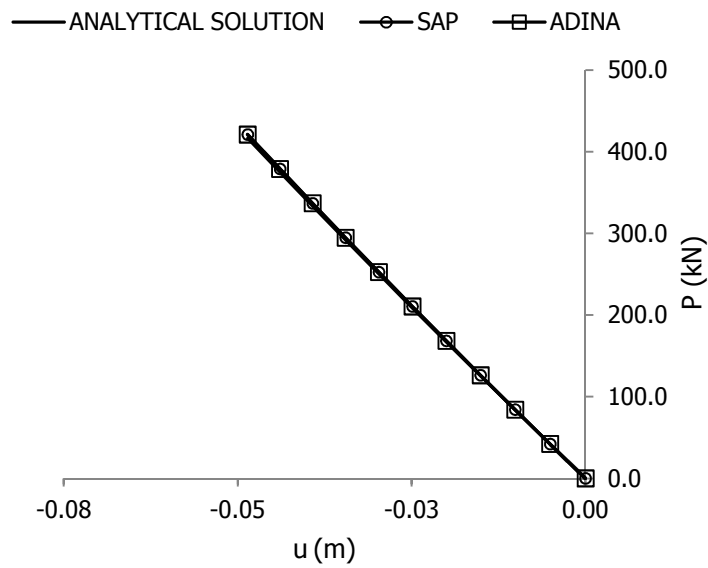


Figure 3-27: Applied load P as function of horizontal deflection u

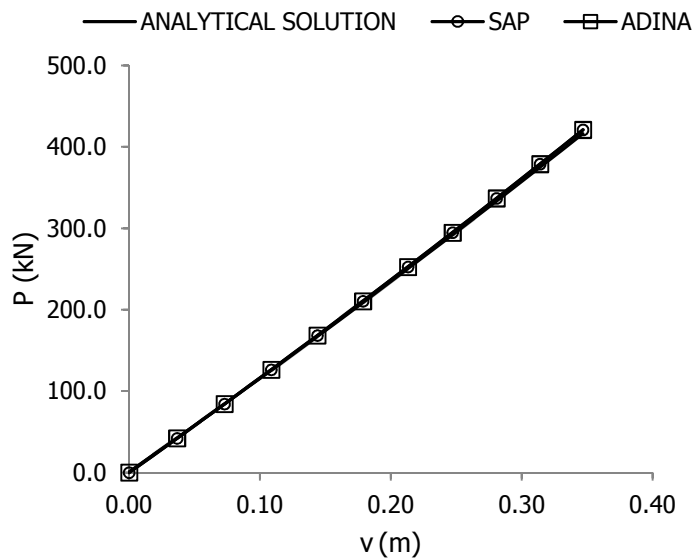
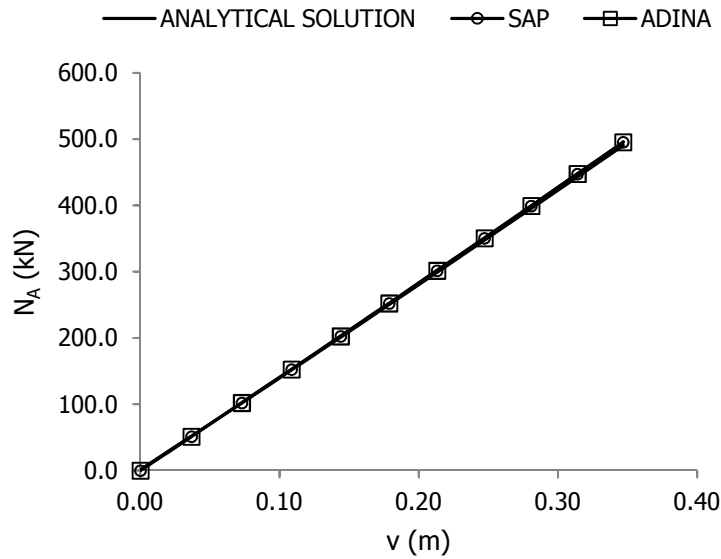
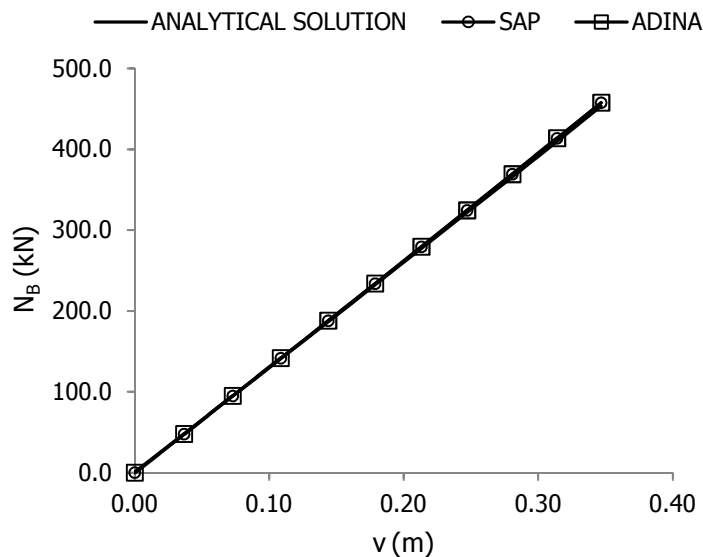


Figure 3-28: Applied load P as function of vertical deflection v

Figure 3-29: Cable's axial force N_A as function of vertical deflection v Figure 3-30: Cable's axial force N_B as function of vertical deflection v

3.2.5 Comparison diagrams of an inclined cable under imposed end displacement

Analytical solution: Paragraph 2.2.4.1

Parametric figures: Paragraph 2.5.5

$$1) \quad S_0 \leq S_{AB}$$

Cables, in this case, are not pre-tensioned as support B is free to move vertical and balance to an unstressed position. Inclined pre-tensioned cables under imposed end displacement are presented analytically in Chapter 5.

2.2.4~S _{AB} =20m~θ=45deg~0.9 - case A -		
θ	45	deg
S ₀	18.000	m
S _{AB}	20.000	m
S ₀ /S _{AB}	0.90	-
E	165	GPa
d _A	20	mm
p ^{max}	310	kN

Table 3-10: Properties of the numerical cable model

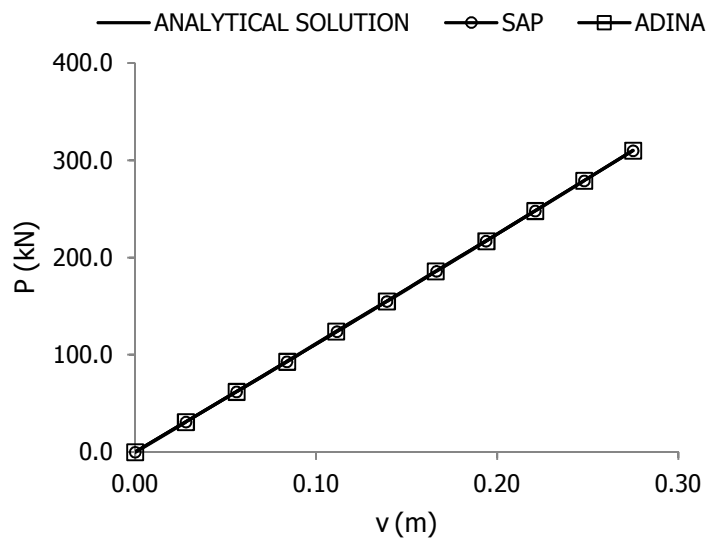


Figure 3-31: Applied load P as function of vertical deflection v

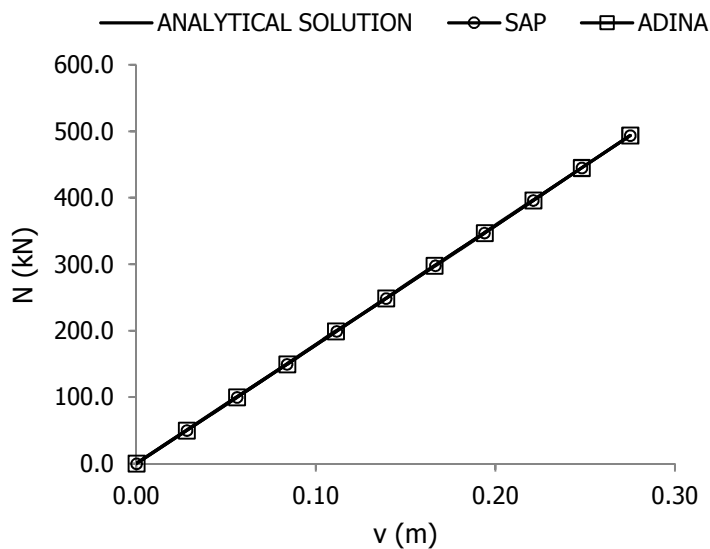


Figure 3-32: Cable's axial force N as function of vertical deflection v

2) $S_0 = S_{AB}$

2.2.4~SAB=20m~ $\theta=45\text{deg}$ ~0%		
- case A -		
θ	45	deg
S_0	20.000	m
E	165	GPa
d_A	20	mm
p^{\max}	354	kN

Table 3-11: Properties of the numerical cable model

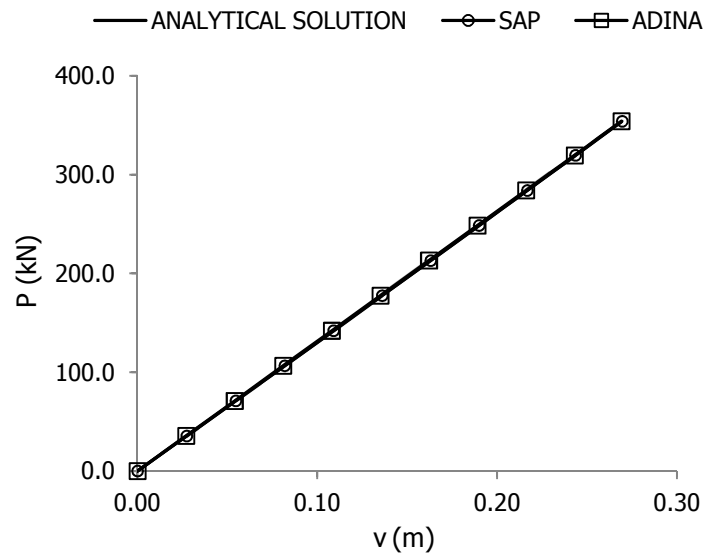


Figure 3-33: Applied load P as function of vertical deflection v

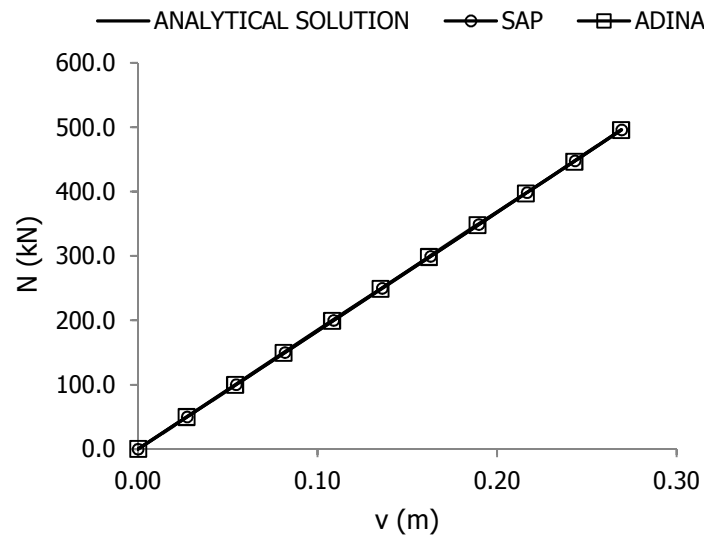


Figure 3-34: Cable's axial force N as function of vertical deflection v

$$3) \quad S_0 \geq S_{AB}$$

2.2.4~S _{AB} =20m~θ=45deg~1.1 - case A -		
θ	45	deg
S ₀	22.000	m
S _{AB}	20.000	m
S ₀ /S _{AB}	1.10	-
E	165	GPa
d _A	20	mm
p ^{max}	380	kN

Table 3-12: Properties of the numerical cable model

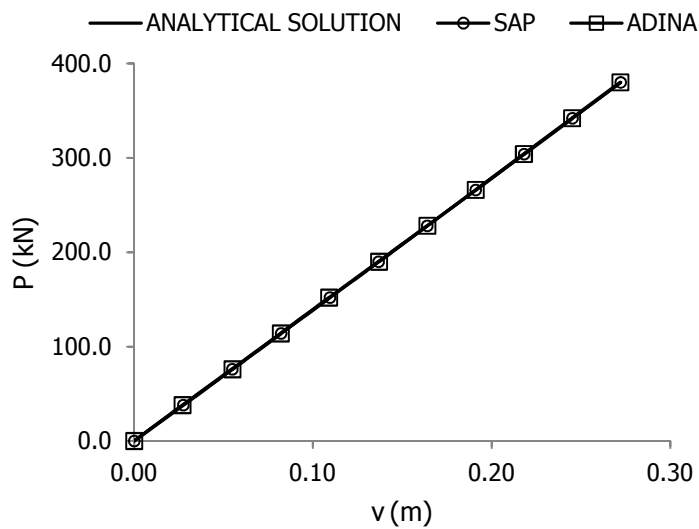


Figure 3-35: Applied load P as function of vertical deflection v

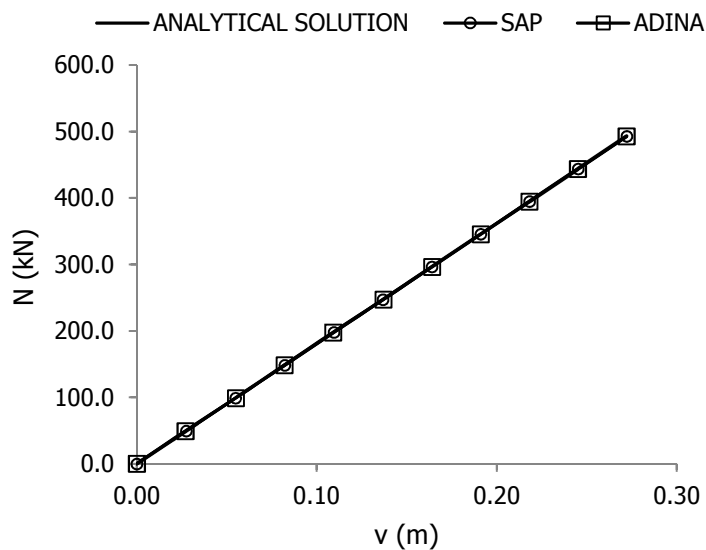


Figure 3-36: Cable's axial force N as function of vertical deflection v

3.3 SIMPLE CABLES UNDER UNIFORMLY DISTRIBUTED LOADS

3.3.1 Results of comparison between analytical and numerical solutions

The comparison between analytical and numerical curves, for the case of uniformly distributed loads along cable's horizontal projection and cable's arc length, arises an inaccuracy of the analytical solution due to an assumption that made.

The analytical procedure, that presented in Paragraph 2.3, takes into account only the vertical deflection v of the cable and omits its horizontal u one. Under virtual circumstances, a simple cable responds to a uniformly distributed load by deploying not only vertical v but also horizontal u deflections. The accurate analytical solution, containing both deflections, is too complex and is out of the context of this diploma thesis. So, the simplification in mathematics leads to a deviation in cable's curves, as shown below.

The comparison between curves of an inclined cable under uniformly distributed load indicates that, the bigger the angle θ is the larger the deviation between analytical and numerical curves becomes. In other words, the effect of the horizontal deflection u in the analytical solution increases as cable inclination increases. Figures referring to applied load p/q as function of horizontal deflection u confirm the agreement between ADINA and SAP programs. In case of a horizontal cable, there is identification between analytical and numerical curves, which is an expected result, as a horizontal cable lacks of horizontal deflection u , due to its symmetric geometry and loading.

The examination of a cable with initial unstressed length S_0 equal to the distance spanned S_{AB} is sufficient to illustrate the disagreement between analytical and numerical solutions and provide the reader a qualitative guide to his design procedure. The comparison for a pre-tensioned cable or a cable with initial unstressed length S_0 larger than the distance spanned S_{AB} is not considered as requisite as leads to similar results.

3.3.2 Comparison diagrams of an inclined cable under uniformly distributed load along its horizontal projection

Analytical solution: Paragraph 2.3.1

Parametric figures: Paragraph 2.5.6

Here, $v = d_m$ as $S_0 \leq S_{AB}$.

2.3.1~SAB=20m~θ=20deg~0%		
θ	20	deg
S₀	20.000	m
E	165	GPa
d_A	20	mm
p^{max}	11.280	kN/m

Table 3-13: Properties of the numerical cable model

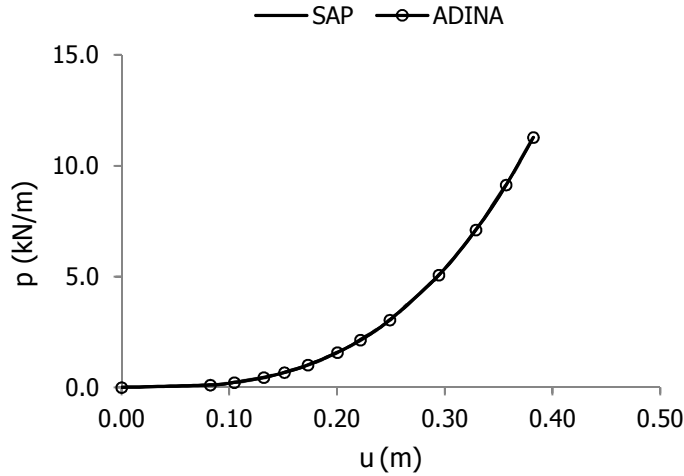


Figure 3-37: Applied load p as function of horizontal deflection u

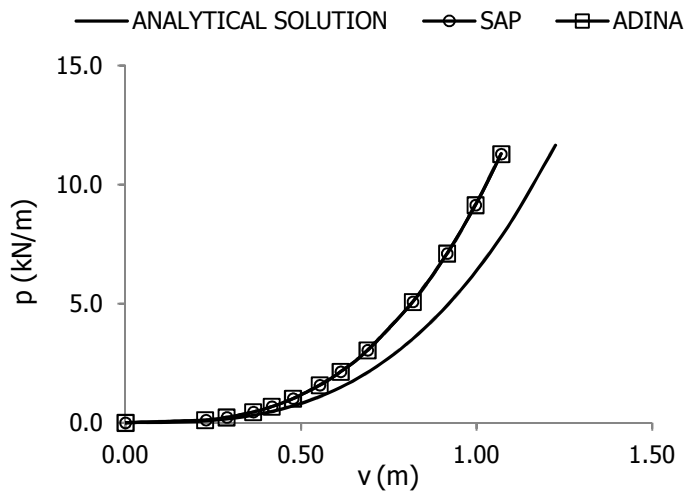


Figure 3-38: Applied load p as function of vertical deflection v

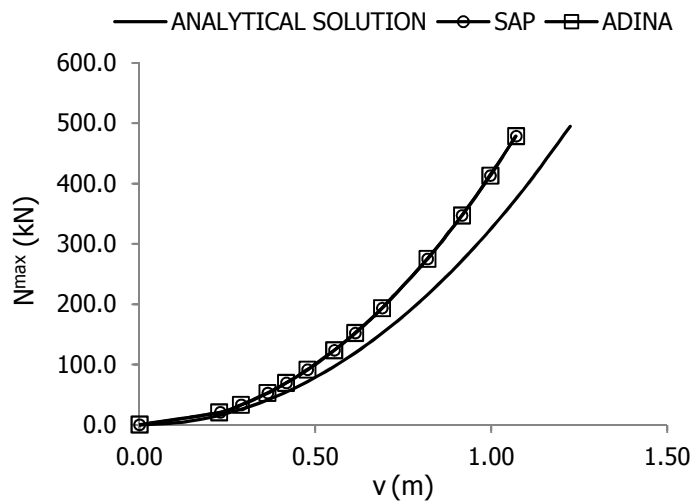
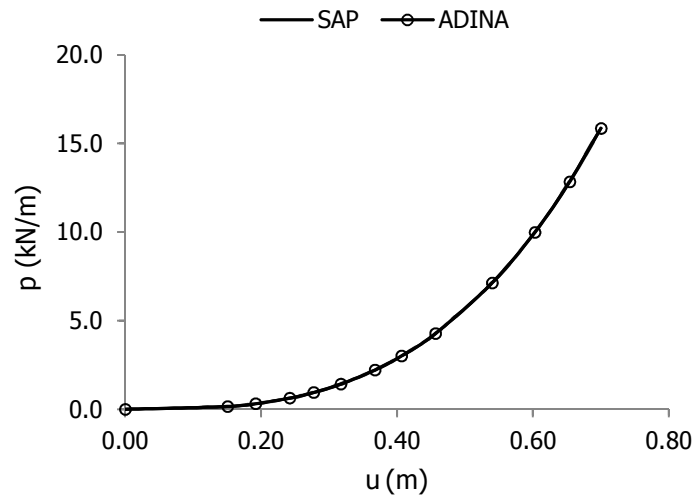
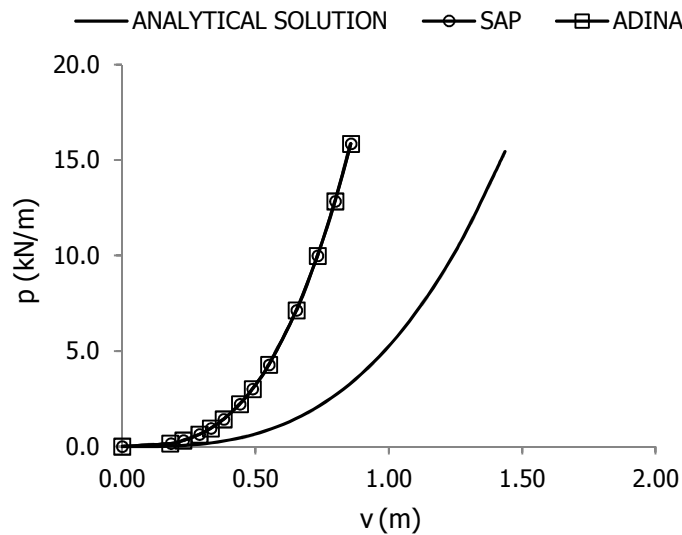


Figure 3-39: Maximum axial force N^{\max} as function of vertical deflection v

2.3.1~SAB=20m~$\theta=40\text{deg}$~0%		
θ	40	deg
S_0	20.000	m
E	165	GPa
d_A	20	mm
p^{\max}	15.850	kN/m

Table 3-14: Properties of the numerical cable model

Figure 3-40: Applied load p as function of horizontal deflection u Figure 3-41: Applied load p as function of vertical deflection v

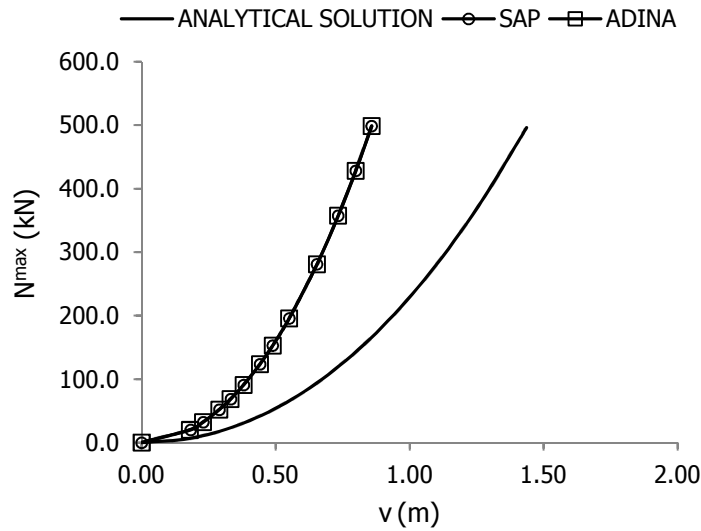


Figure 3-42: Maximum axial force N^{\max} as function of vertical deflection v

3.3.3 Comparison diagrams of a horizontal cable under uniformly distributed load along its horizontal projection

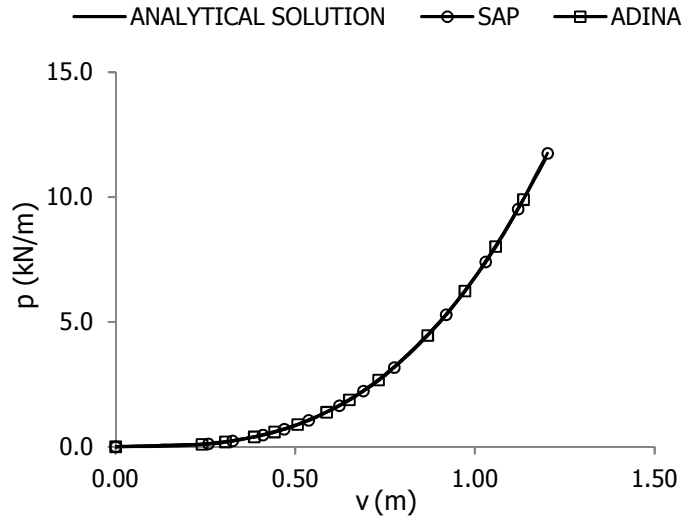
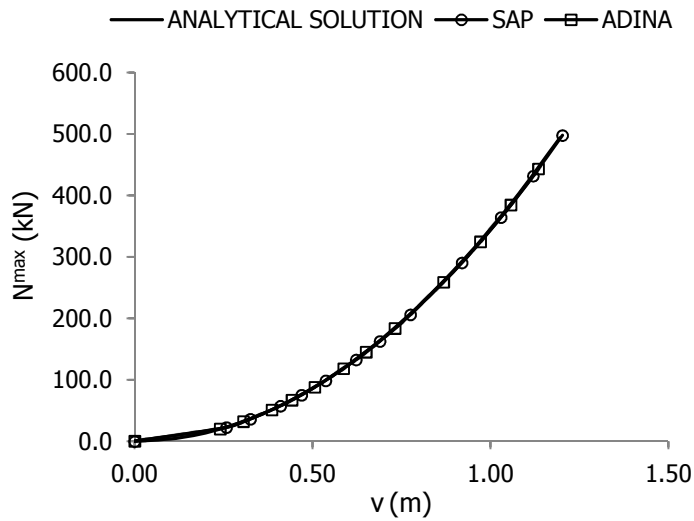
Analytical solution: Paragraph 2.3.2

Parametric figures: Paragraph 2.5.7

Here, $z^* = 0$ as $S_0 \leq S_{AB}$ and, so, $v = z = d_m$.

2.3.2~SAB=20m~θ=0deg~0%		
θ	0	deg
S₀	20.000	m
E	165	GPa
d_A	20	mm
p^{max}	11.750	kN/m

Table 3-15: Properties of the numerical cable model

Figure 3-43: Applied load p as function of vertical deflection v Figure 3-44: Maximum axial force N^{\max} as function of vertical deflection v

3.3.4 Comparison diagrams of an inclined cable under uniformly distributed load along its arc length

Analytical solution: Paragraph 2.3.3

Parametric figures: Paragraph 2.5.8

Here, $v = d_m$ as $S_0 = S_{AB}$.

2.3.3~SAB=20m~θ=20deg~0%		
θ	20	deg
S₀	20.000	m
E	165	GPa
d_A	20	mm
q^{max}	10.582	kN/m

Table 3-16: Properties of the numerical cable model

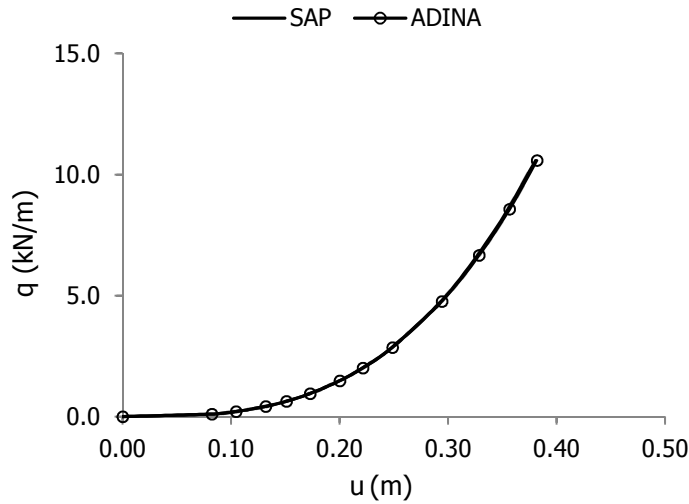


Figure 3-45: Applied load q as function of horizontal deflection u

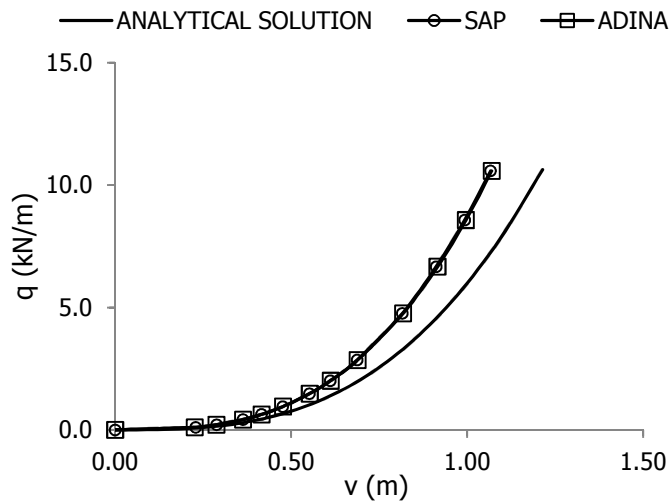


Figure 3-46: Applied load q as function of vertical deflection v

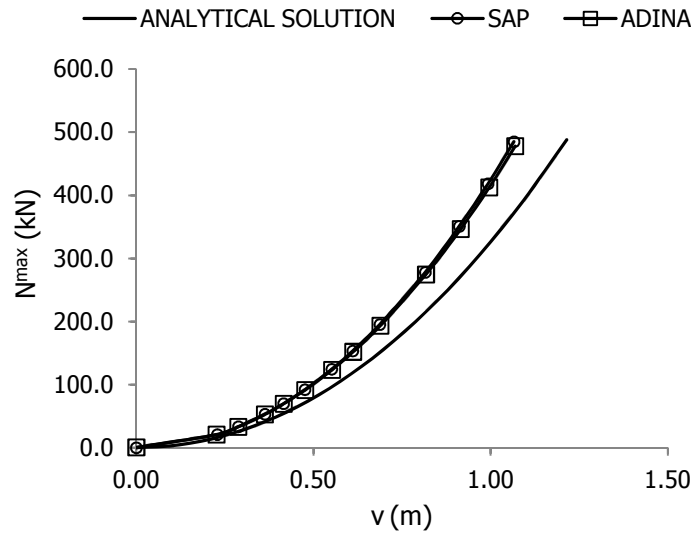


Figure 3-47: Maximum axial force N^{\max} as function of vertical deflection v

2.3.3~SAB=20m~θ=40deg~0%		
θ	40	deg
S_0	20.000	m
E	165	GPa
d_A	20	mm
q^{\max}	11.947	kN/m

Table 3-17: Properties of the numerical cable model

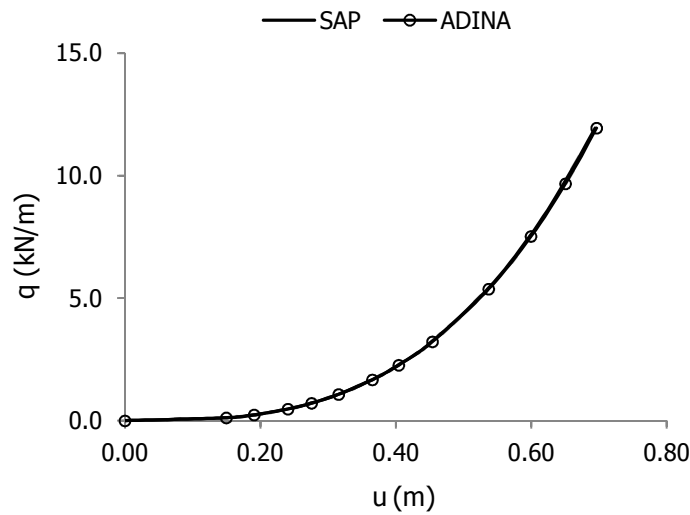


Figure 3-48: Applied load q as function of horizontal deflection u

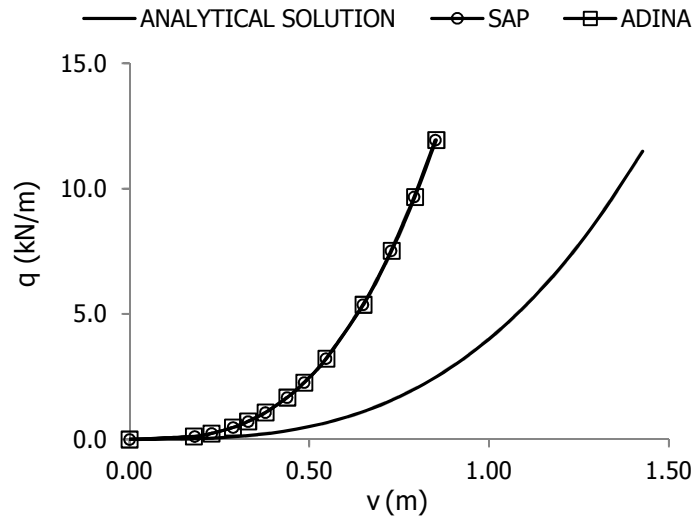


Figure 3-49: Applied load q as function of vertical deflection v

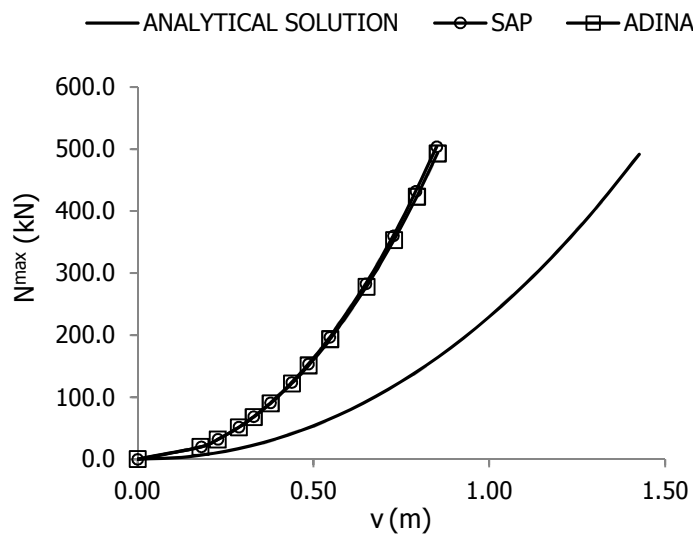


Figure 3-50: Maximum axial force N^{\max} as function of vertical deflection v

3.3.5 Comparison diagrams of a horizontal cable under uniformly distributed load along its arc length

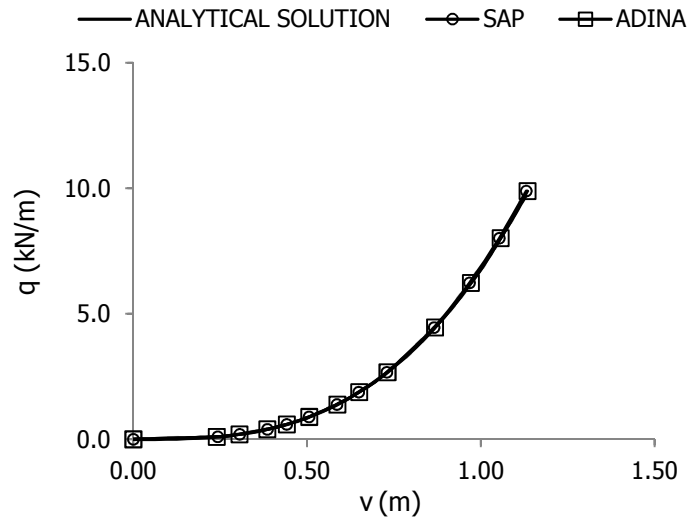
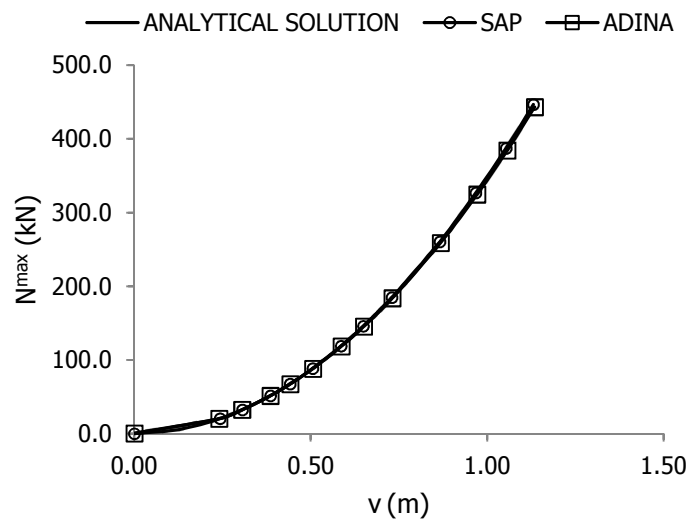
Analytical solution: Paragraph 2.3.4

Parametric figures: Paragraph 2.5.9

Here, $z^* = 0$ as $S_0 = S_{AB}$ and, so, $v = z = d_m$.

2.3.4~SAB=20m~$\theta=0$deg~0%		
θ	0	deg
S_0	20.000	m
E	165	GPa
d_A	20	mm
q^{\max}	9.891	kN/m

Table 3-18: Properties of the numerical cable model

Figure 3-51: Applied load q as function of vertical deflection v Figure 3-52: Maximum axial force N^{\max} as function of vertical deflection v

4 STATIC BEHAVIOR OF SIMPLE 1-DOF CABLE NET UNDER CONCENTRATED LOAD

4.1 SIMPLE 1-DOF CABLE NET MODEL

Figure 4-1 illustrates a simple 1-DOF cable net model in 2-D. The 3 Cartesian axes are defined in the figure. The plane which is perpendicular to z-axis and includes points A and A' is the reference plane for z-coordinates. Supports B and B' could lay over or under this reference plane. Here, the first case is shown. Equations of Chapter 4 are valid for both cases. Cables' supports have coordinates:

A $(x_A, 0, 0)$
A' $(-x_A, 0, 0)$
B $(0, y_B, z_B)$
B' $(0, -y_B, z_B)$

Cable 1 has as supports points A and A' while cable 2 has points B and B'. The geometry of the cable net gives:

$$L_1 = 2|x_A| \tag{4-1}$$

$$L_2 = 2|y_B| \tag{4-2}$$

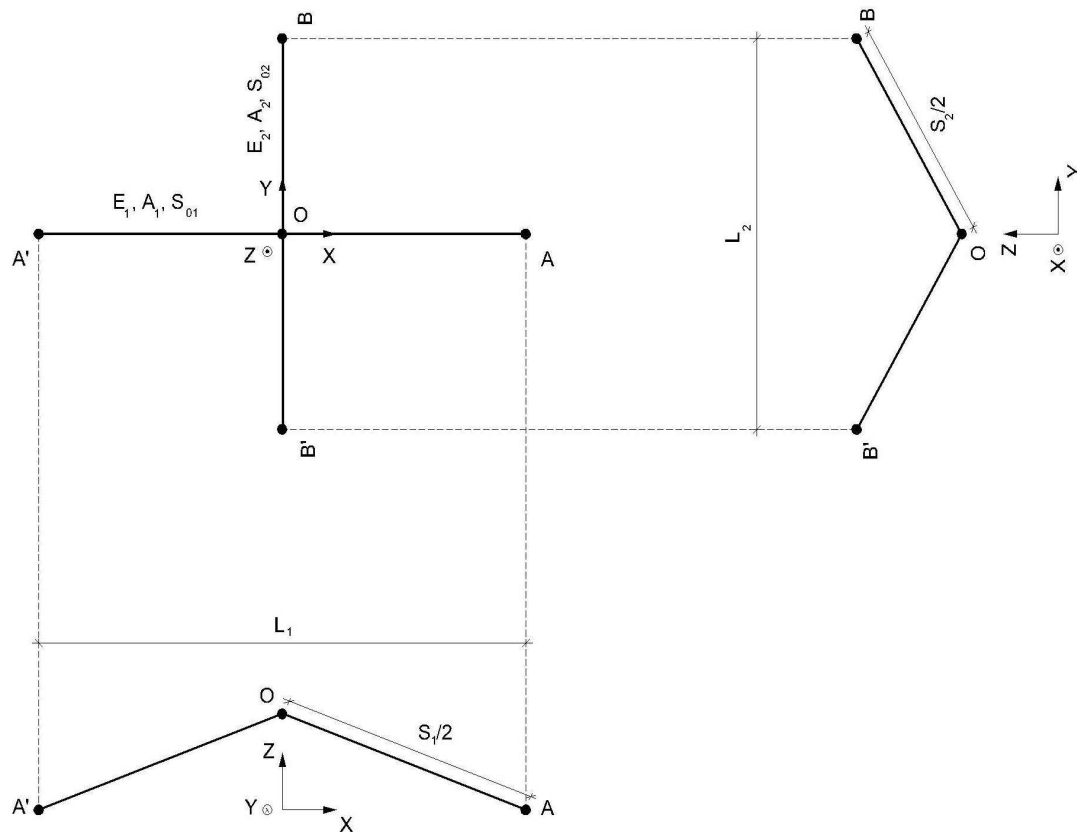


Figure 4-1: Geometry of a simple 1-DOF cable net

In addition, the following cables' characteristics are noted on Figure 4-1:

- $E_{\$}$: modulus of elasticity of cable $\$$
- $A_{\$}$: cross-section of cable $\$$
- $S_{0\$}$: initial unstressed length of cable $\$$
- $S_{\$}$: length of cable $\$$ at the equilibrium state

where $\$ = 1, 2$.

4.2 FORM FINDING

Form finding is the initial step for nonlinear analysis of a simple 1-DOF cable net under concentrated load. Cables, with initial unstressed length $S_{0\$} \geq L_{\$}$, have pre-tension $w_{\pre . The pre-tension $w_{\pre is defined as:

$$w_{\$}^{pre} = 100 \frac{N_{\$}^{pre}}{N_{\$}^{cap}} \quad (4-3)$$

where,

$$N_{\$}^{cap} \text{ is cable's axial force capacity: } N_{\$}^{cap} = A_{\$} f_{y\$} \quad (4-4)$$

$f_{y\$,}$ is the material's yield strength

and $\$ = 1, 2$.

Figure 4-2 shows each single cable, in the equilibrium state, with the corresponding forces in case of cable 2 over the reference plane. The nodal point has coordinates:

$O(0,0,z_0^*)$.

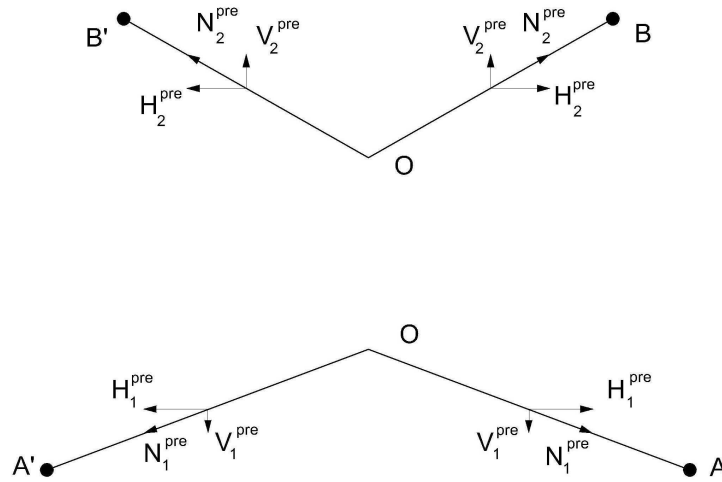


Figure 4-2: Equilibrium state of a simple 1-DOF cable net without concentrated load (cables are not in the same plane)

Assuming cables' material as linearly elastic, Hooke's law gives:

$$\sigma_{\$}^{pre} = E_{\$} \epsilon_{\$}^{pre} \Rightarrow \frac{N_{\$}^{pre}}{A_{\$}} = E_{\$} \frac{S_{\$} - S_{0\$}}{S_{0\$}} \Rightarrow N_{\$}^{pre} = E_{\$} A_{\$} \left(\frac{S_{\$}}{S_{0\$}} - 1 \right) \quad (4-5)$$

where $S_{\$}$ is defined as:

$$S_1 = 2\sqrt{(z_0^*)^2 + x_A^2} \quad (4-6)$$

$$S_2 = 2\sqrt{(z_B - z_0^*)^2 + y_B^2} \quad (4-7)$$

The combination of Eqs. (4-3) and (4-5) leads to:

$$S_{0\$} = \frac{S_{\$}}{\frac{w_{\$}^{pre} f_{y\$,}}{100E_{\$}} + 1} \quad (4-8)$$

The equation of static equilibrium in z-axis gives:

$$2V_1^{pre} = 2V_2^{pre} \Rightarrow V_1^{pre} = V_2^{pre} \quad (4-9)$$

where,

$$\frac{V_1^{\text{pre}}}{N_1^{\text{pre}}} = \frac{|z_0^*|}{\frac{S_1}{2}} \quad \text{and} \quad \frac{V_2^{\text{pre}}}{N_2^{\text{pre}}} = \frac{|z_B - z_0^*|}{\frac{S_2}{2}} \quad (4-10)$$

The combination of Eqs. (4-6), (4-7), (4-9) and (4-10) gives:

$$\frac{|z_0^*| N_1^{\text{pre}}}{\sqrt{(z_0^*)^2 + x_A^2}} = \frac{|z_B - z_0^*| N_2^{\text{pre}}}{\sqrt{(z_B - z_0^*)^2 + y_B^2}} \quad (4-11)$$

Cables' axial force N_{\S}^{pre} comes from Eq. (4-3), given the pre-tension w_{\S}^{pre} , or from Eq. (4-5), given initial unstressed length $S_{0\S}$. The solution of nonlinear Eq. (4-11) is the unknown z-coordinate of nodal point O z_0^* .

4.3 NONLINEAR ANALYSIS

Usual loads of a simple 1-DOF cable net are the snow and the wind. Tension structures are not sensitive in seismic loads. The snow and the wind are distributed loads applied perpendicularly on the membrane which covers the cable net. The shape of the membrane is assumed rhombus, as shown in Figure 4-3, and the 50% of the distributed load is delivered by the central node. The other 50% goes, through the cables, to the supports. The equivalent concentrated load P on the nodal point O has value:

$$P = \frac{1}{4} q_n L_1 L_2 \quad (4-12)$$

where q_n is the distributed snow/wind load (pressure).

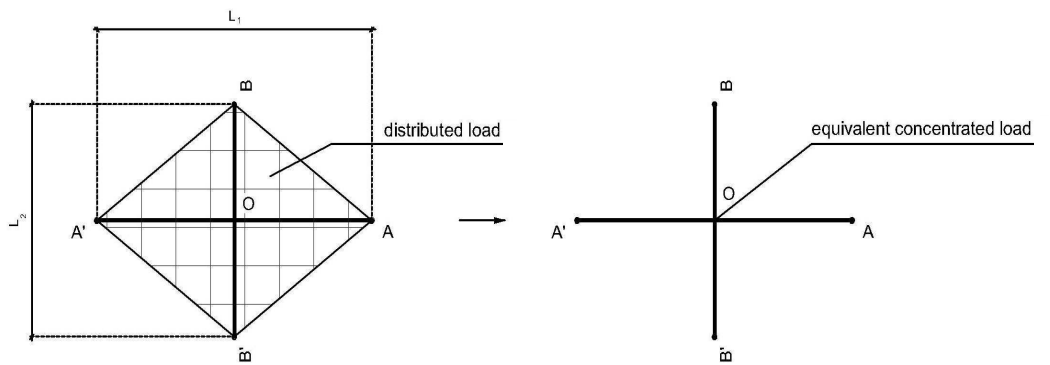


Figure 4-3: Distributed load and its equivalent concentrated

The analysis of Paragraph 2.2.1 is implemented, given the initial unstressed length $S_{0\S}$ from Eq. (4-8). The nodal point has coordinates:

$$O (0,0,z_0).$$

Assuming cables' material as linearly elastic, Hooke's law gives:

$$\sigma_{\$} = E_{\$} \varepsilon_{\$} \Rightarrow \frac{N_{\$}}{A_{\$}} = E_{\$} \frac{S_{\$} - S_{0\$}}{S_{0\$}} \Rightarrow N_{\$} = E_{\$} A_{\$} \left(\frac{S_{\$}}{S_{0\$}} - 1 \right) \quad (4-13)$$

where $S_{\$}$ is the length of cable $\$$ at the equilibrium state:

$$S_1 = 2\sqrt{z_0^2 + x_A^2} \quad (4-14)$$

$$S_2 = 2\sqrt{(z_B - z_0)^2 + y_B^2} \quad (4-15)$$

The geometry of cable net, for both load directions, gives:

$$\frac{V_1}{N_1} = \frac{|z_0|}{\frac{S_1}{2}} \quad \text{and} \quad \frac{V_2}{N_2} = \frac{|z_B - z_0|}{\frac{S_2}{2}} \quad (4-16)$$

The vertical component $V_{\$}$ of axial force $N_{\$}$ derives from Eqs. (4-13) to (4-16). So:

$$V_1 = 2|z_0| E_1 A_1 \left(\frac{1}{S_{01}} - \frac{1}{2\sqrt{z_0^2 + x_A^2}} \right) \quad (4-17)$$

$$V_2 = 2|z_B - z_0| E_2 A_2 \left[\frac{1}{S_{02}} - \frac{1}{2\sqrt{(z_B - z_0)^2 + y_B^2}} \right] \quad (4-18)$$

Cable's axial force $N_{\$}$ can be expressed as the percentage $w_{\$}$ of cable's axial force capacity $N_{\$}^{\text{cap}}$ as:

$$w_{\$} = 100 \frac{N_{\$}}{N_{\$}^{\text{cap}}} \quad (4-19)$$

where $\$ = 1, 2$.

A simple 1-DOF cable net under concentrated load in the direction $-z$, for instance snow or external wind, is illustrated in Figure 4-4.

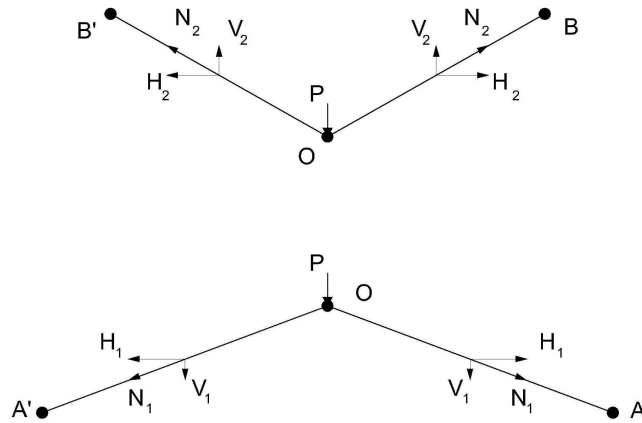


Figure 4-4: Equilibrium state of a simple 1-DOF cable net under concentrated load in the direction $-z$ (cables are not in the same plane)

The equation of static equilibrium in z -axis gives:

$$2V_1 + P = 2V_2 \quad (4-20)$$

Using Eq. (2-11), the concentrated load P applied at the middle of simple cable 2 derives from:

$$(2-11) \Rightarrow P = 2E_2A_2 \left[\frac{2}{S_{02}} - \frac{1}{\sqrt{(z_B - z_0)^2 + \frac{L_2^2}{4}}} \right] (z_B - z_0) \quad (4-21)$$

Replacing Eqs. (4-17), (4-18) and (4-21) into (4-20) and solving nonlinear Eq. (4-20), the new value of z -coordinate of nodal point O z_0 is calculated.

In case of a concentrated load in the direction $+z$, for example internal wind, the equation of static equilibrium in z -axis is:

$$2V_2 + P = 2V_1 \quad (4-22)$$

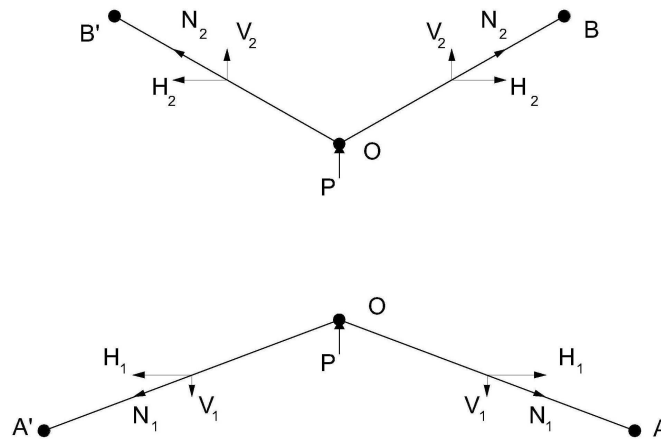


Figure 4-5: Equilibrium state of a simple 1-DOF cable net under concentrated load in the direction +z (cables are not in the same plane)

V_1 and V_2 come from Eqs. (4-17) and (4-18) correspondingly. The concentrated load P applied at the middle of simple cable 1 comes from Eq. (2-11):

$$(2-11) \Rightarrow P = 2E_1A_1 \left(\frac{2}{S_{01}} - \frac{1}{\sqrt{z_0^2 + \frac{L_1^2}{4}}} \right) z_0 \quad (4-23)$$

The solution of nonlinear Eq. (4-22) gives the new value of z-coordinate of nodal point O z_0 .

4.4 MODELING WITH MATLAB

Eqs. (4-11), (4-20) and (4-22) are nonlinear and, so, the finding of the solution is a complex and time-consuming procedure. In such cases, MATLAB can provide accurate and quick solutions. MATLAB is a high-performance language for technical computing. It integrates computation, visualization, and programming in an easy-to-use environment where problems and solutions are expressed in familiar mathematical notation. MATLAB is an interactive system whose basic data element is an array that does not require dimensioning. This allows user to solve many technical computing problems, especially those with matrix and vector formulations, in a fraction of the time it would take to write a program in a scalar noninteractive language such as C or FORTRAN [10].

In the context of this diploma thesis, the form finding of Paragraph 4.2 and the nonlinear analysis of Paragraph 4.3 are modeled in MATLAB. For this purpose, software for the nonlinear static analysis of 1-DOF cable net is developed. User can easily define input values, take instant nonlinear solutions, check if they are acceptable, change specific cables' parameters or applied loads and produce graphical results. The software and its manual are contained in the accompanied CD or can be found at the link of reference [9].

EXAMPLE

A simple 1-DOF cable net is analyzed. At first, the form of the 1-DOF cable net is found without external loads and, afterwards, distributed loads at $\pm z$ direction are imposed. The input data and the results of the analyses are presented in the following screenshots.

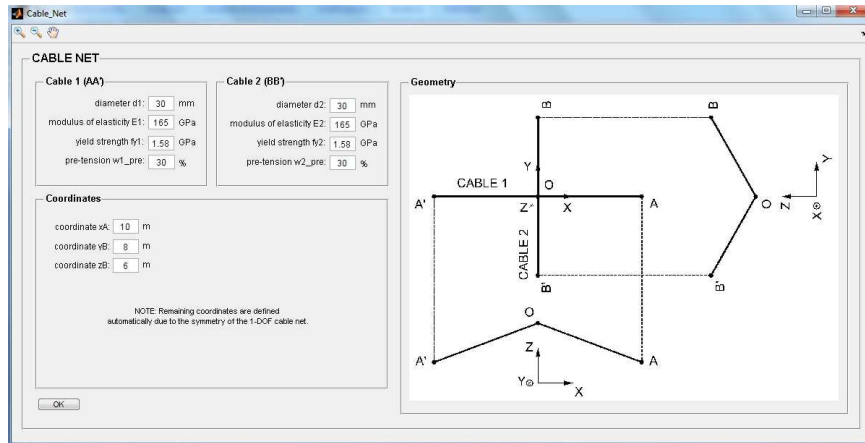


Figure 4-6: Screenshot for 1-DOF cable net geometry

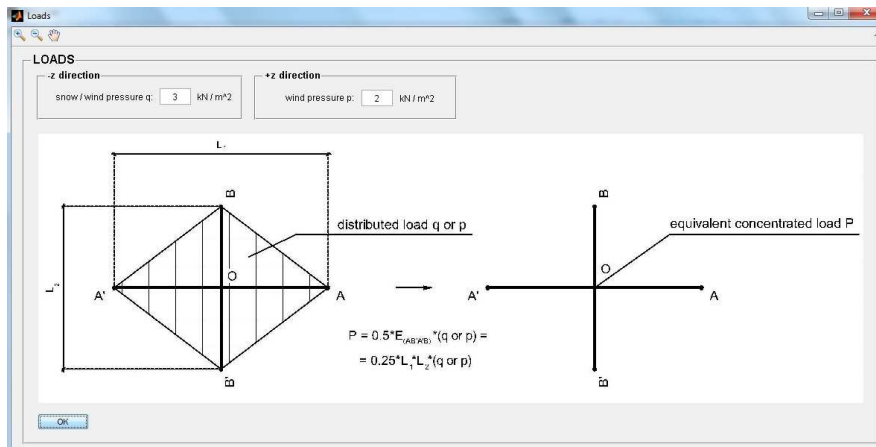


Figure 4-7: Screenshot for loads

STEP 1: FORM FINDING

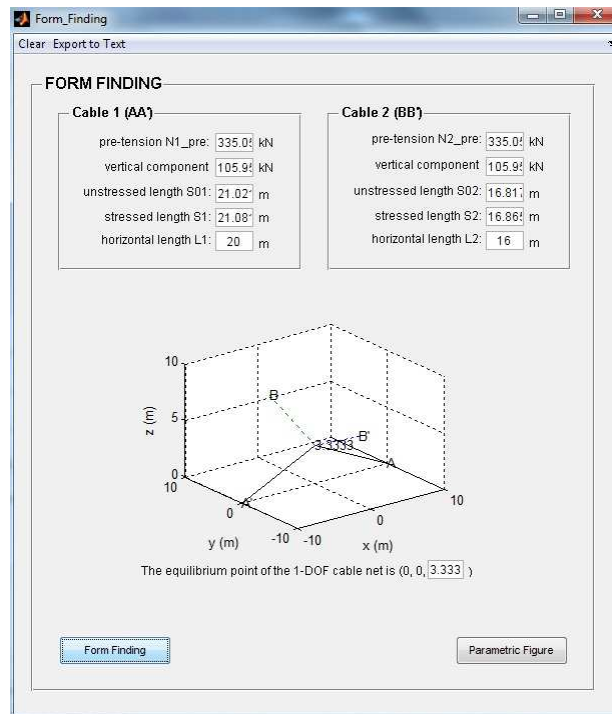


Figure 4-8: Screenshot for form finding

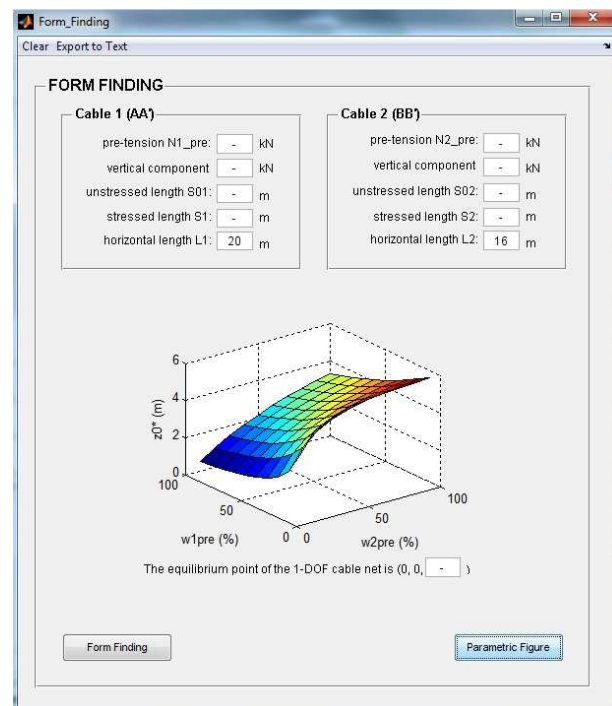


Figure 4-9: Screenshot for parametric figure

STEP 2: NONLINEAR ANALYSIS FOR CONCENTRATED LOADS P

-z direction

pressure $q = 3.0 \text{ kN/m}^2$

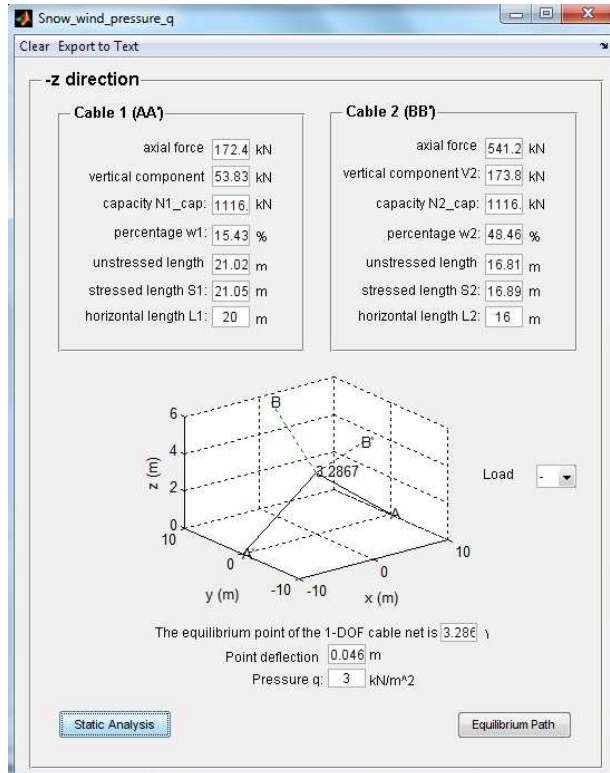


Figure 4-10: Screenshot for static analysis

+z direction

pressure p = 2.0 kN/m²

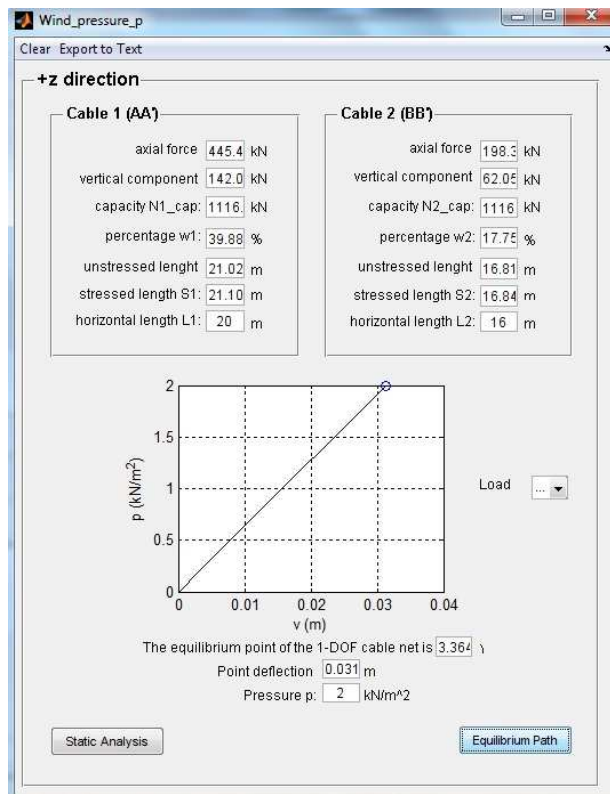


Figure 4-11: Screenshot for equilibrium path

4.5 PARAMETRIC ANALYSIS

What affects, in a significant way, the final place of nodal point O and the axial force N_s of cable s is the initial pre-tension w_s^{pre} . The geometry of cable net at the equilibrium state should fulfill architectural demands while axial force N_s neither can reach N_s^{cap} , as cable s might break, nor the value 0, as it might get loose. Here, parametric figures of a 1-DOF cable net are presented.

EXAMPLE

Below, a 1-DOF cable net model for parametric analysis is presented. Figure 4-12 shows a screenshot from the tab of input data. As $w1_{\text{pre}}$ and $w2_{\text{pre}}$ change their values in parametric figures, values on the screenshot are just a possible combination.

CABLE NET

Cable 1 (AA)

diameter d1: 30 mm

modulus of elasticity E1: 165 GPa

yield strength fy1: 1.58 GPa

pre-tension w1_pre: 30 %

Cable 2 (BB)

diameter d2: 30 mm

modulus of elasticity E2: 165 GPa

yield strength fy2: 1.58 GPa

pre-tension w2_pre: 30 %

Coordinates

coordinate xA: 10 m

coordinate yB: 8 m

coordinate zB: 6 m

NOTE: Remaining coordinates are defined automatically due to the symmetry of the 1-DOF cable net.

Figure 4-12: Screenshot for input data

For the purposes of the parametric analysis, distributed loads, such as snow and wind, are considered. These loads are applied perpendicularly on the membrane which covers the 1-DOF cable net. The equivalent concentrated nodal load P , in kN, applied on the central node is defined in Eq. (4-12).

The parametric figures contain the following symbols.

Form finding

z_0^* : z-coordinate of the central node, before the application of external loads, in m

w_1^{pre} : pre-tension of cable 1, at the equilibrium state, as a percentage (%) of the cables' axial force capacity N_1^{cap}

$$w_1^{\text{pre}} = 100 \frac{N_1^{\text{pre}}}{N_1^{\text{cap}}} = 100 \frac{N_1^{\text{pre}}}{f_{y1} \frac{\pi d_{A1}^2}{4}} \quad (6-24)$$

w_2^{pre} : pre-tension of cable 2, at the equilibrium state, as a percentage (%) of cables' axial

force capacity N_2^{cap}

$$w_2^{\text{pre}} = 100 \frac{N_2^{\text{pre}}}{N_2^{\text{cap}}} = 100 \frac{N_2^{\text{pre}}}{f_{y2} \frac{\pi d_{A2}^2}{4}} \quad (6-25)$$

$S_{0\$}$: initial unstressed length of cable \$, where \$ = 1, 2

Static analysis

z_0 : z-coordinate of the central node, after the application of external loads, in m

w_1 : axial force of cable 1, at the equilibrium state, as a percentage (%) of cables' axial force capacity N_1^{cap}

$$w_1 = 100 \frac{N_1}{N_1^{\text{cap}}} \quad (6-26)$$

w_2 : axial force of cable 2, at the equilibrium state as a percentage (%) of cables' axial force capacity N_2^{cap}

$$w_2 = 100 \frac{N_2}{N_2^{\text{cap}}} \quad (6-27)$$

STEP 1: FORM FINDING

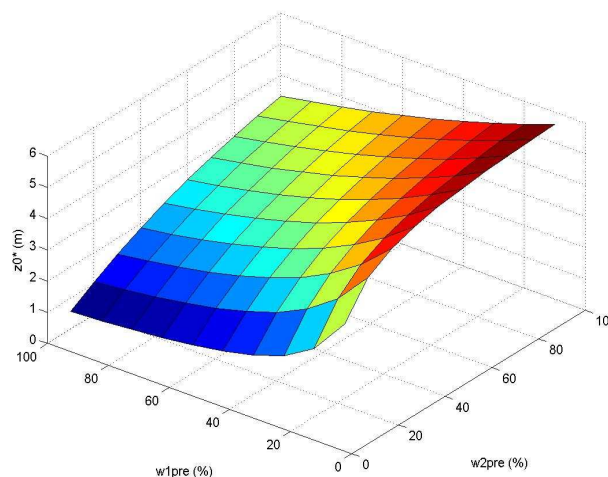


Figure 4-13: z-coordinate of nodal point O, for different values of pre-tensions (w_1^{pre} , w_2^{pre})

Figure 4-13 presents a parametric surface, which describes the z-coordinate of nodal point O for different values of pre-tensions (w_1^{pre} , w_2^{pre}). As w_1^{pre} increases and w_2^{pre} decreases, the equilibrium point O tends to poise lower. Increase of w_1^{pre} means increase of the axial force N_1^{pre} , in other words cable 1 tends to drag to its side the equilibrium point O.

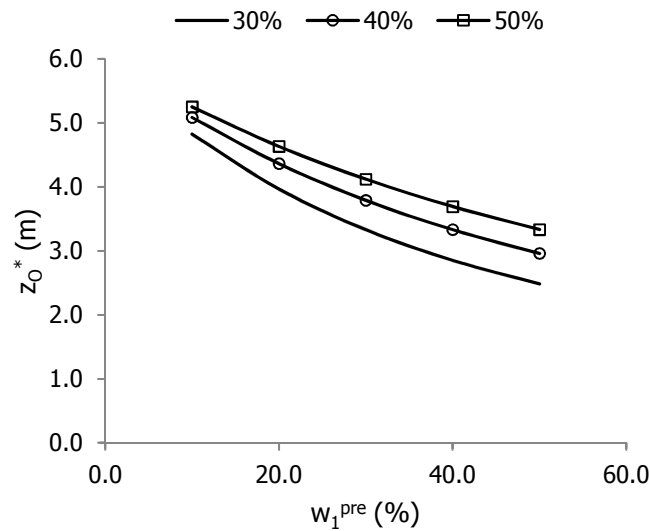


Figure 4-14: z_0^* – pre-tension w_1^{pre} curves, at the equilibrium state, for different values of pre-tension w_2^{pre}

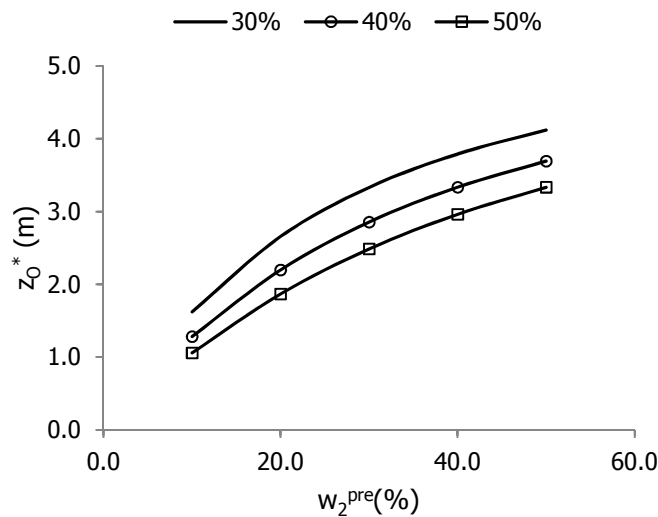


Figure 4-15: z_0^* – pre-tension w_2^{pre} curves, at the equilibrium state, for different values of pre-tension w_1^{pre}

The dependence of form finding on pre-tensions w_1^{pre} and w_2^{pre} is presented in Figures 4-14 and 4-15. The larger the pre-tension w_2^{pre} is, the higher the equilibrium point stands. The reverse correlation incurs for pre-tension w_1^{pre} . These figures prove that the increase of pre-tension makes cables reduce their stressed length by moving the equilibrium point nearer to the level of their supports, as larger values of cable tension occur.

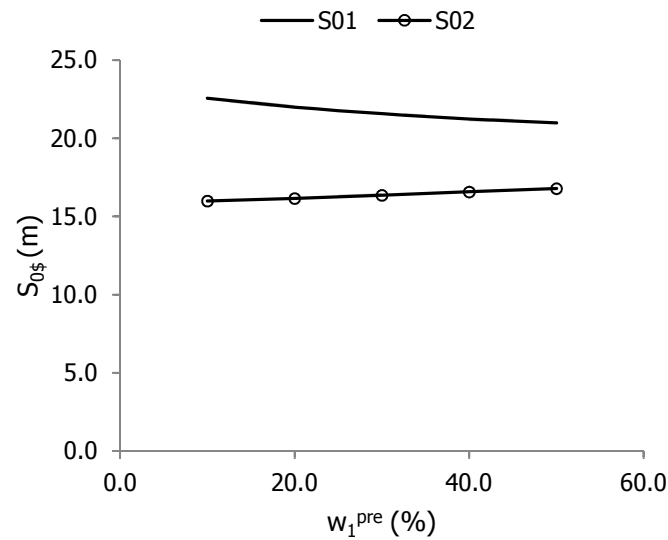


Figure 4-16: $S_{0\$,}$ – pre-tension w_1^{pre} curves, at the equilibrium state, in case that pre-tension $w_2^{pre} = 50\%$

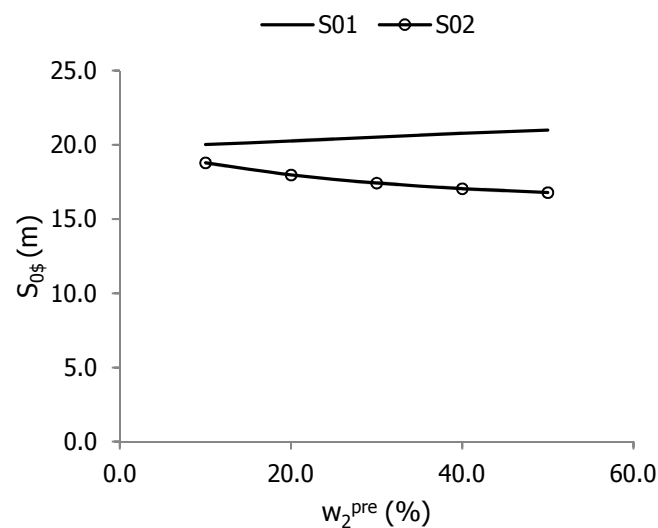


Figure 4-17: $S_{0\$,}$ – pre-tension w_2^{pre} curves, at the equilibrium state, in case that pre-tension $w_1^{pre} = 50\%$

Figures 4-16 and 4-17 indicate that the increase of pre-tension in cable $\$,$ leads to decrease of its initial unstressed length $S_{0\$,}$, where $\$ = 1, 2$. This is in accordance with the fact that, pre-tension in cables is caused by an initial unstressed length shorter than the distance spanned. The shorter the cable is the larger pre-tension acquires. The initial unstressed length of the second cable increases.

STEP 2: NONLINEAR ANALYSIS FOR CONCENTRATED LOADS P

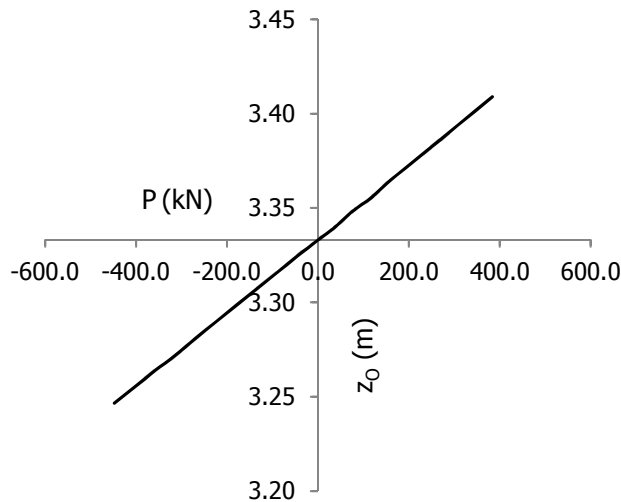


Figure 4-18: $z_0 - P$ curve for $w_1^{pre} = w_2^{pre} = 30.0\%$

Figure 4-18 shows the response of the central node to concentrated nodal load P . The curve is, almost, linear indicating that the geometric nonlinearity is not intense, as cables with reverse curvatures tend to eliminate it. Figure 4-18 occurs from the combination of two separate analyses for concentrated nodal load P at $\pm z$ directions.

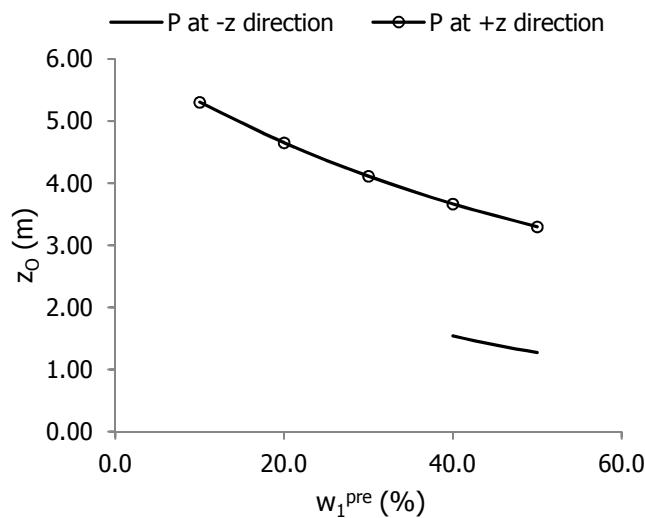


Figure 4-19: $z_0 - w_1^{pre}$, in case that pre-tension $w_2^{pre} = 14\%$ (-z direction) and 46% (+z direction)

Figure 4-19 describes the relationship between z_0 and w_1^{pre} . The larger the pre-tension w_1^{pre} is, the lower the equilibrium point stands, both cases of concentrated load P . Figures 4-14 and 4-15 show that the larger the pre-tension w_1^{pre} is, the lower the equilibrium point stands, in case of form finding. The same behavior occurs for a concentrated nodal load P . In case of load P at $-z$ direction, the equilibrium point stands lower, in comparison to this in case of load P at $+z$ direction, as the direction of the load indicates the direction of the nodal deflection. Pre-tension w_2^{pre} remains constant but has different values in $\pm z$ direction, as there is not a common section, within cables do not break and do not loose, in the range of its values for different kinds of loads P .

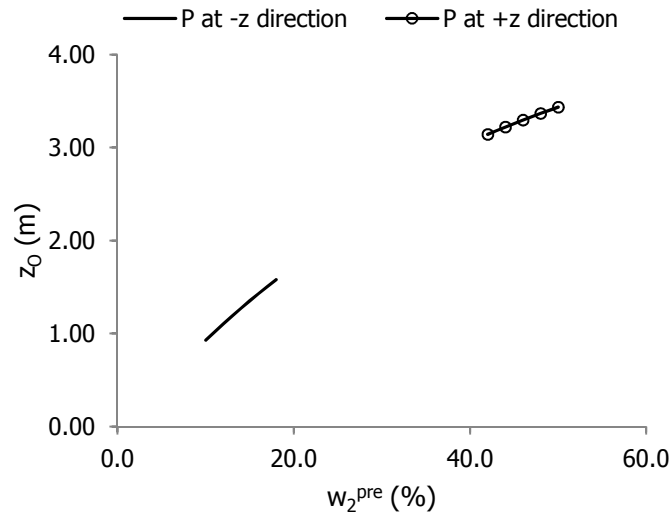


Figure 4-20: $z_0 - w_2^{pre}$, in case that pre-tension $w_1^{pre} = 50\%$

Figure 4-20 describes the relationship between z_0 and w_2^{pre} . Here, the larger the pre-tension w_2^{pre} is, the higher the equilibrium point stands, both cases of concentrated load P . According to Figures 4-14 and 4-15, the larger the pre-tension w_2^{pre} is, the higher the equilibrium point stands, in case of form finding. The same behavior occurs for a concentrated nodal load P . In case of load P at $-z$ direction, the equilibrium point stands lower, in comparison to this in case of load P at $+z$ direction, as the direction of the load indicates the direction of the nodal deflection.

The values of P at $\pm z$ directions are defined below.

direction $-z$

pressure $q = 12.00 \text{ kN/m}^2 \Rightarrow P = 960 \text{ kN}$

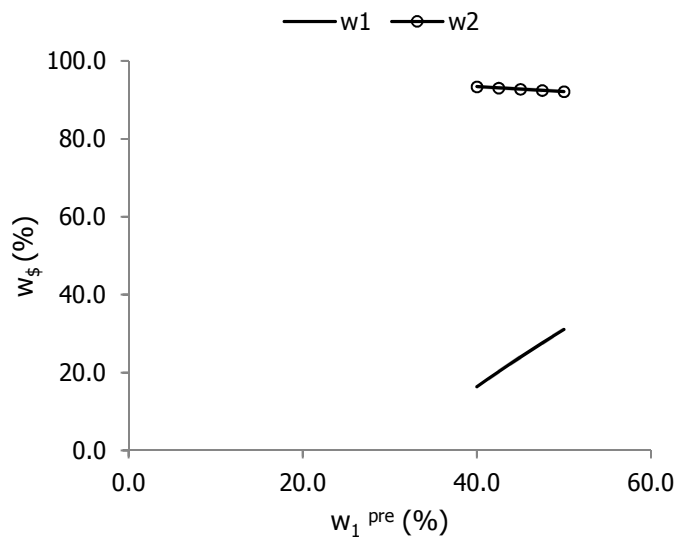


Figure 4-21: $w_\phi - w_1^{pre}$ curves, at the equilibrium state, in case that pre-tension $w_2^{pre} = 14\%$

According to Figure 4-21, the larger the pre-tension w_1^{pre} is, the larger axial force w_1 and the smaller axial force w_2 occur, given constant values of pre-tension w_2^{pre} and concentrated nodal load P . A larger value of axial force w_1 arises for higher starting level of pre-tension w_1^{pre} and constant value of concentrated nodal load P . What is more, Figure 4-16 indicates that the larger the pre-tension w_1^{pre} is, the larger initial unstressed length S_{02} occurs, in other words smaller pre-tension w_2^{pre} or smaller axial force w_2 , for constant value of concentrated nodal load P .

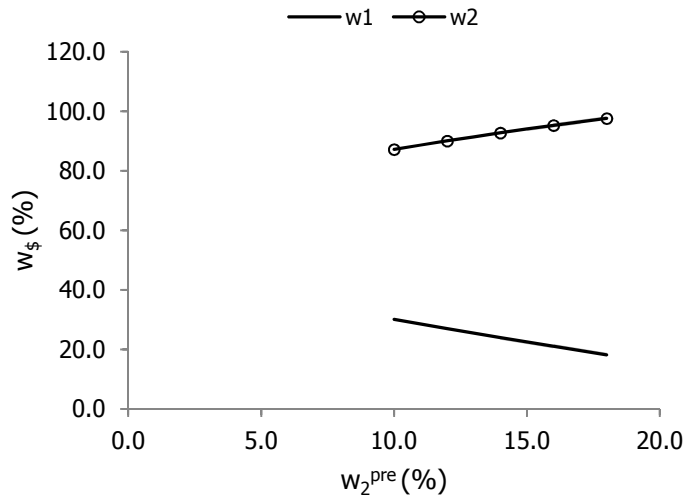


Figure 4-22: $w_§$ – pre-tension w_2^{pre} curves, at the equilibrium state, in case that pre-tension $w_1^{pre} = 45\%$

Figure 4-22 indicates that the larger the pre-tension w_2^{pre} is, the smaller axial force w_1 and the larger axial force w_2 occur, given constant values of pre-tension w_1^{pre} and concentrated nodal load P . This is true, as for higher starting level of pre-tension w_2^{pre} and constant value of concentrated nodal load P , a larger value of axial force w_2 arises. Moreover, Figure 4-17 indicates that the larger the pre-tension w_2^{pre} is, the larger initial unstressed length S_{01} occurs, in other words smaller pre-tension w_1^{pre} or smaller axial force w_1 , for constant value of concentrated nodal load P .

direction +z

pressure $p = 6.6 \text{ kN/m}^2 \Rightarrow P = 526 \text{ kN}$

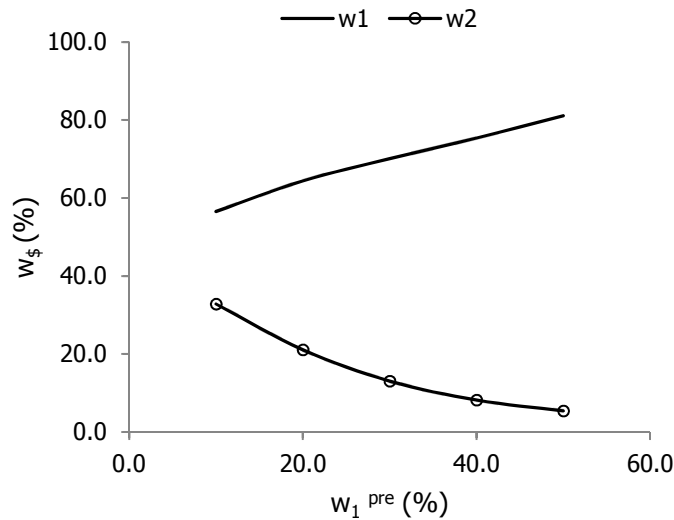


Figure 4-23: w_ξ – pre-tension w_1^{pre} curves, at the equilibrium state, in case that pre-tension $w_2^{pre} = 46$ %

According to Figure 4-23, the larger the pre-tension w_1^{pre} is the larger axial force w_1 and the smaller axial force w_2 and occur, given constant values of pre-tension w_2^{pre} and concentrated nodal load P . A larger value of axial force w_1 arises for higher starting level of pre-tension w_1^{pre} and constant value of concentrated nodal load P . What is more, Figure 4-16 indicates that the larger the pre-tension w_1^{pre} is, the larger initial unstressed length S_{02} occurs, in other words smaller pre-tension w_2^{pre} or smaller axial force w_2 , for constant value of concentrated nodal load P .

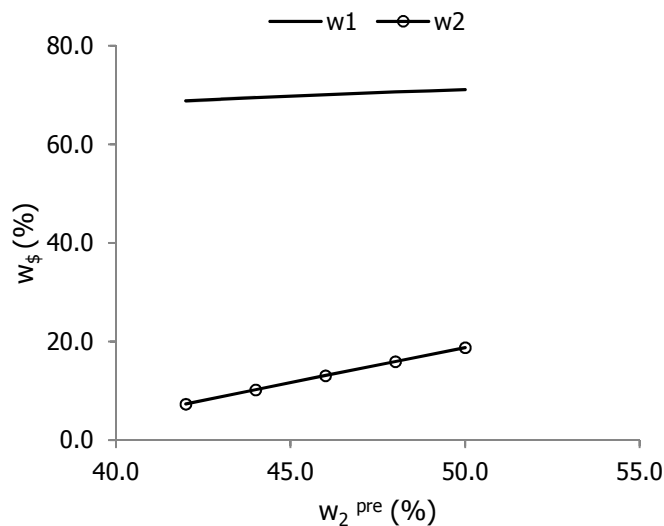


Figure 4-24: w_ξ – pre-tension w_2^{pre} curves, at the equilibrium state, in case that pre-tension $w_1^{pre} = 30$ %

Figure 4-24 indicates that the larger the pre-tension w_2^{pre} is the larger axial force w_2 and occurs, given constant values of pre-tension w_1^{pre} and concentrated nodal load P . This is true, as for higher starting level of pre-tension w_2^{pre} and constant value of concentrated nodal load P , a larger value of axial force w_2 arises. Moreover, axial force w_1 remains almost

constant with a slight increase. This occurs from the load conditions and cable net geometry of the model and cannot provide a physical explanation of cable net response.

Notice in Figures 4-21 to 4-24 that, the additional axial force ($w_{\$} - w_{\$}^{\text{pre}}$), due to the concentrated nodal load P , is significantly larger than the initial pre-tension $w_{\$}^{\text{pre}}$, where $\$ = 1, 2$. For instance, as presented in Figure 4-21, for $w_1^{\text{pre}} = 40.0\%$ and $w_2^{\text{pre}} = 14.0\%$, w_2 is around 90%. In other words, $90 - 14 = 76\%$ of axial force of cable 2 occurs from the concentrated nodal load P and is according to a good design policy. The range of $w_{\$}^{\text{pre}}$, where $\$ = 1, 2$, in STEP 2 differs in $\pm z$ -directions of concentrated nodal load P , as it depends on cables' diameter and cables' axial force capacity.

4.6 NUMERICAL SOLUTION

The comparison between analytical and numerical curves verifies the rightness of the analytical solutions developed in Paragraphs 4.2 and 4.3. Reader can use either analytical formulas or the finite element software ADINA and SAP for the analysis of a 1-DOF cable net, as identical results occur. In the accompanied CD, there is a list of the numerical models, which contains the attributes of each model case. The model used in this chapter is commented with the word 'comparison'. In the same CD, the .idb file for ADINA and the .sdb file for SAP can be found.

Analytical solution: Paragraph 4.2 and 4.3

Parametric figures: Paragraph 4.5

4~2_crossed_cables_pre-tensioned		
x_A	10.000	m
y_B	5.000	m
z_B	8.000	m
E₁ = E₂	165	GPa
f_{y1} = f_{y2}	1.58	GPa
d_{A1} = d_{A2}	20	mm

Table 4-1: Characteristic values of numerical cable model

ADINA

- Form finding

The pre-tension is applied by defining the value of initial strains. At first, random values of initial strains are chosen. The results of solution, for different combinations of initial strains, are presented below.

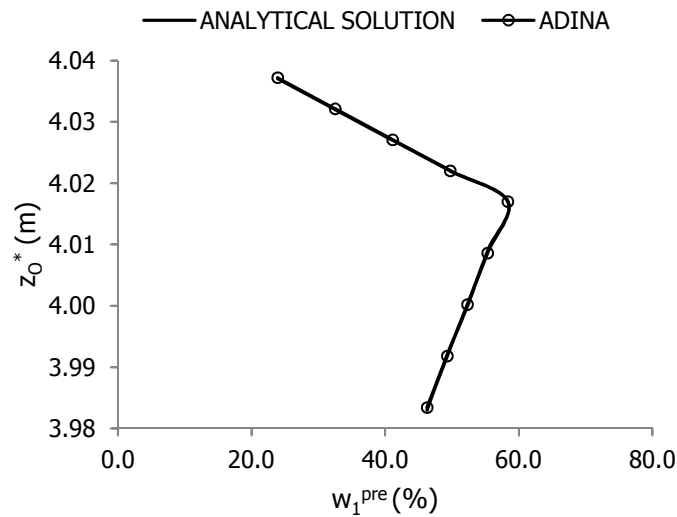


Figure 4-25: z_0^* – pre-tension w_1^{pre} curves, at the equilibrium state

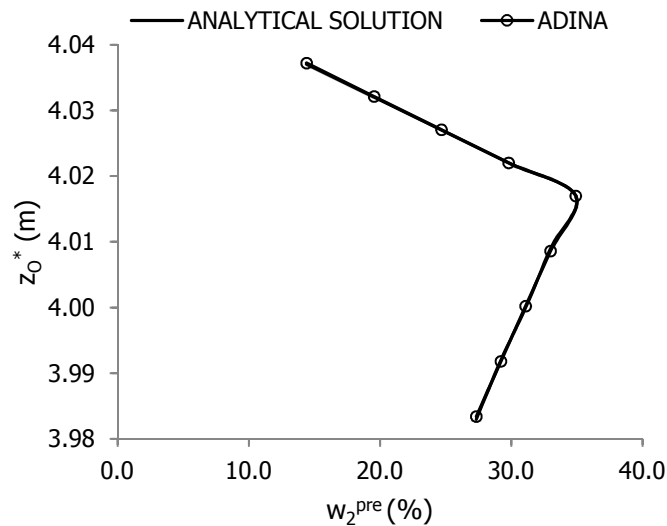


Figure 4-26: z_0^* – pre-tension w_2^{pre} curves, at the equilibrium state

The combination of pre-tensions (w_1^{pre} , w_2^{pre}) derives from the same value of z_0^* of Figures 4-25 and 4-26.

- Nonlinear analysis for concentrated load

The random input values of initials strains are:

Initial strain of cable 1 = 0.004

Initial strain of cable 2 = 0.005

The results of the solution without concentrated load P , for these input values, are considered as the pre-tensions for nonlinear analysis for concentrated load P .

- z direction

$$P^{\max} = 530.0 \text{ kN}$$

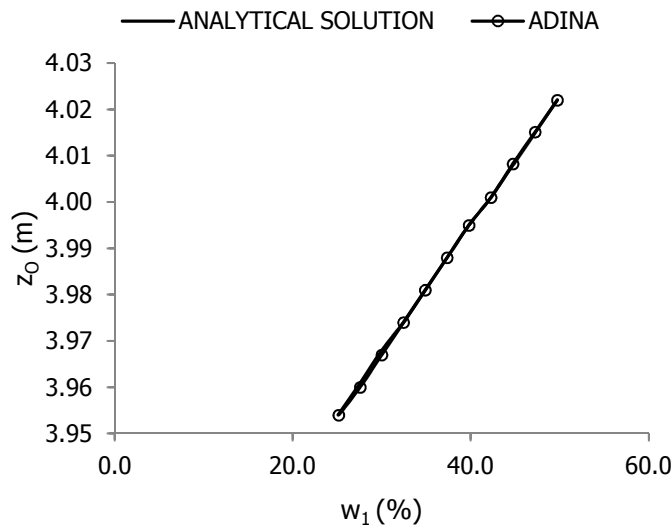


Figure 4-27: $z_0 - w_1$ curves, at the equilibrium state, for various values of P

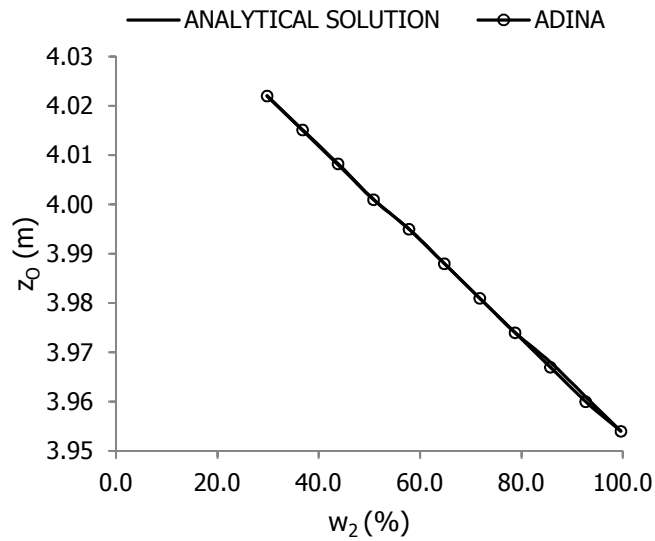


Figure 4-28: $z_0 - w_2$ curves, at the equilibrium state, for various values of P

Points of Figures 4-27 and 4-28 having the same value of z_0 correspond to the same value of applied P.

+ z direction

$$P^{\max} = 220.0 \text{ kN}$$

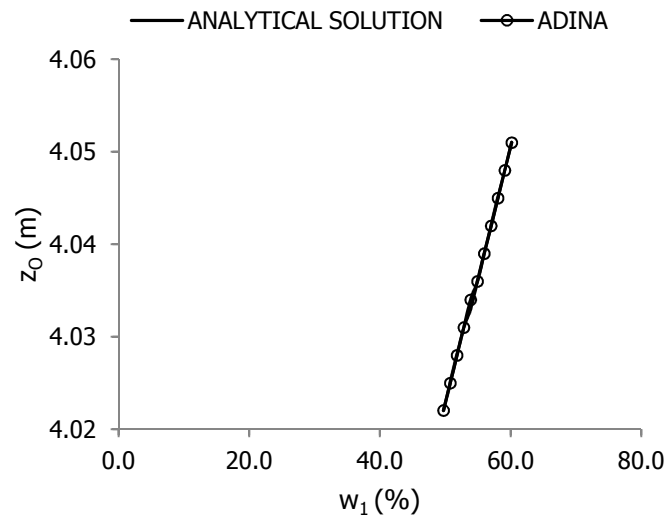


Figure 4-29: $z_0 - w_1$ curves, at the equilibrium state, for various values of P

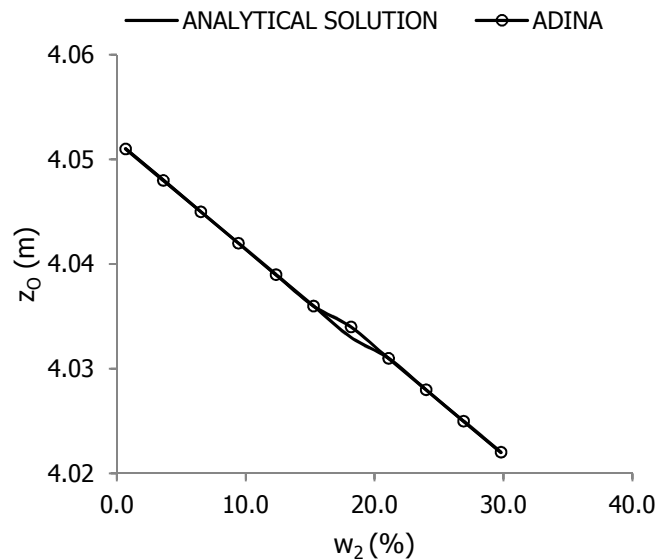


Figure 4-30: $z_0 - w_2$ curves, at the equilibrium state, for various values of P

Points of Figures 4-29 and 4-30 having the same value of z_0 correspond to the same value of applied P . The local difference in Figure 4-30 is 0.001 m, which is a negligible value.

SAP

- Form finding

The pre-tension is applied by defining the value of tensions at I-End of each cable. At first, random values of tensions at I-End of each cable are chosen. The results of solution, for different combinations of tensions at I-End of each cable, are presented below.

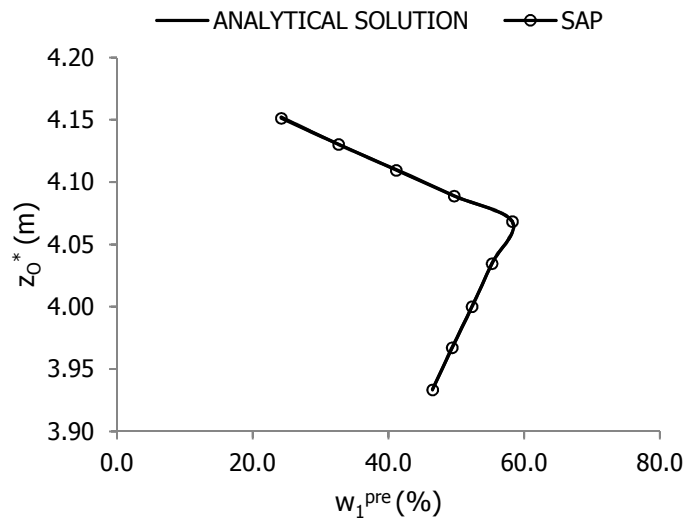


Figure 4-31: z_0^* – pre-tension w_1^{pre} curves, at the equilibrium state

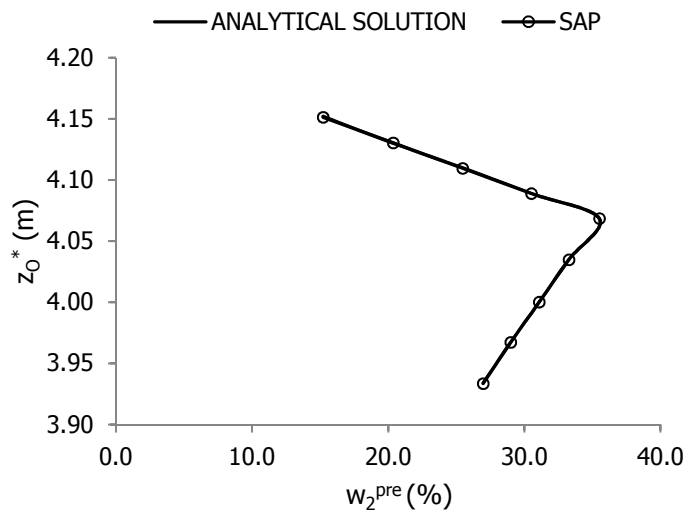


Figure 4-32: z_0^* – pre-tension w_2^{pre} curves, at the equilibrium state

The combination of pre-tensions (w_1^{pre} , w_2^{pre}) derives from the same value of z_0^* of Figures 4-31 and 4-32.

- Nonlinear analysis for concentrated load

The random input values of tensions at I-End of each cable are:

Axial force at I-End of cable 1 = 259.050 kN

Axial force at I-End of cable 2 = 207.240 kN

The results of the solution without concentrated load P, for these input values, are considered as the pre-tensions for nonlinear analysis for concentrated load P.

- z direction

$$P^{\max} = 506.0 \text{ kN}$$

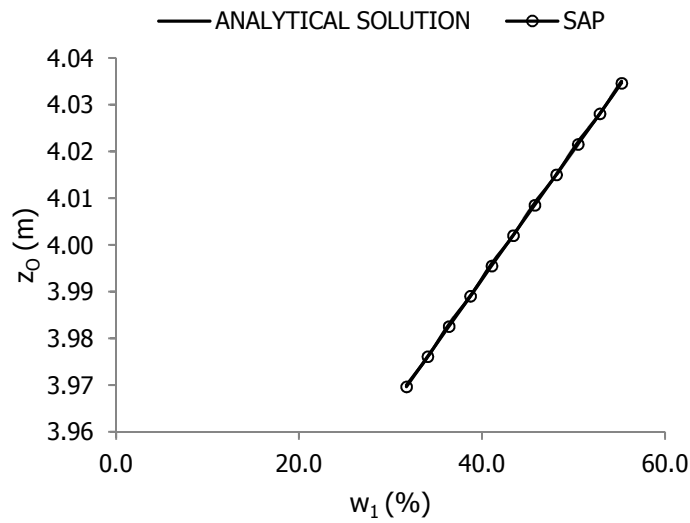


Figure 4-33: $z_0 - w_1$ curves, at the equilibrium state, for various values of P

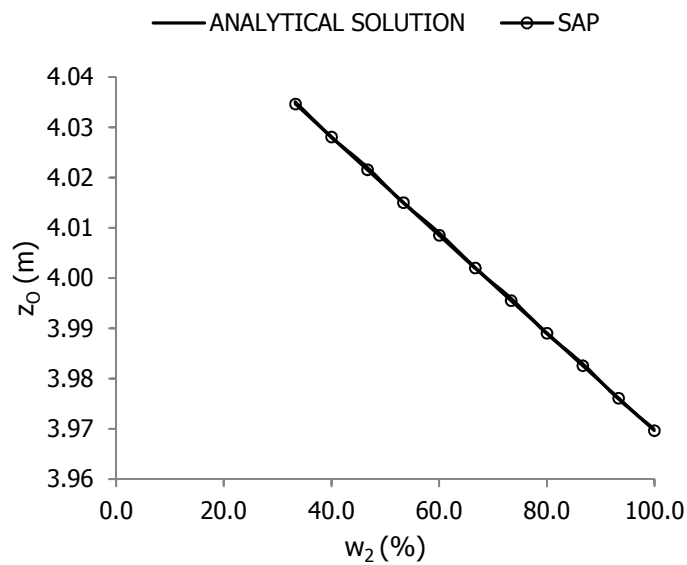


Figure 4-34: $z_0 - w_2$ curves, at the equilibrium state, for various values of P

Points of Figures 4-33 and 4-34 having the same value of z_0 correspond to the same value of applied P .

+ z direction

$$P^{\max} = 250.0 \text{ kN}$$

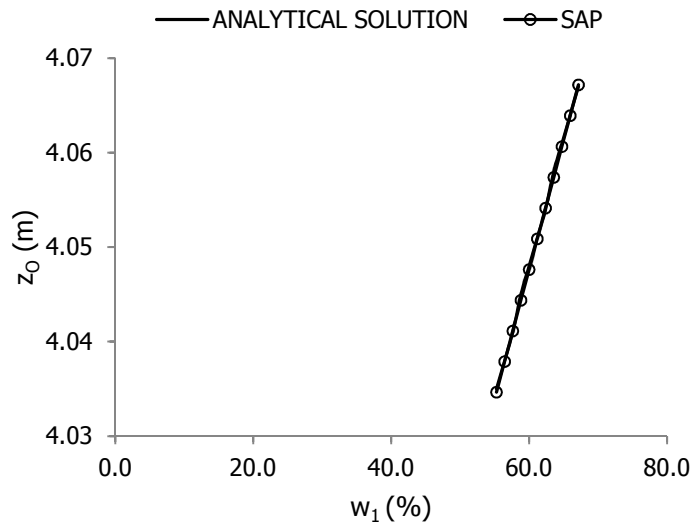


Figure 4-35: $z_0 - w_1$ curves, at the equilibrium state, for various values of P

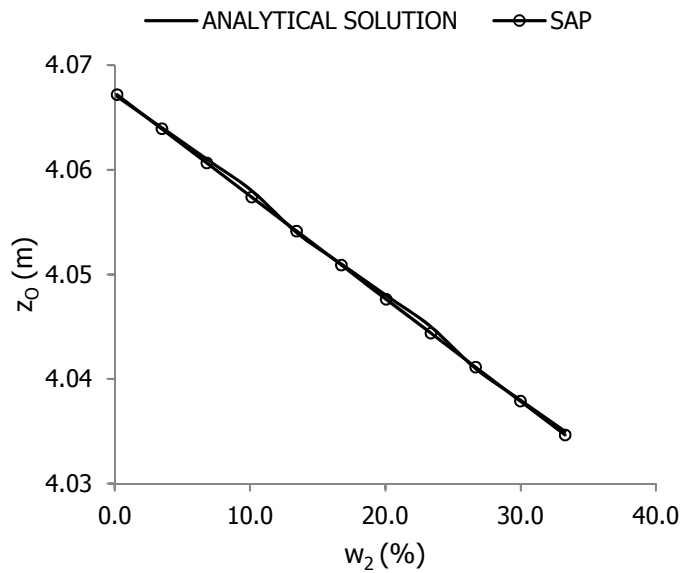


Figure 4-36: $z_0 - w_2$ curves, at the equilibrium state, for various values of P

Points of Figures 4-35 and 4-36 having the same value of z_0 correspond to the same value of applied P . The local differences in Figure 4-36 are less than 0.001 m, which is a negligible value.

5 RADIO MAST WITH PRE-TENSIONED CABLES

5.1 ANALYTICAL SOLUTION

A radio mast is, typically, a tall structure designed to support antennas for telecommunications and broadcasting, including television. It is sensitive to horizontal loads, such as seismic loads, and, due to its height, significant values of moment can occur at its base. Pre-tensioned cables are placed, in a symmetric way, along its height in order to improve structure's stability. Figure 5-1 illustrates a radio mast having two symmetric pre-tensioned cables. Both cables have initial unstressed length $S_0 \leq S_{AC} = S_{BC}$, where S_{AC} (S_{BC}) is the distance between points A (B) and C. The following analysis does not take into account cables' self weight. In such tall structures, self weight provokes cables' curvature, which cannot be omitted during the design procedure. Moreover, the vertical deflection of point C is omitted for simplification reasons. Curves' limits are defined by the axial force capacity N^{cap} of each cable.

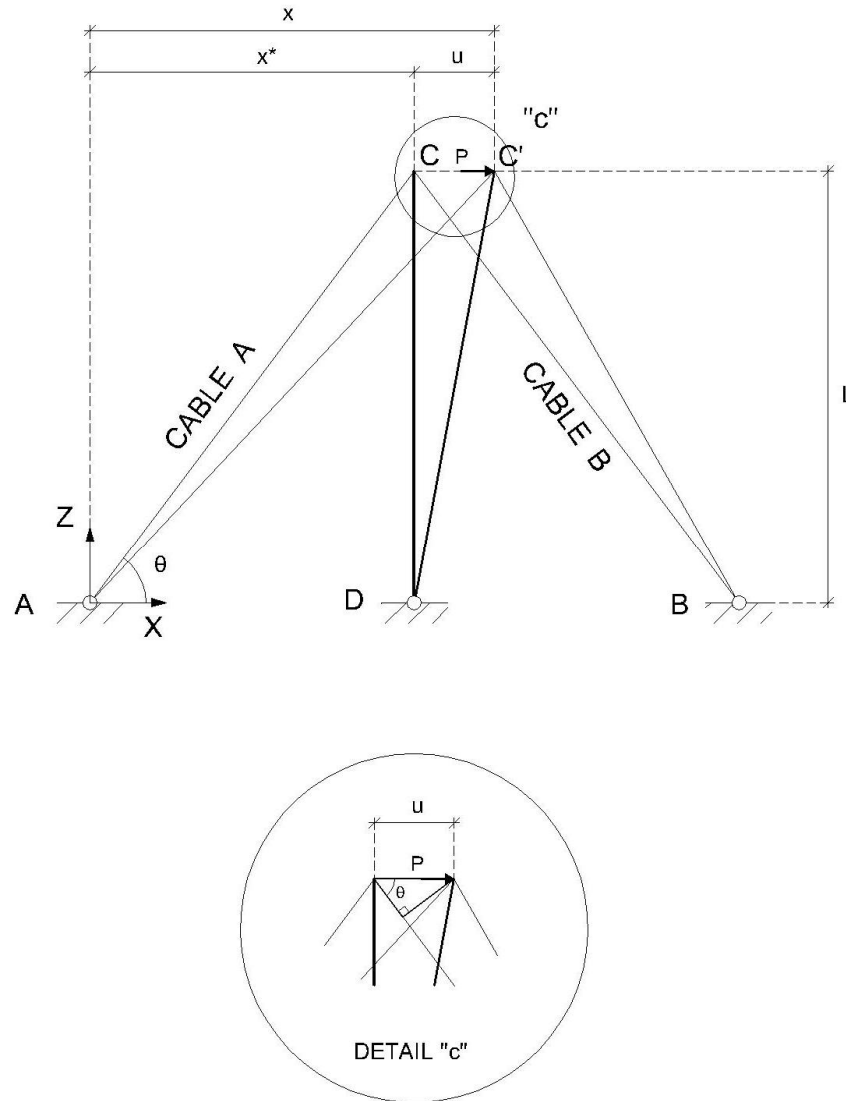


Figure 5-1: Radio mast model with pre-tensioned cables

A horizontal concentrated load P provokes horizontal displacement u of mast's peak and, as a result, horizontal imposed end displacement u of cables. Axial force of cable A N_A comes out from Eq. (2-77) and, in non-dimensional terms, from Eq. (2-78), for $S_0 < S_{AC}$. Pre-tension N_A^{pre} is defined as follows:

$$(2-77) \Rightarrow N_A^{pre} = N_A(x=x^*) = EA \left[\frac{x^*}{S_0} \sqrt{1 + (\tan\theta)^2} - 1 \right] \quad (5-1)$$

or

$$(2-78) \Rightarrow N_A^{pre} = N_A'(x'=x^{*'}) = \frac{x^{*'}}{S_0} \sqrt{1 + (\tan\theta)^2} - 1 \quad (5-2)$$

Axial force of cable B N_B is defined by Hooke's law as:

$$\sigma = E\varepsilon \Rightarrow \frac{N_B}{A} = E \frac{\Delta S}{S_0} \Rightarrow N_B = EA \frac{(S_{BC} - u \cos \theta) - S_0}{S_0} \quad (5-3)$$

where A is the cross-section and E is the modulus of elasticity of both cables.

Correspondingly:

$$(5-3) \Rightarrow N_B (u=0) = N_B^{\text{pre}} \quad (5-4)$$

Pre-tension N_i^{pre} is expressed as the percentage w_i^{pre} (%) of cable's axial force capacity N_i^{cap} , as defined in Paragraph 2.5.1, where $i = A, B$. In case of a radio mast:

$$w_A^{\text{pre}} = w_B^{\text{pre}} = w^{\text{pre}} \quad (5-5)$$

Parameter r (%) describes the axial force of cable B N_B as function of the horizontal end displacement u , according to the following equation:

$$r = 100 \frac{N_B}{N_B^{\text{pre}}} = 100 \frac{(S_{BC} - u \cos \theta) - S_0}{S_{BC} - S_0} \quad (5-6)$$

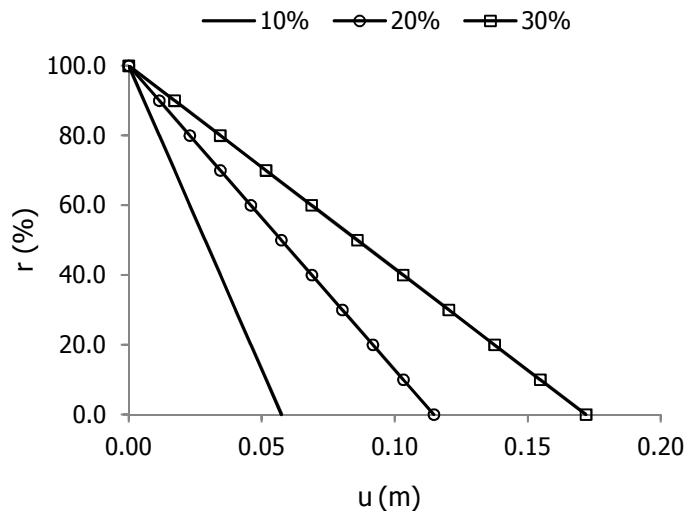


Figure 5-2: $r - u$ curves for different values of pre-tension w^{pre} , in case that $\theta = 60$ deg, $S_{BC} = 30$ m, $E = 165$ GPa and $d = 30$ mm

Figure 5-2 shows the dependence of parameter r on the pre-tension w^{pre} . Radio masts with larger values of pre-tension w^{pre} keep cable B tensioned for larger values of horizontal end displacement u , as the starting level of axial force N_i^{pre} is higher, where $i = A, B$.

The maximum value of the horizontal end displacement u^{max} is determined from the following restraints:

- Axial force of cable A N_A must not exceed $N_A^{\text{cap}} = Af_y$
- Cable B must not loosen. Cable's looseness provokes, in due course, attritions in cable's joints decreasing its efficiency.

So,

$$(2-77) \Rightarrow N_A^{\max} = N_A(x^{\max}) = Af_y \Rightarrow u^{\max} = \sqrt{\left[\left(\frac{f_y + E}{E}\right)S_0\right]^2 - L^2 - x^*} \quad (5-7)$$

and

$$(5-6) \stackrel{r=0\%}{\Rightarrow} u^{\max} = \frac{S_{BC} - S_0}{\cos\theta} \quad (5-8)$$

Finally:

$$u^{\max} = \min\left(\sqrt{\left[\left(\frac{f_y + E}{E}\right)S_0\right]^2 - L^2 - x^*}, \frac{S_{BC} - S_0}{\cos\theta}\right) \quad (5-9)$$

5.2 EQUIVALENT SIMPLE 1-DOF CABLE NET MODEL

The development of an analytical relationship between the horizontal concentrated load P and the horizontal deflection u is a complicated and time-consuming procedure. The comparison between the radio mast model, as shown in Figure 5-1, and the simple 1-DOF cable net, which is presented in Chapter 4, reveals equivalence. Indeed, if one cable of the simple net of Figure 4-1 is twisted 90 degrees, in order both cables lay on the same plane, an alternated cable net model is created, as shown in Figure 5-3. This new cable net model is equivalent to two mirrored radio masts. Notice that, the vertical deflection of point C cannot be implemented in the case of the twisted cable net, as exists in a real radio mast.

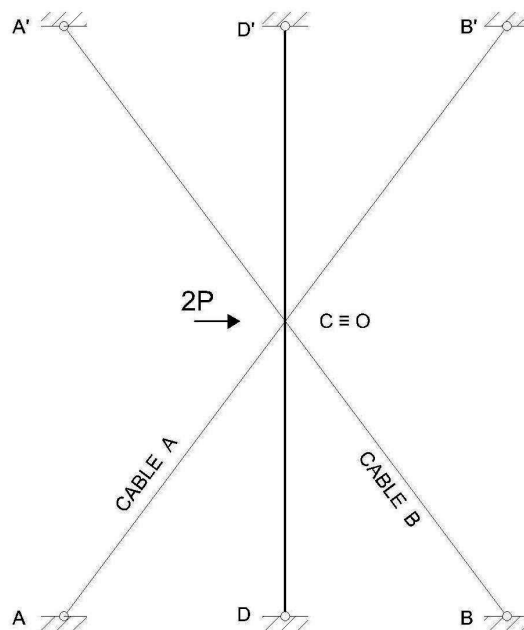


Figure 5-3: Equivalence of a twisted simple 1-DOF cable net with two mirrored radio masts

The application of a concentrated load $2P$ at the nodal point O of the twisted simple 1-DOF cable net gives the same results as if there was a single radio mast imposed under horizontal concentrated load P . This assumption is proven by the figures of Paragraph 5.4. Using MATLAB program, the analysis of a simple 1-DOF cable net imposed under concentrated nodal load $2P$ gives results for the deflection $z_0^* - z_0$ and cables' axial force $N_{\$}$, where $\$ = 1, 2$, for different values of load $2P$. Retaining the same values of deflection $u = z_0^* - z_0$ and cables' axial force N_i , where $i = B, A$, and assuming horizontal concentrated load $\frac{2P}{2} = P$ curves for the radio mast are designed in Paragraph 5.4.

The equivalence of these models gives the opportunity to extract an analytical expression of the stiffness K_{mast} of a radio mast. Otherwise, the mathematical procedure would be quite complex. It is considered that both cables remain tensioned or, in other words, that cable B does not get loose sometime, as this provokes attritions in cable's joints.

The simple 1-DOF cable net of Figure 4-4 is assumed. Eq. (4-20) describes the static equilibrium in z -axis, in case of a nodal concentrated load P . The replacement of Eqs. (4-17) and (4-18) into (4-20) gives:

$$P(z_0) = 4 \left\{ (z_B - z_0) EA \left[\frac{1}{S_0} - \frac{1}{2\sqrt{(z_B - z_0)^2 + y_B^2}} \right] - z_0 EA \left(\frac{1}{S_0} - \frac{1}{2\sqrt{z_0^2 + x_A^2}} \right) \right\} \quad (5-10)$$

where,

$$\begin{aligned} E_1 &= E_2 = E \\ A_1 &= A_2 = A \\ S_{01} &= S_{02} = S_0 \\ x_A &= y_B \end{aligned} \quad (5-11)$$

The expansion of Eq. (5-10) in Taylor series around the value $z_0 = z_0^*$ gives:

$$\begin{aligned} P(z_0) &= P(z_0^*) + \\ &+ \left\{ \frac{2EA(z_B - z_0^*)^2}{\left[(z_B - z_0^*)^2 + y_B^2 \right]^{\frac{3}{2}}} - \frac{2EAz_0^{*2}}{(z_0^{*2} + x_A^2)^{\frac{3}{2}}} + EA \left[\frac{2}{\sqrt{(z_B - z_0^*)^2 + y_B^2}} - \frac{4}{S_0} \right] + EA \left(\frac{2}{\sqrt{z_0^{*2} + x_A^2}} - \frac{4}{S_0} \right) \right\} (z_0 - z_0^*) + \dots \end{aligned} \quad (5-12)$$

The equilibrium point, in the form finding step, has z -coordinate $z_0^* = \frac{z_B}{2}$, as cables have the same characteristics and the cable net is symmetric. So:

$$P(z_0^*) = 0 \quad (5-13)$$

Comparing Figures 4-1 and 5-1 and taking into account the equivalence indicated on Figure 5-3, the symbols of Eq. (5-12), which refer to a cable net, can be replaced by the following symbols, which refer to a radio mast:

$$x_A = y_B \rightarrow L = \sin\theta S_{AC}$$

$$S_0 \rightarrow 2S_0$$

$$z_B \rightarrow 2\cos\theta S_{AC}$$

$$z_O^* \rightarrow \cos\theta S_{AC}$$

$$z_O \rightarrow \cos\theta S_{AC} - u = z_O^* - u$$

Eq. (5-12) turns into:

$$(5-12) \Rightarrow P = 4EA \left[\frac{\cos\theta^2}{S_{AC}} - \left(\frac{1}{S_{AC}} - \frac{1}{S_0} \right) \right] u = K_{net} u \quad (5-14)$$

The simple 1-DOF cable net has stiffness K_{net} . So, the radio mast, which is considered as the half of a cable net, has stiffness K_{mast} :

$$K_{mast} = \frac{K_{net}}{2} = 2EA \left[\frac{\cos\theta^2}{S_{AC}} - \left(\frac{1}{S_{AC}} - \frac{1}{S_0} \right) \right] \quad (5-15)$$

According to Paragraph 2.2.4.2, Eq. (5-15) is the equivalent spring constant K_s , in kN/m, of a linear spring. Using Eq. (2-183), the following parametric figure is created:

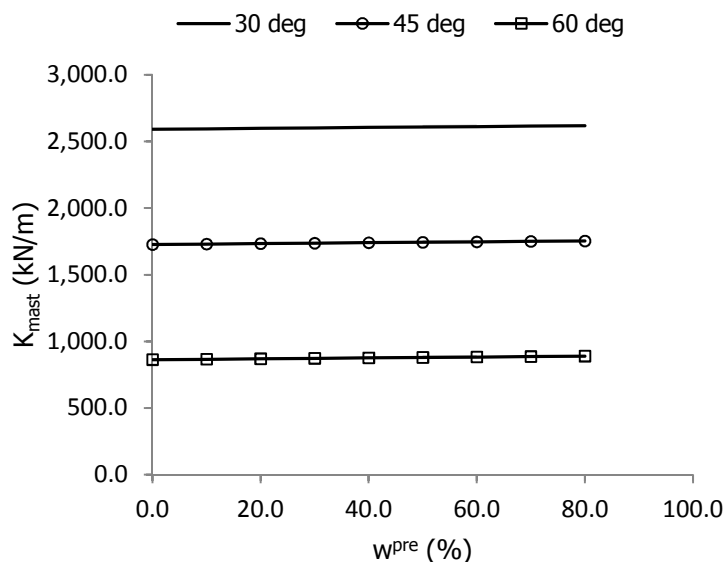


Figure 5-4: $K_{mast} - w^{pre}$ curves for different values of angle θ , in case that $S_{AC} = 30$ m, $E = 165$ GPa, $f_y = 1.58$ GPa and $d = 30$ mm

Figure 5-4 describes the stiffness K_{mast} of a radio mast as function of angle θ and pre-tension w^{pre} . As the angle θ increases, stiffness K_{mast} decreases because the horizontal component of axial force of cable A, which opposes to the horizontal deflection, decreases. Moreover, increase of w^{pre} leads to a slight increase of K_{mast} , as pre-tension w^{pre} adds stiffness K_{mast} in the model.

5.3 EFFECTS OF PRE-TENSIONING

Radio masts are stabilized by pre-tensioned cables. This pre-tension w^{pre} is applied by initial unstressed length S_0 shorter than the distance spanned S_{AC} or S_{BC} . Here, parametric diagrams of a radio mast are presented, for different values of pre-tension w^{pre} . Sample values of pre-tension w^{pre} are increased, corresponding to real situations. Figures are designed using the SAP model with title '5~SAC=30m~ θ =45deg~10-30%.SDB'.

θ	45	deg
S_{AC}	30.000	m
E	165	GPa
d_{A}	20	mm

Table 5-1: Parameters of the radio mast model

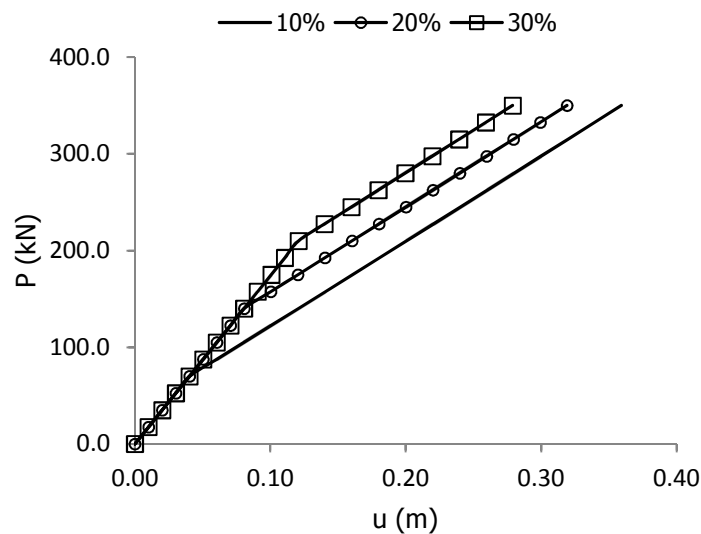


Figure 5-5: P – u curves for different values of pre-tension w^{pre}

The response of radio mast, as shown in Figure 5-5, is almost independent from pre-tension w^{pre} , when both cables are tensioned. When cable B gets loose, the stiffness K_{mast} decreases abruptly, as only cable A contributes to the response to the horizontal concentrated load P , and is larger (slightly steeper curve) for larger values of pre-tension w^{pre} , as pre-tension w^{pre} adds stiffness K_{mast} in the model.

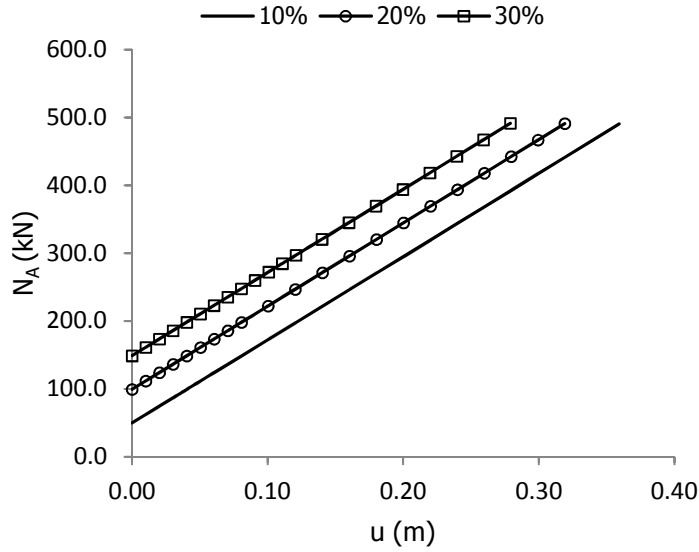


Figure 5-6: Axial force of cable A N_A as function of horizontal deflection u for different values of pre-tension w^{pre}

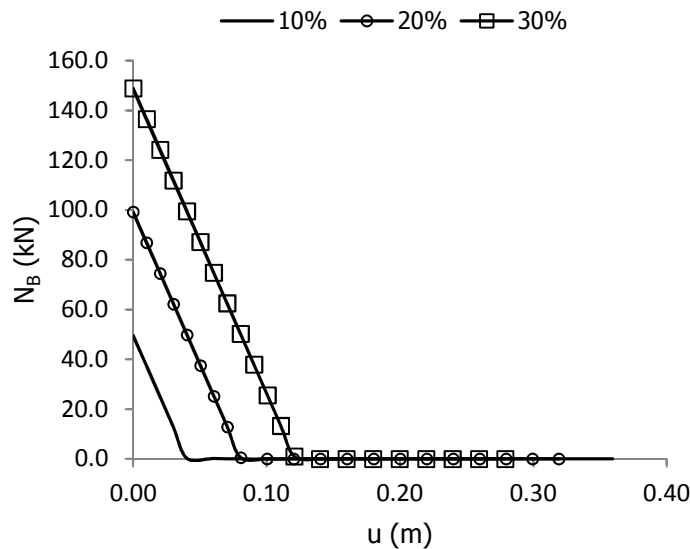


Figure 5-7: Axial force of cable B N_B as function of horizontal deflection u for different values of pre-tension w^{pre}

Radio masts with larger pre-tension w^{pre} have larger values of axial force N_i , where $i = A, B$, for the same value of horizontal deflection u as the starting level of axial force N_i^{pre} is higher, and sustain cable B tensioned for larger values of horizontal deflection u . As a consequence, the maximum value of the horizontal concentrated load P^{max} is depended on cables' pre-tension w^{pre} .

5.4 NUMERICAL SOLUTION

5~SAC=30m~θ=60deg~20% - radio mast -		
θ	60	deg
S_0	29.943	m
S_{AC}	30.000	m
w^{pre}	20.0	%
N^{pre}	223.254	kN
E	165	GPa
d_A	30	mm
p^{max}	225.000	kN

Table 5-2: Characteristic values of numerical cable models

The maximum value of the horizontal concentrated load P^{max} is chosen according to the restraints of Eq. (5-9). Figures 5-8 to 5-10 show the identification between numerical models and analytical solution. Moreover, they prove the assertion of equivalence between a radio mast and a twisted simple 1-DOF cable net, as described in Paragraph 5.2. Figure 5-8 indicates that the assumption of an equivalent linear spring gives identical results with the numerical solution with truss elements. In the accompanied CD, there is a list of the numerical models, which contains the attributes of each model case. The model used in this chapter is commented with the word 'comparison'. In the same CD, the .idb file for ADINA and the .sdb file for SAP can be found.

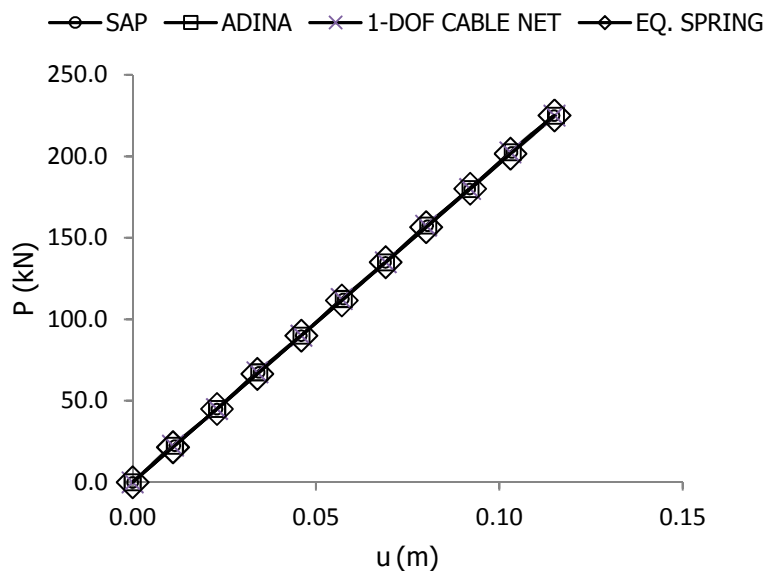


Figure 5-8: P – u

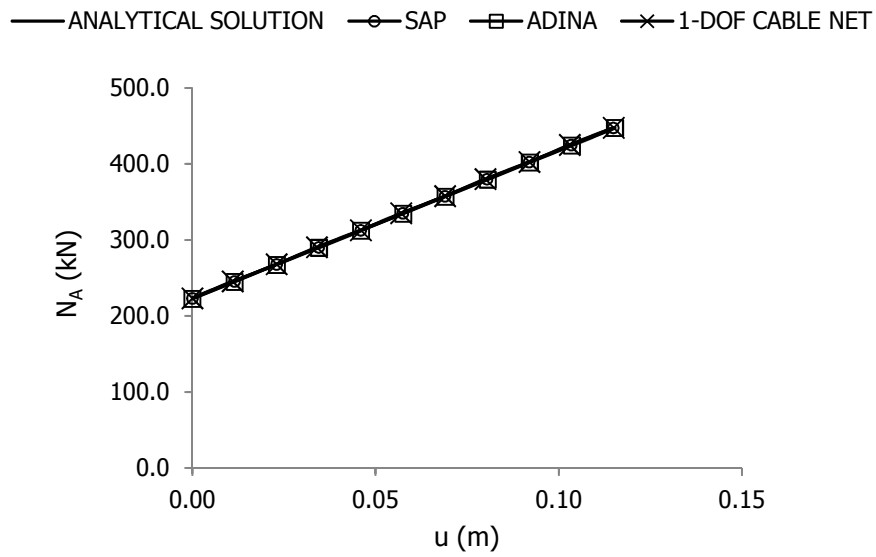


Figure 5-9: Axial force of cable A N_A as function of horizontal deflection u

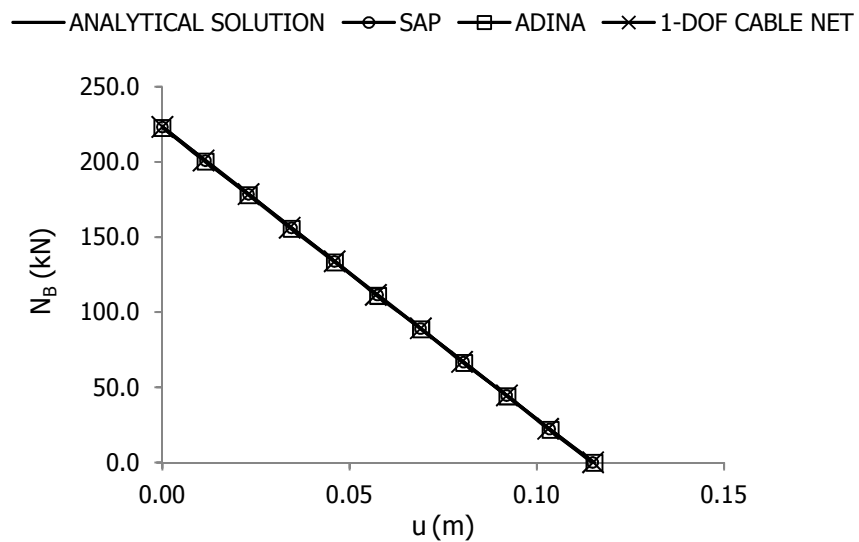


Figure 5-10: Axial force of cable B N_B as function of horizontal deflection u

6 STATIC BEHAVIOR OF CABLE NETS

6.1 THE FORCE DENSITY METHOD

Such as the simple 1-DOF cable net of Chapter 4, the analysis of an extended cable net is divided into two steps, the form finding and the nonlinear analysis under concentrated loads. The complexity of cable nets stems the development of an analytical solution. To overcome this difficulty, various methods, which describe the response of a cable net, are produced. The force density method, presented in this paragraph, is one of them. The force density method was developed for the case of cable nets (Figure 6-1), from Schek and expanded for the form finding of membranes.

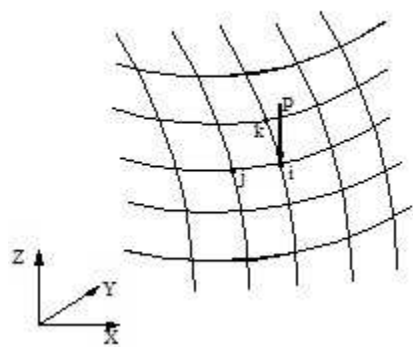


Figure 6-1: Cable net

Consider the node i of the cable net, which is connected with nodes j , k etc. An external concentrated load p_i is applied on the node i . F_{ij} is the axial force of the cable segment having length L_{ij} . The equilibrium equations for the node i , at the global coordinate system, are written as below:

$$\begin{aligned}
F_{ij} \frac{X_j - X_i}{L_{ij}} + F_{ik} \frac{X_k - X_i}{L_{ik}} + \dots &= p_{ix} \\
F_{ij} \frac{Y_j - Y_i}{L_{ij}} + F_{ik} \frac{Y_k - Y_i}{L_{ik}} + \dots &= p_{iy} \\
F_{ij} \frac{Z_j - Z_i}{L_{ij}} + F_{ik} \frac{Z_k - Z_i}{L_{ik}} + \dots &= p_{iz}
\end{aligned} \tag{6-1}$$

The force density, for each cable element, is defined as:

$$f_{ij} = \frac{F_{ij}}{L_{ij}} \tag{6-2}$$

Replacing Eq. (6-2) into (6-1), the equilibrium equations are transformed into:

$$\begin{aligned}
f_{ij} (X_j - X_i) + f_{ik} (X_k - X_i) + \dots &= p_{ix} \\
f_{ij} (Y_j - Y_i) + f_{ik} (Y_k - Y_i) + \dots &= p_{iy} \\
f_{ij} (Z_j - Z_i) + f_{ik} (Z_k - Z_i) + \dots &= p_{iz}
\end{aligned} \tag{6-3}$$

Corresponding equations can be written for all internal nodes of the cable net, while for border nodes equations are reduced, proportionally to node's degrees of freedom. The solution of the system defines the coordinates of nodes, given the values of force density and the external nodal loads. Then, the length of each element and, so, its tensile force are calculated from the following equation:

$$F_{ij} = f_{ij} \sqrt{(X_j - X_i)^2 + (Y_j - Y_i)^2 + (Z_j - Z_i)^2} \tag{6-4}$$

Benefits of force density method

The strategy and the numerical part of form finding are alternated, in contrast to other methods, as the equations of force density are linear and, so, the solution of the system of linear equations Eq. (6-3) gives an equilibrium shape. This system has a unique solution, if the following parameters are considered as constant:

- the coordinates of immovable nodes of the cable net
- the values of force density for all cables of the net

The second parameter seems to be an obstacle for the implementation of the method as the values of force density, for a given equilibrium shape, are not known a priori. Extended researches and experiments have shown that inaccurate approximations of these values are adequate to produce equilibrium shapes which can operate as the starting point for the iterative method of form finding. Thus, it is sufficient to consider, in most cases, as input values in the first step the non-tensioned cable lengths in the formulas of force density, referring to the internal net cables, and values inversely proportional to cable lengths, referring to the boundary zone of the cable net. This consideration does not seem to be self-evident. Nevertheless, it simplifies the calculation method which is rendered as a useful computer aided tool for form finding.

The force density equations do not contain parameters referring to the material of the cables and, so, their solution describes an equilibrium shape independent from the material. In

advanced steps of form finding procedure, the definition of an arbitrary material is demanded.

6.2 PARAMETRIC ANALYSIS – THE PEACE AND FRIENDSHIP STADIUM

6.2.1 The CANED program

The parametric analysis is a useful tool for obtaining a more spherical perception of construction's behavior. Changing gradually critical parameters of the cable net, effects of geometric nonlinearity, pre-tensioning etc can be illustrated in a legible way. The force density method, which is presented in Paragraph 6.1, is used for extracting the following parametric figures. The complexity and the number of the equilibrium equations, even though they are linear, for a real cable net inducts to the use of computer aided procedures. The CANED program is developed in this direction and is chosen for the parametric analysis.

The CANED program, which is developed as student work in the context of a Master course, is based on the force density method for the analysis of cable nets. It is written in MATLAB language producing the final program file in an executive format. At first, user determines the attributes of the cable net and the analysis/design procedure, as he can:

- choose the geometry of the net (rectangle, rhombus, circle or ellipse)
- define the number of cables in two axes
- import characteristics of the material
- set initial values of cross-section and pre-tension
- define the Newton-Raphson nonlinear analysis method
- determine the design procedure

The program is divided into two separate steps, the form finding and the nonlinear analysis for concentrated nodal loads in z axis. Moreover, the program has the ability to design cable nets. At each iteration of the second step, the values of stress are checked if they exceed the permitted range and, in such case, the algorithm returns to the first step re-calculating the values of cross-section and pre-tension. The successful completion of the analysis gives as output:

- figure for the form finding of the cable net
- stress and pre-tension distributions for form finding
- figure for the deformed model
- stress distribution for concentrated loads
- load-deflection diagram for the central node

Detailed results are available in text format, including the final values of cross-section and pre-tension.

[11]

6.2.2 Simulation of the Stadium of Peace and Friendship with CANED program

For the purposes of the parametric analysis, a real cable net is considered as model. It concerns the Stadium of Peace and Friendship in Greece, an example of a saddle-shaped cable net. It was constructed in 1983 and it was used, among other stadiums, for the Olympic Games of 2004. Its circular plan view has a diameter of 114 m, and the sag of the roof is 6.15 m, equal in both directions. The net consists of 27 cables in each direction and the cable spacing is constant and equal to 4 m in both directions. The main cables have a diameter of 60 mm and a breaking load of 3000 kN, while the diameter of the secondary

cables is 46 mm and their breaking load is 1850 kN. The edge ring is made of pre-stressed concrete, with a box cross-section of dimensions 6.40 m \times 8.15 m. The thickness of its horizontal walls is 20 cm and of the vertical ones 50 cm. The ring seats on bearings which are placed on 32 pylons. These pylons consist of radially oriented concrete walls. The bearings allow small radial translations of the ring, but in case of violent horizontal forces, for example during a seismic event, the ring is restrained in the radial direction of the roof. The parametric figures of this cable net model are designed by the implementation of CANED program.

[12]

Figure 6-2 shows a general view of the stadium and the simulation of its roof, using CANED program.

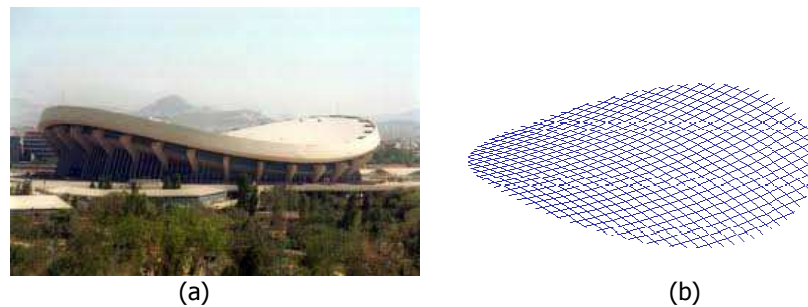


Figure 6-2: The Stadium of Peace and Friendship: (a) general view, (b) simulation of its roof

The plan of the cable net is a circle having two axes as shown in Figure 6-3. Cables parallel to x-axis, shaping a concave surface, are called main while these parallel to y-axis, shaping a convex surface, are called secondary or stabilizing. z-axis is perpendicular to the plan of the cable net. User sets the geometry of the cable net, as described above, and the program numbers each node and cable element with a unique label. Lengths are measured in m and forces in kN. The self weight of the cables is neglected.

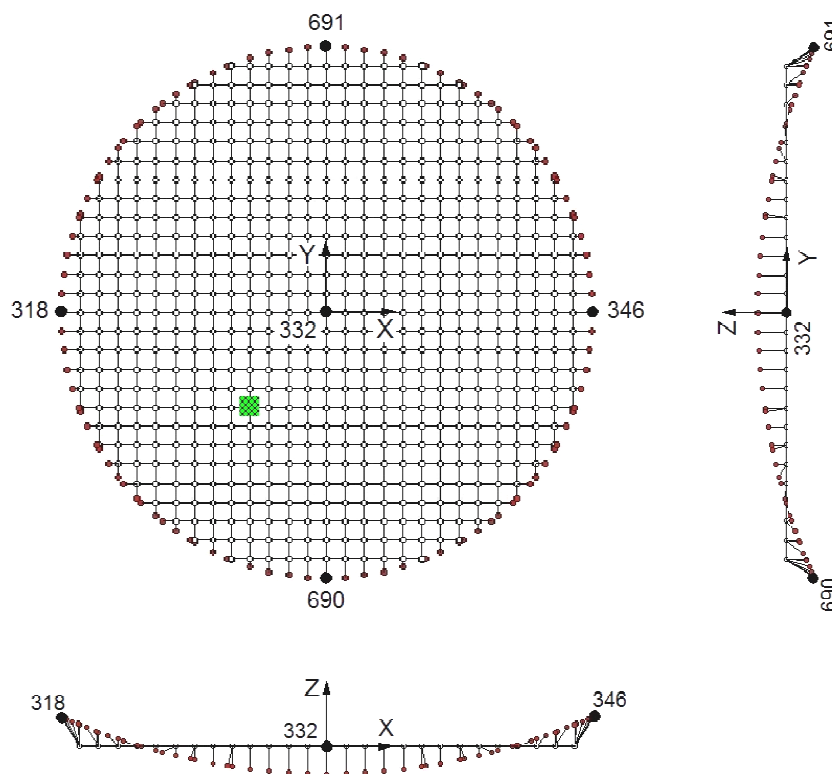


Figure 6-3: Views of the cable net, before the design procedure

Here, some characteristic nodes of the cable net, before the design procedure, are referred:

- 318 (-57,0,6.15)
- 332 (0,0,0) – central reference node
- 346 (57,0,6.15)
- 690 (0,-57,-6.15)
- 691 (0,57,-6.15)

The value of the modulus of elasticity E is 165 GPa. Regarding the limits of cables' tension, the maximum value is calculated as:

$$\sigma^{\max} = \min(\sigma_{\text{main}}^{\max}, \sigma_{\text{sec.}}^{\max}) = \min(1.57 \cdot 10^6 \text{ kPa}, 1.62 \cdot 10^6 \text{ kPa}) = 1.57 \cdot 10^6 \text{ kPa} \quad (6-5)$$

[12]

The tension limits in kPa in both axes, which are chosen for the parametric analysis, are presented in Table 6-1. The range of values for the form finding is smaller than this for the static analysis for safety reasons. The lower limit $\sigma^{\min} = 0$ kPa ensures that cables do not get loose.

step	Form finding	Static analysis
σ^{\max}	$1.0 \cdot 10^6$	$1.57 \cdot 10^6$
σ^{\min}	0	0

Table 6-1: Tension limits of cables in both axes, in kPa

For the purposes of the parametric analysis, distributed loads q_n , such as snow and wind, are considered. These loads are applied perpendicularly on the membrane which covers the cable net. The equivalent concentrated nodal load P, in kN, applied on an internal nodal point has value:

$$P = q_n A \quad (6-6)$$

where,

q_n is the distributed load in kN/m²

A is the hatched green area of Figure 6-3 with value 16.57 m² (for the figures presented on Paragraph 6.2.3, the value of 16.0 m² is considered)

The parametric figures contain the following symbols.

Form finding

z_0^* : z-coordinate of the central node, with label 332, from the starting point (0,0,0), in m

w_x^{pre} : horizontal component of pre-tension of central main cables, with label 318 and 319, at x-axis, at the equilibrium state as a percentage (%) of the maximum axial force N_x^{\max}

$$w_x^{\text{pre}} = 100 \frac{N_x^{\text{pre}}}{N_x^{\max}} = 100 \frac{N_x^{\text{pre}}}{\sigma_{\text{ff}}^{\max} \frac{\pi d_{\text{main}}^2}{4}} = 100 \frac{N_x^{\text{pre}}}{2827 \text{ kN}} \quad (6-7)$$

w_y^{pre} : horizontal component of pre-tension of central secondary cables, with label 954 and 955, at y-axis, at the equilibrium state as a percentage (%) of cables' maximum axial force N_y^{\max}

$$w_y^{\text{pre}} = 100 \frac{N_y^{\text{pre}}}{N_y^{\text{max}}} = 100 \frac{N_y^{\text{pre}}}{\frac{\sigma_{\text{ff}}^{\text{max}} \pi d_{\text{sec.}}^2}{4}} = 100 \frac{N_y^{\text{pre}}}{1662\text{kN}} \quad (6-8)$$

Static analysis

z_0 : z-coordinate of the central node, with label 332, from the equilibrium point $(0,0,z_0^*)$, in m

w_x : axial force of central main cables, with label 318 and 319, at x-axis, at the equilibrium state as a percentage (%) of cables' maximum axial force N_x^{max}

$$w_x = 100 \frac{N_x}{N_x^{\text{max}}} = 100 \frac{N_x}{\frac{\sigma_{\text{sa}}^{\text{max}} \pi d_{\text{main}}^2}{4}} = 100 \frac{N_x}{4439\text{kN}} \quad (6-9)$$

w_y : axial force of central secondary cables, with label 954 and 955, at y-axis, at the equilibrium state as a percentage (%) of cables' maximum axial force N_y^{max}

$$w_y = 100 \frac{N_y}{N_y^{\text{max}}} = 100 \frac{N_y}{\frac{\sigma_{\text{sa}}^{\text{max}} \pi d_{\text{sec.}}^2}{4}} = 100 \frac{N_y}{2609\text{kN}} \quad (6-10)$$

Figure 6-4 shows the referred cable elements, within the frames, and the corresponding edge nodes.

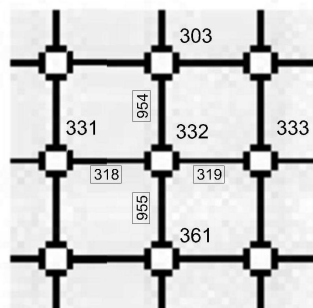


Figure 6-4: Definition of cable nodes and elements

Below, characteristic screenshots from the design procedure are presented.

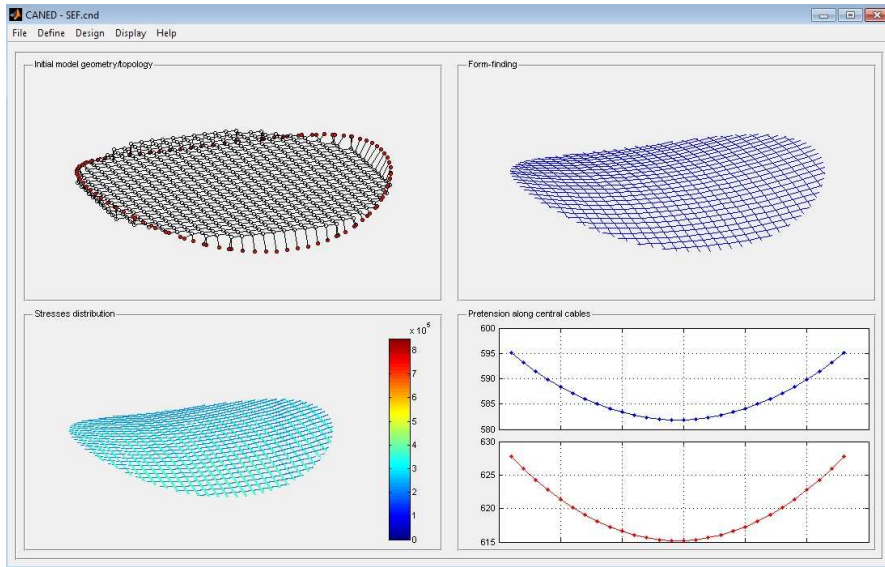


Figure 6-5: Screenshot from form finding

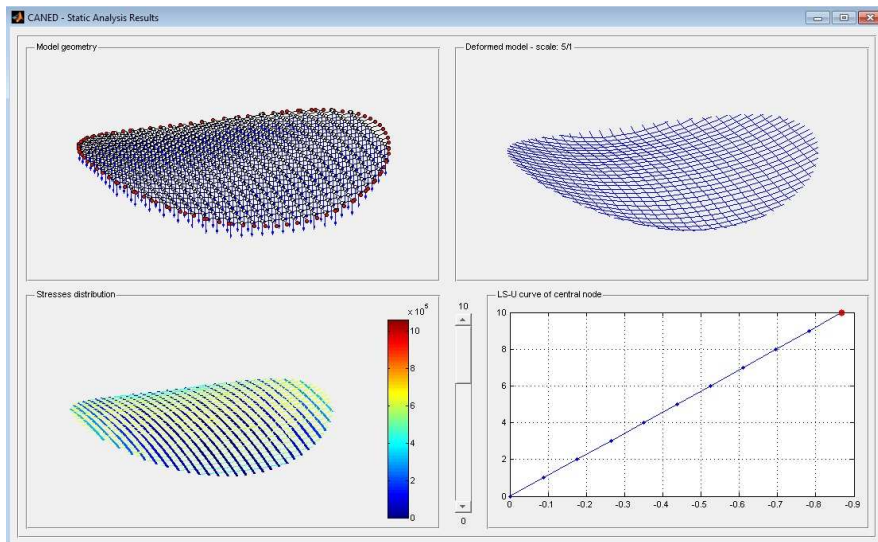


Figure 6-6: Screenshot from static analysis for load at $-z$ direction

6.2.3 Parametric figures

Curves' limits are defined by the maximum axial force N^{\max} of each cable.

STEP 1: FORM FINDING

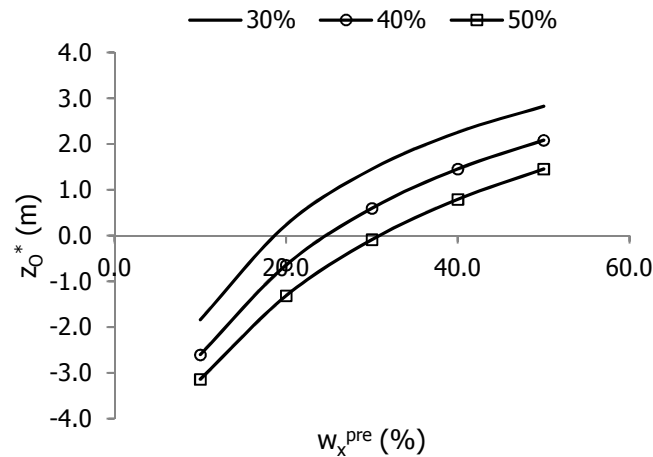


Figure 6-7: $z_0^* - w_x^{\text{pre}}$ curves, at the equilibrium state, for different values of pre-tension w_y^{pre}

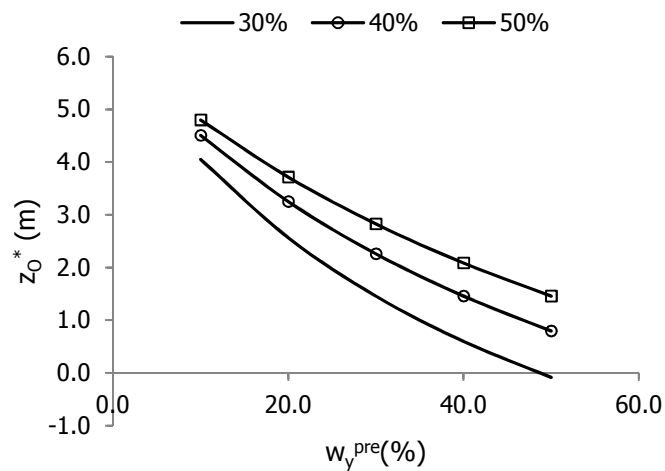


Figure 6-8: $z_0^* - w_y^{\text{pre}}$ curves, at the equilibrium state, for different values of pre-tension w_x^{pre}

The dependence of form finding on pre-tensions w_x^{pre} and w_y^{pre} is presented in Figures 6-7 and 6-8. The larger the pre-tension w_x^{pre} is, the higher the equilibrium point stands. The reverse correlation incurs for pre-tension w_y^{pre} . These figures prove that the increase of pre-tension makes central cables reduce their curvature by moving the equilibrium point nearer to the level of their supports, as larger values of cable axial force occur.

STEP 2: NONLINEAR ANALYSIS FOR CONCENTRATED NODAL LOAD P

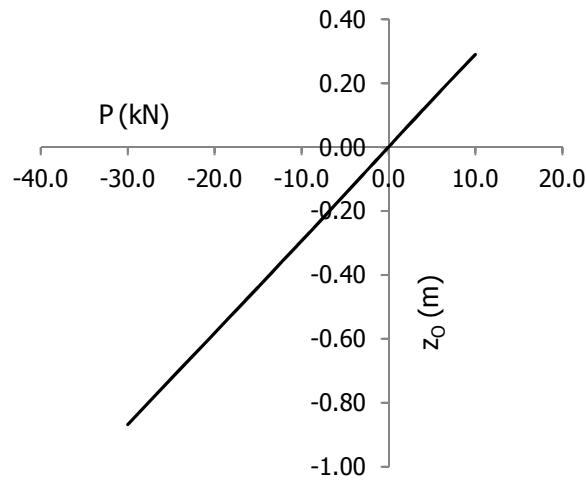


Figure 6-9: $z_0 - P$ curve for $w_x^{pre} = 13.1\%$ and $w_y^{pre} = 22.9\%$

Figure 6-9 shows the response of the central node with label 332 to concentrated nodal load P , with range of values $[-30.0, 10.0]$, in kN. The curve is, almost, linear indicating that the geometric nonlinearity is not intense, as the central cables with reverse curvatures, in x - and y -axes, tend to eliminate it. Pre-tensions w_x^{pre} and w_y^{pre} are equal to these of the construction as built. Figure 6-9 occurs from the combination of two separate analyses for concentrated nodal load P at $\pm z$ directions.

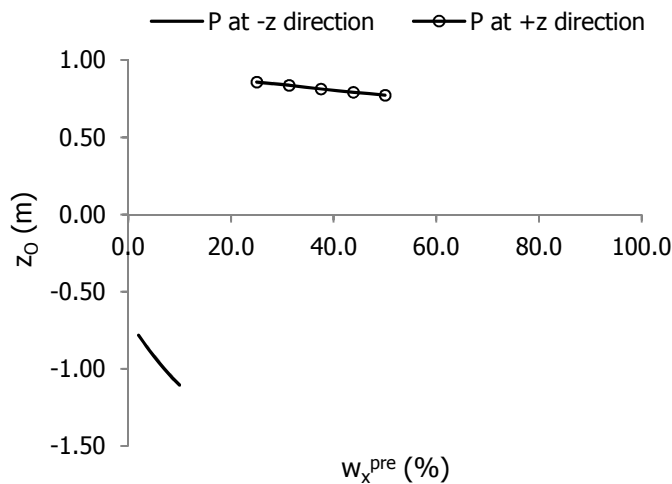


Figure 6-10: $z_0 - w_x^{pre}$ curve, in case that pre-tension $w_y^{pre} = 35.0\%$

Figure 6-10 describes the relationship between z_0 and w_x^{pre} . The larger the pre-tension w_x^{pre} is, the larger the z -coordinate z_0 , in absolute value, becomes, in case of P at $-z$ direction, and the reverse correlation incurs for P at $+z$ direction. Figures 6-7 and 6-8 show that the larger the pre-tension w_x^{pre} is, the higher the equilibrium point stands. So, the unstressed length of central main cables is smaller but this of central secondary cables, given constant value of

w_y^{pre} , is larger. According to Figure 2-63, the larger the ratio $\frac{S_0}{S_{AB}}$ of a cable is the larger stiffness has for the same concentrated nodal load P . This observation is valid for a horizontal cable with concentrated load in the middle but it can be generalized for the case of net cables. As a consequence, larger stiffness of central secondary cables means reduce of z_0 , for constant value of concentrated nodal load P . Correspondingly, the reduction of length of central main cables leads to reduction of their stiffness, in other words increase of z_0 , in absolute value.

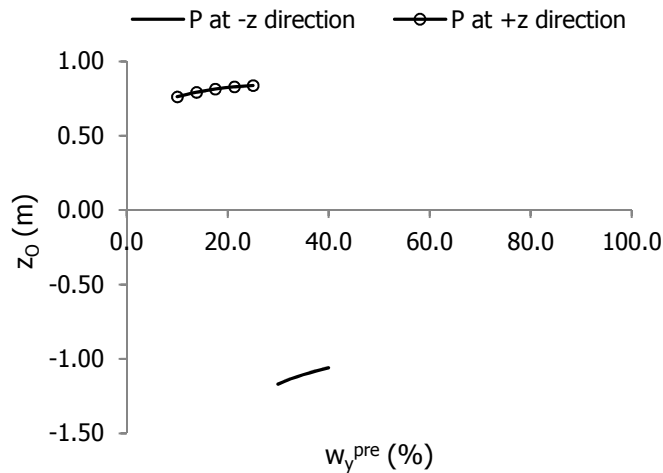


Figure 6-11: $z_0 - w_y^{pre}$ curve, in case that pre-tension $w_x^{pre} = 10.0\%$

Regarding the Figure 6-11, the larger the pre-tension w_y^{pre} is, the smaller the z_0 , in absolute value, becomes, in case of P at $-z$ direction, and the reverse correlation incurs for P at $+z$ direction. Figures 6-7 and 6-8 show that the larger the pre-tension w_y^{pre} is, the lower the equilibrium point stands. So, the unstressed length of central main cables, given constant value of w_x^{pre} , is larger but this of central secondary cables is smaller. According to Figure 2-63, the larger the ratio $\frac{S_0}{S_{AB}}$ of a cable is the larger stiffness has for the same concentrated load P . This observation is valid for a horizontal cable with concentrated load in the middle but it can be generalized for the case of net cables. As a consequence, larger stiffness of central main cables means reduce of z_0 , in absolute value, for constant value of concentrated nodal load P . Correspondingly, the reduction of length of central secondary cables leads to reduction of their stiffness, in other words increase of z_0 .

The values of P at $\pm z$ directions are defined below.

$-z$ direction

$$\text{pressure } q = 3.0 \text{ kN/m}^2 \Rightarrow P = 48.0 \text{ kN}$$

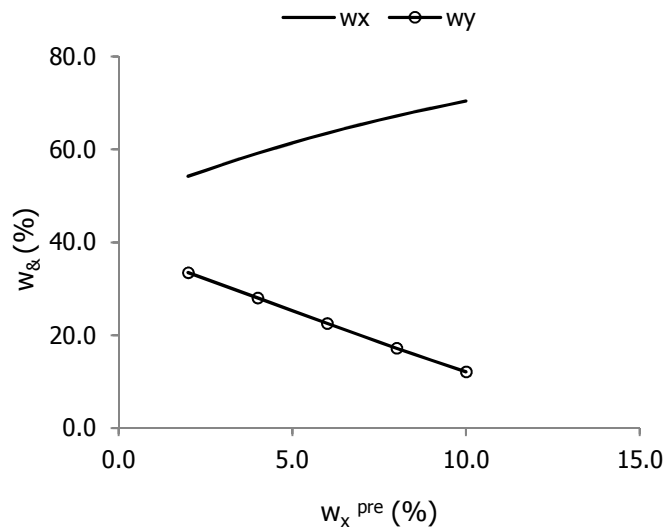


Figure 6-12: $w_x - w_y^{pre}$ curves, at the equilibrium state, in case that pre-tension $w_y^{pre} = 35.0$ %

Figure 6-12 indicates that the larger the pre-tension w_x^{pre} is, the larger axial force w_x and the smaller axial force w_y occur, given constant values of pre-tension w_y^{pre} and concentrated nodal load P . This is true, as for higher starting level of pre-tension w_x^{pre} and constant value of concentrated nodal load P , a larger value of axial force w_x arises. Moreover, Figure 6-10 shows that the larger the pre-tension w_x^{pre} is, the larger the z_0 , in absolute value, is and, so, the increase of stressed length of central secondary cables is smaller provoking smaller values of axial force w_y .

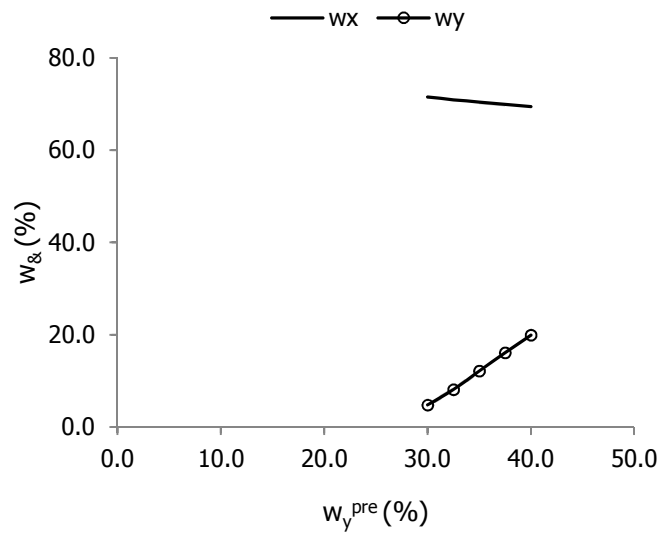


Figure 6-13: $w_x - w_y^{pre}$ curves, at the equilibrium state, in case that pre-tension $w_x^{pre} = 10.0$ %

According to Figure 6-13, the larger the pre-tension w_y^{pre} is, the smaller axial force w_x and the larger axial force w_y occur, given constant values of pre-tension w_x^{pre} and concentrated nodal load P . A larger value of axial force w_y arises for higher starting level of pre-tension w_y^{pre} and constant value of concentrated nodal load P . What is more, Figure 6-11 indicates that the larger the pre-tension w_y^{pre} is, the smaller the z_0 , in absolute value, is and, so, the increase of stressed length of central main cables is smaller provoking smaller values of axial force w_x .

+z direction

pressure $p = 1.65 \text{ kN/m}^2 \Rightarrow P = 26.4 \approx 26.0 \text{ kN}$

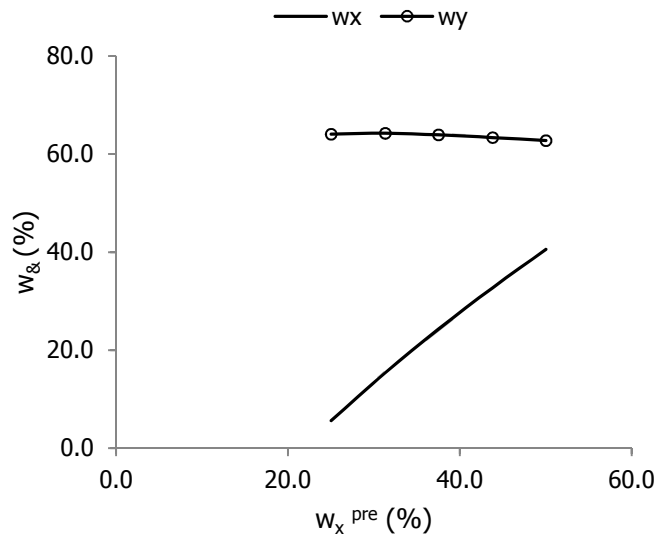


Figure 6-14: $w_g - w_x^{\text{pre}}$ curves, at the equilibrium state, in case that pre-tension $w_y^{\text{pre}} = 17.5 \%$

Figure 6-14 indicates that the larger the pre-tension w_x^{pre} is, the larger axial force w_x and the smaller axial force w_y occur, given constant values of pre-tension w_y^{pre} and concentrated nodal load P . This is true, as for higher starting level of pre-tension w_x^{pre} and constant value of concentrated nodal load P , a larger value of axial force w_x arises. Moreover, Figure 6-10 shows that the larger the pre-tension w_x^{pre} is, the smaller the z_0 is and, so, the increase of stressed length of central secondary cables is smaller provoking smaller values of axial force w_y .

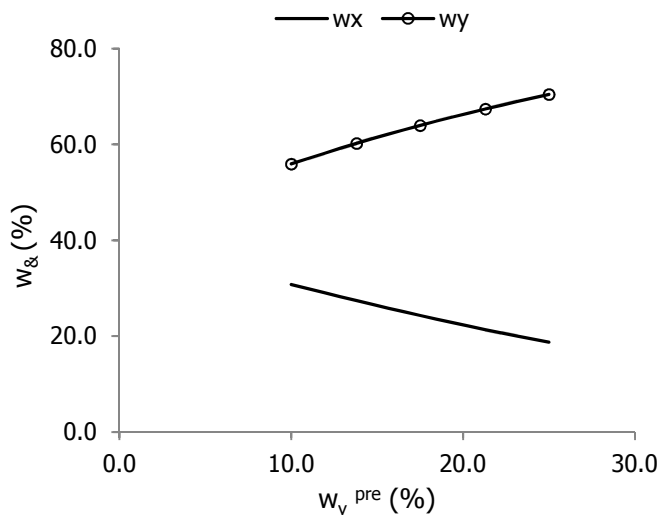


Figure 6-15: $w_g - w_y^{\text{pre}}$ curves, at the equilibrium state, in case that pre-tension $w_x^{\text{pre}} = 37.5 \%$

According to Figure 6-15, the larger the pre-tension w_y^{pre} is, the smaller axial force w_x and the larger axial force w_y occur, given constant values of pre-tension w_x^{pre} and concentrated nodal

load P . A larger value of axial force w_y arises for higher starting level of pre-tension w_y^{pre} and constant value of concentrated nodal load P . What is more, Figure 6-11 indicates that the larger the pre-tension w_y^{pre} is, the larger the z -coordinate z_0 is and, so, the increase of stressed length of central main cables is smaller provoking smaller values of axial force w_x .

Notice in Figures 6-12 to 6-15 that, the additional axial force ($w_{\&} - w_{\&}^{\text{pre}}$), due to the concentrated nodal load P , is significantly larger than the initial pre-tension $w_{\&}^{\text{pre}}$, where $\& = x, y$. For instance, as presented in Figure 6-12, for $w_x^{\text{pre}} = 5.0\%$ and $w_y^{\text{pre}} = 35.0\%$, w_x is around 60% . In other words, $60 - 5 = 55\%$ of axial force of central main cables occurs from the concentrated nodal load P and is according to a good design policy. The range of $w_{\&}^{\text{pre}}$, where $\& = x, y$, in STEP 2 differs in $\pm z$ -directions of concentrated nodal load P , as it depends on cables' diameter and cables' maximum tension.

7 REFERENCES

- [1] I. Vassilopoulou, "Nonlinear dynamic response and design of cable nets", Doctoral thesis, NTUA, Greece, 2011
- [2] M. Irvine, "Cable structures", Dover Publications, Inc., U.S.A., 1981
- [3] EUROCODE 3, PART 1.11, "Design of structures with tension components", 2003
- [4] J. W. Leonard, "Tension structures: Behavior and analysis", McGraw-Hill, Inc., U.S.A., 1988
- [5] C. Gantes, Class notes of the subject "Cable structures", NTUA, 2002
- [6] E. Kreyszig, "Advanced engineering mathematics", 8th Edition, John Wiley & Sons, Inc., U.S.A., 1999.
- [7] <http://www.adina.com/tutorials.shtml>
- [8] <http://www.comp-engineering.com/products/SAP2000/sap2000.html>
- [9] <http://mycourses.ntua.gr/document/document.php?cmd=exChDir&file=%2F%CB%EF%E3%E9%F3%EC%E9%EA%FC> (password is demanded)
- [10] http://www.mathworks.com/help/pdf_doc/matlab/getstart.pdf
- [11] A.A. Vrakas, "Development of software for the design of cable nets", Student work, NTUA, Greece, 2010
- [12] I. Vassilopoulou, "Behavior and analysis of cable net roofs", Graduate thesis, NTUA, Greece, 2001 (in Greek)
- [13] Rassias T. (2004), "Mathematic analysis 1, vol. A", Savalas Publishers, Greece

APPENDIX A: Hyperbolic functions

Appendix A contains a short presentation of hyperbolic functions, which are used in Paragraphs 2.3.3 and 2.3.4, in case of a simple suspended cable under uniformly distributed load along its arc length.

Standard algebraic expressions:

$$\sinh x = \frac{e^x - e^{-x}}{2} = \frac{e^{2x} - 1}{2e^x} = \frac{1 - e^{-2x}}{2e^{-x}} \quad (\text{A-1})$$

$$\cosh x = \frac{e^x + e^{-x}}{2} = \frac{e^{2x} + 1}{2e^x} = \frac{1 + e^{-2x}}{2e^{-x}} \quad (\text{A-2})$$

$$\tanh x = \frac{\sinh x}{\cosh x} = \frac{e^x - e^{-x}}{e^x + e^{-x}} = \frac{e^{2x} - 1}{e^{2x} + 1} = \frac{1 - e^{-2x}}{1 + e^{-2x}} \quad (\text{A-3})$$

Useful relations:

$$\sinh(-x) = -\sinh(x) \quad (\text{A-4})$$

$$\cosh(-x) = \cosh(x) \quad (\text{A-5})$$

$$\tanh(-x) = -\tanh(x) \quad (\text{A-6})$$

$$\cosh^2(x) - \sinh^2(x) = 1 \quad (\text{A-7})$$

Sums of arguments:

$$\cosh(x + y) = \sinh(x)\cosh(y) + \cosh(x)\sinh(y) \quad (\text{A-8})$$

$$\sinh(x + y) = \cosh(x)\sinh(y) + \sinh(x)\cosh(y) \quad (\text{A-9})$$

$$\tanh(x + y) = \frac{\tanh(x) + \tanh(y)}{1 + \tanh(x)\tanh(y)} \quad (\text{A-10})$$

Sum and difference of cosh and sinh:

$$\cosh(x) + \sinh(x) = e^x \quad (\text{A-11})$$

$$\cosh(x) - \sinh(x) = e^{-x} \quad (\text{A-12})$$

Inverse functions as logarithms:

$$\operatorname{arsinh}(x) = \ln(x + \sqrt{x^2 + 1}) \quad (\text{A-13})$$

$$\operatorname{arcosh}(x) = \ln(x + \sqrt{x^2 - 1}), x \geq 1 \quad (\text{A-14})$$

$$\operatorname{artanh}(x) = \frac{1}{2} \ln\left(\frac{1+x}{1-x}\right), |x| < 1 \quad (\text{A-15})$$

Derivatives:

$$\frac{d}{dx} \sinh x = \cosh x \quad (\text{A-16})$$

$$\frac{d}{dx} \cosh x = \sinh x \quad (\text{A-17})$$

$$\frac{d}{dx} \tanh x = 1 - \tanh^2 x \quad (\text{A-18})$$

Standard Integrals:

$$\int \sinh(ax) dx = a^{-1} \cosh(ax) + C \quad (\text{A-19})$$

$$\int \cosh(ax) dx = a^{-1} \sinh(ax) + C \quad (\text{A-20})$$

$$\int \tanh(ax) dx = a^{-1} \ln[\cosh(ax)] + C \quad (\text{A-21})$$

[13]

TABLE OF SYMBOLS

Symbol	Definition	Unit
labels		
\$	label \$ (= 1, 2,...) of a cable	-
i	label i (= A, B, ...) of a point/node	-
&	label & (= x, y, z) of direction	-
ij	chord with endpoints i and j	-
coordinates		
X, Y, Z	Cartesian axes	-
x, y, z	coordinates of the examined point after the application of the load P, p or q	m
x^{\max}	maximum x-coordinate of the examined point	m
x_i, y_i, z_i	coordinates of point i	m
x_p, y_p, z_p	coordinates of the starting application point of the concentrated load P	m
x^*, y^*, z^*	coordinates of the point from which cable tension, due to the load P, p or q, occurs	m
z_0^*	z-coordinate of the central node, at form finding	m
z_0	z-coordinate of the central node, at static analysis	m
lengths		
u, v	deflections/displacements of the examined point $u = x - x^*$ $v = z - z^*$	m
u^{\max}	maximum horizontal deflection/displacement $u^{\max} = x^{\max} - x^*$	m
d	vertical distance of the stressed cable from the chord AB	m

d_m	vertical distance of the stressed cable from the chord AB at midpoint	m
d_{mP}	vertical distance of the stressed cable from the chord AB at midpoint, in case of equivalent concentrated load $P = pL$ at midpoint	m
ε	elongation of the cable	-
ε_i	elongation of the cable segment supported on point i	-
ε^{\max}	maximum elongation of the cable	-
s	stressed length of the cable from the start of the axes to the point (x,z)	m
s_0	initial unstressed length of the cable from the start of the axes to the point (x,z)	m
S	stressed length of the cable	m
S_0	initial unstressed length of the cable	m
S_{0i}	initial unstressed length of the cable segment supported on point i	m
S_i	stressed length of the cable segment supported on point i	m
S_{ij}	distance between points i and j	m
L	horizontal/vertical length, as defined on figures	m
loads		
P	applied concentrated load	kN
p^{\max}	maximum applied concentrated load	kN
p	uniformly distributed load along the horizontal projection	kN/m
p_{\perp}	component of the applied load p perpendicular to the cable segment ds	kN/m
p_{\parallel}	component of the applied load p parallel to the cable segment ds	kN/m
p^{\max}	maximum uniformly distributed load along the horizontal projection	kN/m
q	uniformly distributed load along the arc length of the cable	kN/m
q_{\perp}	component of the applied load q perpendicular to the cable segment ds	kN/m
q_{\parallel}	component of the applied load q parallel to the cable segment ds	kN/m
q^{\max}	maximum uniformly distributed load along the arc length of the cable	kN/m
stresses		
σ	axial tension of the cable	kPa
σ_i	axial tension of the cable segment supported on point i	kPa
σ^{pre}	pre-tension of the cable	kPa
σ^{\max}	maximum axial tension of the cable	kPa
σ^{\min}	minimum axial tension of the cable	kPa
f_y	yield stress of the cable	GPa
E	modulus of elasticity of the cable	GPa
forces		
N	axial force of the cable	kN
N_i	reaction at point i	kN
N_p	axial force of the cable, in case of equivalent concentrated load $P = pL$ at midpoint	kN
N^{pre}	axial force of the cable due to pre-tension	kN
N^{\max}	maximum axial force of the cable	kN

N^{cap}	axial force capacity of the cable	kN
w	axial force of the cable as percentage of its capacity	%
w^{pre}	axial force of the cable due to pre-tension as percentage of its capacity	%
r	axial force of the cable as percentage of its pre-tension	%
H	horizontal component of the axial force of the cable	kN
H_i	horizontal reaction at point i	kN
V	vertical component of the axial force of the cable	kN
V_i	vertical reaction at point i	kN
F	restoring force of a spring	kN
other important symbols		
M	bending moment	kNm
K	stiffness of the cable	kN/m
K_S	(equivalent) spring constant	kN/m
K_{mast}	stiffness of a radio mast	kN/m
K_{net}	stiffness of 1-DOF cable net	kN/m
θ	angle of inclination	deg ($^\circ$)
d_A	the diameter of the cable	mm
A	the cross-section of the cable	m^2
defined in paragraph		
$g_k, w_k, f, A_u, f_u, F^{\text{min}}, R_r, K_r, \sigma_e, \sigma_u$	symbols defined in Paragraph 1.2.1	-
$c_1, c_1^\#, c_2, c_2^\#, a, \beta, \beta^\#, \gamma, \gamma^\#, \Gamma, \Gamma^\#, \Delta, \Delta^\#, \Theta, \Theta^\#, \Lambda, \Lambda^\#, \Xi, \Xi^\#$	symbols defined in Paragraph 2.2.2	-
$c_1^h, c_2^h, \beta^h, \gamma^h, \Gamma^h, \Delta^h, \Theta^h, \Lambda^h, \Xi^h$	symbols defined in Paragraph 2.2.3	-
$K_{Si}, P_i, v_i, \theta_i$	symbols defined in Paragraph 2.2.4.3, for the cable i of the cable-braced bridge	-
ρ, ρ_A, ρ_B	symbols defined in Paragraph 2.3.1	-
δ, ζ	symbols defined in Paragraph 2.3.3	-
$\varepsilon_\$, \varepsilon_\$, S_{0\$}, S_\$, L_\$, q_n, \sigma_\$, \sigma_\$, f_{y\$}, E_\$, w_\$, w_\$, N_\$, N_\$, H_\$, H_\$, V_\$, V_\$, N_\$, A_\$, d_{A\$}$	symbols defined in Chapter 4 for cable $\$$	-
$N_i^{\text{pre}}, w_i^{\text{pre}}, N_i^{\text{cap}}, N_i^{\text{max}}$	symbols defined in Paragraph 5.1	-
$X_i, Y_i, Z_i, L_{ij}, p_i, p_{ix}, p_{iy}, p_{iz}, F_{ij}, f_{ij}$	symbols defined in Paragraph 6.1	-
$\sigma_{\text{main}}^{\text{max}}, \sigma_{\text{sec}}^{\text{max}}, \sigma_{\text{ff}}^{\text{max}}, \sigma_{\text{sa}}^{\text{max}}, w_{\&}, w_{\&}^{\text{pre}}, N_{\&}, N_{\&}^{\text{pre}}, N_{\&}^{\text{max}}$	symbols defined in Paragraph 6.2	-

$d_{main}, d_{sec.}$		
----------------------	--	--

Table T-1: Table of symbols

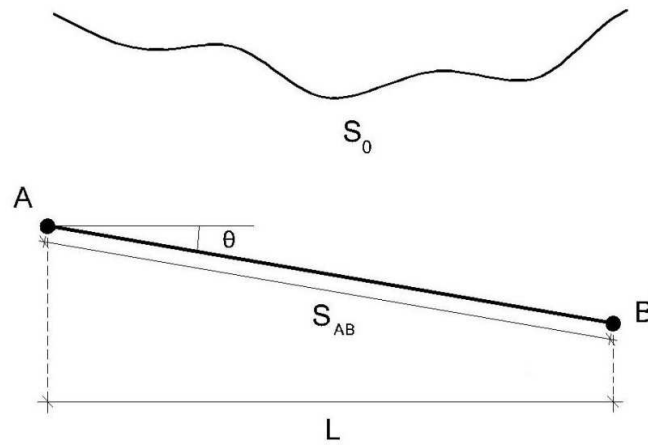


Figure T-1: General cable model

Dimensional parameters are transformed to non-dimensional using the following multiplications:

- coordinates and lengths: $\times \frac{1}{L}$
- concentrated loads: $\times \frac{1}{EA}$
- distributed loads: $\times \frac{L}{2EA}$
- forces: $\times \frac{1}{EA}$
- stiffness: $\times \frac{1}{\frac{EA}{L}}$

